Development of Sodium-Sulfur Batteries for Utility Application

EPRI

EPRI EM-683
Project 128-4
Interim Report
May 1978

Keywords:
Energy Storage
Sodium-Sulfur Battery
Battery

Prepared by
General Electric Company
Schenectady, New York 12301

ELECTRIC POWER RESEARCH INSTITUTE

Development of Sodium-Sulfur Batteries for Utility Application

EM-683
Research Project 128-4

Interim Report, May 1978

Prepared by

GENERAL ELECTRIC COMPANY
Electrochemistry Branch
Corporate Research and Development
Schenectady, New York 12301

Principal Investigator
S. P. Mitoff

Project Manager
D. Chatterji

Prepared for

Electric Power Research Institute
3412 Hillview Avenue
Palo Alto, California 94304

EPRI Project Manager
J. R. Birk
Fossil Fuel and Advanced Systems Division

LEGAL NOTICE

This report was prepared by General Electric Company, Corporate Research and Development as an account of work sponsored by the Electric Power Research Institute, Inc. (EPRI). Neither EPRI, members of EPRI, General Electric Company, Corporate Research and Development, nor any person acting on behalf of either: (a) makes any warranty or representation, express or implied, with respect to the accuracy, completeness, or usefulness of the information contained in this report, or that the use of any information, apparatus, method, or process disclosed in this report may not infringe privately owned rights; or (b) assumes any liabilities with respect to the use of, or for damages resulting from the use of, any information, apparatus, method, or process disclosed in this report.

ABSTRACT

The results of the past sixteen months of a project aimed at developing sodium-sulfur batteries for utility applications are presented in this report. During this period Laboratories de Marcoussis of Compagnie Generale d'Electricite, France, joined the program as a subcontractor. The report, therefore, includes the results obtained by CGE-Marcoussis under the subcontract.

During the reporting period over 150 small (16 Ah) cells were placed on test. Life times up to 12,000 hours and up to 1,150 Ah/cm^2 were obtained. Cell capacities of over 80% have been achieved and sustained for over 250 cycles. The most common failure mode during the period involved degradation of the glass seal between the beta-alumina tube and the alpha-alumina header.

Several container materials have been judged unsatisfactory from the corrosion standpoint. These are: 347 stainless steel, aluminided steel, molybdenum foil, and plasma sprayed molybdenum or chromium. Apparently satisfactory is a chromium base coating, which is thin, and remains conductive during test periods (about 1 year) employed so far.

Thermocompression bonding of steel containers to the alpha alumina insulator was chosen as the first choice for the exterior seals. It has been shown to be thermally and chemically stable, and no seal failures have been observed in a six month

testing period. A new glass formulation has so far eliminated our problem with the interior beta to alpha alumina seal. The glass shows no signs of deterioration or reaction with beta alumina, and no failures have occurred in the six months of cell testing since it was put into use.

No further beta alumina compositional modifications were made during the reporting period. The ceramic as produced today has a fine and uniform grain size, shows a rupture strength of over 50 kpsi, and is not a life limiting cell component within the completed test periods. Large tubes for 300 WH cells have been formed by both electrophoresis and isostatic pressing. However, firing of the large tubes has not yet reached the status of a routine activity.

Battery system design is in an advanced stage. In our present design, the basic unit of the system is a module which is a thermally self-sufficient package. It consists of 360 cells (300 WH each). The cells within the module are arranged in nine bundles in series, each bundle consisting of forty cells connected in parallel.

Manufacturing and cost studies of two kinds are presented in this report. One is a cost projection for a battery system of commercial size, 100 megawatt hours. The system is designed for a seventy five percent efficiency operating on a 5 hour discharge, 7 hour charge cycle. The estimated selling price is projected to be about $38/KWH. The other study is an examination of the effect of the ceramic electrolyte tube size on the system selling price. The optimum size range was found to be between 2

and 3 cm O.D. and 30 to 45 cm long.

Finally, a summary of supporting research activities is given. Major emphasis was placed on understanding the behavior of the sulfur electrode. This included real-time examination of cells by x-radiography.

EPRI PERSPECTIVE

PROJECT DESCRIPTION

This report is one in a series of progress reports that reviews the status of the development of the sodium-sulfur battery for utility application. This battery, along with the zinc halogen systems, are the leading battery systems being developed to improve the capacity factor of base-load generation plants and to reduce oil consumption by the electric utility industry. The sodium-sulfur battery is one of five systems that EEI and, subsequently, EPRI began to support in the 1971-1974 time frame. Presently, the EPRI battery subprogram is narrowing down the number of battery technology options to two or three by 1979, before scale-up to the 5-10 MWh prototype level. It is unlikely, however, that the sodium-sulfur battery system will be one of the systems dropped. The sodium-sulfur battery is now being developed under a $3.4 million, 32-month contract initiated in May 1976. General Electric is also providing significant financial contribution to this project. This report covers work on the first half on this contract.

PROJECT OBJECTIVES

The ultimate objective of this project is to commercialize the sodium-sulfur battery for electric utility energy-storage application. An intermediate objective is to install a 5 MWh battery in the Battery Energy Storage Test (BEST) Facility (RP255) by 1985. The specific objectives for the period covered by this report were (1) to develop low-cost sulfur-electrode containers, (2) to increase life of small laboratory cells from about 500 to about 1000 cycles, and (3) to assess ultimate battery price.

CONCLUSIONS AND RECOMMENDATIONS

The objectives stated above were achieved. The small (30Wh) laboratory cells have consistently shown excellent performance and long life. Considering these cells use the materials and components anticipated for commercial hardware, the performance and life are meaningful indicators of development status. The cost studies have shown that the sodium-sulfur battery can achieve the cost objective for utility application. These studies have been objective and thorough. In addition, the results of the costing exercise are in good agreement with independent work done by Compagnie Générale d'Electricité (France) under a separate EPRI contract. The previous work at G.E. justifies scale-up of cells from 3 Wh to full-scale size (300 Wh) and a hard look at commercialization strategy. Testing of full-scale cells is to commence in April, 1978 and by the end of the contract period (December 1978) 10 kWh bundles (40 cells in parallel) should be on test. However, since this is an ambitious schedule, it is unlikely that the transition to larger hardware can be accomplished smoothly.

James R. Birk
Project Manager
Advanced Battery Development

ACKNOWLEDGMENTS

This report describes work performed between May 1, 1976 and August 31, 1977 under Electric Power Research Institute Project RP 128-4, "Development of Sodium-Sulfur Batteries for Utility Application", and the work of a planned, on-going, in-house program at General Electric Corporate Research and Development. The work was principally carried out by the Electrochemistry Branch in the Power Systems Laboratory of General Electric Corporate Research and Development in Schenectady, New York. Laboratoires de Marcoussis, Compagnie Generale d'Electricite, Paris, France, became a major subcontractor to General Electric, beginning January 1, 1977.

Dr. D. Chatterji, Manager-Electrochemistry Branch, General Electric Corporate Research and Development, was the Program Manager for EPRI Project RP 128-4, and Dr. S.P. Mitoff was the Principal Investigator. Dr. J.R. Birk of EPRI was designated by the Institute as the Project Manager.

GE contributors during this reporting period were:

J.D. Arcuri
J.C. Bielawski
Dr. M.W. Breiter
J.L. Briant
V.J. DeCarlo
R.R. Dubin
Dr. B. Dunn
T.M. Evenden
D.L. Hollinger
T.J. Jordan
R.N. King
H.E. Major
Dr. L. Navias
Dr. R.H. Norris
Dr. D.S. Park
H.T. Plant
Dr. R.W. Powers
M.C. Schmidt
E. Szymalak

Major CGE-Marcoussis contributors were:

G. Desplances
J.P. Dumas
Dr. G. Fenillade
J. Jacqueline
G. Kaltenbach
J.B. Pompon
R.L. Vic
Dr. A. Wicker

TABLE OF CONTENTS

PART ONE

INTRODUCTION, SUMMARY, AND REPORT ORGANIZATION

Section A
INTRODUCTION AND SUMMARY

The sodium-sulfur battery is a potentially low cost, high energy density, rechargeable battery. It utilizes molten sodium as the anode (in discharge mode) and molten sulfur/sodium polysulfide as the cathode, and beta-alumina as the solid electrolyte-separator. The sodium-sulfur battery is one of several electrochemical systems currently being developed for use by electric utilities for large scale storage of energy during low demand periods for discharge during subsequent high demand periods.

At General Electric, work on beta-alumina synthesis, characterization and property/application evaluation began in 1967. A program was initiated around 1971 to develop beta-alumina-based batteries. In 1973 the program was focussed, under joint GE-EPRI sponsorship, toward developing a sodium-sulfur battery system for utility energy storage application. In 1977, Laboratoires de Marcoussis, Compagnie Generale d'Electricite (CGE), France, joined the GE-EPRI program as a major subcontractor.

The ultimate goal of the multiyear, multiphase GE-EPRI program is to successfully demonstrate in the 1981-82 timeframe a GE battery of 1 MW/5 MWh rating at the Battery Energy Storage Test (BEST) Facility; this facility is now under construction at a Public Service Electric & Gas site in New Jersey under EPRI-ERDA-PSE&G sponsorship. The Phase I of the GE-EPRI program, scheduled to end in 1977, had the following objectives:

1. Development of a fabrication process for beta-alumina ceramic ware;
2. Optimization of ceramic composition and processing for best combination of physical and chemical properties;
3. Identification and demonstration of practical cell construction materials and design concepts; and
4. Generation of statistically significant life and performance data on small, 16 Ah capacity, "prototype" cells and establishing the effects of design, material and process changes.

The Phase II of the GE-EPRI program began in 1976 and is targeted for completion by end of 1978. Its objectives are:

1. Demonstration of equivalent of 5 years life and sustained high performance in prototype test cells;
2. Fabrication, evaluation and optimization of full-size cells and cell "bundles"; and

3. Design optimization for the BEST battery.

This Interim Report covers the period May 1, 1976 through August 31, 1977. Since Phase I and Phase II efforts overlapped during this period, the program saw continuation of efforts started in 1975 as well as initiation of tasks to be continued through 1978. (Also certain aspects of a number of tasks were subcontracted to CGE-Marcoussis beginning January 1, 1977.) The following areas of R&D received the primary attention during the report period:

1. Evaluation and improvement of prototype cell life and performance.
2. Development of corrosion-resistant, high conductivity containers for the cathode (sulfur/polysulfide) compartment.
3. Development of exterior and interior seals with long life and low cost potential.
4. Improvement in ceramic properties.
5. Design for the BEST battery system/module/bundle/cell.
6. Manufacturing engineering and cost studies.
7. Electrochemical modeling of the sulfur electrode, real-time X-radiography of cells, and other supporting research areas.
8. Scale-up of components, processes and facilities to insure success in fabrication and operation of full size cells in the September 1977 - December 1973 period.

Progress made in these areas are summarized in this Interim Report.

Some of the above-mentioned R&D activities were sponsored by EPRI and others were supported by GE (and CGE-Marcoussis in some cases) as part of a planned, on-going in-house program. At the discretion of the General Electric Company, parts of the information generated under its in-house program are included in this report. Section B of this report describes the EPRI, the GE, and the CGE programs, and explains the organization of this report vis-a-vis the three programs. The following paragraphs provide brief summaries of progress made in the listed areas during the report period.

Prototype Cell Life and Performance: During the report period, substantial improvements were made in the areas of cell life and performance. Table A.1 offers a chronological history of progress in these areas; very substantial gains have been made during the report period in all areas important to utility application: cell life, cell efficiency, and utilization of cell capacity. Some 150 cells were placed on test during the last 15 months, and a number of design and materials advances were incorporated to improve cell life and performance.

The longest lived cell logged more than 12,000 hours before failure, and cycled at 54 mA/cm^2 current density. Another cell, placed on test somewhat later, has logged $\sim$ 11,000 hours and is still on test, cycling at 108 mA/cm^2; thus the ceramic electrolyte in this cell has withstood $\sim$ 1150 Ah/cm^2 of charge transport.

Electrolyte quality has been improved to such an extent that the electrolyte is rarely the cause of cell failure at this time. Seal failures presently limit the cell life to a typical value of ∿ 500 cycles (∿ 500 Ah/cm^2). Cells with new, improved seals are performing very well; however, the exact magnitude of improvement will not be known until substantial test time has been logged.

As a result of advances in sulfur electrode design and container material, cells can now be routinely cycled at ∿ 80% capacity over hundreds of cycles. Also because of improved sulfur container material, the cell resistance increase with cycling is low.

Container Development: The selection of suitable cell container materials is an important part in the successful development of a long-life sodium-sulfur battery. Many low cost materials such as aluminum and low carbon steel appear to be adequate as sodium container material. However, finding a suitable container material for the sulfur compartment has been a difficult problem.

From the results of previous contract periods, the choice for sulfur container had been narrowed down, considering both corrosion resistance and materials cost, to the following candidate materials: stainless steel, aluminum with suitable coating, and low carbon steel with suitable coating. (In addition, earlier work at GE had demonstrated that SiC had

TABLE A.1: PROGRESS IN THE DEVELOPMENT OF Na/S BATTERY:

PERFORMANCE IMPROVEMENTS IN 16 Ah TEST CELLS

Parameter	4/75 Status	4/76 Status	9/77/ Status
Maximum Cycle Life			
- In Test Hours	2,400 @ 54 mA/cm^2 --	5,500 @ 54 mA/cm^2 3,800 @ 108 mA/cm^2	12,000 @ 54 mA/cm^2 11,250 @ 108 mA/cm^2
- In Ah/cm^2(*)	115	337	1135
- In Cycles	250	650	1500
Typical Cycle Life	∿70 Ah/cm^2	∿100 Ah/cm^2	∿400 Ah/cm^2
Ceramic Resistivity	26Ω-cm(β)	22Ω-cm(β)	14Ω-cm(β) 7Ω-cm(β")
Typical Cell Resistance			
- Initial	∿0.30Ω	∿0.25Ω	∿0.15Ω
- End-of-Life	∿0.40Ω	∿0.30Ω	∿0.20Ω
Typical Cell Efficiency	∿60%	∿70%	∿77%
Capacity Utilization			
- Peak	80%	>90%	95%
- "Average"	∿50%	∿60%	∿80%

*This is a common measure for cell "life", for it represents the integrated amount of "electrochemical action" by the cell, inclusive of depth-of-discharge, number of cycles, and test hours. The accomplishments to-date may be compared to the goal for pre-BEST cells: 1780 Ah/cm^2 = 5 yrs x 260 cycles/yr x (7 hrs charge x 0.96 A/cm^2 + 5 hrs discharge x 0.140 A/cm).

outstanding corrosion resistance and excellent electrical conductivity. It was nevertheless excluded from further considerations because of possible cost difficulties.)

Significant conclusions were reached and advances made during the contract period as results of intensive materials investigations:

1. 347 stainless steel, both untreated and treated, forms a corrosion scale which is not stable in the sodium polysulfide melt.

2. Cell tests with aluminide coatings on low carbon steel are not conclusive. While aluminiding offers some improvement in corrosion resistance, the formation of a resistive Fe-Al-S layer is a serious shortcoming.

3. Molybdenum has intrinsic chemical stability and electrical conductivity characteristics which made it an attractive coating material candidate, provided the coating is thin, defect-free and obtained through a low cost process. The same comments apply to chromium except for the cost constraints which are less severe for chromium.

4. Coatings of Mo or Cr onto Al or low carbon steel substrates made by plasma spray techniques are too porous to give long term corrosion protection. A pore-free, diffusion-bonded coating is desirable.

5. Low carbon steel containers with Cr-base coatings made by a proprietary process have performed extremely well in

in-cell tests. The coatings are thin, dense, electrically conductive and chemically stable, and the coating process is amenable to significant cost reduction. Intensive efforts are now underway to optimize the coating properties, predict and validate life limits, and develop low-cost manufacturing processes.

Seal Development: Significant improvements were made during the past year in the development of seals for the sodium-sulfur cell. For the exterior ceramic-metal seal, two solid-state sealing methods were investigated: thermocompression bonding (TCB) and field-assisted bonding (FAB). TCB appears to offer an improved, cost-effective alternative to the mechanical seal so far used in test cells. Helium leak-tight seals are routinely produced between alpha-alumina and aluminum, 347 stainless steel, or chrome-coated mild steel. The nature of the intermetallic phase formed at the seal during the bonding operation determines whether a leak-tight, corrosion-resistant seal is produced. Seal properties were evaluated by CGE, and excellent resistance to thermal cycling and to molten sodium and polysulfides under static and electrochemical conditions was demonstrated. In summary, TCB seals appear to be chemically and thermally stable and have yet to fail in a Na/S cell.

The concept of FAB was successfully reduced to practice. It is now being developed as a back-up alternative to TCB.

The interior ceramic-ceramic seal now utilizes an alumino-borate glass; this proprietory composition 2093 is vastly superior to the silicate glasses used earlier. Sodium resistance has been greatly enhanced and devitrification problems seem to have been eliminated. Cell testing results using this glass are extremely encouraging. Seals were virtually crack-free and without visible Na-attack after 100 days of cycling. None of the 25 or so cells with 2093 glass seals have failed so far (i.e., in $\sim$ 6 months) due to seal failure. Experiments are in progress to establish the life limits for the 2093 glass.

Ceramic Electrolyte Development: At the beginning of this report period, a little over 300 Ah/cm^2 of life testing experience had been logged on our longest lived Na/S cell, one containing a Generation V beta-alumina tube (composition: 8.4% Na_2O, bal. Al_2O_3). This ceramic had excellent physical properties; however, its resistivity at 300°C was $\sim$ 22 ohm-cm.

During this report period, over 1100 Ah/cm^2 of ceramic life has been achieved in metal cells undergoing deep discharges. This has been accomplished with Generation VI beta-alumina ceramic of composition 9.6% Na_2O and 0.25% Li_2O, bal. Al_2O_3, and 16 ohm-cm conductivity at 300°C. The physical properties of the ceramic have been improved to the extent that the average fracture strength in diametral compression tests exceeds 50 Kpsi.

It was found, however, that the goal of a specific resistivity of less than 9 ohm-cm, imposed by the battery system

design, was not likely to be achieved with a beta-alumina ceramic without sacrificing the microstructural quality. Consequently, beta"-alumina ceramics with less than 7.5 ohm-cm resistivities (at 300°C) and without exaggerated grain growth were developed.

In addition to work on ceramic property improvement, alternative ceramic forming methods were evaluated during the report period. Free-flowing beta- and beta"-alumina powders were produced by a spray-drying process developed in-house, and were isostatically-pressed into tubes at 20 Kpsi. Specimens formed this way were sintered to > 99% of theoretical density.

The sintered properties of ware formed by electrophoretic deposition and isostatic pressing have been compared for both beta- and beta"-ceramics. Electrophoretically formed specimens were found to sinter more nearly to full density and at lower sintering temperatures. In addition, the grain size was found to be more uniform with pores of smaller size with this forming technique. The cost of the two forming methods were projected to be nearly the same for large volume production.

At this time both beta- and beta"-alumina tubes of the size required for the BEST cells have been formed satisfactorily by both electrophoretic deposition and isostatic pressing.

Battery System Design: During the report period, the Mark III design was developed. In this design, the building block for

the battery system is a "bundle" of individual cells, each essentially a scaled-up version (300 Wh) of our present test cells (30 Wh). A bundle is designed to consist of a 5 x 8 array of individual cells connected in parallel. Nine of these bundles are connected in series to form a 100 KWh "module", i.e. a thermally self-sufficient unit. Twenty four of these modules are then arranged into 500 V (End-of-Charge)/360 V (Discharge), multi-level sections with 1500 amps rating. Each module is enclosed in a gas-tight steel container under a slight positive pressure of nitrogen gas to permit cooling of a failed module without oxidation of any sodium or sulfur and escape of SO_2 gas or Na_2O smoke. Thermal control is maintained separately in each module by circulating hot nitrogen vertically through the bundles of cells. Circulation is performed within each module with a fan connected with a shaft to a motor placed outside the module. Excess heat is removed by heat exchangers employing a liquid heat transfer fluid. Electric heating elements are provided in the gas stream of each module for initial warm-up and temperature maintenance during long idle periods.

The entire battery is designed to be weatherproof for outdoor installation on a concrete slab. The large size of each bank of batteries reduces insulation cost drastically. The overall footprint for the battery is > 3 KWh/ft^2 because of the modular, multi-level design.

Battery Manufacturing and Cost Studies: During 1976-1977, a group of engineers from GE's Manufacturing Engineering Consulting Services completed a number of manufacturing engineering/cost studies. In this report, two major studies are summarized:

1. Cost Projections for Commercial-Size (20 MW/100 MWh) Batteries.
2. Battery Cost as a Function of Electrolyte Tube Dimensions.

The first study included 1) conceptualization of a battery plant capable of producing 25 battery systems per year, each rated at 20 MW/100 MWh; 2) preliminary estimates of resources needed (investment, materials, labor and space), and 3) projections for the factory cost and the FOB selling price of the battery. The manufacturing conceptualizations and cost estimates were based on EPRI definitions of standard battery, standard production plant, and semi-mature market and technology, and EPRI recommendations on depreciations, taxes, overhead, G&A, ROI, and other cost parameters. For a 5 hr discharge battery, the FOB selling price for the battery was projected by this study to be $\sim$ \$38/KWh. The sensitivity of these estimates to changes in technological or accounting assumptions has not yet been established.

The second study was conducted to determine if the electrolyte tube dimensions chosen for the Mark III battery design are "optimum" from manufacturing cost viewpoints. For the study, eleven different beta"-alumina tube sizes were considered. In one analysis, the diameters were varied from

2.0 to 5.0 cm with tube lengths being 15 times the diameter and wall thickness 0.06 times the diameter. In a second analysis, diameter and thickness were varied the same way but tube length was held constant. It was found that optimum (lowest) manufacturing cost resulted for the electrolyte tube diameter in the 2-3 cm range, with the actual choice depending slightly upon the particular scaling formula used to relate other dimensions to tube diameter.

Supporting Research: Although research was conducted in many areas to support the more development-oriented tasks such as container development or prototype cell evaluation, results of two investigations are summarized in this report for their general appeal:

1. Sulfur Electrode Studies.
2. Real-Time X-Radiography of Na/S Cells.

In the area of sulfur electrode studies, the resistance of various carbon mat arrangements was determined under simulated operating conditions. These independent measurements enabled models to be formulated for total cell resistance and the electrochemical reaction rate distribution within the sulfur electrode. In the former a series resistance approximation for the one phase region led to values which agreed extremely well with the lowest observed cell resistances. The analysis therefore offers a viable means of predicting the minimum attainable resistance. The reaction rate distribution model

indicated that the graded mat resistance design effectively suppressed the formation of sulfur at the beta-alumina interface. This explains the ability of sodium/sulfur cells to consistently cycle into the two phase region.

X-radiography was successfully used during the report period to observe the flow of electrochemically active materials in a Na-S cell as it cycled at operating temperature. Differential and densitometric techniques were applied to detect differences in electrochemical activity at various locations in test cells and to observe composition changes in the extended sulfur electrode.

Scale-Up Activities: Ths sodium-sulfur battery development program at General Electric now stands at a crossroads. The program emphasis is shifting from feasibility demonstration with test cells to detailed design, development and demonstration of battery systems of much larger scales. The program therefore faces the usual but demanding challenges associated with scale-up of laboratory processes and devices. Furthermore, a number of anticipatory actions have now become necessary to lay the groundwork for the BEST battery production program. A number of significant activities were initiated during 1977 on cell size and component production scale-up as well as on safety, manufacturing process development, battery control strategies, failure modes analysis, and similar design and/or cost-related subjects.

List of Tables

Section B
PROGRAM AND REPORT ORGANIZATION

The EPRI Project RP128-4 consists of the following tasks:

1. Prototype Cell Development and Evaluation.
2. BEST Cell Design and Development.
3. BEST Module Design, Engineering and Cost Studies.

In addition, as part of a planned, on-going, in-house program, GE carried out R&D activities in a number of areas. Among them are: ceramic electrolyte development, seal development, sulfur electrode studies, x-radiography of Na/S cells, and container failure mechanisms.

In January 1977, CGE-Marcoussis joined RP128-4 as a subcontractor to GE to carry out investigations in the areas of prototype cell evaluation/development and BEST cell development. Under this subcontract, CGE evaluated the physico-chemical properties of its proprietary coatings for the sulfur container and ceramic-metal and ceramic-ceramic seals. In addition, CGE carried out a parallel program on seal optimization, sulfur electrode studies and other areas.

This report provides detailed accounts of work performed by GE and CGE under the EPRI contract. In addition, summaries of parts of GE-funded in-house investigations are included in this report at GE's discretion. For simplicity, information in the text of this report is not classified according to source; instead, it is segmented into generic areas of R&D. Table L.1 lists the Sections in this report, the tasks they correspond to in the GE-EPRI project, and the sponsors and contractors.

TABLE B.1: PROGRAM AND REPORT ORGANIZATION

Task Under GE-EPRI Program	Section No. in Report	Sponsor	Contractor
Prototype Cell Evaluation and Development	C	EPRI	GE
	D	EPRI	GE
	L	EPRI	CGE
BEST Cell - Multitube Design	K	EPRI	GE
	L	EPRI	CGE
	App. I	EPRI	GE
Module Development	G	EPRI	GE
	H	EPRI	GE
	K	EPRI	GE
	App. II	EPRI	GE
Ceramic Development	F	GE	--
Seal Development	E	GE	--
Fundamental & Applied Research	J	GE	--

List of Tables

PART TWO

GENERAL ELECTRIC COMPANY

PROGRESS REPORT

Section C
PROTOTYPE CELL LIFE AND PERFORMANCE

The prototype laboratory cell evaluation program consists of the following elements:

1. Cell Design
2. Materials and Process Development
3. Component Fabrication and Cell Assembly
4. Cell Testing
5. Post-Test Cell Evaluation

The relationship among the program elements is illustrated in Fig. C.1.

The overall approach for prototype cell evaluation has been to start with small test cells of a design which approaches as closely as possible the smallest individual cell unit of a utility battery system. These cells are then subjected to electrical cycling similar to utility load-leveling use. Starting from this basis, excursions are made in testing parameters which are judged best to pinpoint design and materials limitations.

As before,[1-3] the small test cells fabricated and evaluated in the laboratory are of tubular design with 15-16 Ah capacity (Fig. C.2). Significant design and material

changes were introduced during 1976-77 to improve cell life and performance; some of these modifications and improvements are discussed in this Section.

Most of the test cells were cycled at a constant current of 2A. This corresponded to a current density of 108 mA/cm^2 referred to the geometric surface area of the beta-alumina tube. A few cells underwent cycling at 54 mA/cm^2. Current was automatically reversed when the cell voltage reached 2.8 V at the end of charge or 1.3 V at the end of discharge. For a limited number of cells, a constant current of 2A was maintained for the same preset time during both charge and discharge. Up to 30 test cells could be tested simultaneously and the test data collected in a fully automated facility, designed and constructed for this purpose. The test data were then analyzed through a central computer to provide graphs indicating the state of charge at the end of charge and discharge, the position of the two phase sulfur/polysulfide boundary and the cell resistance at the start and at the middle of the discharge cycle.

C.1. Summary of Test Results

As in previous reports,[1-3] the useful life of a sodium-sulfur cell for the load-leveling application is evaluated in the following three ways:

1. Time to reach uneconomic capacity
2. Time to reach uneconomic resistance
3. Time to abrupt failure

Frequently the failure modes 1 and 2, reflecting a large, unacceptable loss in performance, occur simultaneously. Failure mode 3 is usually caused by internal short circuits arising out of ceramic failure of one kind or another. There are of course additional extrinsic failure modes, such as cycling equipment malfunction, cell/component mishandling, etc.

Table C.1 traces the progress in cell performance and life and the evolution in material, design and fabrication of test cells for the period April 1975 through September 1977. Needless to say, very substantial gains have been made in all areas important to utiltity application: utilization of cell capacity, cell efficiency, and cell life. These gains are discussed in some detail later in this Section.

Table C.2 contains information on observed failure modes and their frequency for two successive periods: May 1975-April 1976 and May 1976-April 1977. To make the comparison meaningful, periods of comparable lengths had to be chosen. For this reason the second period (May 1976-April 1977) does not coincide with the report period (May 1976-August 1977).

It is clear that among the abrupt failure modes, the failure of the alpha-alumina insulating header (see Table C.2) was the more predominant problem during the second period

TABLE C.1: PROGRESS IN THE DEVELOPMENT OF Na/S BATTERY:

PERFORMANCE IMPROVEMENTS IN 16 Ah TEST CELLS

Parameter	4/75 Status	4/76 Status	9/77 Status
Maximum Cycle Life			
- In Test Hours	2,400 @ 54 mA/cm^2 --	5,500 @ 54 mA/cm^2 3,800 @ 108 mA/cm^2	12,000 @ 54 mA/cm^2 11,250 @ 108 mA/cm^2
- In Ah/cm^2(*)	115	337	1135
- In Cycles	250	650	1500
Typical Cycle Life	∿70 Ah/cm^2	∿100 Ah/cm^2	∿400 Ah/cm^2
Ceramic Resistivity	26Ω-cm(β)	22Ω-cm(β)	14Ω-cm(β) 7Ω-cm(β")
Typical Cell Resistance			
- Initial	∿0.30Ω	∿0.25Ω	∿0.15Ω
- End-of-Life	∿0.40Ω	∿0.30Ω	∿0.20Ω
Typical Cell Efficiency	∿60%	∿70%	∿77%
Capacity Utilization			
- Peak	80%	>90%	95%
- "Average"	∿50%	∿60%	∿80%

* This is a common measure for cell "life", for it represents the integrated amount of "electrochemical action" by the cell, inclusive of depth-of-discharge, number of cycles, and test hours. The accomplishments to-date may be compared to the goal for pre-BEST cells: 1780 Ah/cm^2 = 5 yrs x 260 cycles/yr x (7 hrs charge x 0.96 A/cm^2 + 5 hrs discharge x 0.140 A/cm)

TABLE C.2

OBSERVED CELL FAILURE MODES AND FREQUENCY OF OCCURRENCES FOR TWO SUCCESSIVE PERIODS

Period I May 1975 to End of April 1976		Period II May 1976 to End of April 1977	
Total Number of Cells:	125	Total Number of Cells:	101
Number of Failed Cells:	98	Number of Failed Cells:	74
Failure Due To:		Failure Due To:	
Equipment Breakdown:	20	Equipment Breakdown:	5
Handling:	2	Handling:	
Abrupt Failure:		Abrupt Failure:	1
A) Cracked Alpha-Alumina:	4	A) Cracked Alpha-Alumina:	25
B) Cracked Beta-Alumina:	31	B) Cracked Beta-Alumina:	9
C) Seal Failure:	14	C) Seal Failure:	9
D) Combinations of A,B,C:	8	D) Can Failure:	2
Poor Performance: (Capacity Loss and/or Resistance Increase)	19*	Poor Performance: (Capacity Loss and/or Resistance Increase)	23*

* It appears from the data presented that poor performance was responsible for more cell failures (in absolute numbers and in percentage) in 1976-77 than in 1975-76. In reality, it was not the case. A number of experimental containers, coatings were tested during 1976-1977, and were removed as soon as test objectives were met. Poor performance thus had different meanings in the two periods.

whereas the beta-alumina electrolyte was the bigger problem in the first period. The causes behind these have been established and are discussed subsequently in detail. (Losses from equipment breakdown, mainly due to cooling of furnaces resulting from power failures, were reduced in the second period by installing dedicated power lines and automated emergency warning systems in the test facility.) During the second period, seal failures became quite common, and seal development became an important task.

C.2. Improvements in Cell Performance

As indicated in Table C.1, capacity utilization of up to 95% (based on the lower limit of discharge, which is usually near the composition Na_2S_3, as "complete discharge" and pure sulfur as "full charge") are now being obtained for single cycles and over 80% on sustained cycling at a constant current density of 108 mA/cm^2. (It is worth reiterating at this point that all General Electric test experience was gained from fabrication and evaluation of what are commonly called "metal cells".) While peak utilization of material increased from 80% to 90% during the 1975-77 period, typical average (i.e. over $\sim$ 100 cycles) values increased from about 50% to 80%. This is reflected by the data compiled in Table C.3. In many cells it has been possible to sustain high capacity and low resistance to 400 cycles ($\sim$ 400 Ah/cm^2) or more. An example of the performance of such a cell is shown in

Fig. C.3. The upper plot in Fig. C.3 demonstrates the constancy in cell capacity at 108 mA/cm^2, and the lower plot reflects the constancy in cell resistance. The asterisks in the upper plot mark the position of the two-phase sulfur/polysulfide boundary; it barely shifts for the cell under consideration. The cell resistance at the beginning and middle of discharge is shown by the asterisk and the symbol M, respectively, in the lower part of Fig. C.3.

The recent generation of cells has initial resistance values varying between 0.12 and 0.15 ohms. Although these resistance values are lower than the resistance values observed in earlier generation cells,[1-3] the resistance of most cells increases some with cycling and approaches a steady value between 0.17 and 0.20 ohm after 50-100 cycles at 108 mA/cm^2 (Table C.4). The cell capacity at the same time decreases only slightly. The causes for these behaviors are presently under investigation.

It should not be concluded from the scatter in the data presented in Tables C.3 and C.4 that cell-to-cell reproducibility in capacity and resistance has not been achieved. Each of the cells reported in Tables C.3 and C.4 differed from the rest in some material or design aspects. For example, Cell 289 had a pre-oxidized stainless steel sulfur container whereas Cell 303 had a chemically-treated stainless steel can.

TABLE C.3: PERFORMANCE OF PROTOTYPE LABORATORY CELLS:

CHANGE IN CAPACITY WITH CYCLE LIFE

Cell No.	Capacity Utilization			
	5th Cycle	50th Cycle	100th Cycle	300th Cycle
195	73%	73%	77%	75%
287	96	87	77	61
288	80	67	67	60→
289	94	98	88	70
294	95	96	84	45
303	95	96	82	--
306	86	83	84	80
311	91	76	66	57→
314	43	66	66	80→
315	60	97	95	80
318	89	87	89	--
320	95	90	86	67→
328	92	88	79	77→
330	95	95	80	--

Note: The cells reported herein were not identical in constructional features. Almost every cell represents some design/material modification.

(Arrows indicate that the cells are still on test as of Sept. 7, 1977).

TABLE C.4: PERFORMANCE OF PROTOTYPE LABORATORY CELLS:

CHANGE IN RESISTANCE WITH CYCLE LIFE

Cell No.	Cell Resistance			
	5th Cycle	50th Cycle	100th Cycle	300th Cycle
195	0.2 Ω	0.2 Ω	0.2 Ω	0.2 Ω
287	0.19	0.25	0.27	0.29
288	0.18	0.25	0.26	0.24→
289	0.14	0.15	0.18	0.19
294	0.14	0.16	0.18	0.21→
303	0.15	0.19	0.23	--
306	0.15	0.17	0.19	0.22
311	0.18	0.19	0.20	0.27→
314	0.16	0.19	0.19	0.21→
315	0.16	0.18	0.21	0.23
318	0.16	0.17	0.20	--
320	0.13	0.19	0.23	0.26→
328	0.14	0.18	0.20	0.20→
330	0.14	0.16	0.15	--

Note: The cells reported herein were not identical in constructional features. Almost every cell represents some design/material modification.

(Arrows indicate that the cells are still on test as of Sept. 7, 1977).

The improvements in cell capacity and initial cell resistance are attributed to our increased understanding of the factors controlling the sulfur electrode performance and the material and design modifications resulting therefrom.

In the new design/material modification, Thornel MAT Grade VM0032 is uniformly pushed into a cylindrical mould of Teflon. (Previously WDF-grade carbon felt was used; its replacement by the pitch-derived MAT Grade VM0032 represents a significant cost-reduction.) Purified sulfur of a given weight is then poured into the mold. Attention is paid to uniform distribution of sulfur. After cooling, the carbon fiber/sulfur composite "plug" is removed from the mould machined. A longitudinal hole of appropriate diameter is then drilled through the center of the plug.

A high utilization of cell capacity has been achieved in two different ways. In the *first* method, additional small holes (four or five) were drilled in the carbon fiber/sulfur plug. (Figure C.4a) The arrangement of the small holes around the center hole was symmetrical. The space between the plug and the ceramic tube was stuffed with another grade of Thornel MAT. Taken in equal volumes, the latter material possessed a larger electronic resistance than Thornal MAT grade VM0032. The electronic resistance of the carbon fiber matrix increases toward the beta-alumina surface and prevents the preferential formation of sulfur layers close to the beta-alumina tube during charge. Both the holes and the

stuffing in the space between the plug and the beta tube produce the resistance gradient. Experimental verification of the role of the small holes in the plug was obtained by filling them with solid glass rods in some cells. The performance of cells, constructed with the same materials and beta-alumina tubes of equivalent properties, was independent of the presence of glass rods in the small holes. This result represents experimental proof that convection of polysulfide or sulfur in the small holes is not responsible for the better performance of the cells. The latter conclusion is confirmed by the visual observation that sulfur or polysulfide was not discovered inside the small holes of failed cells which had been opened.

The *second* (and the preferred) method is also based on the principle of a resistance gradient. After machining, the carbon fiber plug is split into two halves (Figure C.4b). Two pieces of the MAT with the higher resistance are cut and placed inside the center groove of each of the halves. Then the two halves are placed around the beta-alumina tube and the cell is assembled. The second approach is simpler because it does not require the time-consuming process of drilling additional small holes.

C.3. Improvements in Cell Life

As shown in Table C.2, more cells have been removed from life test for abrupt failure than for performance decay.

As mentioned earlier, there has been a marked change among the abrupt failure modes in the past year. Failures due to cracked alpha-alumina increased greatly in the second period. Since the cracking of the alpha-alumina header becomes apparent only after 1 to 2 months of cycling, it was not realized for some time that certain properties of the new shipments of alpha-alumina discs were different. Sodium was found to penetrate the alpha-alumina and cause cracking. Once the cause of the problem was identified, different types of high purity alpha-alumina underwent accelerated testing to determine susceptibility to sodium attack. The types of alpha-alumina showing negligible attacks by sodium were chosen as header material in the most recent test cells. Failure due to cracking of the alpha-alumina header was reduced significantly.

The number of cell failures due to beta-alumina cracking decreased significantly in recent months. This fact reflects the considerable improvement in the quality of our solid electrolyte. Best results were obtained with tubes of sodium enriched beta-alumina without additive or with 0.25% Li_2O as additive.

As the average life of our test cells improved, it became apparent that the glass seal between alpha-alumina header and beta-alumina tube was slowly attacked by liquid sodium. Sodium penetration led to cracking of the glass seal. To overcome this problem, a new series of sodium resistant glasses was developed and tested for sodium attack in

separate experiments. The most promising of these glasses is being used in the more recent cells.

Penetration of the sulfur container has resulted in failure only in a few cells. Usually in these cases a crack developed in the area directly below the flange. Precautions were taken in the spinning operation of the cans to reduce the thinning of the wall in this critical region.

Data on the cell life are compiled in Table C.5. Only those cells which were cycled as sodium-sulfur cells at either 54 or 108 mA/cm^2 are considered there. In contrast, Table C.2 also contains information on cells cycled at other current densities or as sodium-sodium cells. The data in Table C.5 show that the average cell life, measured in Ah/cm^2, increased markedly in recent years. The better quality of the beta-alumina tubes is largely responsible for this result. The best cell lifes achieved as of September 1977 are: 1135 Ah/cm^2 (Cell 244) at 108 mA/cm^2 and 584 Ah/cm^2 at 54 mA/cm^2 (Cell 162).

The improved design of the sulfur electrode discussed in the preceeding section has allowed us to cycle most of our cells at 108 mA/cm^2 in the recent period.

We believe that the three factors, in addition to improved, electrolyte, which contributed to the extended cell life are:

TABLE C.5: IMPROVEMENT IN CELL LIFE

(Status as of Sept. 6, 1977)

Period	Number of Cells Cycled	Current Density In mA/cm^2	Number of Cells Which Reached					Number of Cells Still Cycling At End of Period
			50 Ah/cm^2	100 Ah/cm^2	200 Ah/cm^2	400 Ah/cm^2	800 Ah/cm^2	
3/9/73 to 3/15/75	104	54	3	0	0	0	0	0
5/1/75 to 4/30/76	71	54	21	4	2	0	0	0
	41	108	16	10	5	0	0	0
5/1/76 to 9/6/77	15	54	11	7	2	2	0	0
	137	108	76	64	31	10	2	28

- Improved uniformity of current distribution at the surface of the beta-alumina tube.
- Lower ceramic surface resistivity.
- Improved uniformity of contact at the carbon fiber/container interface.

Satisfactory current distribution, as well as low surface resistivity, was obtained by improved processing techniques of the beta-alumina tubes. Essentially, the formation of a porous layer, which was responsible for an inhomogeneous current distribution because of regions with different resistivity, was overcome. Improved uniformity of the contact at the carbon fiber/ceramic interface and of the current distribution inside the sulfur electrode was achieved through the changes in the production procedures of the carbon fiber/sulfur plug discussed earlier.

References

1. S.P. Mitoff and J.B. Bush, Jr., Proc. Ninth Inter-Society Energy Conversion Engineering Conf., San Francisco, August 1974, pp. 916-923.

2. M.W. Breiter, et al., Proc. Symp. on Energy Storage, Eds. J.B. Berkowitz and H.P. Silverman, Electrochemical Society, NJ, 1976, pp. 165-178.

3. Development of Sodium-Sulfur Batteries for Utility Application, EPRI Project 128-3 Annual Report (EPRI Report No. EM-266), General Electric Co., Schenectady, NY, December 1976.

List of Figure Captions

List of Tables

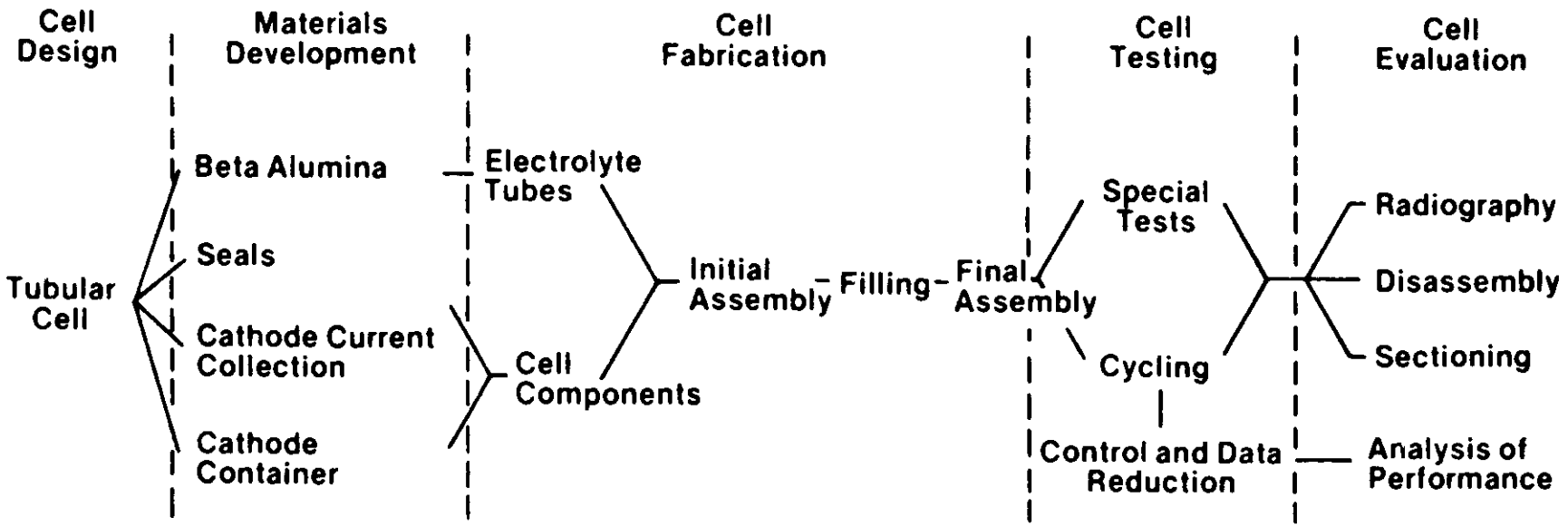

Figure C.1. Relationship Among Program Elements

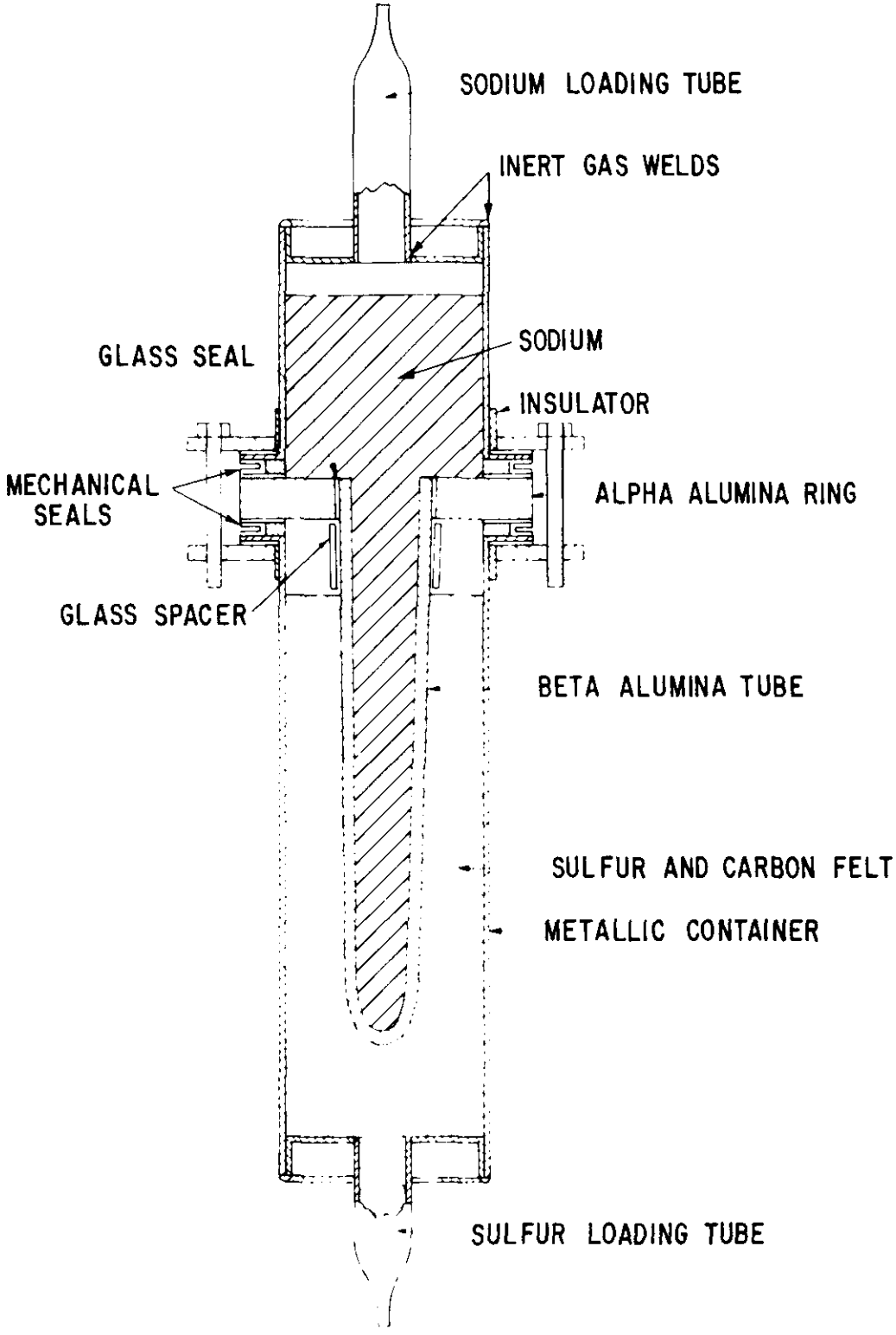

Figure C.2. Test Cell of 15-16Ah Capacity

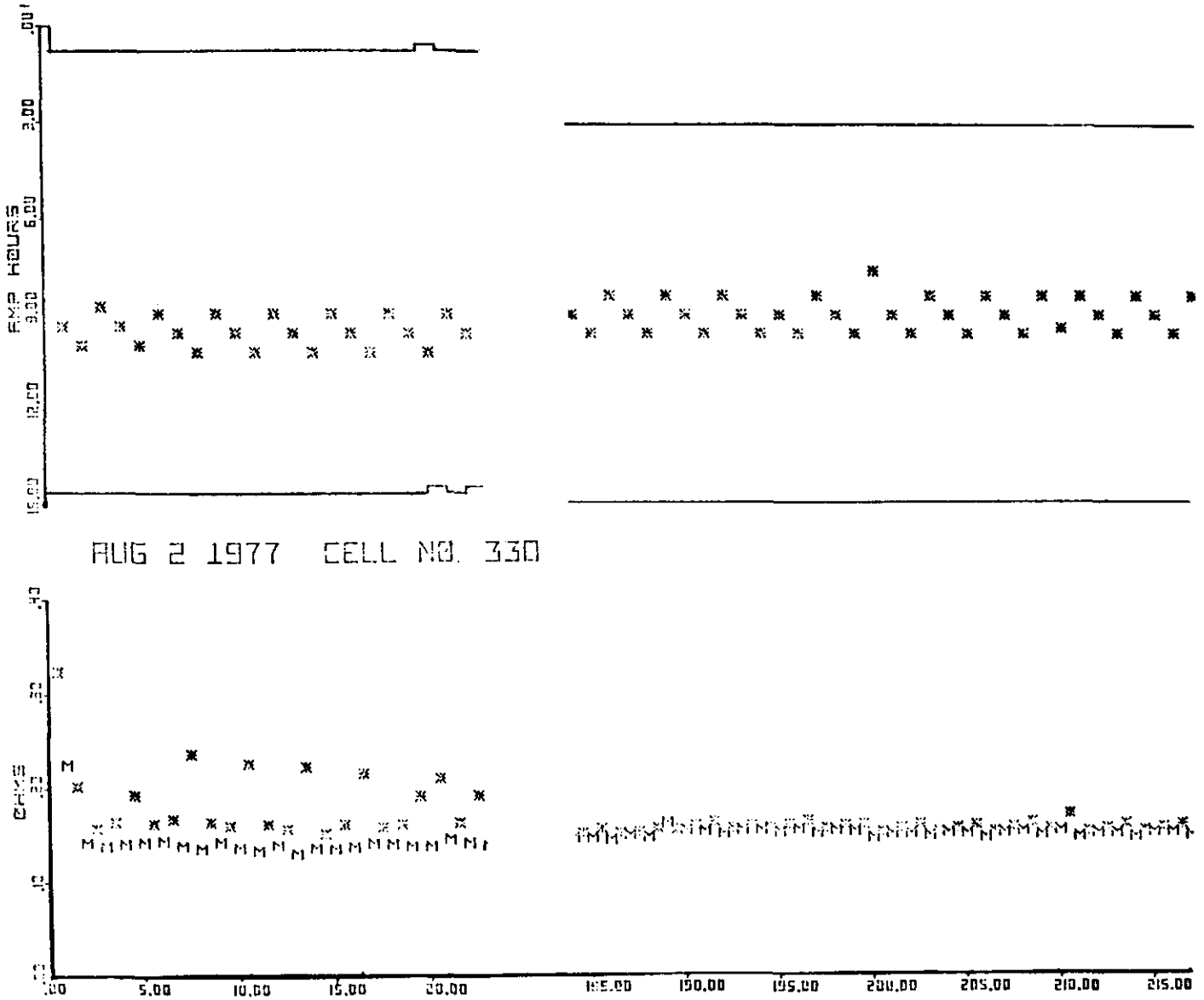

Figure C.3. Performance of Cell With Sustained High Capacity and Low Resistance

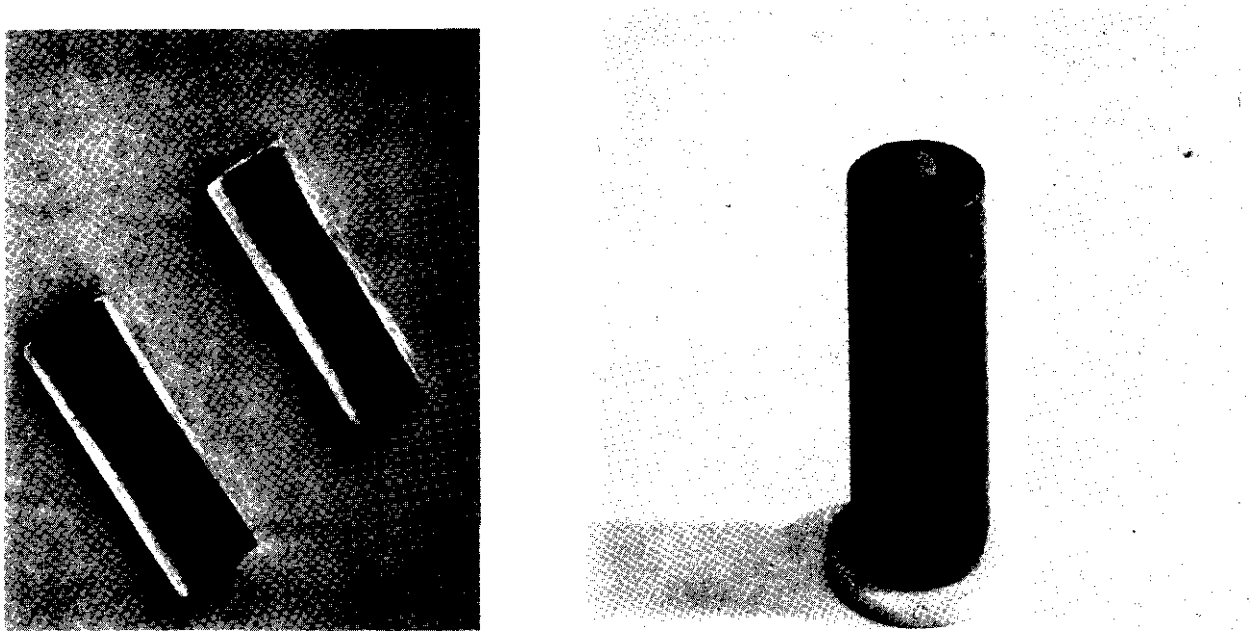

(b) (a)

Figure C.4. Sulfur Plugs, a - With Drilled Holes, b - With Split Configuration

Section D

CONTAINER DEVELOPMENT

The selection of suitable cell container materials is an important part of the successful development of a long life sodium-sulfur battery for load leveling. Many low-cost materials such as aluminum and low carbon steel appear to be adequate for sodium container. However, finding a suitable container material for sulfur compartment has been a difficult problem because of formation of corrosion scales due to the reactive chemical environment. The corrosion products not only cause an increase in cell resistance and a decrease in cell capacity, but also may lead to degradation of beta-alumina as well, thus adversely affecting cell performance.

From the results of previous contract periods, the choice of sulfur container had been narrowed down, considering both the corrosion resistance and cost of the material, to the following candidate materials: stainless steel, aluminum with suitable coating and low carbon steel with suitable coating. Mo and Cr were among the most promising coating materials. (In addition it has been demonstrated[1] that SiC is a very promising material as sulfur container. However, with the manufacturing techniques available presently, SiC appears to be expensive.)

Work during the present contract period was thus aimed at studying the behavior of the metallic container materials cited above and at developing suitable coating techniques. An emphasis was placed on an in-depth study of corrosion behavior of stainless steel with grade 347, which is a stabilized austenitic stainless steel. Preliminary results of cell tests had shown that 347 stainless steel had a reasonably good corrosion resistance, better than most of other materials studied in the previous contract periods. Thus, it was intended to utilize 347 stainless steel as a standard material to extract a maximum information to help formulate guidelines for developing the most suitable container material. On the other hand, aluminum and low carbon steel containers were chosen primarily because of their low cost. Development of suitable coatings and a proper evaluation of them were major concerns with those materials.

Earlier studies of container corrosion behavior at both GE and other places were concentrated on accelerated tests, often carried out in the medium of one specific composition of Na_2S_x, usually Na_2S_4. Such accelerated tests have been very helpful in establishing a certain group of materials as most promising container materials. However, it has been realized that such accelerated tests have some serious limitations. With preliminary information available from the results of previous contract periods, it has been decided that the most helpful and reliable information can be

obtained from actual cell tests. This is particularly true when one realizes that a "trivial" difference in the container and/or melt condition often leads to a substantially different result. Some of the significant discrepancies regarding corrosion resistance of some container materials are likely due to some experimental conditions which were not fully under control.

In the present contract period, the corrosion behavior of container materials was thus studied by post-mortem examination of containers after actual cell tests under cycling conditions. The cell tests were made as described in Section C, and cells were on test up to a period of 17 months. In selective cases, cells were taken out after a predetermined time to examine the corrosion behavior of containers.

A number of different techniques were utilized to study the corrosion behavior: metallographic cross-sectioning, x-ray analysis, chemical analysis, electron microprobe analysis, Auger spectroscopic analysis and scanning electron microscopy.

D.1 General Considerations

Careful experimental examinations of selective materials would be best to correctly assess the suitability of those materials as sulfur container. It is, however, helpful to formulate a set of general guidelines which any candidate container material should meet for the material to offer a long term corrosion protection. Such guidelines are particularly helpful for a proper evaluation of experimental observations which follow in the next section.

From thermodynamic considerations, most of metallic containers are expected to form sulfides in the sulfur/ sodium polysulfide melt. For the container material to offer a long-term corrosion protection, the sulfide scale should meet two major requirements:

1) Chemical and electrochemical stability of the sulfide in the melt. This is the most essential requirement; otherwise, the sulfide will be dissolved out and it cannot form a protective scale onto the container.

2) Slow mass transport in the sulfide. This ensures a slow growth of the sulfide layer. While this kinetic aspect is of importance, it has a true significance only when the first requirement is met.

When a protective material is used as a coating, the following points are of importance, in addition to the above requirements:

3) The coating should be free of pores and cracks.

4) To give an adequate strength, a chemically bonded (cr alloyed) coating is desirable rather than a physical coating.

D.2 Materials Investigation

D.2.1 347 Stainless Steel

Untreated Cans

347 stainless steel is an austenitic stainless steel stabilized with Cb and Ta. A typical analysis of cans used in our Na/S cells is as follows (in weight %):

Ni	Cr	Mn	Si	C	S	P	Mo	Cb/Ta	Fe
11.25	17.80	1.68	0.59	0.06	0.006	0.014	0.03	0.74	balance

347 stainless steel as sulfur containers in laboratory cells has shown in general a pretty good behavior. Its corrosion resistance is better than most of other container materials investigated including those studied in the previous contract periods. Typically, however, cells with 347 stainless steel container have shown a gradual increase in cell resistance and decrease in cell performance. A typical cell would show an increase in cell resistance from 0.12 ohm to about 0.20 ohm in about two months.

One of the most notable characteristics of the corrosion behavior of 347 stainless steel containers is the unpredictability of its corrosion morphology. Post-mortem examinations have shown a number of different corrosion morphologies; quite different morphologies have often been observed even under nominally the same conditions. No clear correlation could be made between the length of time on test and the corrosion morphology or the extent of corrosion. Some containers have shown a relatively small amount of corrosion products even after being on test for several months while others have shown a heavy corrosion product within a short period of time, e.g., one month. These observations indicate that a small difference in some uncontrolled factors can make a substantial change in the corrosion behavior. Those factors can include, among others, moisture content

and presence of chloride ions as contaminant.

In many cases a layer of emulsion-like black/dark brown material, sometimes several mils thick, was observed adjacent to the container. The emulsion-like material could be washed away easily by water, and then the container itself showed a bright metallic sufrace, as can be seen in Figure D.1. After such washing the container surface would show no indication of any graphite fiber contact to the can. This can be compared with the case of Mo containers to be discussed later. Auger analysis shows that there is very little sulfur in the surface layer of the container. This indicates that whatever sulfide layer was formed, it had been dissolved out. In some containers somewhat adherent corrosion scale was observed, as shown in Figure D.2. Even in these cases, however, the scale was not very adherent and would flake off rather easily. In most of 347 stainless steel containers the corrosion morphology showed a mixture of the two cases described above. Table D.1 summarizes the various corrosion morphologies observed with 347 stainless steel containers.

Even though 347 stainless steel containers have shown a number of different corrosion morphologies, x-ray analysis has shown that in all cases the major part of the corrosion product consists of FeS_2 (cubic pyrite). In addition, the corrosion scale has shown a number of minor phases such as NiS_2, Cr_3S_4, $FeCr_2S_4$, Fe_7S_8, $Fe_{1-x}S$, Cr_2S_3, etc. Not all of these, however, appear in one container.

Table D.1

Summary of Corrosion Morphologies of 347 Stainless Steel Containers

Shiny Surface	Almost free of sulfides; a thin oxide layer, rich in CrO_3, on the surface.
Emulsion-like Material	Can be washed out easily by water. Observed in most of containers to a certain amount; a thick layer is accompanied by a bright container surface.
Adherent Corrosion Scale	Not frequently observed. Even when observed, the scale is neither uniform no very adherent.
Pitted	Very localized attack; might have been caused by chloride ions as contaminant.
Mixed	Some parts covered with a corrosion scale, and other parts showing a shiny surface. Most frequently observed.

The emulsion-like corrosion product near the container, which consists of mostly FeS_2, indicates that the sulfide layer formed on the container does not remain stable in the melt. Instead, it is dissolved out and is accumulated near the bottom of the container. The dissolution of corrosion scale is believed to be more active in the lower polysulfide, i.e., near the end of discharge cycle. The extent and rate of dissolution would also depend on other factors such as the amount of minor phases and the different microstructure of the scale, and the condition of the melt. Thus, the corrosion scale ends up showing a variety of different corrosion morphologies.

The emulsion-like material consists of mostly metal sulfides; there is, however, some evidence that it also contains a substantial amount of sulfur. If so, that can be a major factor in cell resistance increase because of the high resistivity of sulfur compared to metal sulfides. This is another deteriorating effect, in addition to a faster rate of sulfide formation, when the sulfide scale is dissolved out. Also, the graphite fiber contact to the container is deteriorated.

From above observations we can see that the corrosion behavior of 347 stainless steel container is primarily a problem of an inadeaquate chemical and electrochemical stability. In other words, 347 stainless steel has an intrinsically unsatisfactory corrosion resistance in the melt even though it is better than most of other materials. To utilize 347 stainless steel as sulfur container for a long

term use, a further treatment will be required which helps form a stable corrosion scale.

Treated Cans

In the first two treatments an attempt was made to form a layer of high Cr_2O_3 layer. Based on information on oxidation and sulfidation rates, it is estimated that the rate controlling mass transport is about four orders of magnitude lower in Cr_2O_3 than in Cr_2S_3 at 700°C. A limited information also indicates that Cr_2O_3 is stable in Na_2S_4. If Cr_2O_3 remains stable during the whole charge/discharge cycle, one can utilize a compact Cr_2O_3 layer on top of the container for corrosion protection, which can cut down the corrosion rate of 347 stainless steel container.

Oxidized Cans: 347 stainless steel containers were oxidized at 960°C for 20 minutes either in air or in oxygen. It is well known that oxidizing stainless steel at an elevated temperature enriches the surface chromium content. The heat-treatment formed an adherent black layer of about 2 μm thickness. (It is to be noted that the layer is black rather than green color of Cr_2O_3). A composition profile of surface layer of Auger analysis confirms the enrichment of chromium in the surface layer as shown in Figure D.3. In addition to Cr_2O_3 as the major component in the surface layer, x-ray analysis has shown other oxides of spinel structure, ($MnFe_2O_4$ and $MnCr_2O_4$) and a small amount of Fe_2O_3.

Cell tests have shown that the above preoxidizing treatment is not very effective for an improvement of corrosion resistance. Both cell performance and corrosion morphology of preoxidized containers are not very different from those of untreated containers. One of the containers, which was on test for 64 days, is shown in Figure D.4. It is to be noted that the original black oxide layer disappeared.

There seem to be two major possibilities for the very limited effectiveness of the treatment:

1. Even though Cr_2O_3 appears stable in Na_2S_4, it may become unstable in a lower sulfide, say Na_2S_3.

2. The amount of Cr_2O_3 in the surface layer was very limited. Therefore, the oxidation treatment did not provide an adequate way of utilizing Cr_2O_3 layer for improvement of corrosion protection.

Passivated Cans: Another way of forming Cr_2O_3 layer on stainless steel is by passivating it in a suitable solution such as nitric acid. While the oxide layer formed by this method is extremely thin, it is more compact than the one formed by high temperature oxidation.

Several 347 stainless steel containers were passivated in 50% HNO_3 or in 50% HNO_3 + 2% HF at 40°C up to a few hours. Figure D.5 shows a profile of chromium and oxygen content in the surface obtained from Auger analysis. As can be seen from the figure the surface chromium content has increased substantially. However, the oxide layer is very thin and the

surface chromium content is still below 50%.

Cell tests have shown that the passivation treatment does not make much improvement in the corrosion behavior of 347 stainless steel containers. Basically the same type of mixed corrosion morphologies as observed with untreated cans have been obtained.

Mechanically Polished Cans: This method of surface treatment is based on the following hypothesis: mechanical polishing just prior to cell assembly induces plastic deformation on the surface, which increases grain boundaries. This is supposed to enhance the preferential migration of chromium along grain boundaries, thus increasing the concentration of Cr_2S_3, which is stable in the corrosive melt.

Cell tests show that the polishing treatment described above has only a limited effectiveness. Cells with polished containers have shown some indication of a better initial performance. However, the overall behavior appears to be about the same. In particular, the same corrosion behavior has been observed.

As seen above the treated containers show a corrosion behavior which is more or less the same as that of untreated cans. In all cases the major part of corrosion product consisted of FeS_2, which does not form a protective layer as described earlier.

In contrast to this, a stable, adherent sulfide layer can be formed if we coat the container with some metallic

element such as Mo or Cr in a suitable way. This has been confirmed in cells having a Cr-coated container which is presently under development: cell tests with these containers have shown a uniform, very thin and adherent Cr_2S_3 layer formed on 347 stainless steel containers.

D.2.2 Molybdenum

Mo was identified in an earlier study[1] as one of the materials which show a good corrosion resistance in the sulfur/sodium polysulfide melt. Laboratory cell tests with Mo container have confirmed the earlier findings. Mo containers have shown a very thin and uniform black corrosion scale. No indication of any dissolved corrosion product was observed. In contrast to the case of 347 stainless steel containers, a number of graphite fibers were seen on the surface of Mo containers after the polysulfides were washed out with water. This is a further indication of the fact that the corrosion product has not been dissolved out to any significant degree, if any at all.

X-ray analysis has identified the corrosion layer as MoS_2. Since Mo forms an adherent sulfide layer in the melt under actual cycling conditions, the kinetic aspect of the sulfide growth becomes more significant than, for example, in the case of 347 stainless steel containers. Metallographic examination of a container, which was on test for 80 days, shows that the sulfide layer is about 1 μm thick. A further experimental study on the growth rate of MoS_2 layer is underway.

From diffusion data, however, a reasonable estimate can be made in the following way. In MoS_2, it is known that diffusivities of both sulfur and Mo are comparable and have a similar activation energy[3]. An extrapolation of available high temperature data on diffusion coefficients in MoS_2 gives an estimate of $D \sim 10^{-15} - 10^{-18}$ cm^2/sec at 350°C. The thickness of the sulfide layer X can be calculated approximately from

$$X \simeq (4Dt)^{1/2}$$

where t represents time. If we take $D = 10^{-16}$ cm^2/sec, then the following estimate on the thickness of MoS_2 layer is obtained:

time	one month	one year	ten years
X(μm)	0.32	1.12	3.53

Thus, from both thermodynamic stability and kinetic viewpoints it appears that Mo can offer a good corrosion protection for a period of many years without forming a thick sulfide layer.

There are, however, two aspects which deserve a careful attention. The first relates to the cost of the material. A solid Mo container is prohibitively expensive to be considered as a practical container material. An estimate shows that even a thin foil of 2 mil thickness will cost over $6.00 per container of BEST cell. This means that Mo can be attractive only when a thin coating can be applied inexpensively

onto some low-cost container material such as low carbon steels. The second aspect concerns with the high polarization observed in cells with Mo container. This in itself is not a corrosion problem, but it is an important concern where the container has a dual purpose of container and current collector.

D.2.3 Coated Aluminum

Aluminum forms a sulfide layer (Al_2S_3), which has a high electrical resistivity. To minimize the effect of such a resistive sulfide layer, two types of protective coatings have been tried: Cr-coating and Mo-coating, both made by plasma spray to a thickness of about 5 mils.

In both types of coating, a relatively heavy subscale has been observed underneath the coating. The scale caused the coating to separate from the can as can be seen from the container shown in Figure D.6. The container was coated with Mo and was on test for 81 days. All aluminum containers with Mo or Cr-coating showed a similar corrosion behavior.

The improvement of corrosion protection of Al containers by plasma spray coating of Mo or Cr thus appears to be very limited. The main reasons for the only marginal improvement of cans with such coatings can be twofold: firstly, the coatings made by plasma spray were too porous; secondly, the coatings were made as a physical coating without forming a diffusion bonding to the container. Thus, once the subscale is formed by the polysulfide melt creeped through pores, the coating appears to be peeled off easily. These observations

confirm the belief that for a long-term corrosion protection the coating should be free of pores, and that an alloyed (or diffusion bonded) coating is desirable.

D.2.4 Coated Low Carbon Steel

Low carbon steel containers are badly attacked by the sulfur/polysulfide melt. To protect the steel container, Cr-coating was applied by plasma spray to a thickness of about 5 mils. While the coating made a definite improvement in corrosion resistance, it was only for a short period of time of usually less than a month. Post-mortem examinations have shown that the coating had peeled off from the steel container as in the case of coated Al. The reasons for poor corrosion protection and possible remedies would be the same as those discussed with Al container.

Another coating of a different nature has been tried onto low carbon steel containers: the containers were pack-aluminided at an elevated temperature to form an Al-Fe alloy on the surface. Aluminiding is a well known process and has been used in industry to improve oxidation/sulfidation resistance of steels and many superalloys. The steel containers used in cell tests were pack-aluminided at 1060°C for 3 hours. It resulted in a surface Al concentration of 8-10%, which decreases gradually over a thickness of about 150 μm. It is to be noted that unlike coatings made by plasma spray, the aluminiding offers a layer of alloyed "coating".

Cell test results of aluminided steel containers have shown a substantial improvement in corrosion protection over

uncoated steel containers. However, corrosion scale was still quite heavy, and not adherent. Probably a more significant aspect of cells with aluminided steel containers is a higher cell resistance than observed with other cells. This aspect appears to be common to cells with aluminum containers and aluminided steel containers. It is most likely that the high resistance is related to the resistive Al_2S_3 layer. By selecting a right composition of Al in the surface layer of steel container, it may be possible to have a satisfactory corrosion resistance while avoiding the troublesome aspect of the resistive layer. From a practical viewpoint, however, this appears to be too delicate to be fully relied upon. A further study is being made.

D.3 Work in Progress

Presently Cr-rich coatings on low carbon steel are being developed as the most viable sulfur container. The Cr-coatings are made as pore-free, diffusion-bonded coatings; they have shown very promising results in cell tests both in the corrosion resistance and the cell performance. It has been observed that sulfur containers with the coatings form a stable corrosion scale under actual cycling conditions: The corrosion layer is very thin, uniform and remains adherent to the container, thus forming a protective scale. Typically, about one micron thick scale has been observed after cell test for 3 months. Another important characteristic in the corrosion behavior

of the Cr-coated steel container is the good reproducibility of the corrosion morphology. All of these characteristics are in contrast to the corrosion behavior of 347 stainless steel containers, which form non-adherent corrosion scales with a number of different corrosion morphologies.

Laboratory cells with Cr-coated steel containers have shown a very good cell performance characterized by good charge/discharge characteristics and a very stable cell capacity. The cell resistance has also shown a slower and smaller increase than in cells with 347 stainless steel container (It is to be remembered that the increase in cell resistance can be due to other factors such as degradation of β-alumina and of sulfur electrode as well as due to the formation of corrosion scale). The excellent cell performance can be clearly seen in the following examples. In all cells described below the container was Cr-coated but three different modifications in coating techniques were utilized.

Figure D.7 shows the cycling result of Cell #330, which was on test for 134 days. As can be clearly seen in the figure, both the cell capacity and cell resistance remained very stable until it failed, which was due to the glass-seal failure. The cycling data of another cell with a similar coating condition of container is shown in Figure D.8. The cell has been on test for 4 months, and a very good cell performance can be clearly seen. Figure D.9 illustrates the cell performance of Cell #360, which has been on test for 4 months; the container of the cell was Cr-coated by a somewhat different method

from that of the previous two containers. Here again an excellent cell performance has been observed. Figure D.10 shows the cycling result of cell #357; the container of the cell was Cr-coated by a third method. The cell has been on test for over 4 months and a remarkably stable cell performance has been observed.

It is clear from the cell performance data exemplified above that the Cr-rich coatings on carbon steel do offer an excellent corrosion protection of sulfur container as well as good charge/discharge characteristics (It is to be noted that Mo container has a good corrosion resistance, but shows a less-than-satisfactory cell performance). This is further substantiated by additional experimental results with 347 stainless steel: when Cr-coated, 347 stainless steel formed a thin, adherent corrosion scale and a much better cycling result as observed with Cr-coated carbon steel containers. These observations leave us little doubt that the Cr-coated containers offer the best practical sulfur containers so far developed by us and also by other groups as far as we are aware of.

Presently, efforts are being made with the Cr-coated steel containers with an emphasis on the following aspects:

1) An in-depth study on the long-term corrosion protection by studying the kinetic growth of the corrosion scale, which in turn determines the required coating thickness.

2. Improvement in coating techniques to have uniform

defect-free coatings.

3. A careful study to monitor even a minute and slow dissolution of corrosion scale, if there is any. Efforts to further enhance the stability of the corrosion scale by introducing small modifications into the Cr-rich coatings.

4. A comparative evaluation and development of Cr-coating techniques which can offer the best method from viewpoints of both cost and corrosion protection.

D.4 Summary

1. 347 stainless steel, both untreated and treated, forms a corrosion scale which is not stable in the melt.

2. Mo has a good corrosion resistance, which appears to be able to offer a corrosion protection for a 10-year period without problem. However, the high cost of the material will have to be overcome by some suitable coating technique. The high polarization observed with Mo containers is a problematic area.

3. Coatings of Mo or Cr onto Al or low carbon steel made by plasma spray are too porous to give a long-term corrosion protection. A pore-free, diffusion-bonded coating is desirable.

4. Results on aluminided steel are not conclusive; while aluminiding offers some improvement in corrosion resistance, the formation of a resistive layer is a serious

shortcoming.

5. Low carbon steel containers with Cr-rich coatings form a thin, stable corrosion scale under actual cell cycling conditions. They have shown very promising cell performance and are believed to be able to offer the long-term corrosion protection required in sodium-sulfur batteries. An in-depth study is being made to further characterize and to optimize the coatings.

References

1. Development of Sodium-Sulfur Batteries for Utility Application, GE-EPRI Annual Report, December 1976.

2. See for example, R. Bauer, W. Fisher, W. Haar, H. Kleinschmager, R. Langpape and G. Weddigen, Intersociety Energy Conversion and Engineering Conference, Stateline, Nevada, September 1976.

3. M. S. Koval'chenko, V. V. Sychev, D. Z. Yurchenko and Yu G. Takachenko, Russian Metal. 5, 180 (1974).

Figure Captions

Figure D.1 Corrosion morphology of a 347 stainless steel container after cell test for one year and 142 days. The shiny metallic surface appeared when the black corrosion product, shown in the bottom piece, was washed out.

Figure D.2 Corrosion morphology of a 347 stainless steel container after cell test for 148 days; the corrosion scale is somewhat adherent, but not uniform.

Figure D.3 Concentration of metallic elements in the oxide layer of 347 stainless steel.

Figure D.4 Corrosion morphology of a 347 stainless steel container after cell test for 64 days. The container was preoxidized at 960°C for 20 minutes.

Figure D.5 Profile of Cr and oxygen concentrations in the surface layer of 347 stainless steel samples. Cell #195 was on test for 134 days and the container showed a bright metallic surface.

Figure D.6 Corrosion morphology of an Al container coated with Mo by plasma spray after cell test for 81 days.

Figure D.7 Cycling record of Cell #330; the cell had a Cr-coated steel container and was on test for 134 days.

Figure D.8 Cycling record of Cell #359; the cell has a Cr-coated steel container and has been on test for 4 months.

Figure D.9 Cycling of Cell #360; the cell has a Cr-coated steel container and has been on test for 4 months.

Figure D.10 Cycling record of Cell #357; the cell has a Cr-coated steel container and has been on test for over 4 months.

List of Tables

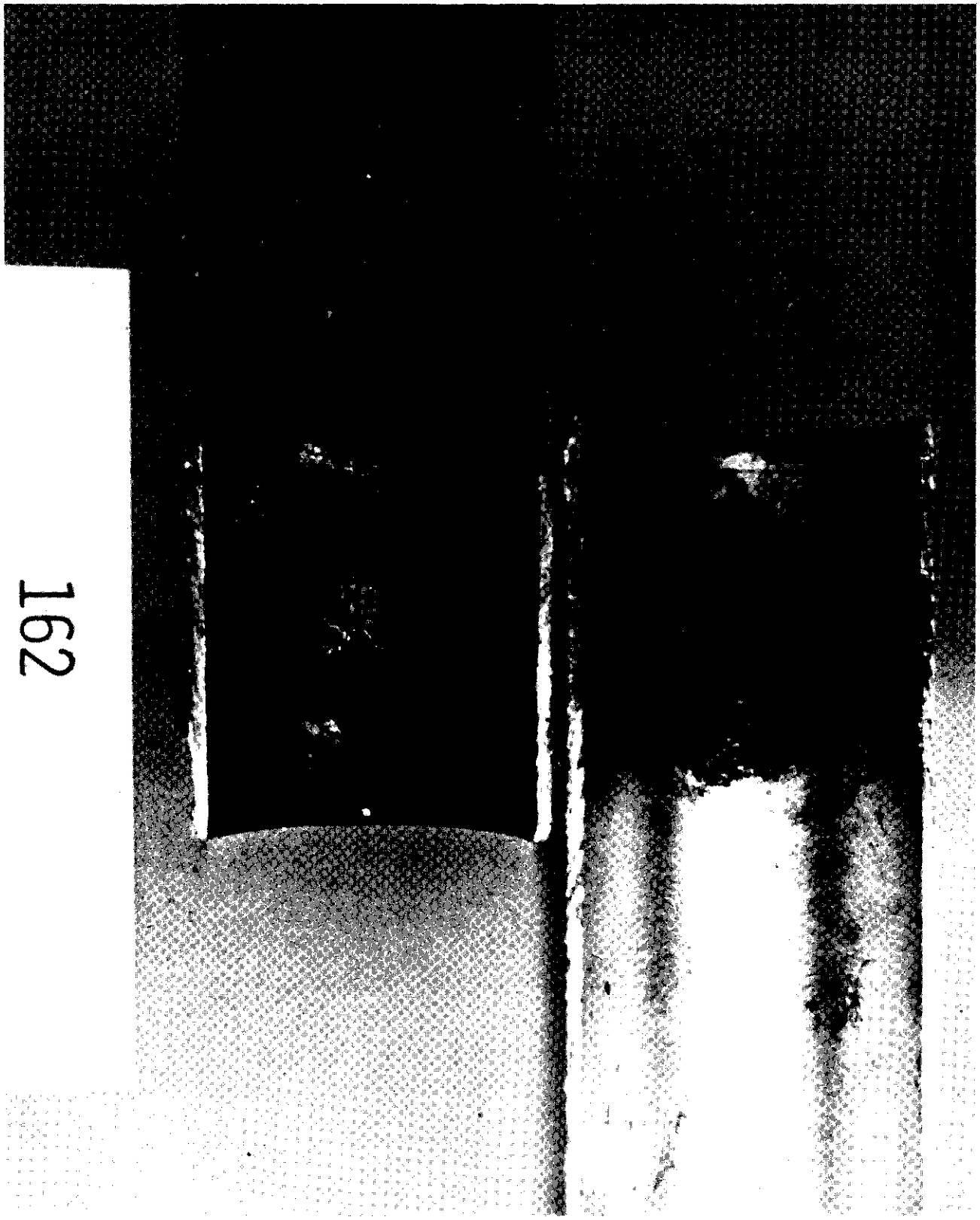

Figure D.1. Corrosion Morphology of a 347 Stainless Steel Container After Cell Test for One Year and 142 Days. The shiny metallic surface appeared when the black corrosion product, shown in the bottom piece, was washed out.

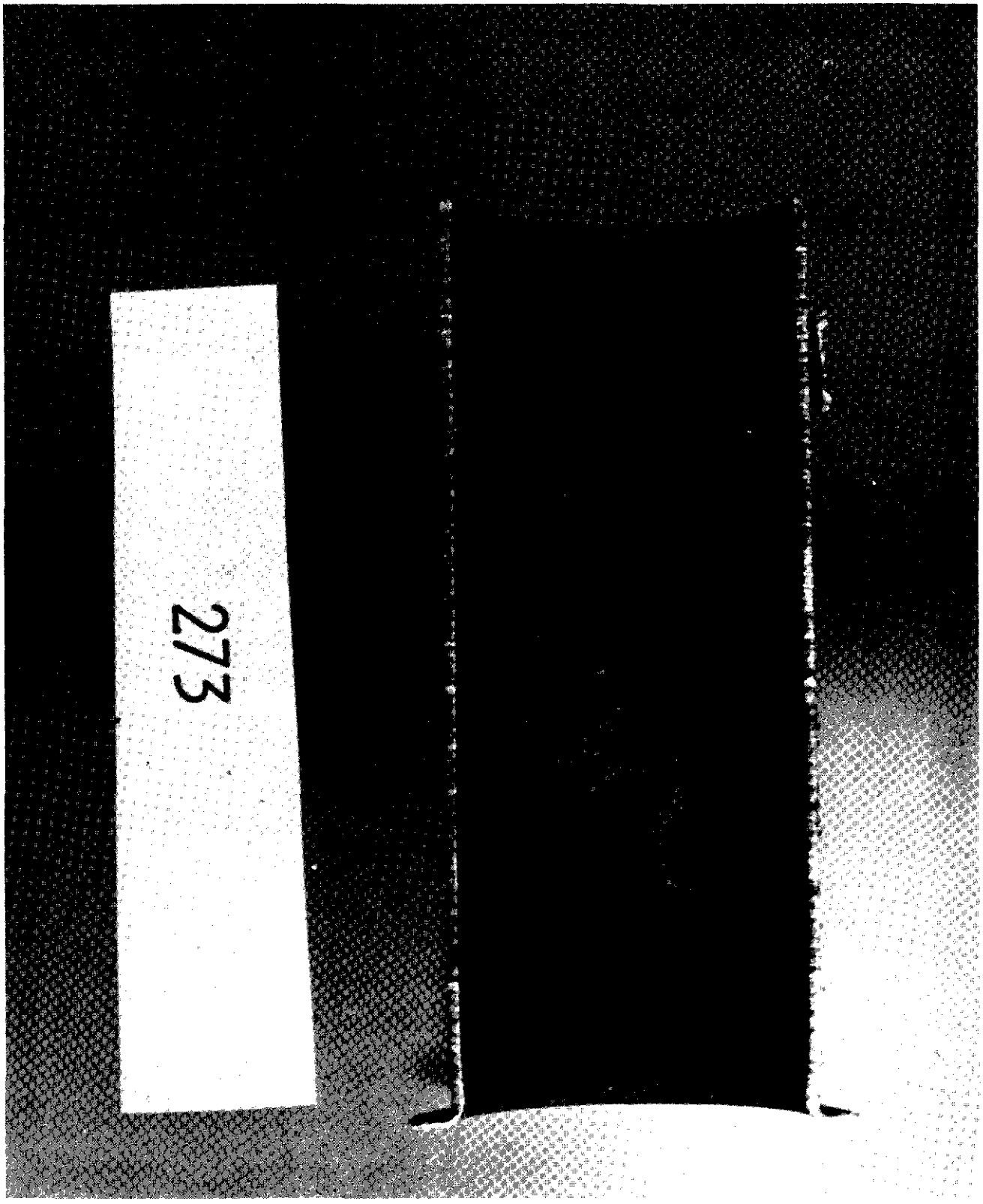

Figure D.2. Corrosion Morphology of a 347 Stainless Steel Container After Cell Test for 148 Days; the Corrosion Scale is Somewhat Adherent, but Not Uniform

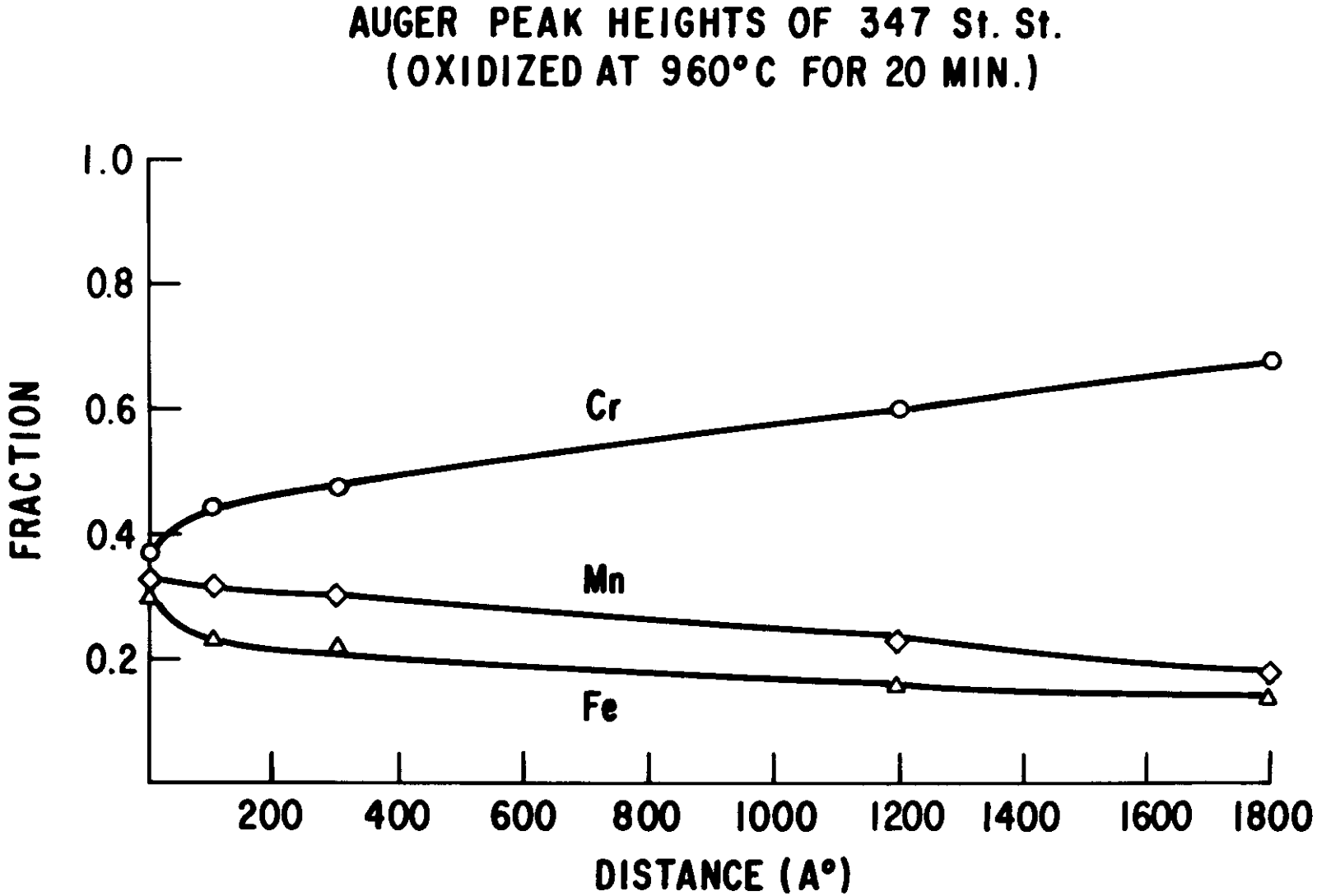

Figure D.3. Concentration of Metallic Elements in the Oxide Layer of 347 Stainless Steel

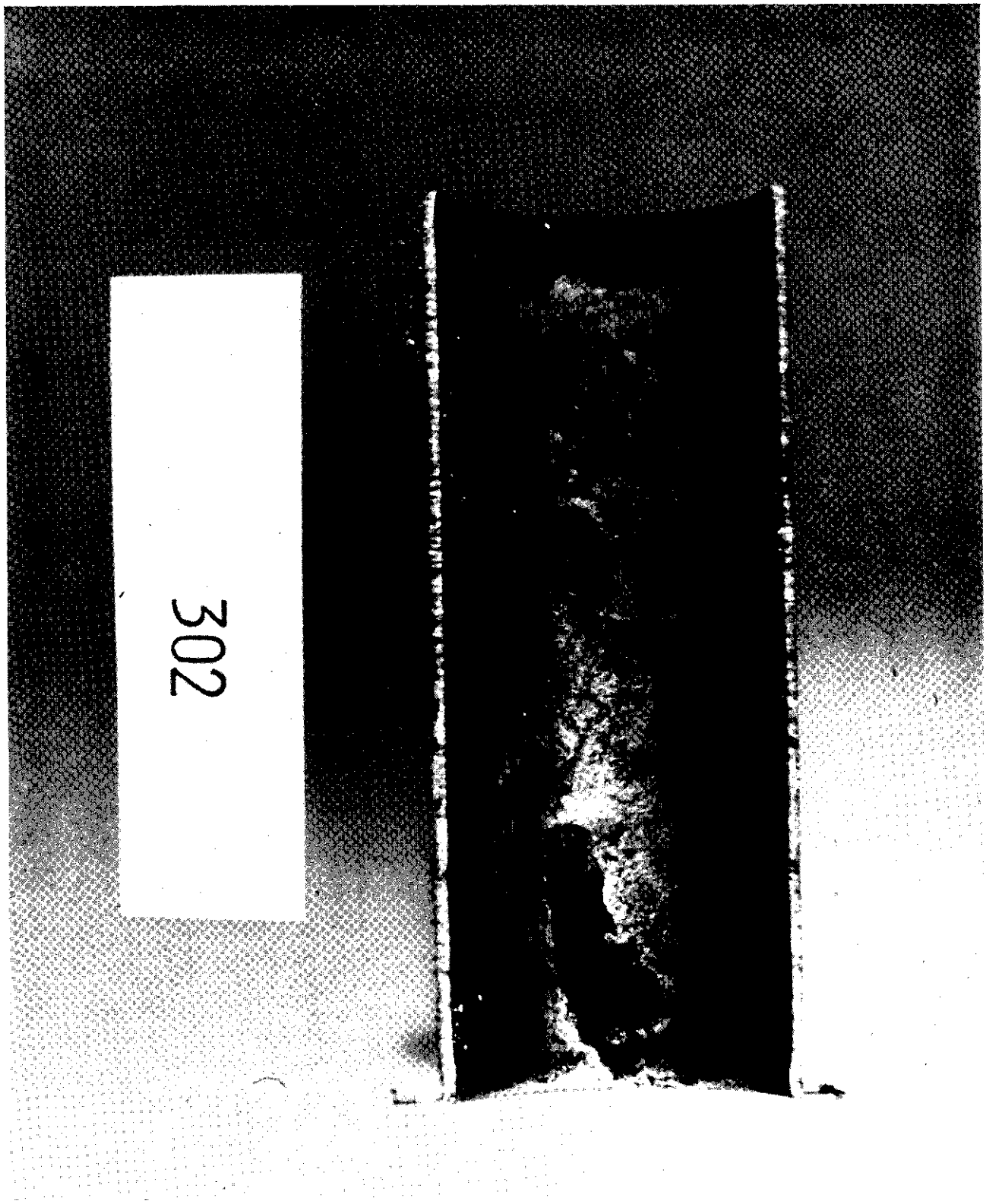

Figure D.4. Corrosion Morphology of a 347 Stainless Steel Container After Cell Test for 64 Days. The container was pre-oxidized at 960°C for 20 minutes.

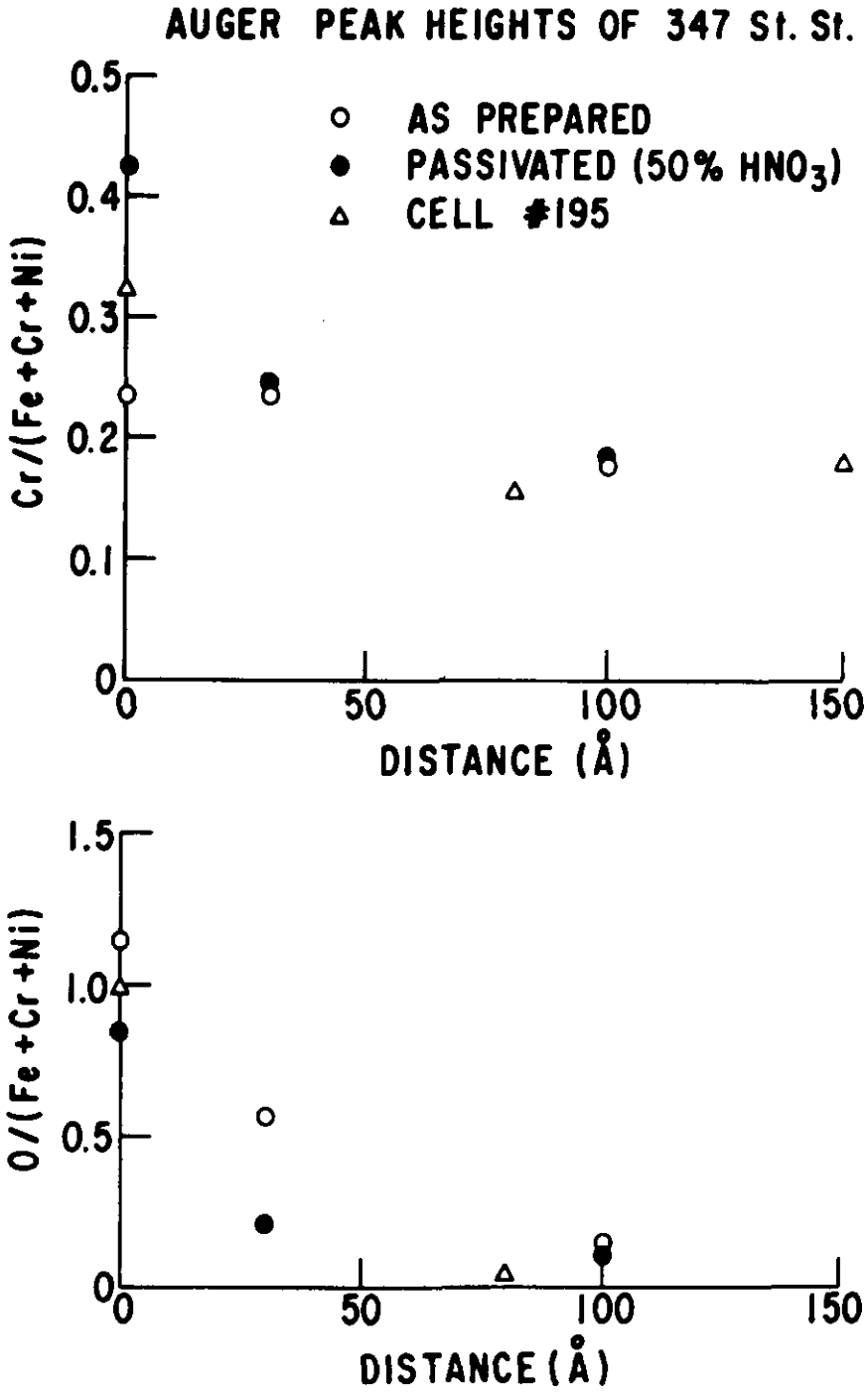

Figure D.5. Profile of Cr and Oxygen Concentrations in the Surface Layer of 347 Stainless Steel Samples. Cell #195 was on test for 134 days and the container showed a bright metallic surface.

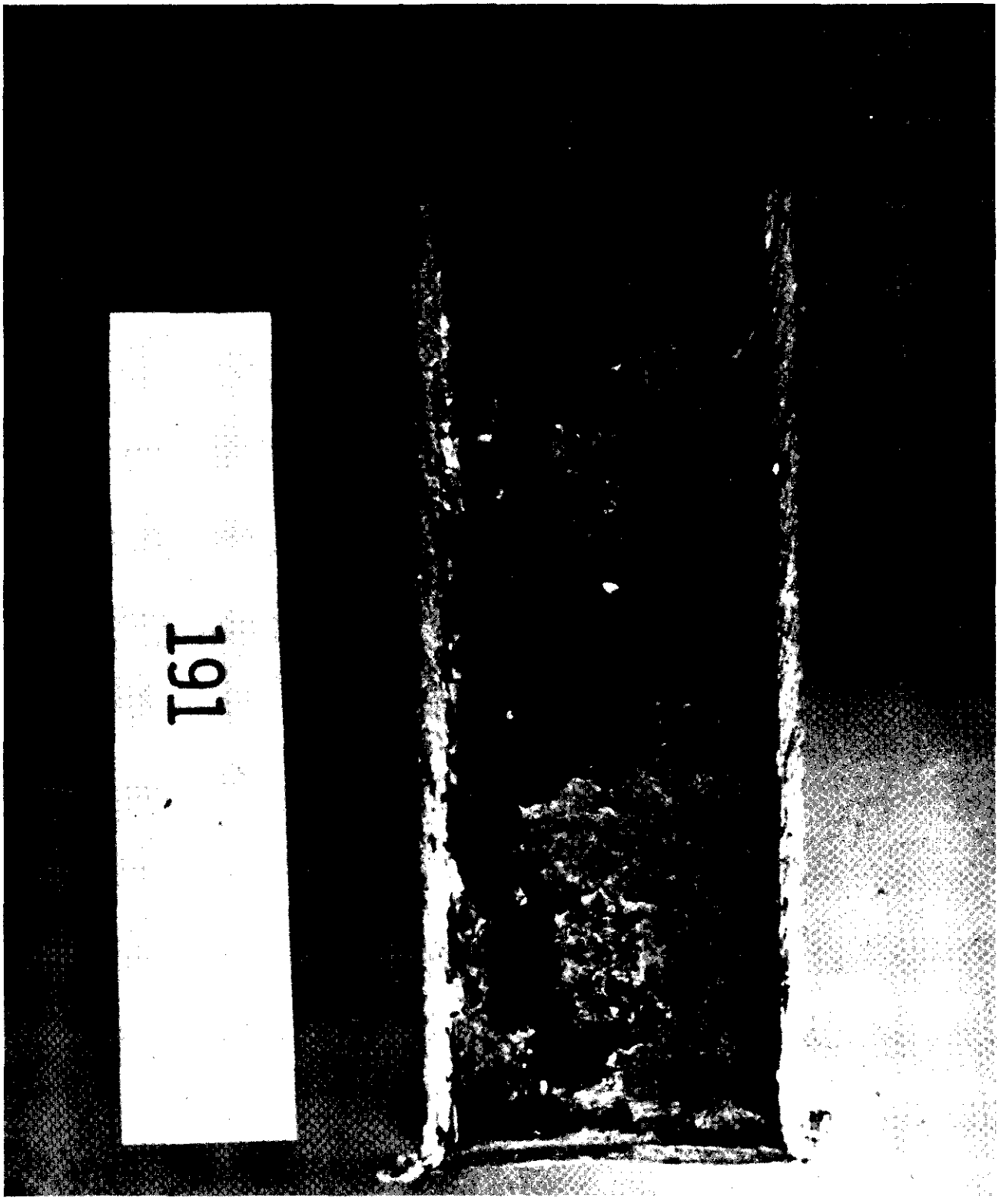

Figure D.6. Corrosion Morphology of an Al Container Coated with Mo by Plasma Spray After Cell Test for 81 Days

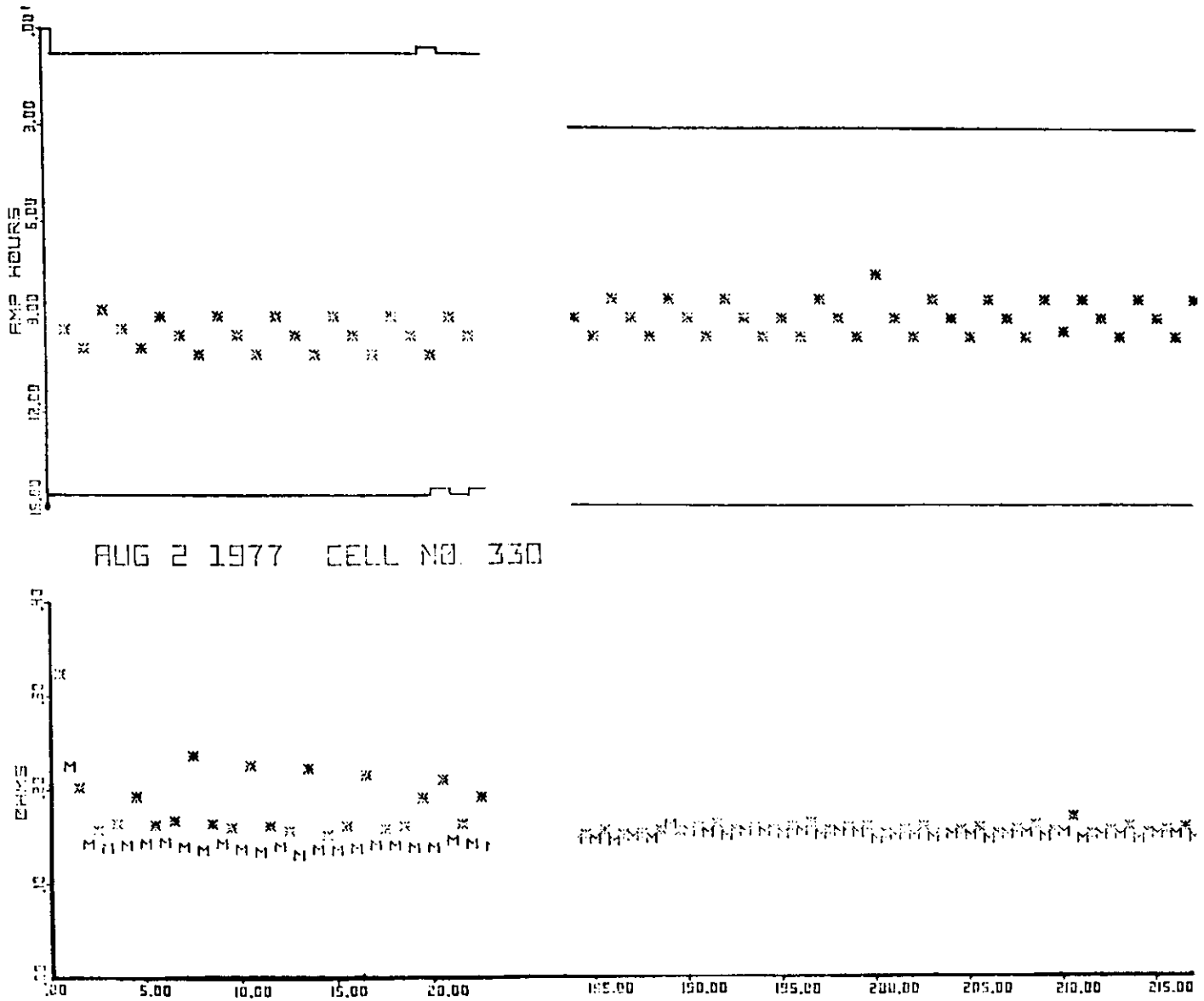

Figure D.7. Cycling Record of Cell #330; the Cell has a Cr-coated Steel Container and was on Test for 134 Days

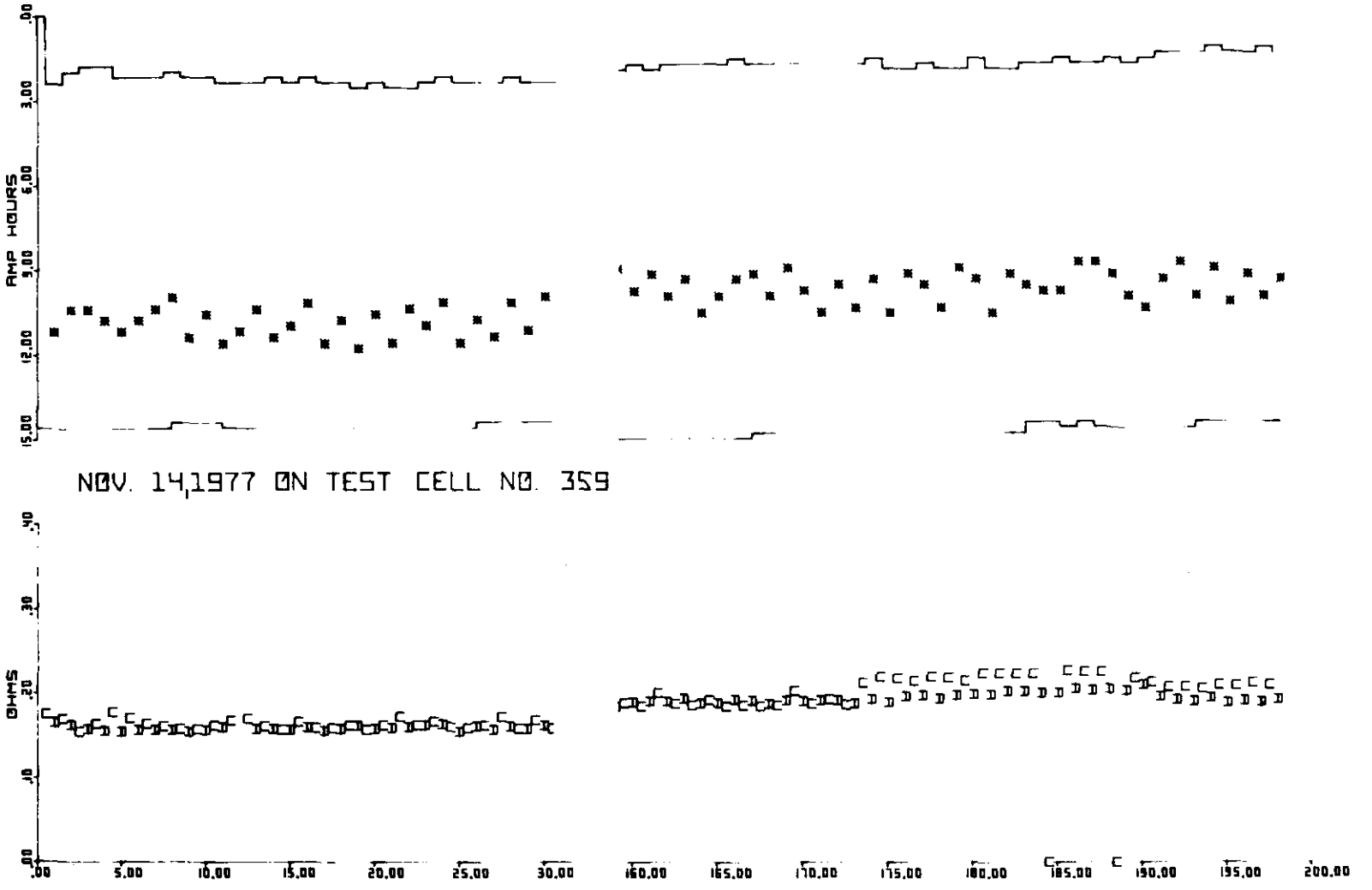

Figure D.8. Cycling Record of Cell #359; the Cell Has a Cr-coated Steel Container and Has Been on Test for 4 Months

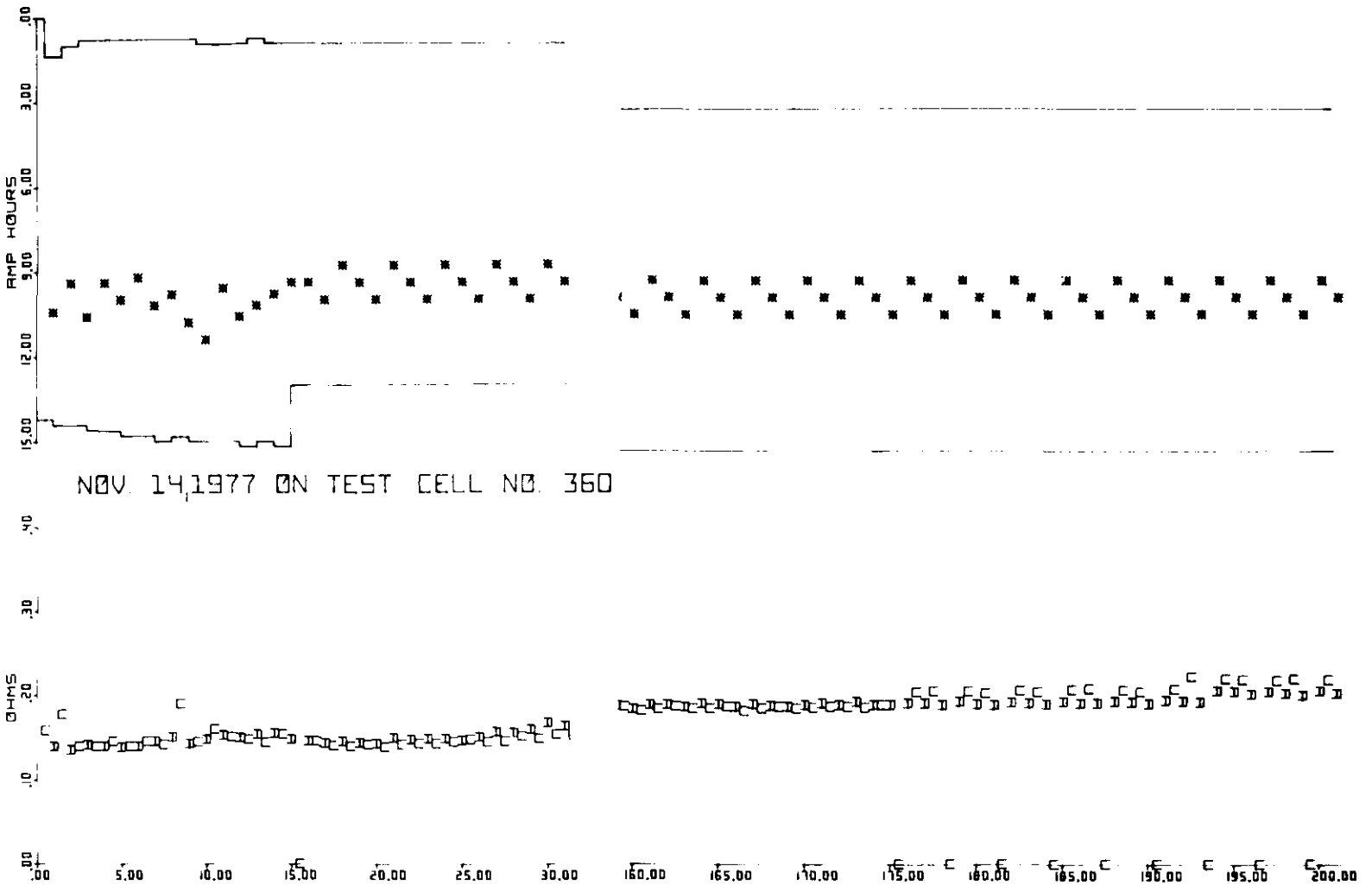

Figure D.9. Cycling of Cell #360; the Cell Has a Cr-coated Steel Container and Has Been on Test for 4 Months

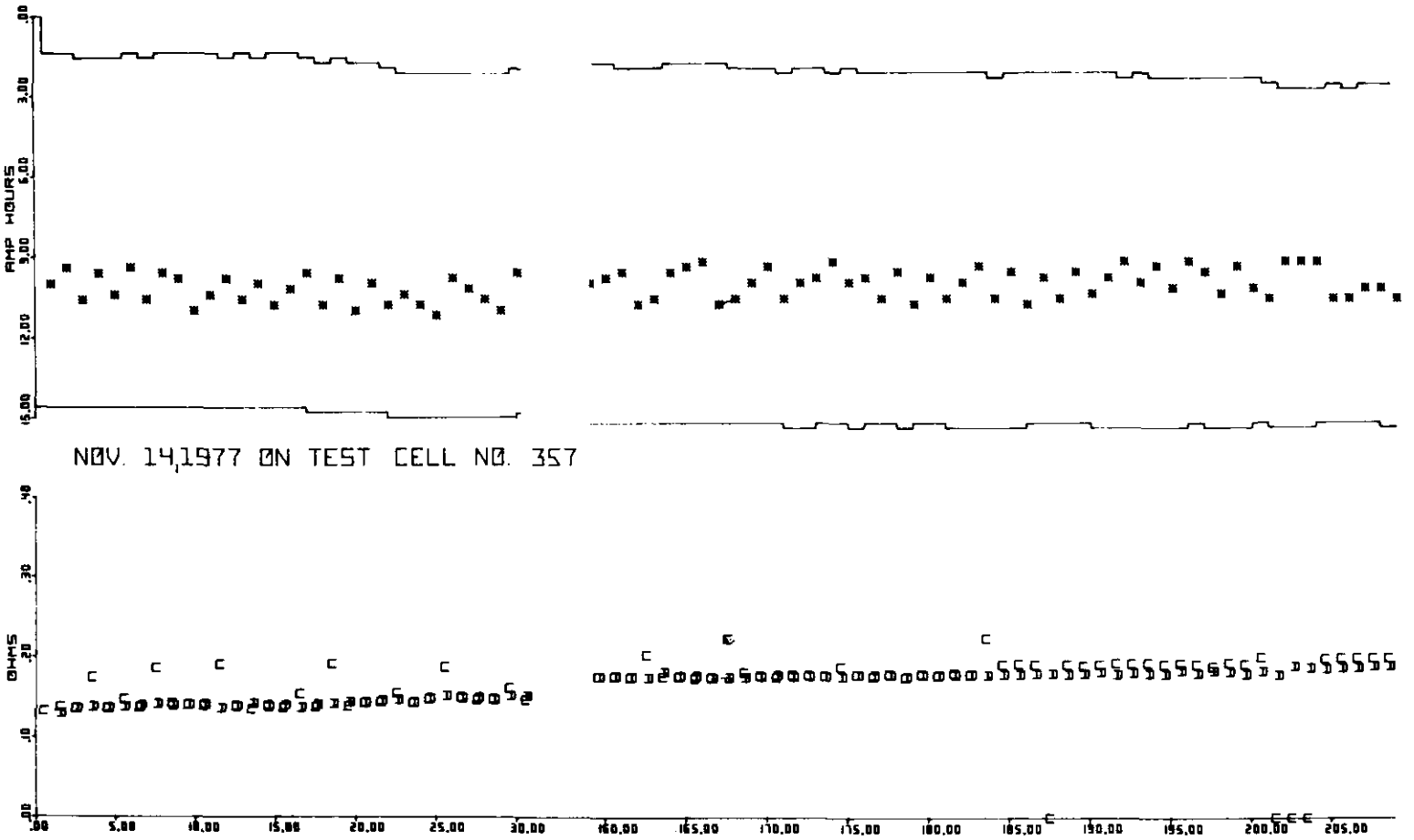

Figure D.10. Cycling Record of Cell #357; the Cell Has a Cr-coated Steel Container and Has Been on Test for Over 4 Months

Section E
SEAL DEVELOPMENT

The seal system in the sodium/sulfur cell consists of a) an outer ceramic metal seal between the metal container and alpha alumina insulator and b) an inner ceramic-ceramic seal between the beta-alumina electrolyte and alpha alumina insulator. The former must provide at least two functions: (1) to hermetically enclose each of the reactant chambers and (2) to electrically isolate the two reactant containers. The mechanical seals presently used in prototype cells are acceptable; however, their long term stability is somewhat suspect. Furthermore, these designs are likely to be expensive for a commercial sodium-sulfur cell.

In the ceramic-ceramic seals, the sealing glasses previously employed were often responsible for limiting cell life. Thermal expansion mismatch and susceptibility to chemical attack led to crack initiation and ultimately, failure of the seal area. During the past year rapid progress was made on both seal topics. Alternative ceramic-metal bonding schemes were developed and improvements in glass composition drastically reduced this mode of failure. The methods and results are reviewed in this section.

E.1 Ceramic-Metal Seals

The solid-state bonding methods for producing ceramic-metal seals appear to offer cost effectiveness as well as superior properties. Their fabrication processes are compatible with battery assembly procedures. Two solid-state techniques are described in this section. In one case a direct bond is made between metal and ceramic, deformation of the metal being instrumental in developing the bond. The other technique depends upon the ionic conductivity of the ceramic.

E.1.1 Thermocompression Bonding

The direct seals require that the ceramic and metal parts be pressed together at elevated temperatures, hence the name thermocompression bonding (TCB). The method has been extensively investigated by researchers at the Compagnie Generale d'Electricite (CGE).[1] A subcontract between GE and CGE has continued the support of this work in several specific areas (see Part II). The transfer of this technology to GE and its subsequent development are discussed below.

Procedures

TCB is essentially a hot pressing technique where an aluminum washer is placed between the flange of the metal container and the ceramic. Plastic deformation of the aluminum plays a major role in establishing the ceramic-

metal bond. The alpha-alumina ceramic is 99.7% pure and is used in either the as-fired state or polished to a 10 micron diamond finish. Components are cleaned in freon prior to sealing.

Results and Discussion

Helium leak-tight seals are routinely obtained with aluminum, stainless steel or Cr-coated mild steel containers. A summary of materials, conditions and geometries for which hermetic seals were made are listed in Table E.1. An outward flange refers to the flange design applied in prototype cells. The two-sided configuration involves the simultaneous bonding of sodium and sulfur compartments. Reproduceability of the TCB method is illustrated in Fig. E.1. Most of the failures were incurred at the inception of the testing program. The use of alpha-alumina with as-fired surfaces does not affect seal hermiticity.

There are two interfaces to consider in the system described in Table E.1; the aluminum/alpha-alumina interface and the container/aluminum interface. The former represents a ceramic-metal bond generally overlooked in the literature because of the large disparity in thermal expansion coefficients and inability of aluminum to resist temperatures greater than 750°C. Nonetheless, strong and leak-tight bonds are achieved. A microstructure of this interface (Fig. 2) indicates that the aluminum deforms and follows the contour

Table E.1

SUMMARY OF THERMOCOMPRESSION BONDING RESULTS

	Containers	Ceramic Surface
Materials	Aluminum 347 Stainless Steel Chromized Mild Steel	Polished (10 micron finish) As-fired
Geometries	• Outward flange • Two sides bonded simultaneously • Inward flange	

of the ceramic extremely well. No interfacial reaction is evident and an analysis of this region by several techniques suggests that no chemical reaction occurs at distances more than 50 A away from the interface.[2,3]

In contrast to the ceramic-metal bond, the container/aluminum boundary is critically dependent upon the nature of the reaction layer formed. A coherent interface is produced when chromized mild steel or 347 stainless steel (Fig. 3) contact aluminum. The intermetallic is somewhat ductile and capable of withstanding strains developed from lattice and thermal expansion mismatches. Porosity is present but it is not interconnected. The mild steel/aluminum boundary is characterized by excessive interfacial porosity. This effect apparently prevents leak-tight seals from being made. When an aluminum container is used, it is virtually welded to the washer. There are hardly any vestiges of a boundary existing between the two components.

Properties of TCB seals were evaluated as part of the CGE seal program. The results (see Part II for additional detail) are extremely impressive; seals are routinely cycled (10 or more times) to 400°C, there is no evidence of chemical attack by molten sodium in 5000 hrs, and the seals are stable under cycling conditions. A cell with TCB seals

has been on test for over 5500 hours and CGE has yet to experience failure of a sodium/sulfur cell due to a TCB seal. These results clearly indicate the superior properties offered by TCB and the advantages to be gained by replacing the mechanical seals. A complementary testing program at GE is presently underway.

Although cell cycling, thermal cycling and corrosion testing results have demonstrated the durability of TCB seals, more quantitative information on seal strength (modulus of rupture, tensile and torsional strengths) is needed.

E.1.2 Field-Assisted Bonding

Description and Procedure

Field-assisted bonding (FAB) is another solid state method for sealing aluminum and other metals to ceramics. The ceramic must possess an appreciable ionic conductivity in order to be successfully bonded. The large conductivity of beta-alumina makes it an excellent candidate for FAB.

A beta-alumina header in sodium-sulfur cells is not altogether unrealistic. Certain multichannel designs require a direct seal between the metal container and electrolyte. In prototype cells there is a concern that the scaled-up versions will exaggerate thermal expansion coefficient mismatches and cause high stresses at the glass seal between beta and alpha alumina. A beta-alumina header would minimize the potential for such an effect. Regardless of the precise application, it is imperative that the beta-alumina be insulated from the container to prevent self-discharge of the cell.

The method used for FAB is shown in Fig. E.4a. A d.c. field is applied across the sample with the metal to be bonded placed at the anode. A certain number of equivalents of charge must be passed in order to develop a bond. Adherence is not critically dependent on voltage provided that a minimum of 1×10^{-5} equivalents/cm^2 are transported. Constant current or constant voltage modes may be employed. The beta-alumina discs are polished to a 20 micron finish. Aside from disc geometry, aluminum containers are also bonded directly to beta-alumina.

Results and Discussion

Aluminum foil anodes (8 cm^2) were bonded to beta-alumina and found to be helium leak-tight. FAB of aluminum containers was also successful although the seals were still slightly permeable. Deposits on the counter electrode hydrated (strongly basic) and evolved gas. Presumably the reaction

$$2Na^\circ + 2H_2O \rightarrow 2NaOH + H_2\uparrow$$

occurred. The cathodic side of the beta-alumina was dark gray in various regions.

It would seem that the application of the d.c. field depletes Na^+ ions from the anode. Al^{3+} ions are transported into this region to preserve electrical neutrality. By introducing substantial numbers of Al^{3+} ions over sufficiently long distances a bond between aluminum and beta-alumina is formed. An electron microprobe trace

verifies that the anode region is depleted in Na^+ and enriched in Al^{3+} ions (Figure E.4b). A photomicrograph of the ceramic-metal interface (Figure E.5) indicates that the aluminum deforms (perhaps from local electrical stresses) and establishes intimate interfacial contact. This enables aluminum to be transported from the electrode to the ceramic. X-ray diffraction of the anodic region shows that alpha-alumina is the primary phase. The formation of alpha-alumina is significant for sodium-sulfur cells because it provides a means of insulating the metal container from the beta-alumina header. This prevents the creation of a sodium-air cell.

E.2. Ceramic-Ceramic Seals

In the past year emphasis was placed on gaining an improved understanding of the processes which cause the seal failures. Actual cell tests were combined with additional tests made outside cells. As a standard test for Na resistance of different sealing glasses, each new glass was subjected to an accelerated test in Na vapor at 350°C for 160 hours. This provided a quick method of comparing chemical stability of the virgin glasses in Na. In addition actual cell testing provided information concerning stability of the seal system under cycling conditions. Micrographic examination was made on a number

of seals, which provided the morphologies in the reaction zones between glass/ceramic interfaces. In addition, electron microprobe scans were made on several seal systems to study the compositional change in the seal system. Combined with observations made in the previous year, the effort has led to a very substantial improvement of the glass seal system as discussed below.

The sealing glass used in previous years was GE 1013 and the difficulties associated with it were reported. Substantial improvements were obtained by the development of alumino-borate compositions. These glasses exhibit extremely good Na resistance in our accelerated tests. This may be attributed to the greater thermodynamic stability of Al_2O_3 and B_2O_3 as compared to SiO_2 and P_2O_5.[5]

The glasses, however, remain susceptible to cracking and the earlier alumino-borate compositions generally failed in cells within three months. Microstructures of the beta-alumina/glass/alpha-alumina interface indicated that crystallites were formed upon sealing (Fig. E.6). Crystal growth was discontinuous and electron microprobe analysis verified that local compositional changes were occurring. In particular, the diffusion of glass modifiers away from the interface appeared to be responsible for the observed interfacial crystallization. The glasses themselves lacked the necessary stability and small changes in composition were able to produce devitrification. This behavior differs

markedly from that of glass 1013 where new phase formation was observed within the beta-alumina; the glass itself did not devitrify.

In the most recent glasses (e.g., 2093) crystallite formation was suppressed because a) interdiffusion of modifiers was reduced and b) the inherent stability of the glass was improved. The former was achieved by reducing concentration gradients while increased stability was acquired by bringing the glass composition well within the glass formation region. A micrograph of the seal cross-section (Fig. 7) represents a substantial improvement from earlier alumino-borate compositions.

Cell testing results of this glass are extremely encouraging. After cycling 100 days seals were virtually free of cracks and Na attack was negligible (6 cells). None of the cells with 2093 glass seals have failed due to seal cracking (over 25 fabricated). It is certain that this glass offers far better behavior than previous glass formations. Experiments in progress are aimed at evaluating the long-term stability of the 2093 glass seal system.

One major consideration in any glass seal system is the stress build-up due to thermal expansion mismatch. The thermal expansion coefficient of the glass must be compatible with those of the components it is sealing (i.e., alpha and beta-alumina). The analysis presented below is helpful in establishing the feasibility of alumino-borate glasses.

Figure E.8 shows the linear thermal expansion of alpha-alumina (AL998), two beta-aluminas and two sealing glasses. (Beta-alumina #1 is a 5th generation tube and beta-alumina #2 is a 6th generation tube.) It is clear that alpha-alumina and both beta-aluminas show a good thermal expansion match up to 1000°C, the 6th generation beta-alumina being more suitable. The sealing glasses also exhibit good thermal expansion match up to about 500°C. This indicates that if the glass seal is cooled slowly to relieve the thermal stress, the residual stress should not be too serious. The difference in thermal expansion is more clearly shown in Fig. E.9 where the abscissa represents the present thermal expansion difference referred to that of AL998 alpha-alumina.

In the above analysis we have tacitly assumed that there is no change in the thermal expansion coefficients of the seal components after the sealing is made. However, we have seen earlier that compositional change of the glass may be significant at the interface. A more detailed analysis shows that in a 2090 glass seal system, for example, the compositional change introduces an additional 7-10% further deviation in the thermal expansion coefficient. Thus, the change in glass composition and crystallite formation introduces additional thermal expansion mismatches which undoubtedly contribute to crack formation.

E.3 Summary

Significant improvements were made during the past year in the development of seals for the sodium/sulfur battery. For the outer, ceramic-metal seal, two solid state bonding methods are reported. Thermocompression bonding appears to offer a viable alternative to the mechanical seals presently used in prototype cells. Helium leak-tight seals are routinely produced between aluminum, 347 stainless steel or chrome-coated mild steel and alpha-alumina with an as-fired surface. The nature of the intermetallic determines whether a leak-tight seal is produced. Seal properties were evaluated by CGE and appear extremely promising. TCB seals are chemically and thermally stable and have yet to fail in a sodium/sulfur cell.

The inner, ceramic-ceramic seal, now utilizes an alumino-borate glass which possesses vastly superior properties to the previous silicate systems. Sodium durability is greatly enhanced and stable compositions which resist devitrification are available. The latter property has enabled crystallite formation at the glass/beta-alumina interface to be suppressed, thus eliminating a source of crack formation. Cell testing results of this glass are very positive; no cells with 2093 glass seals have experienced seal failures.

References

1. G. Desplanches et. al, U.S. Patent 4,037,027.

2. G. Heidt and G. Heimke, J. Mat. Sci. 10, 887 (1975).

3. J.T. Klomp, Sci. Ceramics 5, 501 (1971).

4. Development of Sodium-Sulfur Batteries for Utility Application, GE-EPRI Annual Report, December 1976.

5. C.A. Elyard and H. Rawson, Advances in Glass Technology, Proceedings of VIth Internat. Congress on Glass, Plenum, NY (1962).

List of Figures

List of Tables

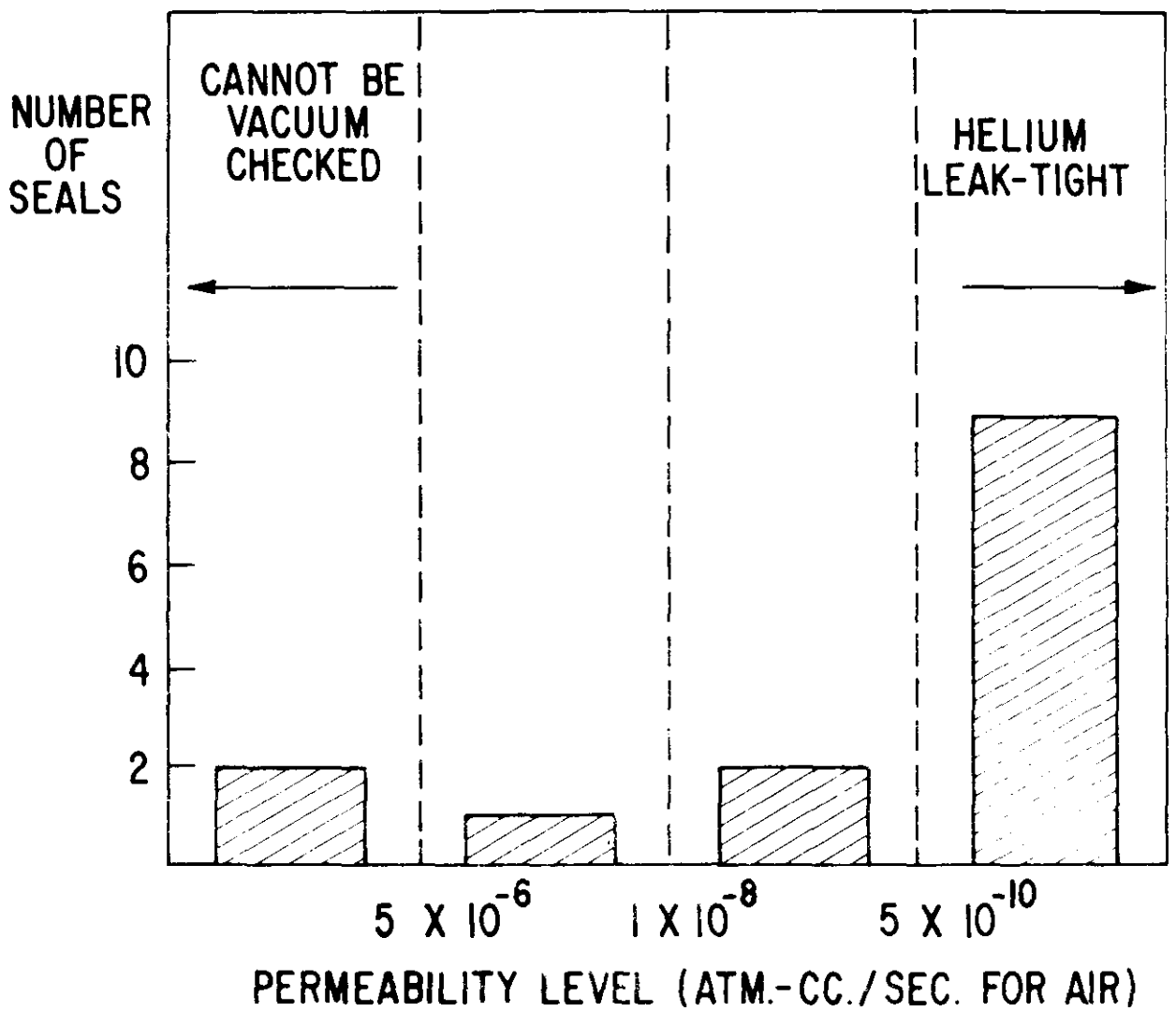

Figure E.1. Permeability of TCB Ceramic-metal Seals

Figure E.2. Aluminum/Alpha-alumina Interface of a TCB Seal (500X)

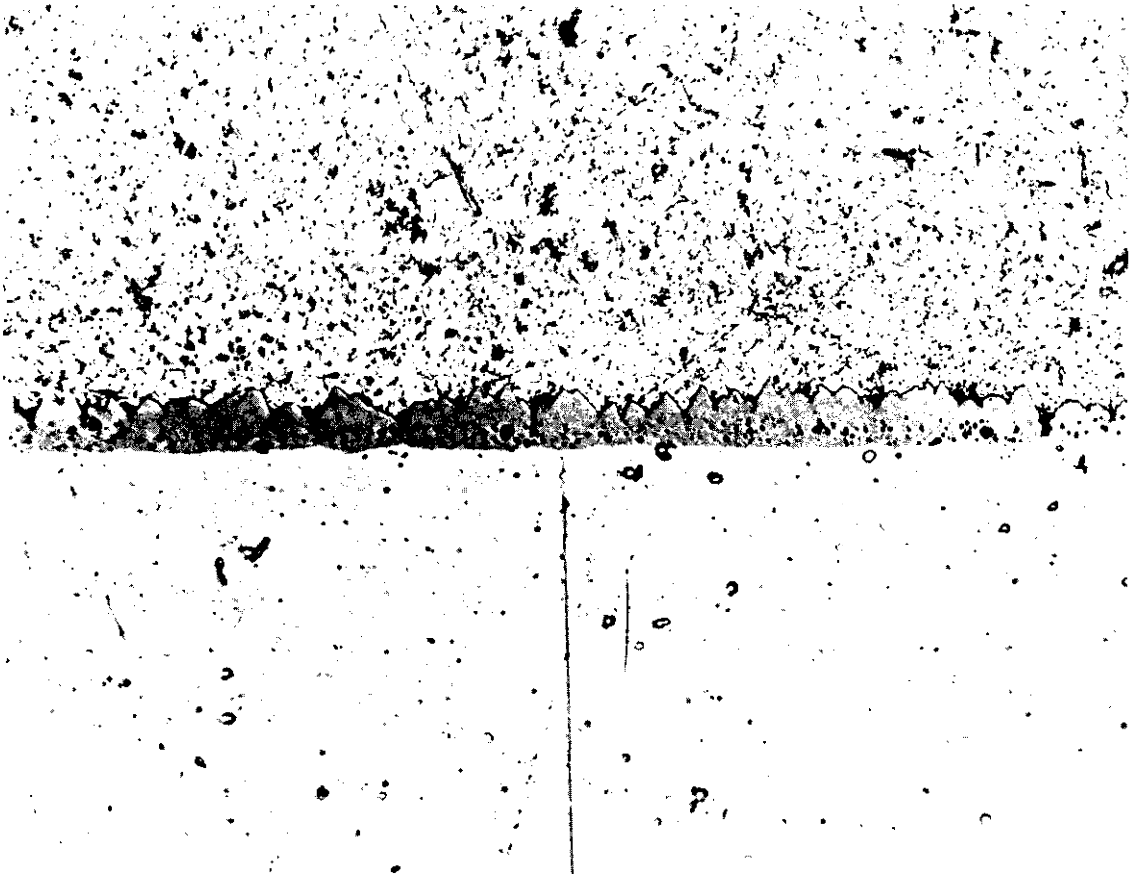

Figure E.3. Intermetallic Formation at the Boundary Between Aluminum (Top) and 347 Stainless Steel (750X)

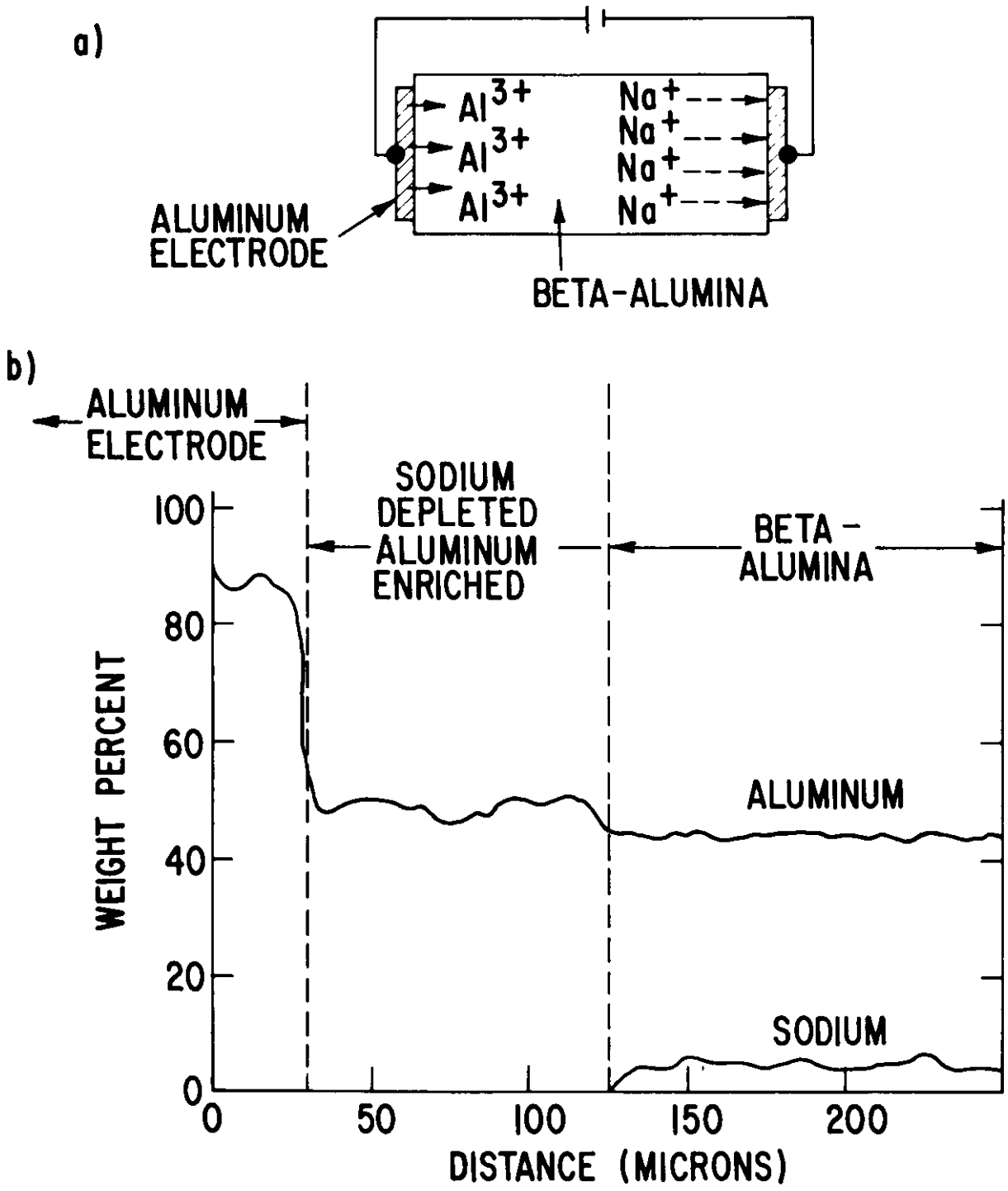

Figure E.4. Field-assisted Bonding of Aluminum

a) Schematic of Bonding Procedure
b) Concentration Profile from Electron Microprobe of Anodic Region

Figure E.5. Aluminum/Beta-alumina Interface of a FAB Seal (1500X)

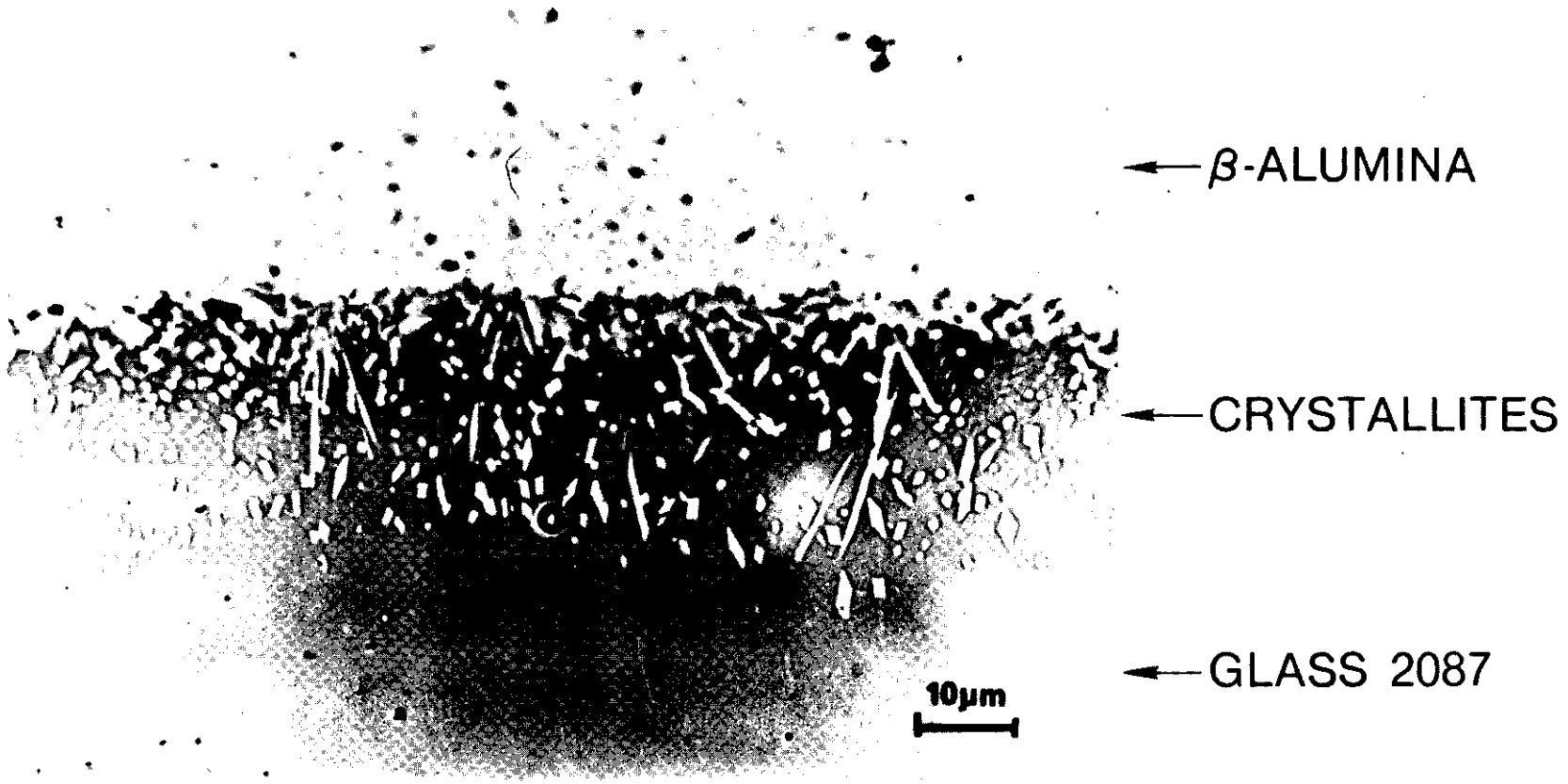

Figure E.6. Cross-section of a 2087 Glass Seal

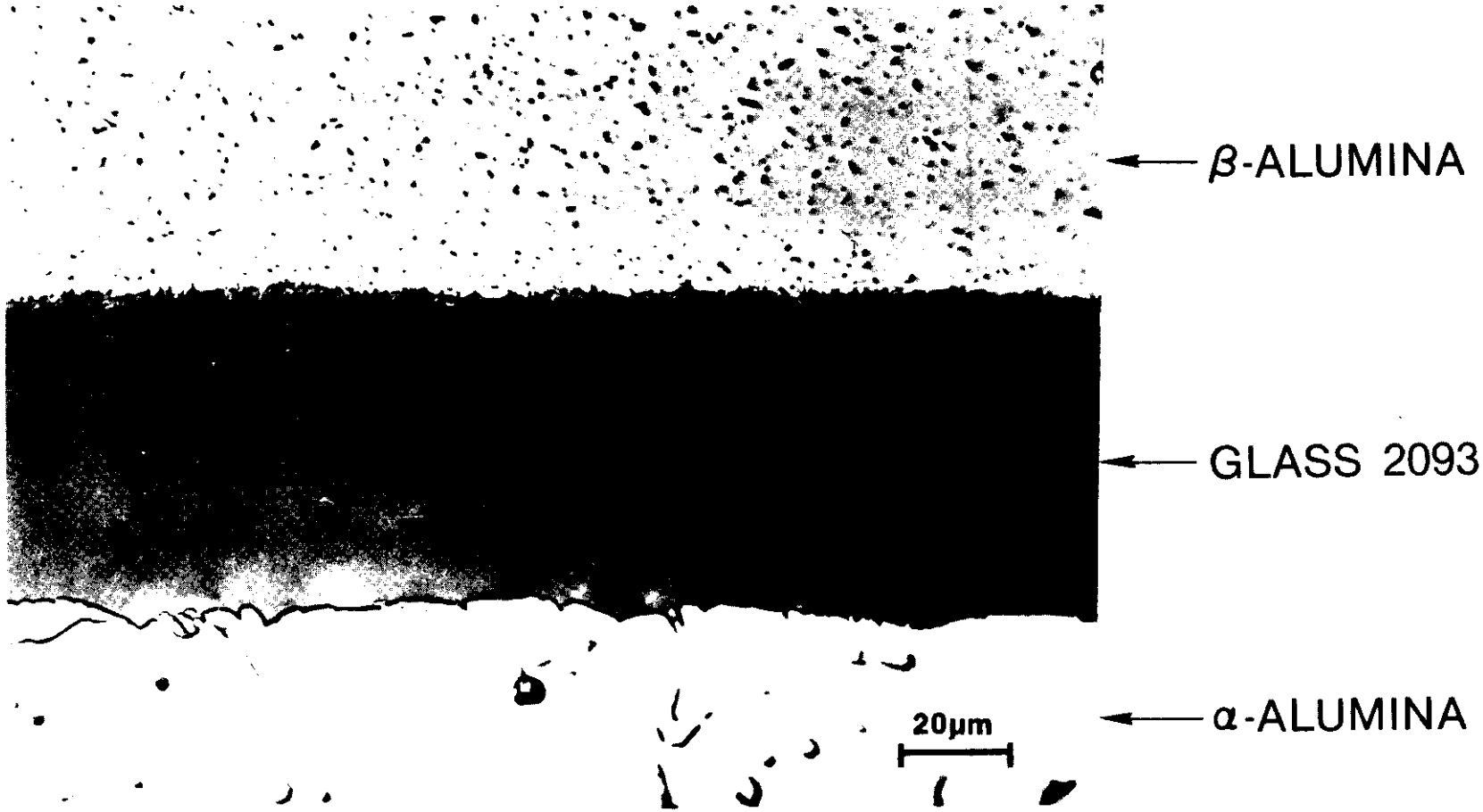

Figure E.7. Cross-section of a 2093 Glass Seal

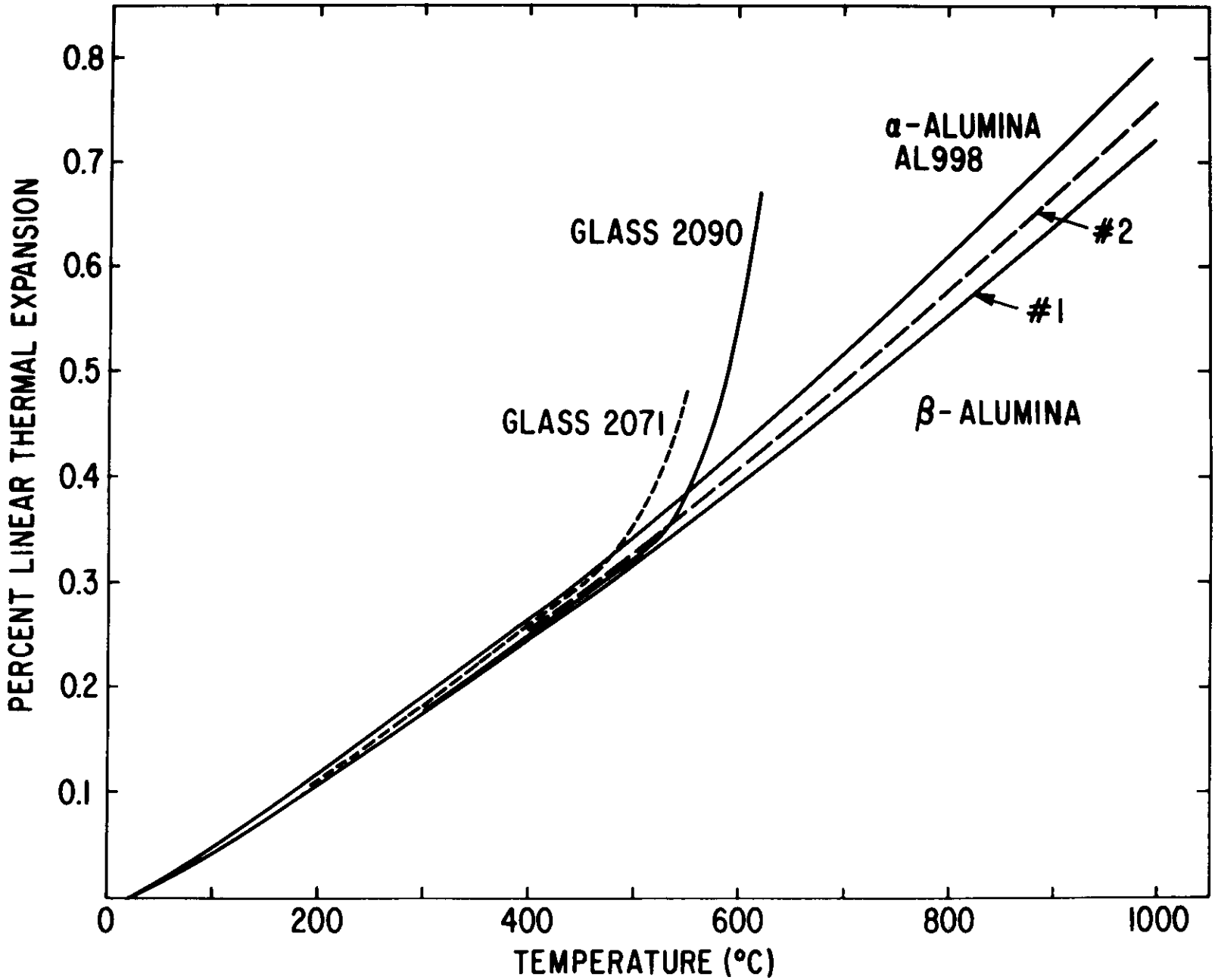

Figure E.8. Thermal Expansion of AL998 Alpha-alumina, 2 Beta-aluminas and Sealing Glasses 2071 and 2090

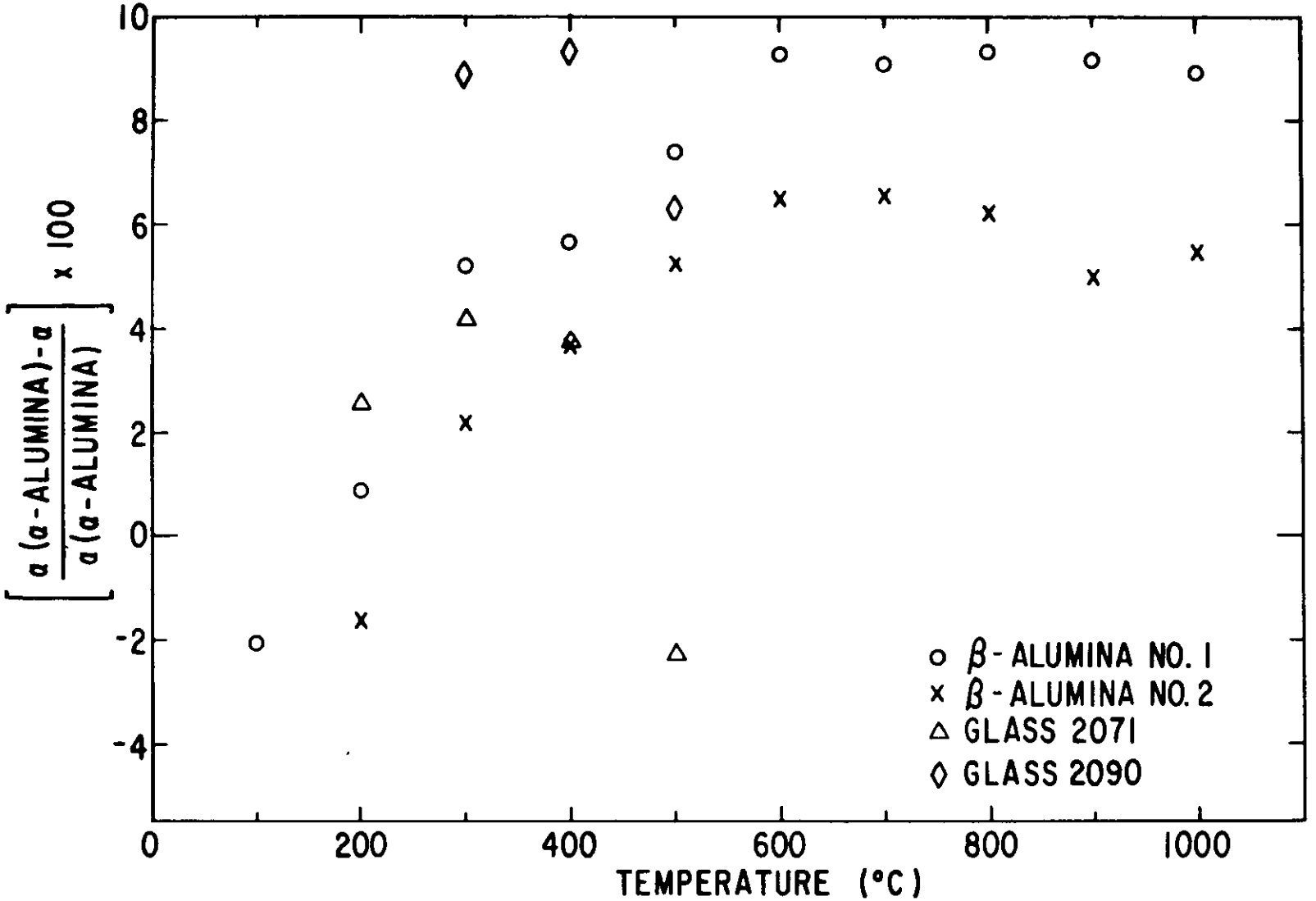

Figure E.9. Differential Thermal Expansion of 2 Beta-aluminas and Sealing Glasses Referred to AL998 Alpha-alumina

Section F
CERAMIC ELECTROLYTE DEVELOPMENT

At the beginning of this report period, a little over 300 ah/cm^2 of life testing experience had been logged on our longest lived Na/S cell, one containing a Generation V beta-alumina ceramic tube. This ceramic contained 8.4% Na_2O without other additives. It had a rather uniform grain size of 3-4 microns with very few exaggerated size grains. Closed end tubes of this composition were noticeably translucent, i.e. the porosity was considerably less than one percent. The resistivity at 300°C was moderately high however, about 22 ohm cm. Another beta-alumina ceramic, Generation VI, with a 300°C resistivity of ca 16 ohm cm had also been developed but little life testing experience had been accumulated on it. This material contained 9.6% Na_2O and 0.25% Li_2O. The microstructure was even better than that of Generation V as no evidence whatsoever of exaggerated size grains could be found.

These ceramics were the products of a development effort, the object of which was to extend operating life in Na/S cells by reducing electric fields at grain boundaries. This approach to longer operating life followed from considerations based on a model of the electrical properties of polycrystalline beta-

alumina shown in Fig. F.1.[1] Here r_c represents the specific resistivity associated with the interior of grains and is usually called the crystal resistivity. The extra resistivity in ceramic specimens associated with the presence of grain boundaries is represented by r_b. The capacitor C_b models the dielectric properties of these grain boundaries. Justification for use of this equivalent circuit is given elsewhere.[2,3]

The model can be viewed as a voltage divider for direct current, apportioning a part of the voltage drop associated with current flow across the grain interiors and a part across grain boundaries. In as much as grain boundaries are very thin and the two resistivity components are very approximately the same size at 300°C, electric fields at grain boundaries can be very large. For a grain boundary thickness of 10A, typical fields are computed to be about 10^5 V/cm. Such large fields might accelerate decomposition of beta-alumina ceramics, particularly at sites close to electronic conductors. Breakdown then might take place in Na/S cells near the electrolyte surface in contact with sodium and then propagate across the wall of the beta-alumina tube, giving rise in this way to an electronic short.

Because sintering aids, materials used to reduce the sintering temperature or to increase densification, often congregate near grain boundaries and consequently might be

reduced there, one aspect of the effort to extend ceramic operating life involved the development of techniques to sinter beta-alumina to high density without use of such aids. The problems encountered and solved in this effort were described in previous contract reports.[4,5] The high average fields at grain boundaries might be further enhanced if local current densities through parts of the ceramic tube greatly exceeded average values. As described previously, several sources of ceramic heterogeneities, such as cracks, exaggerated size grains, pores and second phase particles, were identified and systematically eliminated as they would contribute to field enhancement.[5] Likewise, field enhancement arising from details of tube shape were also eliminated.[4,5] A good inverse correlation was established between the grain boundary resistivities associated with the various ceramic generations and maximum operating life in sodium-sulfur cells.[5]

Techniques for measuring the impedance of beta-alumina ceramic over an extended range of temperature had been developed along with two different procedures for resolving measured impedances into the components characterizing the model shown on Fig.F.1.[2.3] A considerable knowledge about the variation of crystal and grain boundary resistivities with temperature for different ceramic composition and grain sizes had been accumulated.[3] This information was very important to the development of the improved ceramics of Generation V and VI.

While considerable work was carried out in this report period on forming by isostatic pressing, the processing scheme used for the most part for fabricating beta"-alumina ceramics had been developed previously for use with beta-alumina. The main steps in this scheme involve: (1) the use of a commercial beta-alumina or mainly beta"-alumina powder from Alcoa rather than synthesis from a high purity alpha-alumina powder; (2) forming by electrophoretic deposition; and (3) use of the stoker sintering method for firing greenware.

These particular processing steps were selected initially for reasons rather different from those now viewed as their outstanding features. Alcoa XB-2 beta-alumina powder was first employed in this Laboratory because of a conviction derived from cost considerations that ceramic must be fabricated from a base powder of commercial purity rather than from high purity alumina. In this report period, a greater appreciation developed for the homogeneity of this powder and its likely relationship to the suppression of exaggerated grain growth. The technique for forming by electrophoretic deposition was developed initially to obtain closed-end tubes.[6] It was apparent rather early that green tubes could be deposited in a few minutes with good dimensional control by this method. The fact was also soon recognized that the preferred crystallographic orientation of the grains, which has an adverse effect on conductivity, is virtually absent in ware formed by this technique.

However the excellent sinterability, arising from the fine uniform pore structure, became fully appreciated only more recently.

The stoker method for ceramic firing was used initially because it is a continuous rather than a batch process. High production rates can be achieved in a facility of modest size. Since every article of ware experiences the same thermal history on passage through the furnace, property reproducibility is excellent. There is an important but somewhat subtle corollary of this high reproducibility--small effects of processing changes can be readily noted. The accumulative effect of several such changes has been substantial. An example of one processing modification is the use of pure oxygen instead of air as the furnace atmosphere in order to achieve better densification.[7]

With lithia-containing ceramics, a problem is frequently encountered in electrophoretic forming if powder processing is done in a straightforward manner. Deposit weights with these ceramics are often unexpectedly small and not very reproducible. However, use of what has been called the two-powder route circumvents these difficulties. Discussion of these matters was previously given very restricted distribution.

At the beginning of this report period, the largest beta-alumina tubes fabricated in this Laboratory were 15 cm in length

with diameters of one and of two cm. Furthermore, no work had been done carried out on beta"-alumina ceramic. Our experience had been limited exclusively to beta-alumina.

The three major objectives of ceramic development work under the present contract are:

1) to obtain a ceramic electrolyte with a much lower resistivity in the temperature range of 300-350°C while retaining the good qualities of previously developed ceramic;

2) to select the most suitable forming method for the fabrication of large beta-alumina tubes; and

3) to gear up to fabricate large beta-alumina tubes with the required dimensions and properties at a sufficiently high production rate required for a Na/S battery to go into the BEST facility. Progress made in this period towards these objectives is summarized in this report.

The major accomplishments and findings of this period include the following:

1) Confidence in the approach used to develop improved ceramic electrolyte, as described above, was confirmed by two findings: (a) the achievement of over 1100 ah/cm^2 of operation in metal encased Na/S cells subject to deep discharge through the two-phase region and (b) the obtaining of average fracture strengths in diametral compression tests in excess of 50 Kpsi, i.e., equal to the best alpha-alumina values.[5,8]

2) However, it was established that the goal of a specific resistivity less than 9 ohm cm at 300°C was not likely to be achieved with a beta-alumina ceramic with a good microstructure.

A good microstructure is defined to be one with less than 1% porosity distributed in very small pores, no second phase particles, and no exaggerated grain growth. A beta"-alumina ceramic is needed.

3) Consequently beta"-alumina ceramics with specific resistivities less than 7.5 Ωcm at 300°C and microstructures without exaggerated size grains have been developed.

4) Free-flowing beta- and beta"-alumina powders were developed which could be isostatically pressed at 20 Kpsi. Specimens formed in this way have been sintered to over 99% of full density.

5) Both beta- and beta"-alumina tubes of the size required in cells for the BEST facility have been formed satisfactorily by both electrophoretic deposition and isostatic pressing.

6) The sintered properties of ware formed by electrophoretic deposition and isostatic pressing have been compared for both beta- and beta"-alumina ceramics. Electrophoretically formed specimens sinter more nearly to full density and at lower sintering temperatures. In addition, the grain size was found to be more uniform with pores of a smaller size with this forming procedure. The cost of the two forming methods was projected to be nearly the same from studies carried out by experienced manufacturing engineers. A cost analysis* was also carried out by Compagnie Generale de Electricite (CGE) on their ceramic processing and forming method. Although the GE and CGE methods are somewhat different it is interesting to note that the independent cost studies gave similar results.

These developments are discussed more fully below.

*Improvements of Electrolyte and Seal Technology for Sodium-Sulfur and Sodium Antimony Trichloride Load Leveling Batteries, EPRI Project 726-1, Final Report (EM-413), Compagnie Generale d'Electricite, Marcoussis, France, June 1977.

F.1. Development of Ceramic Electrolyte with Lower Resistivity

The purpose of having ceramic electrolyte with low resistivity is to reduce battery cost. For some required efficiency level (energy out/energy in), it is always possible to compensate for high ceramic resistivity by operating at low current density, i.e., by increasing the surface area of the electrolyte. This usually means more and/or larger cells. While the required number of cells also depends on the tube dimensions and on the sulfur electrode resistivity, nonetheless this quantity declines monotonically with the electrolyte resistivity. However, because of other sources of cell resistivity, the required number of cells becomes increasingly independent of ceramic resistivity at lower resistivities. A resistivity goal of less than 9 ohm cm at 300°C has been set from our system studies based on these considerations.

For our best beta-alumina ceramic, Generation VI with 9.6% Na_2O, 0.25% Li_2O, the crystal resistivity r_c amounts to 11.8 ohm cm at 300°C and the grain boundary resistivity r_b at that temperature is only 3 to 4 ohm cm for a tube with a fine-grained microstructure as shown on Fig. F.2. A larger field of view is shown on Fig. F.3 to indicate the absence of large grains. With other ceramic compositions, r_c values of less than 6 ohm cm at 300°C were obtained but with r_b values in the range of

10-12 ohm cm even with relatively poor microstructures.[5] There was hope that the best component resistivities could be obtained in a beta-alumina ceramic with a good microstructure. As shown previously, there are several advantages to the use of soda concentrations in excess of about 8.5 weight percent: easier microstructural control, lower r_b values, and lower sintering temperatures.[5] The problem reduced then mainly to lowering r_c values to about 6 ohm cm in a relatively high soda ceramic.

With the use of additives, it was found possible to vary considerably both the pre-exponential constant, σ_o, and the activation energy, E_c, associated with r_c. However, the variation of these two factors, on which r_c depends, are generally correlated with the result that their effects counteract leaving values of r_c at 300°C not greatly changed. This point is illustrated in Table F.1 using data from some of the various compositions studied. While these findings do not prove conclusively that the resistivity goal of less than 9 ohm cm at 300°C is unattainable with a beta-alumina ceramic, they are nonetheless very discouraging. The conclusion that a mainly beta"-ceramic would be needed appears otherwise on balance to involve more unfavorable than favorable points. While beta"-ceramics generally have lower r_c values and sinter at about a 100°C lower temperature than do beta of the same composition, microstructural control, moisture sensitivity,

Table F.1

Variation in Resistivity Parameters of Various
High Soda Beta-Alumina Ceramics

Amt Na_2O - wt%	9.6	9.6	9.6	9.6	9.6
Li_2O	.25	.50	.75	.25	--
MgO		.25			1.0
ZrO_2				1.0	
σ_o deg/Ωcm	6626	10220	16950	7273	
E kcal/mole	5.61	5.97	6.71	5.82	
r_c at 300°C-Ωcm	11.8	10.5	12.9	12.9	ca 12
r_c at 26.8°C-Ωcm	552	656	1520	718	

soda evaporation during sintering, and surface polarization problems are more troublesome. Furthermore, beta"-ceramics are more complicated. A phase stabilizer such as Li_2O and/or MgO is required.

An implicit assumption involved in all past work carried out on resistivity analysis in this Laboratory is that the crystal resistivity of a pure beta-alumina ceramic is a function of the composition but not of the processing history, apart from a small effect arising from preferred orientation. If this quantity should depend rather sensitively on the source of beta-alumina powder however, the worth of this kind of analysis in guiding property optimization would be much more limited. Because the method of preparation of beta-alumina single crystals has been reported to have a rather large effect on their resistivity, a variation of about a factor of 4 having been found, it seemed important to determine if there was a comparable effect in ceramics with greatly different processing history.[10] Resistivity parameters on a ceramic based on Monofrax H, a commercial fused beta-alumina from the Carborundum Co. was compared against those from ceramic based on XB-2, a calcined beta-alumina powder from Alcoa. Additional soda was introduced into the as-received powders to increase the concentration to a level where the resistivity was found previously not to vary significantly with the soda content.[3,9]

The results of resistivity measurements on these two ceramics are given in Table F.2. The resistivity parameters are distinguishable. It is not known whether the differences are indeed attributable to the starting powders or to other causes. However, the important point is that the difference in resistivity values are small in comparison to those on different single crystals. While results such as these cannot prove the point conclusively, it would appear that any differences in crystal resistivity values between powders of different origin are substantially erased by subsequent ceramic processing.

F.2 Fabrication of Mixed Beta, Beta"-Alumina Ceramics

Most commonly, beta- or mixed beta-beta"-alumina powders are prepared by dry blending fine powders of an alumina source, a soda source, and that of a stabilizer for beta"-phase and then calcining the blended mixture. As pointed out by Ray and Subbarao and confirmed in this Laboratory, the calcined mass is not converted completely to beta-alumina or to mixtures of beta- or beta". It is contaminated with alpha-alumina and/or sodium aluminate.[11] This is understandable since homogenization of the blended mixture cannot be carried out to atomic dimensions but only to the size of the particle aggregates, of the order of 10 μm. Segregation effects during calcining can also play a role in causing compositional fluctuations. After the dry blended and calcined product is milled, formed, and sintered, large exaggerated size grains appear in rather

Table F.2

Resistivity Parameters for Ceramics Based on Different Beta-Alumina Starting Powders

Parameter	Carborundum Co. Monofrax H	Alcoa XB-2
Composition $\%Na_2O$	8.8	8.4
r_c intergranular resistivity at 300°C - ohm cm	14.9	17.0
r_c at 26.8°C - ohm cm	334	418
σ_o pre-exponential factor - deg K/ohm cm	2361	2294
E_c activation energy for r_c - Kcal/mole	4.69	4.81
E_b grain boundary activation energy in Kcal/mole averaged between 26.8 °C and		
150°C	7.27	7.48
200	7.45	7.67
250	7.62	7.89
300	7.81	8.11
350	8.05	8.36
400	8.36	8.70

large numbers in the microstructure. Such grains cause a very significant loss of mechanical strength as well as reduced operating life in Na/S cells. While not completely eliminating exaggerated size grains, significantly improved microstructures have been achieved in other laboratories by improving compositional uniformity in dry blended powders.

However, XB-2 beta-alumina powder from Alcoa is phase pure as determined by x-ray diffraction. A more recently available mixed beta-beta" powder from that firm contains only beta"- and beta-alumina. By appropriate processing of these powders, exaggerated size grains can be completely eliminated while sintering to over 99% of full density. Complete elimination is defined operationally to mean that no large elongated grains greater than 25 μm are observed at 500X and at 50X in one or two specimens removed from a tube.

The XB-2 mainly beta"-alumina powder (65% beta"-, balance beta-) has a number of properties similar to those of pure beta-alumina powder. It contains approximately 8.0 percent Na_2O. The BET surface area of as-received powder is 0.9 to 1.0 m^2/g. Such powder is ball-milled dry to increase the surface area to almost 4.0 m^2/g to increase sinterability. Pure (99.5%) alumina grinding cylinders are used for this purpose to keep silica contamination relatively low, i.e., at 0.04 to 0.05 weight percent SiO_2. The processing for forming by electrophoretic deposition is nearly the same as for beta-alumina

ceramics.[6] Only a very small processing change was required to facilitate tube removal from mandrels after electrophoretic deposition. Prior to this change, however, mainly beta"-tubes were somewhat more difficult to remove than those of pure beta-alumina.

The best mainly beta"-alumina ceramic developed in this Laboratory as of this writing, is still not of the quality achieved with Generation VI pure beta-ceramic. It contains 85-90% beta"-alumina, the balance beta-. No sodium aluminate has been found in it. The resistivity is less than 7.5 ohm cm at 300°C. Average fracture strengths on different one cm diameter tubes have ranged from 36-44 Kpsi as determined by diametral compression tests. Sintering is usually carried out to densities in excess of 3.26 g/cc where translucency is noticeably better than in tubes sintered to lower densities. While microstructures of this ceramic can be rated good as defined above, it is still considerably inferior to that achieved with Generation VI beta-alumina ceramic. As shown on Fig. F.4, while most of the specimen volume is occupied by grains 2 μm or less, there is a considerable amount of 10 μm grains and even a few as large as 20 μm.

F.3. Two-Powder Route for the Electrophoretic Forming of Li_2O-Containing Ceramics

As mentioned above, if lithia is incorporated into either a beta- or a mainly beta"-alumina powder, often no deposition

occurs when electrophoretic forming is attempted or it takes place at an unsuitably slow and not very reproducible rate. This problem can be circumvented, however, by use of what has been called the two-powder route. One of the powders is milled XB-2 beta- or mainly beta"-alumina powder while the other is the same powder highly enriched in soda.

Use of the two powder route was discussed in the previous contract report in connection with some studies on the mechanism of sintering of beta-alumina.[5] Perhaps the most surprising fact about the two-powder route is that the sintering kinetics of ware formed by co-electrophoretic deposition of two powders is the same within experimental error as that for a single powder made up to the same soda concentration as the average of the two powders. This fact was demonstrated for both the Generation V and the Generation VI beta-alumina ceramic compositions, the latter containing 0.25% Li_2O.[5] Identical densification for the different powder routes over a range of sintering temperatures have also been found for mainly beta"-alumina containing much higher lithia concentrations. The interpretation placed on this phenomenon is that once the formation of the beta- or beta"-alumina crystal structure is complete, subsequent soda and lithia diffusion during sintering is so rapid that significant gradients cannot be sustained and rapid compositional equlibration occurs.

The addition of a second powder highly enriched in soda increases of course the overall soda content above that in the as-received powder. Since the sintering temperature of both beta- as well as beta"-alumina is decreased as the soda concentration is increased, use of the two powder route lowers the sintering temperature below that required for ceramic maintained at the same soda concentration as as-received powder. As also discussed in a previous report, it was found in the course of these studies on sintering mechanisms that exaggerated grain growth is much less of a problem in beta-alumina ceramics of higher soda contents than in that with the composition of as received powder. And furthermore grain boundary resistivities are lower in higher soda ceramics.[5] The discovery of these facts was central to the development of the improved beta-alumina ceramics of the V and VI Generations. It was in the course of further comparative studies of one- vs two-powder routes that the effect of Li_2O on electrophoretic deposit weights was uncovered.

At first, lithia was incorporated in the low soda powder component. It has been found, however, that it may just as well be put in the highly soda-enriched component--a practice that simplifies fabrication somewhat. This is illustrated in Table F.3 for beta-alumina ceramic of the Generation VI composition. Since the deposition conditions were the same for the four suspensions used, with the same initial concentration of

powder in vehicle, the same deposition times and electric fields, and with mandrels of nearly identical dimensions, the mass of the first specimen deposited from a suspension was proportional to the electrophoretic mobility. It can be seen from the table that the electrophoretic mobility is essentially independent of the powder component into which the lithia was incorporated. After sintering under similar conditions, the fired densities of different tube specimens from the same suspension were not found to differ greatly from each other and average densities from different suspensions varied little with the lithia source. Likewise the room temperature resistivity, which depends mostly on ceramic microstructure and which therefore can be used as a microstructure indicator, does not depend significantly on the powder component containing the lithia. It should be added that the resistivity values given in Table F.3 are not typical of present Generation VI beta-alumina tubes.

Furthermore the concentration of Na_2O can be varied rather widely in the high soda component without much effect on the electrophoretic yield. This is shown in Table F.4 for beta-alumina ceramic containing 9.6% Na_2O and either 0.25 or 0.75 weight percent Li_2O. While early work was carried out with a 30/70 Na_2O/Al_2O_3 mole ratio, satisfactory yields were also obtained at a 35/65 ratio (that of the binary eutectic composition) as well as with a ratio as low as 21/79. However, with the latter, a drop in yield was noted,

Table F.3

Comparative Properties of Ware Formed with Li_2O in XB2 vs. that with Li_2O in the High Soda Component

Suspension No.	Lithia Source	Mass of First Deposit	Fired Density		Room Temp. Resistivity
BG1	XB2	9.7 g	3.268		4.2 KΩcm
			3.268	3.268[1] g/cc	
			3.269		3.9
BG2	High Soda Component	9.3	3.272		4.2
			3.274	3.275[1]	
			3.278		3.7
BG3	XB2	10.1	3.267		5.2
			3.267	3.268[2]	
			3.270		4.9
BG4	High Soda Component	9.8	3.270		5.0
			3.270	3.270[2]	
			3.270		4.3

1 Sintered on June 21, 1976

2 Sintered on June 22, 1976

Table F.4

Electrophoretic Yields for Various Soda Concentrations in the High Soda Powder Component

Na_2O/Al_2O_3 Mole Ratio	Deposit Masses	
	0.25% Li_2O	0.75% Li_2O
35/65	9.5 g	9.4 g
30/70	9.5	9.2
21/79	9.0	8.4

particularly with 0.75% Li_2O.

F.4. Selection of a Forming Method for Large Tubes

While the technique of forming by electrophoretic deposition has served this project very well in providing one cm diameter closed end tubes for small test cells, by no means does it follow that this forming method is necessarily the most suitable for forming large tubes, ca 2.8 cm outer diameter by 40 cm long. These are needed for cells to go into a battery for the BEST facility. The Laboratory is believed to be the only one forming solid electrolyte tubes by electrophoretic deposition exclusively. A battery group at CGE Marcoussis uses a combination of electrophoretic deposition and isostatic pressing while other groups throughout the world use isostatic pressing. It seemed that the two forming methods, isostatic pressing and electrophoretic deposition, should be evaluated as objectively as possible on a quality/cost basis.

An isostatic press was purchased from Olin Energy Systems Ltd. of Sunderland, England and installed at the General Electric Research and Development Center. Meanwhile free-flowing powders were developed using spray drying. Such powders are required to fill very quickly the space in the press between the mandrel and the elastomeric bag. The procedures developed apply to both XB-2 beta- and to mainly beta"-alumina powders. Suitable compaction was obtained at 20 Kpsi to achieve green densities of 62-64 percent of full density. These

compacts were found to sinter as well as others pressed at 27.5 Kpsi. The maximum sintered density achieved with isostatically pressed specimens was 3.26 g/cc. The significance of the low pressure required to achieve compaction is that the Olin press has an almost unlimited life for pressings carried out under 30 Kpsi but an increasingly shorter fatique life on use with pressures over 30 Kpsi.

In order to carry out a valid comparison of the two forming methods, identical starting powders were used. Beta-alumina powders of the Generation VI composition (9.6% Na_2O and 0.25% Li_2O) and our presently best mainly beta" composition were both used in the evaluation of the two forming methods. These compositions were prepared from Alcoa XB-2 powders (8.0 Na_2O) manufactured in 1975. Beta-alumina powder was dry-milled with Coors 99.5% alumina grinding media to increase the surface area to approximately 2.7 m^2/g while mainly beta"-alumina powder was milled to 3.7 m^2/g. Extra soda was introduced by way of sodium carbonate and lithia from lithium oxalate. After mixing of the powders, calcination was carried out at 1200°C for about 24 hours. A single powder of the appropriate composition was used for isostatic pressing. However, electrophoretic forming was carried out by co-depositing a mixture of two powders. One powder was milled XB-2. The second powder was relatively rich in Na_2O

with a Na_2O/AlO_2 mole ratio of 30/70. This second powder also contained the lithia. The weight ratio of the two powders was such as to correspond to the desired overall composition. Use of the two-powder route permits larger and more uniformly thick deposits in the electrophoretic forming of lithia-containing ceramics. However, as discussed above, sintered densities and microstructures are independent of the powder route.

Specimens about 0.5 in. in width and 3 in. long were cut from large green tubes formed by the two methods. Since suitable sintering facilities for green tubes were still undergoing construction, small specimens were required so that sintering could be carried out in the well-controlled furnace used to stoker fire the 1 cm diameter tubes used in small test cells. Specimens formed by electrophoretic deposition and by isostatic pressing were sent through the furnace alternately in an attempt to obtain the most valid comparisons.

Density data for Generation VI beta-alumina specimens sintered at 1650, 1675, and 1700°C after forming by either of the two methods are given in Table F.5. Similar data for the mainly beta"-ceramic after sintering at 1550, 1575, and 1600°C appear in Table F.6. Actually test strips were cut from two isostatically pressed beta" tubes which differed in the manner by which powder was loaded into the press. The data of Table F.6 bring out that the sintered density

Table F.5

Comparison of Sintered Densities for
Generation VI Beta-Alumina Formed by Different Methods

Sintering Temp.-°C	Forming Method	Sample No.	Measured Density-g/cc	Av. Density g/cc	Std. Dev. g/cc
1650	Isostatic Pressing	1	3.159	3.160	0.0010
		2	3.161		
		3	3.161		
		4	3.161		
	Electrophor. Deposition	1	3.271	3.270	0.0006
		2	3.270		
		3	3.270		
1675	Isostatic Pressing	1	3.214	3.212	0.0014
		2	3.212		
		3	3.211		
		4	3.211		
	Electrophor. Deposition	1	3.269	3.271	0.0022
		2	3.271		
		3	3.274		
		4	3.270		
1700	Isostatic	1	3.241	3.242	0.0013
		2	3.242		
		3	3.240		
		4	3.243		
	Electrophor.	1	3.278	3.282	0.0032
		2	3.284		
		3	3.283		

Table F.6

Comparison of Densities of Mainly Beta"-Alumina Ware
Formed by Isostatic Pressing and by Electrophoretic Deposition

Sintering Temperature--°C	1550°		1575°		1600°	
Forming Method						
1. Isostatic Pressing Method A	3.040 3.082	3.061 g/cc	3.215 3.215	3.215	3.255 3.232	3.244
2. Isostatic Pressing Method B	3.122 3.126	3.124	3.233 3.232	3.232	3.256 3.265	3.260
3. Electrophoretic Deposition	3.249 3.247	3.248	3.275 3.276	3.276	3.279 3.276	3.279

depends somewhat on the procedure used to feed the powder. Comparative microstructures for both ceramics for the different sintering temperatures are presented on Figures F.5 and F.6.

Data in the tables indicate clearly that densification of ware formed by electrophoretic deposition proceeded more rapidly and more nearly to full density for both ceramics. Even so, the density of the isostatically pressed ware sintered at the highest temperatures is at least as high, to our knowledge, as that reported by any other group using this forming method. Inspection of the photomicrographs indicates the presence of smaller size pores with the electrophoretic forming method. Smaller size pores are desirable for the purpose of maximizing mechanical strength and minimizing electric field enhancement within the ceramic. Also with this forming method, the grains appear to be of more uniform size except at the highest sintering temperatures where exaggerated grain growth is becoming noticeable.

These results perhaps are not surprising in view of the nature of the two forming processes. In general with isostatic pressing, the green structure is built up using particles of powder aggregates while with electrophoretic deposition, building is done with much smaller crystallite particles. The particles usually observed by eye in fine powders are loosely bonded aggregates of smaller sized crystallites. In preparing stable suspensions for electrophoretic deposition,

i.e., suspensions which settle at a minimum rate, surface charge is developed on the crystallites. The resulting forces of repulsion overwhelm the relatively weak forces of attraction between the crystallites within aggregates. Thus the typically tens of μm size aggregates are broken down into much smaller, ca μm size, crystallite particles. During deposition, the crystallite particles are laid down one by one. In contrast, with isostatic pressing, aggregate size particles much be used. In order to fill the press rapidly with powder to a good density, free-flowing powders, usually more or less spherical aggregates are prepared--usually by a spray drying process. Organic binders are often added to improve inter-crystallite bonding. The important point is that since smaller particles are used with electrophoretic deposition, the pores or space between particles are also much smaller. Small pores are much easier to remove during sintering than large ones. While it is true that during compaction in isostatic pressing, the large interaggregate pores are filled to a certain extend by flow, this process can seldom be complete. When pores on fractured surfaces of sintered specimens formed by electrophoretic deposition are examined by scanning electron microscopy, they are found to be of micron size. On the other hand, pores in the shape of circular arcs, residues of interaggregate porosity, are frequently seen in optical micrographs of specimens that had been isostatically pressed.

Manufacturing cost studies comparing electrophoretic forming (GE process) and isostatic pressing processes have not shown cost advantages for isostatic pressing. In view of these cost studies, the extensive technology developed so far in electrophoretic forming, and the high quality ware consistently produced by this technique, electrophoretic forming has been selected as the preferred forming method for use in the fabrication of ceramic tubes for a BEST battery.

Progress made in scale-up of both the size and production rate of tubes is discussed in another section of this report.

F.5. Status and Plans

A mainly beta"-alumina ceramic has been developed which readily meets our resistivity goal of 9 Ωcm at 300°C. While the microstructure of this ceramic is good, it is nonetheless far inferior to that of our Generation VI beta-alumina ceramic. Work is underway to improve the uniformity of the grain size and to increase the mechanical strength considerably over the present value of about 40 Kpsi in tension. Adequate life and sufficiently low polarization in Na/S cells remain to be demonstrated for this ceramic.

While tubes formed by electrophoretic deposition sinter more nearly to full density, at lower sintering temperatures, and give rise to a better microstructure than those isostatically pressed, some work will nonetheless be carried out to improve the properties of isostatically pressed ware. Tubes formed by isostatic pressing might be required should the cost of

electrophoretic forming prove excessive at high production rates.

However, the major thrust throughout the remainder of this contract will be given to the development of sintering techniques for large tubes for BEST size cells. In addition more realistic specifications must be developed and quality control procedures set up. The fabrication rate of tubes meeting specifications must gradually be increased to that required to produce a BEST size battery.

References

1. S.P. Mitoff, in "Fast Ion Transport in Solids", W. van Gool, Editor, North Holland American Elsevier Publishing Co., NY (1973).

2. R.W. Powers and S.P. Mitoff, J. Electrochem. Soc. 122, 226-231 (1975).

3. R.W. Powers, pp. 351-368 in "Superionic Conductors", G.D. Mahan and W.L. Roth, Editors, Plenum Publishing Corp., NY (1976).

4. "Sodium-Sulfur Battery Development", EPRI Report 128-2, General Electric Co., Schenectady, NY, Sept. 1975.

5. "Development of Sodium-Sulfur Batteries for Utility Application", EPRI Report EM-266, Project 128-3, General Electric Co., Schenectady, NY, Dec. 1976.

6. R.W. Powers, J. Electrochem. Soc. 122, 490-500 (1975).

7. R.W. Powers and S.P. Mitoff, Am. Ceramic Soc. Bull (In Press).

8. "Alumina as a Ceramic Material", W.H. Gitzen, Editor, Am. Ceramic Soc., Columbus, OH (1970).

9. R.W. Powers and S.P. Mitoff, in "Solid Electrolytes", P. Hagenmuller and W. van Gool, Editors, Academic Press, NY (In Press).

10. S.J. Allen, Jr., L.C. Feldman, D.B. McWhan, J.P. Remika and R.E. Walstedt, pp. 279-298, in "Superionic Conductors", G.D. Mahan and W.L. Roth, Editors, Plenum Publishing Corp., NY (1976).

11. A.K. Ray and E.C. Subbarao, Mat. Res. Bull. 10 583 (1975).

List of Figure Captions

List of Tables

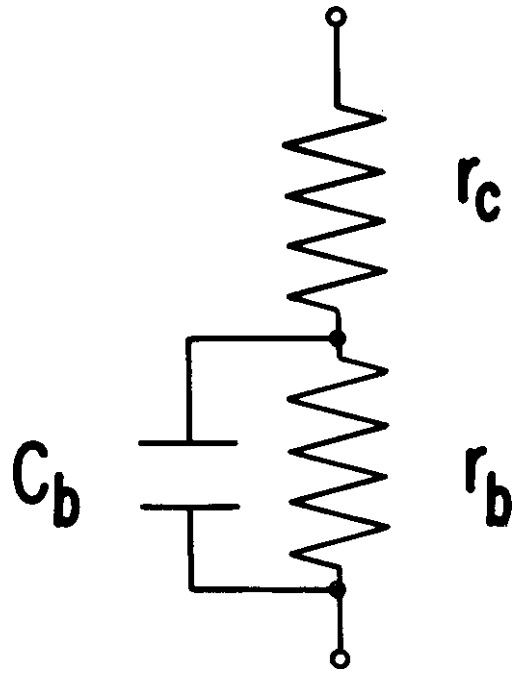

Figure F.1. Simplified Model of Electrical Properties of Polycrystalline Beta-alumina

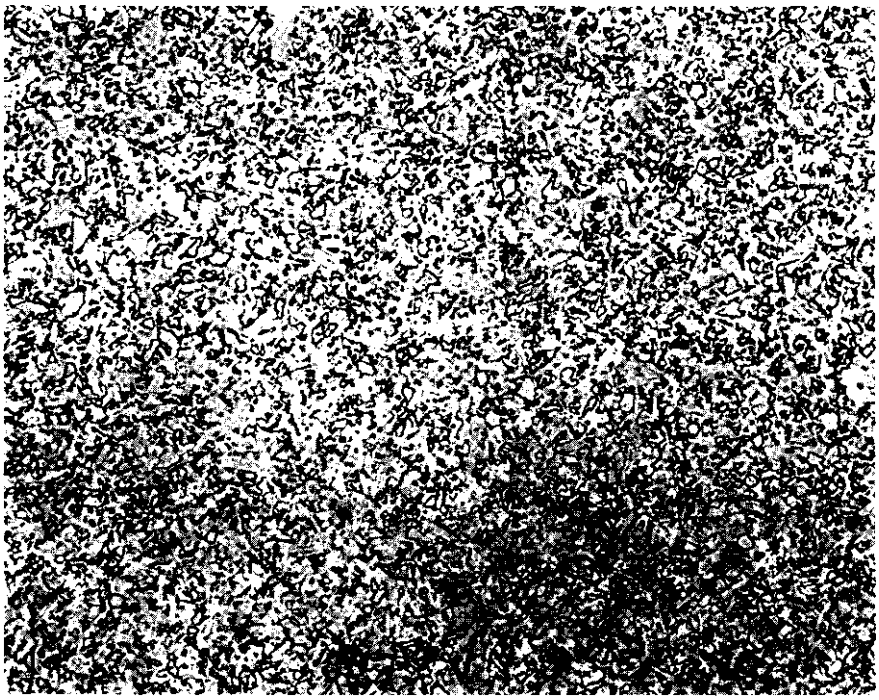

Figure F.2. Photomicrograph of Generation VI Beta-alumina Ceramic with 9.6% Na_2O and 0.25% Li_2O. Density 3.28 g/cc; 500X.

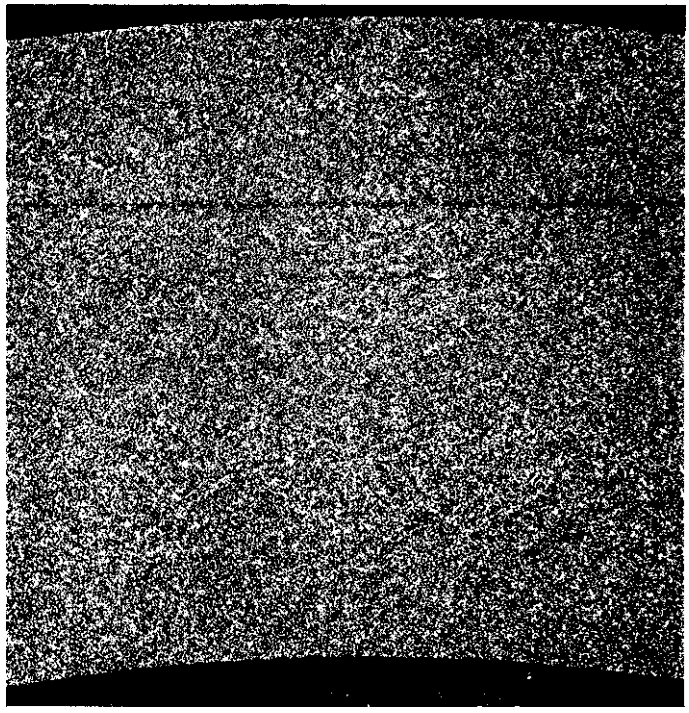

Figure F.3. Same Specimen as Fig. 1 but at 75X

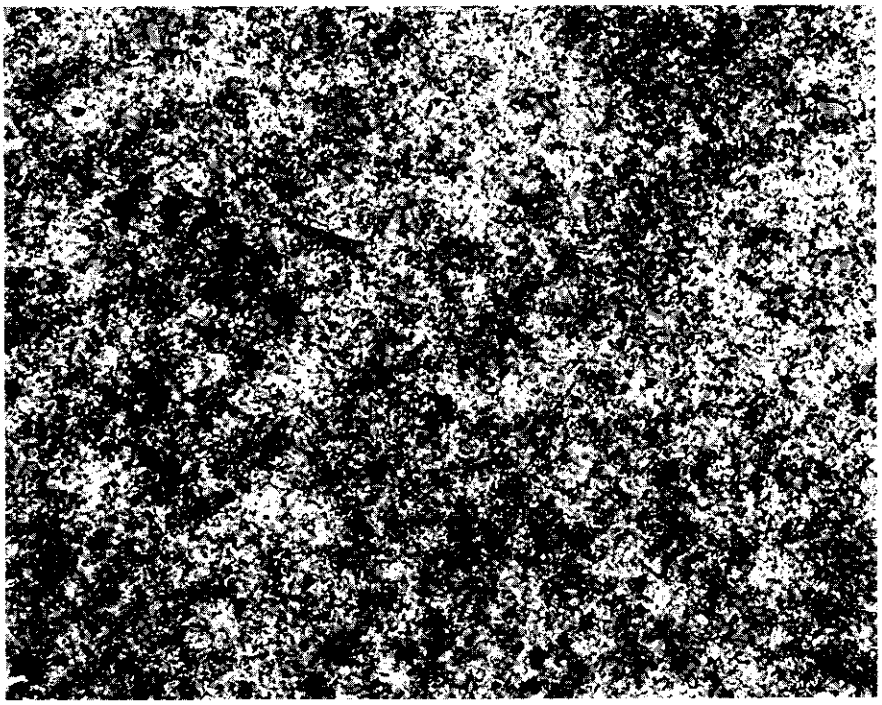

Figure F.4. Photomicrograph of Generation VII Mainly Beta"-Alumina Ceramic. Density 3.26 g/cc; 500X.

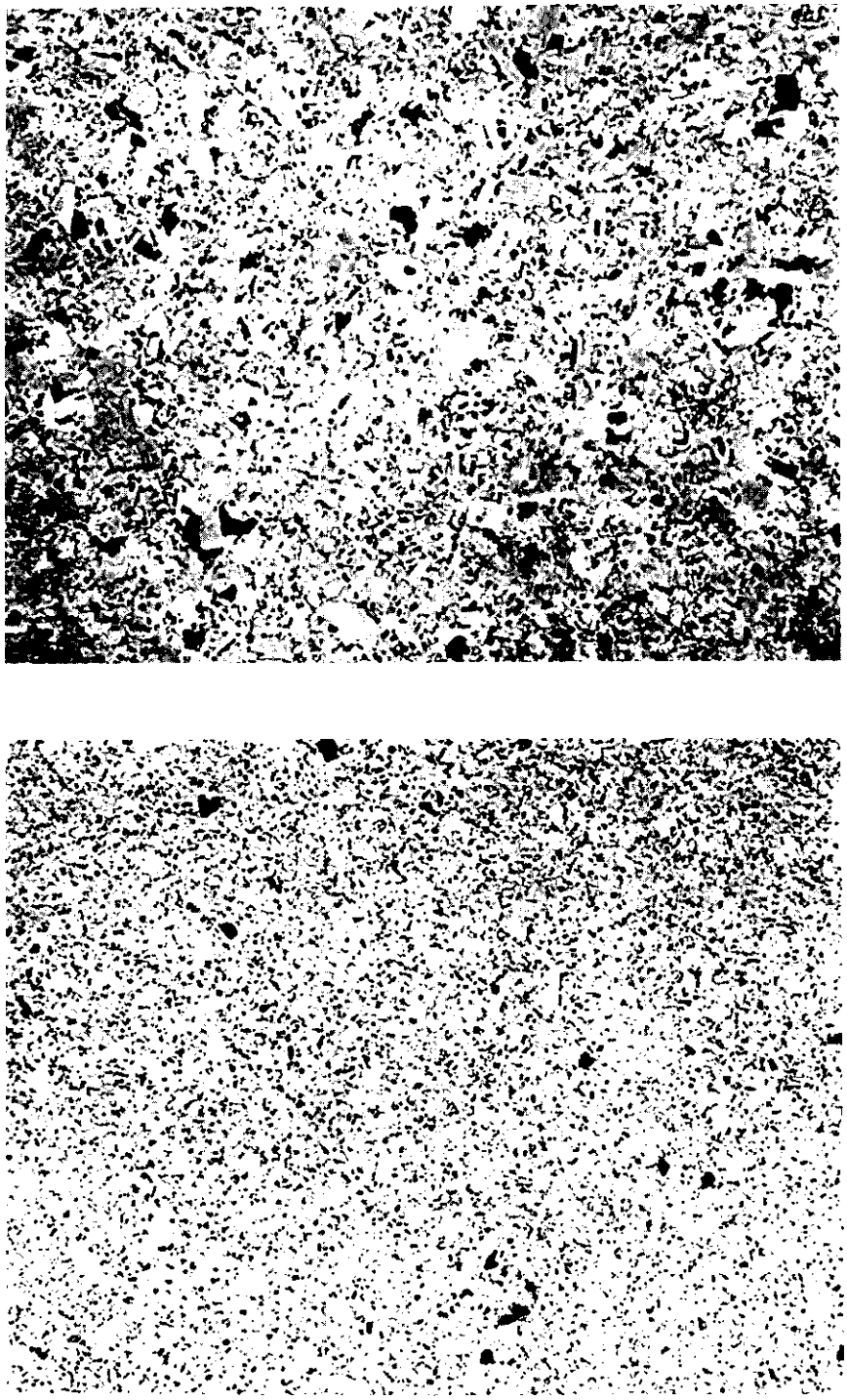

Figure F.5a. Photomicrographs (500X) of Beta-Alumina Ceramics Formed by Either Isostatic Pressing (Upper) or Electrophoretic Deposition (Lower) and Sintered at 1650°C

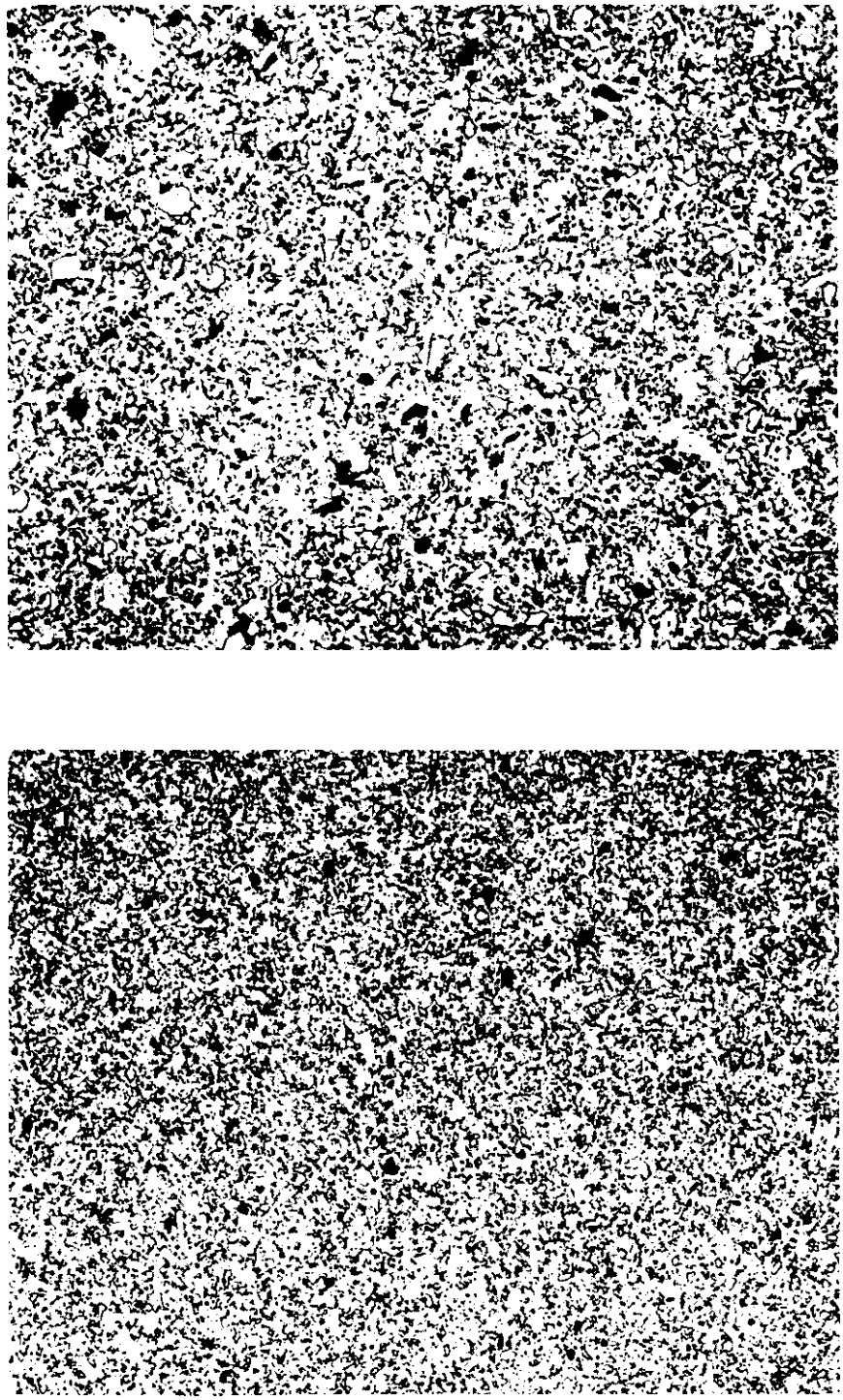

Figure F.5b. Photomicrographs (500X) of Beta-Alumina Ceramics Formed by Either Isostatic Pressing (Upper) or Electrophoretic Deposition (Lower) and Sintered at 1675°C

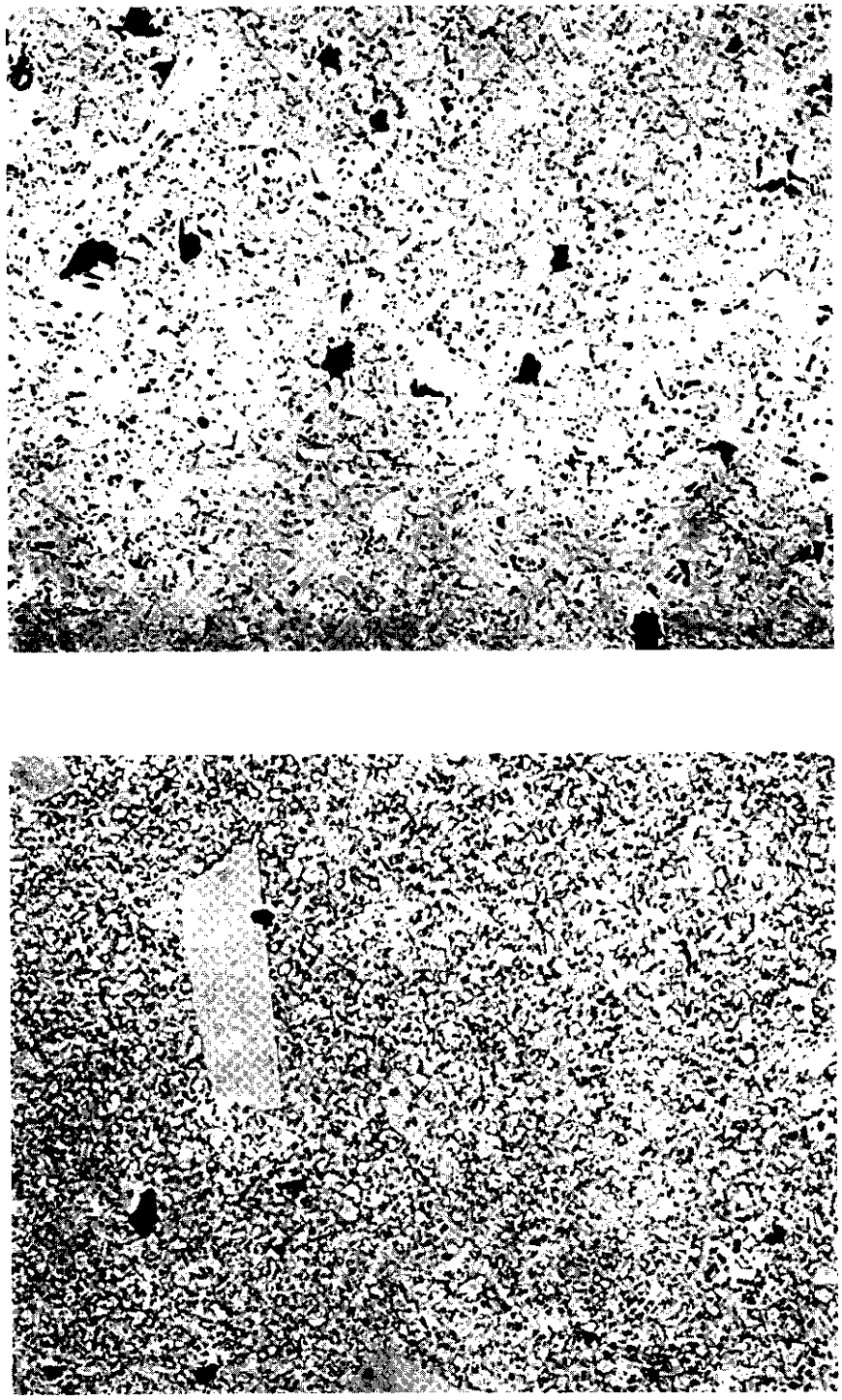

Figure F.5c. Photomicrographs (500X) of Beta-Alumina Ceramics Formed by Either Isostatic Pressing (Upper) or Electrophoretic Deposition (Lower) and Sintered at 1700°C

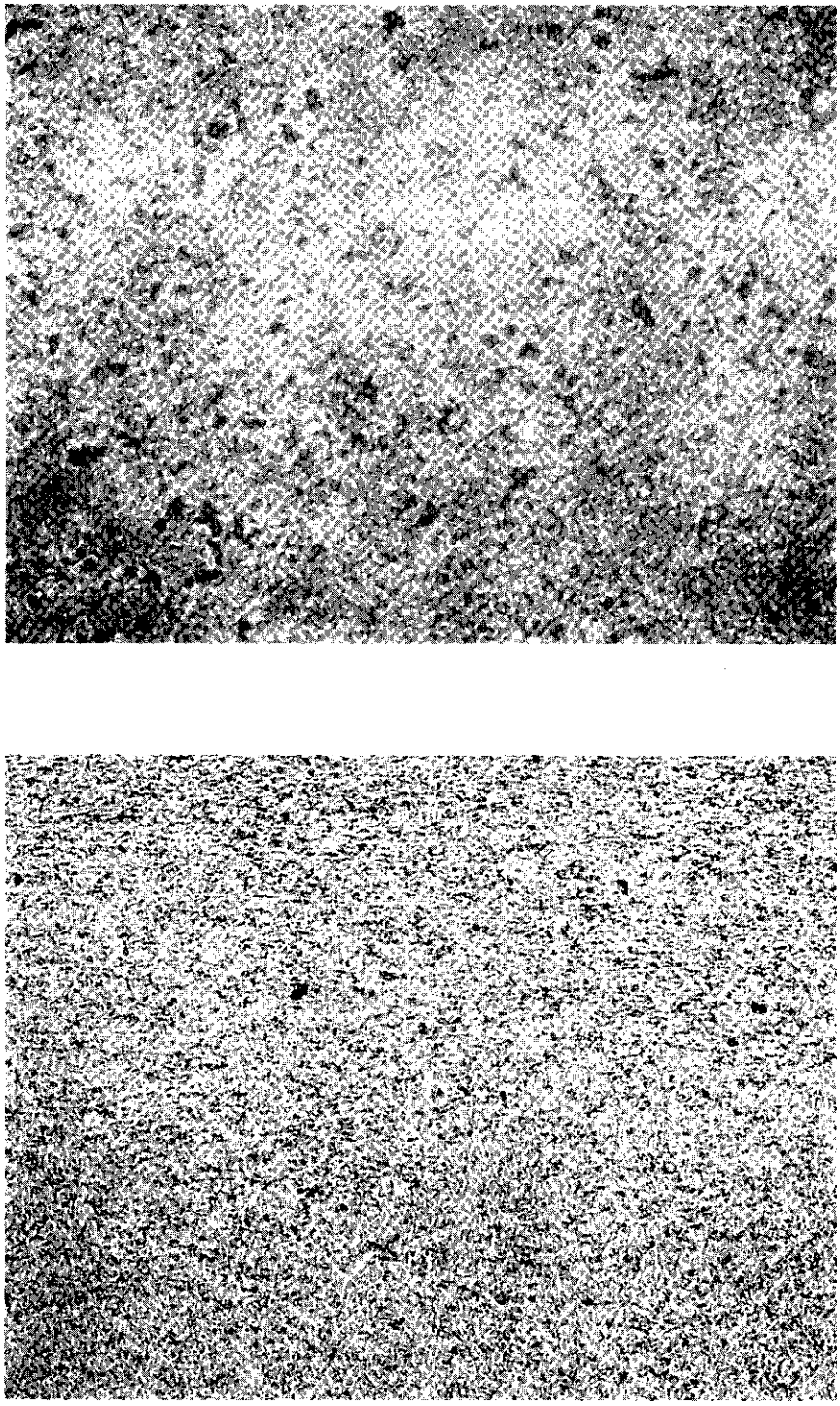

Figure F.6a. Photomicrographs (500X) of Beta"-Alumina Ceramics Formed by Either Isostatic Pressing (Upper) or Electrophoretic Deposition (Lower) and Sintered at 1550°C

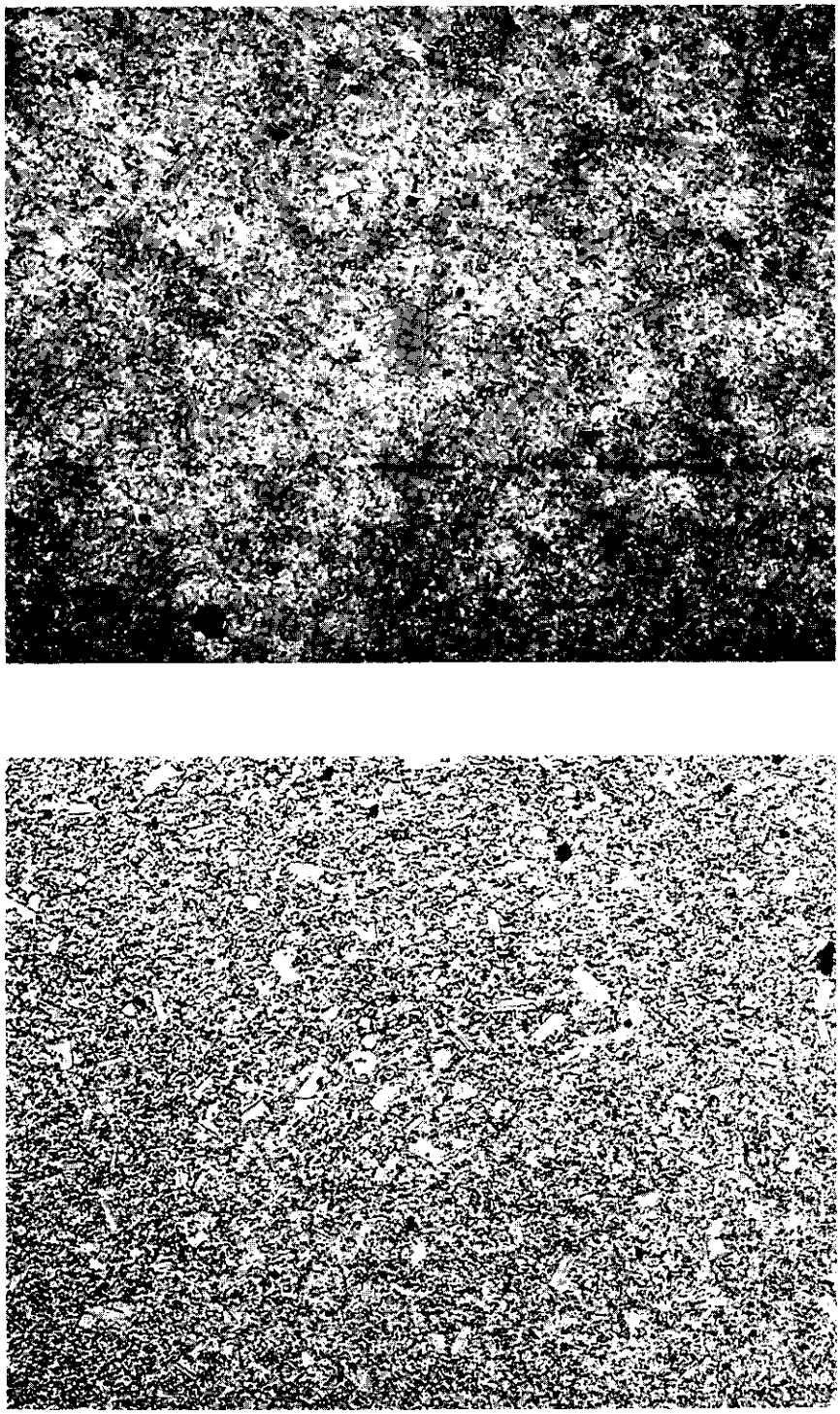

Figure F.6b. Photomicrographs (500X) of Beta"-Alumina Ceramics Formed by Either Isostatic Pressing (Upper) or Electrophoretic Deposition (Lower) and Sintered at 1575^{o}C

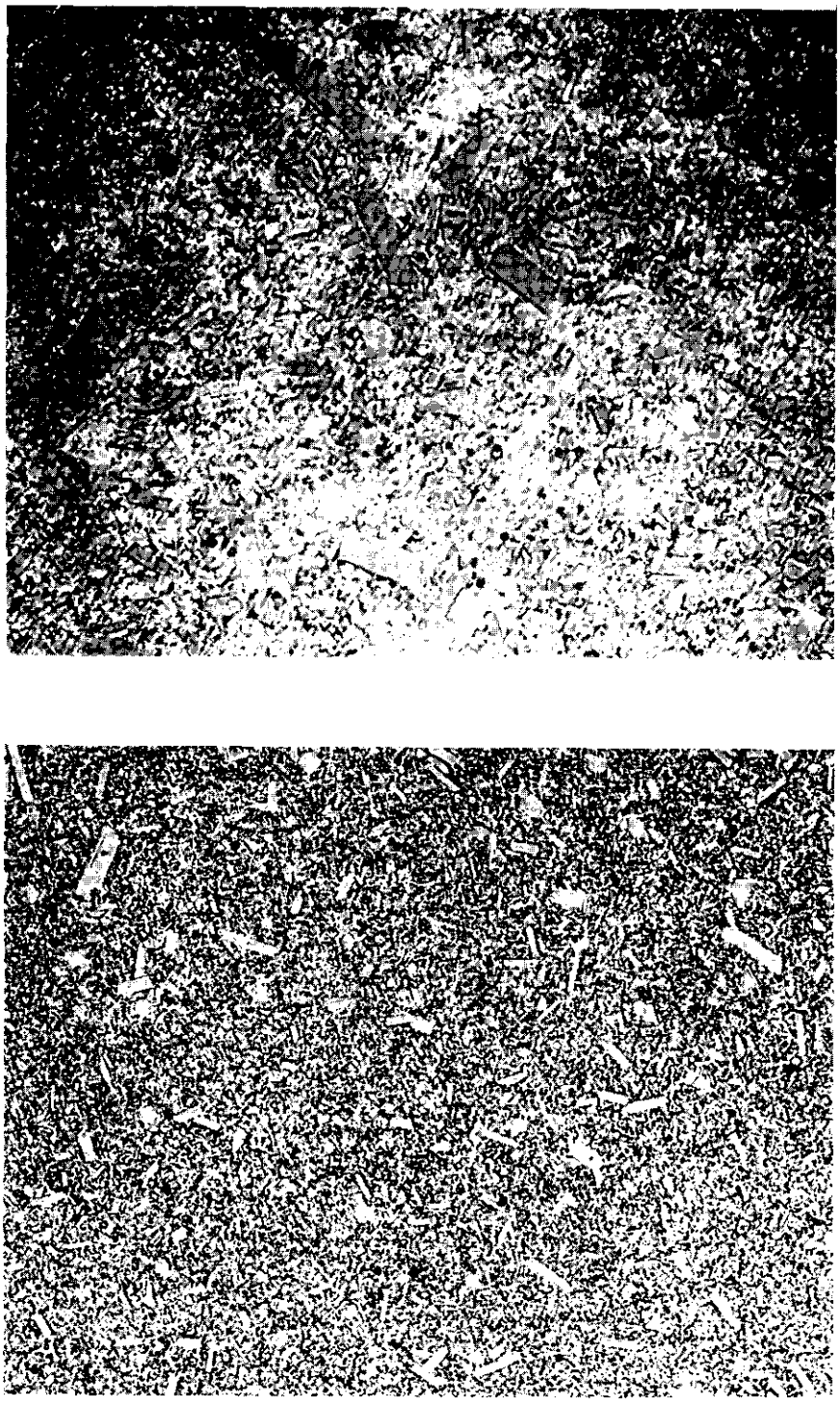

Figure F.6c. Photomicrographs (500X) of Beta"-Alumina Ceramics Formed by Either Isostatic Pressing (Upper) or Electrophoretic Deposition (Lower) and Sintered at 1600°C

Section G

BATTERY SYSTEM DESIGN

At General Electric, work on full-scale battery design was first undertaken in late 1974. The 1974 study[1] indicated that a 2.5 KWHr cell consisting of a 2 x 50 array of 1cmϕ x 15cm beta-alumina tubes mounted in a single insulating header (3.3cm x 80cm x 0.4cm in dimensions) could serve as the basic building block for the battery system. The long narrow construction was chosen so that the heat generated during operation could be removed from the sides by natural convection. Although this design (Mark I) was compact and attractive from electrical and thermal engineering standpoints, its weakness was obvious: the header geometry was impractical for typical ceramic insulators. A design (Mark II) based on a 10 x 10 array of beta-alumina tubes, sealed to a 17cm x 17cm x 0.4cm header, was then developed[2]. This design called for heat removal through forced circulation of low pressure, ambient temperature nitrogen. However, this design was subsequently abandoned because of the large seals basic to this "common header" approach and their cost and reliability implications. One experimental cell of the Mark II type was constructed and is described in the Appendix.

Battery system design is an iterative process that seeks a balance between manufacturing feasibility, operating reliability and overall cost. Mark I and Mark II designs represented two iterations of this evolutionary process. Since these iterations amply demonstrated the problems of the common header approach, an alternate approach (Mark III) is now being examined. In this design, the "building block" for the system is a "bundle" of individual cells, each complete with its own Na-chamber, S-chamber, beta-alumina tube, insulating header, etc. Each individual cell is essentially a scaled-up version of our prototype cells. The basic features of this Mark III design will be presented in this Section of the report.

Before presenting the design details, it is desirable to reiterate the design goals, underscore the considerations involved, and describe the principles applied.

G.1. Design Goals

The goals for the system design were as follows:

Rating:	20 MW/100 MWHr - Full Size Installation 1 MW/5 MWHr - BEST Installation
Operating Voltage:	1000 V dc maximum
Operating Temp.:	300 - 350°C
Battery Efficiency:	75%
Duty Cycle:	5 Hr Discharge/7 Hr Charge

Current Density: 100 ma/cm^2 Charge
140 ma/cm^2 Discharge

Footprint: > 8 KWHr/ft^2

Height: < 20 ft

It was decided that there would be no design differences between the BEST and the full size batteries, except that the latter would be proportionately larger in size than the former.

G.2. Major Considerations

The battery system designer must not only develop a design that is sound from mechanical, electrical and thermal standpoints but also take into account a number of additional considerations:

- Construction must be modular
- On-site labor must be minimum
- Modules must be serviceable
- Battery should be "oversized", if necessary, to insure nominally rated output at end-of-life
- Controlled environment building is not permitted
- Battery should be weather-proofed and insulated
- Safety features must be included to minimize chemical, electrical, fire and explosion hazards
- Impact on the environment must be negligible

Needless to say, these considerations impose on the designer a series of constraints, often with cost, manufactur-

ability and/or reliability implications. They must nevertheless be taken into account, for otherwise the acceptability of the system to utilities may be seriously undermined.

G.3. Design Methodology

Two major steps are involved in arriving at a battery system design. First, for a given set of fixed parameters (system capacity, duty cycle, efficiency - corresponding to the design goals) the system "geometry" is computed as a function of variable parameters such as electrolyte size and resistivity, etc. The second step in the design process involves system "packaging", i.e. developing a modular configuration that is thermally controllable, and footprint-wise acceptable. Many of the considerations mentioned above must be included in the "packaging" exercise.

A computer program has been developed to obtain the optimum battery "geometry", i.e. the number of cells (of given dimensions) needed for a system of specified capacity and power rating (and efficiency). The optimization carried out by this program involves iterative matching of the geometric consequences of the capacity rating with those of the power rating specified, - without sacrificing the efficiency. The basic optimization problem is best described through the following example where the objective is to arrive at the geometry of (i.e. number of individual cells in) a multicell bundle of 2 KW power rating and 10 KWHr capacity.

The parameters governing the geometry of construction of a cell bundle are related to the power rating as follows:

$$\frac{t}{A} = \frac{V_o^2}{P\rho}\left(\frac{1 - E}{1 + XE}\right) \quad 1 - \left[\left(\frac{1 - E}{1 + XE}\right)\right]$$

where t = thickness of the electrolyte tubes, cm

A = total electrolyte surface area, cm^2

V_o = open circuit potential, volts

P = power rating, watts

ρ = electrolyte resistivity, ohm-cm (assuming no losses in cathode compartment)

E = cell efficiency

X = ratio of charge rate-to-discharge rate

A 2 KW bundle with 2V open circuit potential, 5 hr charge rates, 75% efficiency and a ceramic resistivity of 5 ohm-cm would therefore, require t/A of $4.8 \times 10^{-5} cm^{-1}$. If one assumes, based on ceramic manufacturing experience, that

- Electrolyte tube length = 15 x Tube diameter, and
- Tube wall thickness = 0.06 x Tube diameter,

then for tubes of, say, 0.15 cm wall thickness (hence 2.5cm dia and 37.5cm length), a total of about $2.5 \times 10^3 cm^2$ of ceramic surface area would be required. This would correspond to 9 electrolyte tubes of the given dimensions.

The ceramic area, however, must be adequate to meet the capacity or the stored energy specification. Relationship

of the following type exists among the ceramic surface area, the storage capacity and the diffusion path length in the sulfur compartment:

Area = Constant x Energy/Diffusion Path Length

(Note that Na/S cell capacity in present design is governed by sulfur electrode capacity; excess Na is available.)

The stored energy required for the cell fixes the volume of the sulfur compartment. Present test cells have a diffusion path length of 0.65 cm, which is probably near the maximum allowable for obtaining high utilization and low resistive losses. Cells made with electrolyte tubes 2.5 cm diameter and 37.5 long and 0.65 cm thick sulfur compartment, would have enough sulfur for 120 Ah of discharge capacity, - allowing for 10% void volume and 80% utilization. This would correspond to $\sim$ 200 WHr at the 5 hr discharge rate. On this basis, 50, rather than 9, cells are required to meet the 10 KWHr capacity specification.

The above example illustrates the optimization problem faced in battery design. As mentioned before, the program developed at General Electric addresses the optimization problem in an iterative mode. The program

- assumes a certain thickness for the cathode compartment;
- calculates a trial number of tubes needed for the system;
- calculates current to match efficiency;

- compares (current x discharge time) capacity with assumed capacity to give utilization of cell capacity;
- assumes a new cathode (and cell) size;
- iterates until it finds the discrete number of cells which have capacity and efficiency to satisfy all system design goals.

Table G.1 and G.2 summarize some of the most useful outputs from this geometry analysis. Table G.1 shows the non-linear relationship between electrolyte tube size and the number of cells required per MWHr of system capacity. Also shown is the corresponding energy density (assuming 0.1 cm thick steel containers). Table G.2 shows the number of cells required per MWHr of capacity for 20 different combinations of electrolyte resistivity and cathode (S+C) resistivity. This table is for electrolyte tubes of 2.5 cm dia.; similar tables have been generated for other tube sizes as well.

Information presented in Tables G.1 and G.2 are prerequisite to subsequent cost/manufacturing feasibility/ operating reliability trade-offs through which an optimum geometric package must emerge for detailed thermal, mechanical and electrical design.

G.4. Mark III Design Details

It was mentioned before that in the Mark III design, the "building block" for the battery is a bundle of individual cells, each complete with its own ceramic electrolyte tube, Na-chamber, S-chamber, etc. The cell design is shown in

TABLE G.1

DEPENDENCE OF NUMBER OF CELLS AND CELL

ENERGY DENSITY ON ELECTROLYTE TUBE SIZE

Tube Dia. (cm)	No. of Cells Needed (per MWHr)	Correspond. Cell E.D. (WHr/Kg)
1.0	12,428	144
1.5	6,950	148
2.0	4,549	147
2.5	3,261	142
3.0	2,481	134
3.5	1,970	126

Assumptions: Tube Length = 15 x Tube Diameter

Tube Wall Thickness = 0.06 x Tube Diameter

Na- and S-containers are made of 0.1 cm thick steel

System Operated at Constant Power

TABLE G.2

NUMBER OF CELLS REQUIRED FOR 1 MWH SYSTEM
FOR VARIOUS COMBINATIONS OF ELECTROLYTE AND
CATHODE (S+C) RESISTIVITIES

S-Electrode Resistivity Ohm. Cm. \ Electrolyte Resist. Ohm. Cm.	3.5	7.0	10.5	14.0
2.2	2,742	3,261	3,807	4,377
2.8	3,086	3,592	4,125	4,681
3.3	3,403	3,899	4,421	4,965
3.9	3,698	4,187	4,700	5,234
4.4	3,976	4,458	4,963	5,489

Assumptions: Electrolyte Tube Dia = 2.5 cm.
Electrolyte Tube Wall Thickness - 0.15 cm.
Electrolyte Tube Length = 37.5 cm.
System Efficiency = 75%
System Rating - 0.2 MW

cross-section in Fig. G.1. It is very similar to the present test cells, except for size, seals and some safety features not shown in the figure but discussed below. Table G.3 gives the cell dimensions and ratings; it also provides information on number, size and ratings of bundles, modules, sections, banks needed for 100 MWHr full-size battery installation.

A bundle consists of a 5 x 8 array of individual cells connected in parallel. Nine of these bundles are connected in series to form a module. Figure G.2 shows the arrangement of cells and bundles within a module. Thermal controls are shown at the front end of the module. In Figure G.3 two sections are shown, each containing 24 modules connected in series; these two sections constitute the BEST battery. A section will have a maximum voltage rating of 500 volts (end of charge voltage) and an average discharge voltage of 360 volts at 1500 amps. Thus two of these sections in series will form the BEST Facility test battery, with a 1MW, 5KWHr rating. The battery will have 5-hour discharge/7 hour charge rates and 75% overall efficiency (dc-to-dc).

---

* The design described here is more appropriately designated as Mark IIIA to distinguish it from the "Mark III" design discussed in a recent publication[3]. Both designs are based on the same approach; the major differences are in footprints (footprint for the design in Ref. 4 is $\sim$ 2 KWHr/ ft^2) and thermal engineering details.

TABLE G.3

BATTERY SYSTEM SPECIFICATIONS

(MARK IIIA DESIGN)

Cell Rating:	185 Ah/300 WHr/60 W
Cell Size:	20.9" L X 1.77"ϕ
No. of Cells/Bundle:	40 in parallel
Bundle Rating:	7397 Ah/12.1 KWHr/2.42 KW
Bundle Size:	14" L X 17" W X 22" H
No. of Bundles/Module:	9 in series
Module Rating:	7397 Ah/104 KWHr/20.8 KW
Module Size:	10.6' L X 1.5' W X 4' H
No. of Modules/Section:	24 in series
Section Rating:	7397 Ah/2.5 MWHr/500 KW
Section Size:	12' L X 11' W X 20' H
No. of Sections/Bank:	10
No. of Banks/System:	4
System Rating:	100 MWHr/20 MW
System Size:	126' L X 90' W X 20' H
System Footprint:	8.8 KWHr/ft^2

(If 1162 sq. ft. were made available as accessory space, footprint would drop to 8.0 KWHr/ft^2).

Shown in Fig. G.4 is a full size battery installation, with a capacity of 100 MWHr and power rating of 20MW. In this installation groups of ten sections form a bank. Whereas the BEST Facility battery consisted of two sections, each with forty cell modules (432 bundles), the larger number of modules in a 100MWH system permits several alternative series/ parallel combinations. This allows for matching the battery to power conditioning equipment with the most practical current vs. voltage trade off.

Several safety features are provided in the system. Each cell will have a metal diaphram with small holes in it to restrict the flow rate of sodium from the sodium compartment into the inner electrolyte tube. In addition a large fraction of the volume of the electrolyte tube will consist of an inert solid material such as alpha alumina grains. Therefore, in case of fracture of the electrolyte tube there will be less sodium in the vicinity of the sulfur; thus initial energy of the reaction will be reduced, and subsequent reaction from more sodium coming out of the sodium compartment will be retarded. It is projected that these features will limit the failure to this individual cell and not cause failures in adjacent cells.

Each module is enclosed in a gas tight steel container under a slight positive pressure of nitrogen gas to permit cooling a failed module without oxidation of any sodium or sulfur and escape of SO_2 gas or sodium oxide smoke.

Thermal control is maintained separately in each module by circulating hot nitrogen vertically through the bundles of cells. Circulation is obtained with fans connected with a shaft to electric motors which are shown on the exterior of each module (Fig. 3). Excess heat is removed by heat exchangers employing a heat transfer liquid. The heat transfer liquid is also used to supply external heat to each module for initial warm-up and temperature maintenance during long idle periods. (Appendix II provides detailed description of components provided for thermal control of modules.)

Figure G.4 shows some further design features. The battery is weatherproofed for installation outdoors and is placed on a concrete slab (126' x 90'). The two center banks are placed back to back allowing for two 15 foot access aisles which are wide enough to remove a full module. The roof is slanted away from accessible face of the banks. The large size of a bank reduces insulation cost to less than 1% of the total basic raw materials and purchased component costs.

G.5 Summary

During the report period, Mark III design was developed. In this design, the building block for the system is a "bundle" of individual cells, each essentially a scaled-up version of our present test cells. A bundle is designed to

consist of a 5 x 8 array of individual cells connected in parallel. Nine of these bundles are connected in series to form a "module", i.e. a thermally self-sufficient unit. The modules are then arranged into 500 V (End-of-Charge)/ 360 V (Discharge), multi-level sections with 1500 amps rating. Each module is enclosed in a gas-tight steel container under a slight positive pressure of nitrogen gas to permit cooling of a failed module without oxidation of any sodium or sulfur and escape of SO_2 gas or sodium oxide smoke. Thermal control is maintained separately in each module by circulating hot nitrogen vertically through the bundles of cells. Circulation is performed within each module with a fan connected with a shaft to a motor placed outside the module. Excess heat is removed by heat exchangers employing a liquid heat transfer fluid. The heat transfer fluid is also used to supply external heat to each module for initial warm-up and temperature maintenance during long idle periods.

The entire battery is designed to be weatherproof for outdoor installation on a concrete slab. The large size of each bank of batteries reduces insulation cost drastically. The overall footprint for the battery is > 8 KWh/ft^2 because of the modular, multi-level design.

References

1. Sodium-Sulfur Battery Development for Bulk Power Storage: Conceptual Battery Design for BEST Facility, EPRI Project 128-2 (Addendum), General Electric Co. Report SRD-74-130, Schenectady, New York, December 1974.

2. Development of Sodium-Sulfur Batteries For Utility Application, EPRI Project 128-3 Annual Report. (EPRI Report No. EM-226), General Electric Company, Schenectady, New York, December 1976.

3. S.P. Mitoff, M.W. Breiter, and D. Chatterji, Proc. Eleventh Intersociety Energy Conversion Engineering Conference, August 1977.

List of Figure Captions

List of Tables

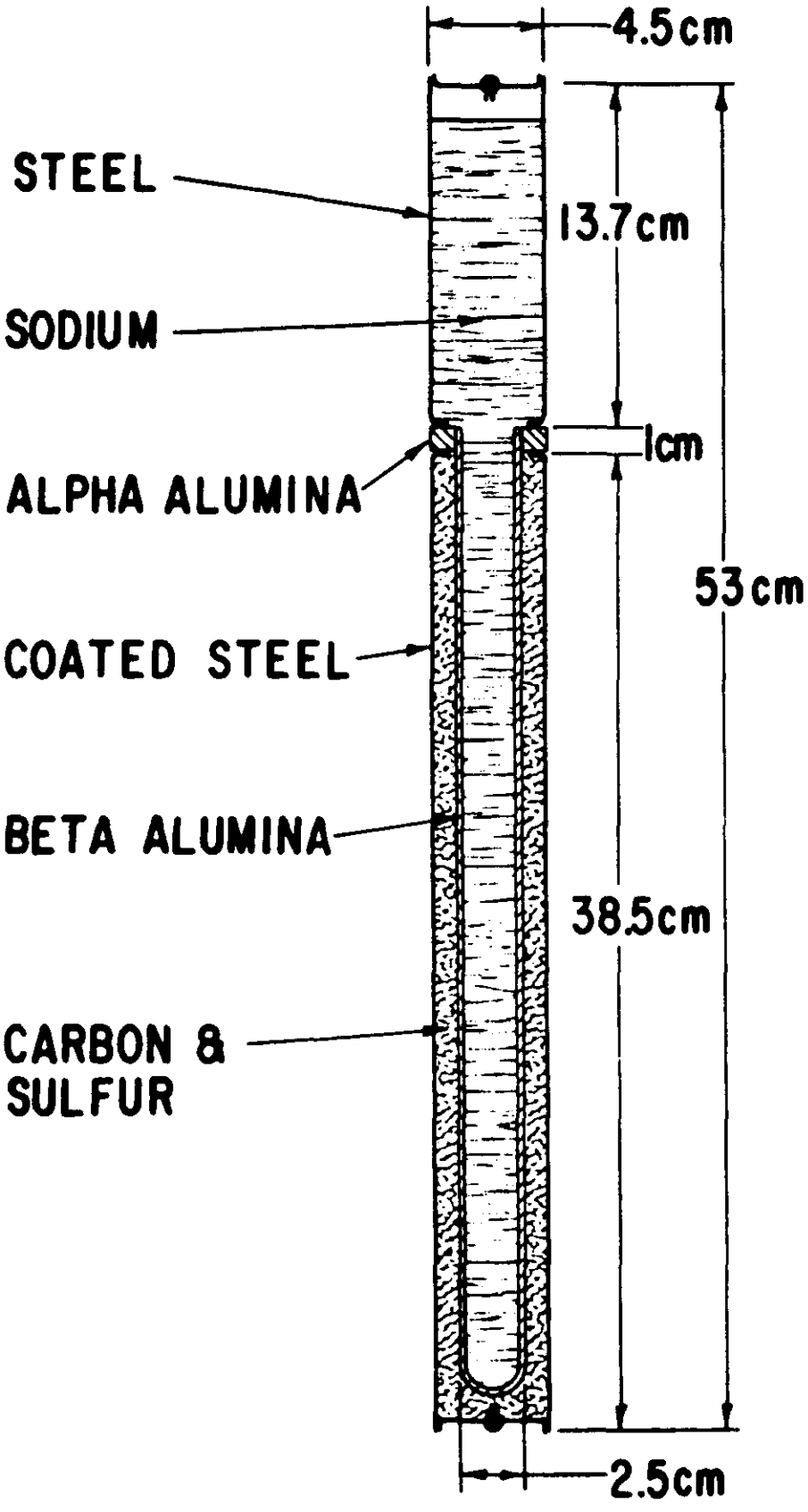

Figure G.1. Cross-Section of the Full Size Cell-185 Ah Capacity (Schematic).

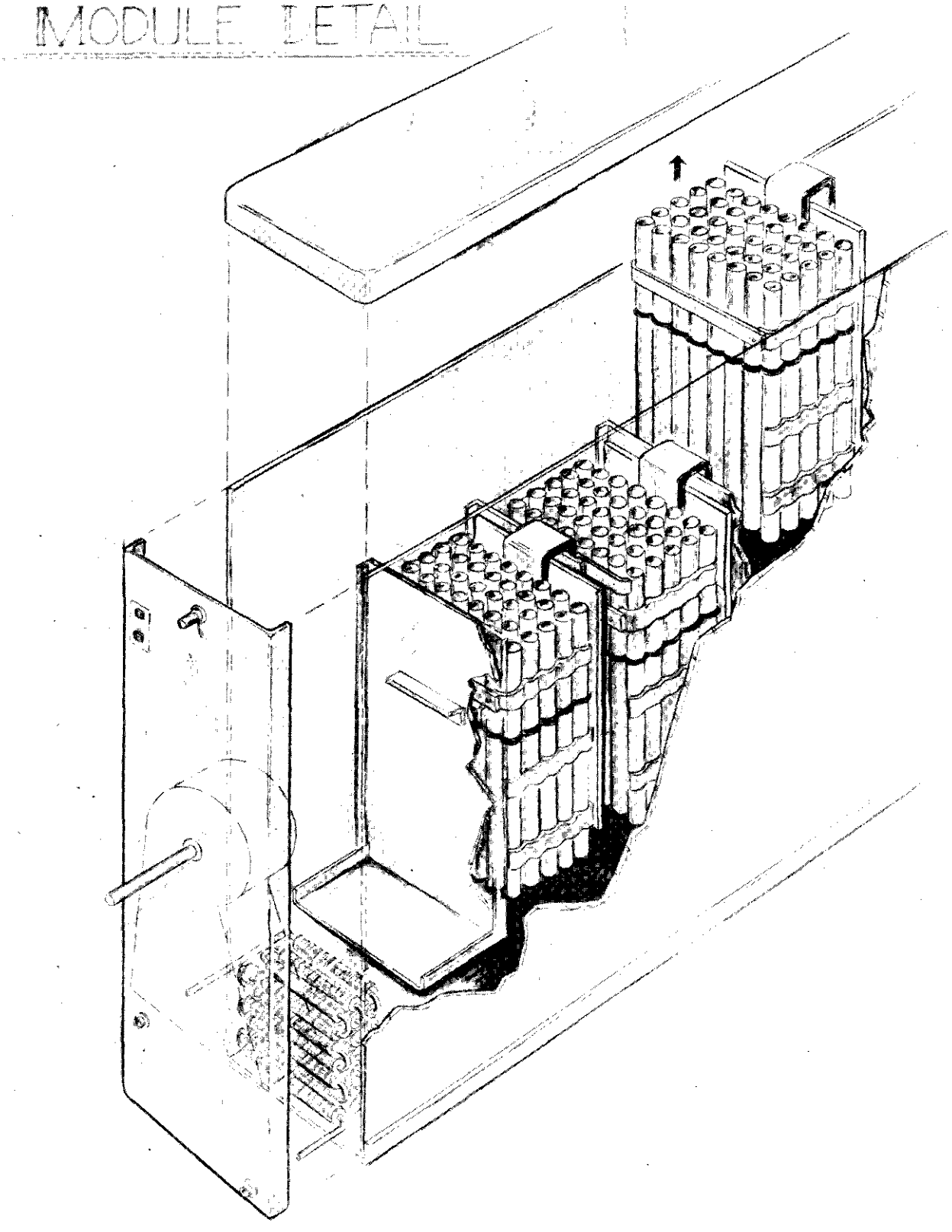

Figure G.2. Arrangement of Cells and Bundles Within a Module (Schematic)

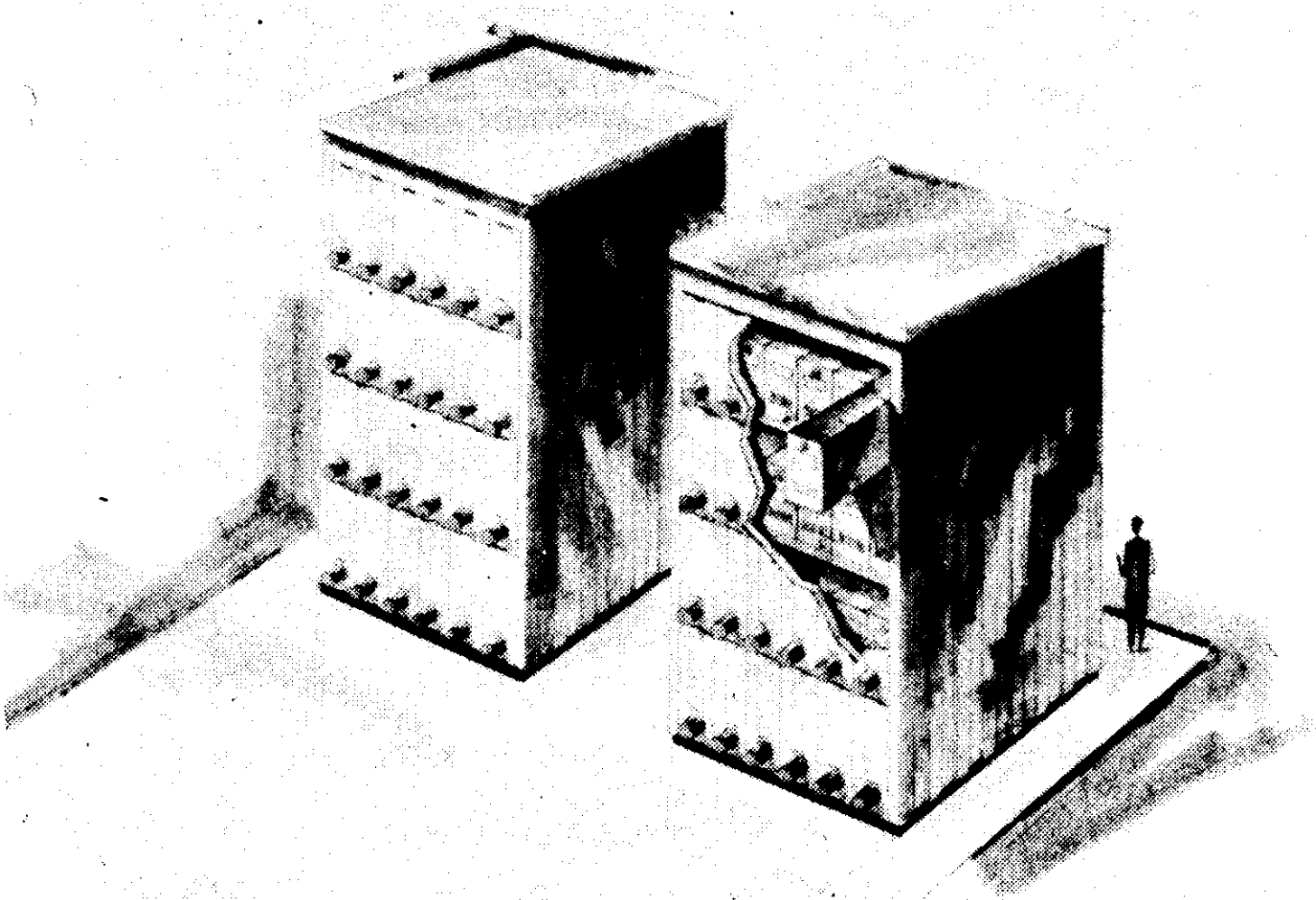

Figure G.3. The BEST Battery in Two Sections: Mark IIIA Design

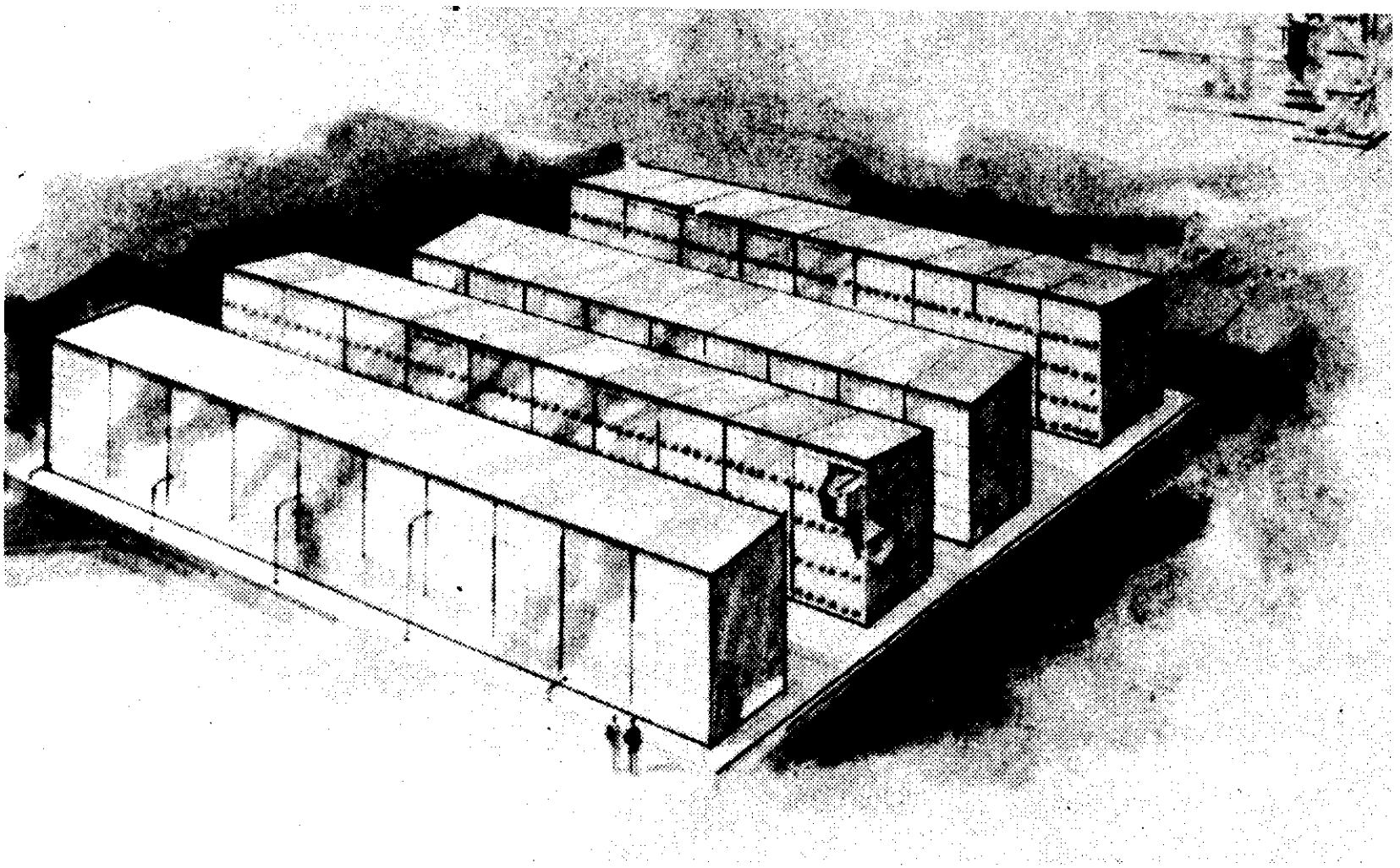

Figure G.4. The Commercial-Size Battery (20 MW/100 mWh) for Utility Application: Mark IIIA Design

Section H

BATTERY MANUFACTURING AND COST STUDIES

During 1976-77 a group of engineers from GE's Manufacturing Engineering Consulting Services completed a number of manufacturing engineering/cost studies. In this Section summaries are given of two such studies. The first consists of conceptualization of a plant capable of producing a number of commercial-size peaking batteries and cost projections for such a facility. The second study examined battery cost as a function of ceramic tube dimensions.

H.1. Cost Projections for Commercial Size (20 MW/100 MWH) Batteries

This study included 1) conceptualization of a battery plant capable of producing 25 battery systems per year, each rated at 20 MW/100 MWHr, 2) preliminary estimates of resources needed (investment, materials, labor and space), and (3) projections for the factory cost and the FOB selling price per battery. These manufacturing engineering and cost studies were based on the EPRI definitions[1] of "standard" battery and "standard" manufacturing plant and the EPRI-recommended cost-calculation procedures. The immediate objective of this analysis is to identify the materials/manufacturing steps where further technological developments could lead to significant cost reduction. The ultimate

objective, of course, is to determine if the projected selling price is compatible, within limits, with the capital cost estimated to be generally acceptable to the utilities[2].

Table H.1 lists the elements of the "factory cost" per year and per battery, and Table H.2 presents the projected "selling price" per battery. As can be seen from Table H.1, materials constitute 85% of the factory cost of the battery. Table H.3 presents a breakdown of the material costs per battery; cost for basic raw materials is roughly comparable to the cost for purchased components. Among the basic raw materials, container materials (steel tubes and sheets) and conductors (copper and aluminum) are the largest cost items. Among the purchased parts, the heat transfer/control related components constitute a large cost element.

The manufacturing cost studies envisioned a plant operating at full capacity in 1985. The costs given in Tables H.1 - H.3, however, refer to 1977 dollars. It must be emphasized that the plant is conceptualized on the basis of the technology status likely to be achieved by the end of 1978. This is not intended to mean that all manufacturing processes would be fully developed and automated production of full scale components at the design yield rates demonstrated by the end of 1978. It is safe to say, however, that by the end of 1978 (hopefully sooner) all design, material and

TABLE H.1

ELEMENTS OF TOTAL FACTORY COST PER YEAR
FOR PRODUCTION OF 25 FULL SIZE BATTERIES,
EACH OF 20 MW/100 MWHr RATING

Total Investment	$13,356,000	
Yearly Amortization @ 10 Yr S/L		$ 1,345,600
Freight & Installation @ 25% of Equip. Investment	3,346,000	
Yearly Amortization @ 10 yr S/L		336,400
Materials		61,925,000
Overhead @ 10% of Materials		6,192,500
Labor @ $7.50/Man-Hour		4,810,500
Overhead @ 150% of Labor		7,215,800
Rent @ $3,75/($ft^2$) (Year)		633,400
Total Factory Cost Per Year		$82,459,200
Total Factory Cost Per Battery @ 25 Batteries/Year		$ 3,298,400

Note: For details on cost calculation procedure, see Ref. 1

TABLE H.2

ESTIMATED SELLING PRICE FOR
A 20 MW/100 MWHr BATTERY

Factory Cost Per Battery (From Table X)		$3,298,400
Working Capital Per Battery: (30% of Factory Cost)	$ 989,510	
Investment Per Battery:	$ 672,800	
ROI Base	$1,662,310	
After-Tax ROI (15% of ROI Base):		$ 249,350
Taxes (=After-Tax ROI)		$ 249,350
Selling Price Per Battery:		$3,797,100
Salvage Value (Present Worth):		$ 27,400
Net Selling Price Per Battery:		$3,769,700

Price Per KWHr:	$ 37.70
Price Per KW :	$188.50

Note: For details on cost calculation procedure, see Ref. 1.

TABLE H.3

BREAKDOWN FOR MATERIAL COST
PER 20 MW/100 MWHr BATTERY

Basic Raw Materials	Cost ($1000)	% of Total
Steel, Tube	400	16.1
Steel, Sheet	294	11.9
Ceramics	266	10.7
Aluminum	116	4.7
Chemicals	108	4.4
Copper	109	4.4
Steel, Structural	35	1.4
Instulation, Thermal	21	0.8
Sub Total	1,347	54.4
Purchased Components		
Isolators, Electrical	221	8.9
Fans and Motors	226	9.1
Controller	211	8.5
Heat Transfer System	191	7.7
Bushings, Electrical	120	4.9
Sensors	71	2.9
Heaters	36	1.5
Miscellaneous	31	1.3
N_2 Replenishment System	21	0.8
Sub-Total	1,128	45.6
Total For 1 Battery	$2,474,000	100.0
Total For Year (25 Batteries)	$61,175,000	100.0

process-related decisions would have been completed, scale-up processes for critical components demonstrated in a pre-pilot plant scale, and the experience base for manufacturing technology development generated. The Mark III design, for example, is based on 7 ohm-cm ceramic resistivity (already achieved) and 0.0087 ohm cell resistance (equivalent of 0.0125 ohm achieved).

It is important to bring out at this point some of the major assumptions involved in the study. These assumptions are listed below.

1. Mark IIIA design will be used.
2. Ceramic electrolyte tubes will be formed electrophoretically.
3. Certain proprietary coating and sealing processes will be used.
4. Within the bundles, the intercell connectors are made of copper, but the inter-bundle connectors are made of aluminum. This scheme requires steel-to-copper and copper-to-aluminum welding technologies.

Needless to say, a number of manufacturing processes had to be envisioned and costed out. Present processes and operations were conceptually scaled up wherever possible (i.e. electrophoretic forming of beta-alumina tubes). In some cases, comparable industrial processes were considered instead of a direct scale-up of the present laboratory practice (e.g. coating operation). In any case, the "standard" battery manufacturing plant was intended to reflect a "semi-

mature" state of technology, i.e. a full-scale production facility in its second or third year of production. No "learning curves" were assumed.

It is indeed encouraging to note that the estimated battery selling price* of $188/KW (∿$38/KWHr) is well within the range of capital cost reported[2] to be acceptable to the utilities: $210 - 440/KW (for a 5-hour battery operating 1000 hours annually). Selling price estimates recently made by other developers[3, 4] of sodium-sulfur batteries are, interestingly enough, comparable to the GE projection.

There are some reasons to believe that the EPRI recommended guidelines followed in computing costs and selling prices may have resulted in low estimates. These should be mentioned, although the actual impact of each has not been well assessed. They include:

a. the lack of any intentional contingency allowance in the estimates for factory cost components,

b. the use of an unrealistically high final product yield (95%) from incoming raw materials and purchased components. There are multiple step processes whose individual yields

---

* The projected selling price does not include the following cost items: battery transportation, site preparation, concrete pad installation, AC/DC power conversion device, computerized control station, central heat disposal/recovery system. The last item may pay for itself if a district-heating market exists for the utility.

affect the output requirements forpreceding steps. For example, yields in the filling and closure of cells affect the output required from cell case fabrication, metal-to-ceramic sealing, beta-to-alpha sealing and beta-tube manufacture,

c. the probability that a manufacturing overhead higher than 150% on direct labor will prevail in a "semi-mature" plant wherein a considerable degree of automation has been included,

d. the lack of provisions for the cost of some necessary business adjuncts such as market development, technical service, legal service, general company management, etc., other than their possible inclusion in the 150% overhead on factory direct labor. For example, a 15%-25% G&A adder to total factory cost would not be unusual,

e. the commonly high percentage of total calculated selling price due to manufacturing materials (72%). Experience would say that this almost certainly means that some important cost contributions have been omitted or underestimated.

H.2. Battery Cost as Function of Electrolyte Tube Dimensions

The computer analysis discussed in Section G under "Design Methodology" cites the number of cells and the geometric constants for each cell as a function of beta alumina tube size. Although this study sets some technological limitations on tube size, the range is broad combining the computer study with a manufacturing cost study which results in an optimum size. For the purposes of the cost study, eleven different beta" alumina tube sizes were considered. In one series the diameters from 2.0 to 5.0 cm were considered with tube lengths being 15 times the diameter and wall thickness 0.06 times the diameter. In the other series diameter and thickness were varied in the same way but tube length was held constant. A report of the findings is summarized below.

We have found that changing the beta-alumina electrolyte tube diameter over the range from 2.00 to 5.00 centimeters (with length and wall thickness correspondingly varied according to the two different formulae) produces a variation in manufacturing cost of approximately $500,000 per battery or $5 per kilowatt hour capacity. The largest effect is in materials costs, which steadily increase with tube diameter. Labor cost, which decreases continuously as tube diameter increases over this range, is of a lower magnitude.

Optimum (lowest) manufacturing cost is in the 2-3 cm diameter range, with the actual choice depending slightly upon the particular scaling formula used to relate other dimensions and material quantities to the beta-tube diameter.

The analysis was made on the basis of materials and labor costs given earlier in this section which showed that overheaded materials and labor account for more than 97% of the factory cost (See Table H.1). Therefore, it was deemed unnecessary to consider the effects of varying tube size on equipment investment or factory floor space, since any perturbations on those costs would have insignificant impact on the total factory cost.

H.2.1. Material Costs

Of the basic raw materials used in manufacture (See Table H.3), those expected to vary significantly with

beta-alumina tube size and number are the following:

1. Steel tube (for cell cases)
2. Steel sheet (for module cases)
3. Ceramics (for beta-tubes and alpha-separator, saggers, bedding beta-alumina)
4. Chemical - sodium (total sulfur and carbon are held constant)

The total copper and aluminum for current collectors was assumed to remain relatively constant because the total power output of the battery and total resistance losses of the current collector system outside the cells, proper, were expected to be the same.

Structural steel for frames and insulation, while they both would vary somewhat, were not evaluated since they contribute very small percentages to total material cost.

All purchased components depend only on the number of modules, which was chosen to remain nearly constant, or are independent of number of modules over a considerable range. Thus, the total cost for purchased components can be expected to remain nearly constant as tube size and number of tubes vary.

The data for material quantities utilized in making the cells were derived from a series of computer runs and are presented in Table H.4. Calculated costs for cell materials for each of the 11 cases and the original case from reference #1 are given in Table H.5.

The other major source of variable material cost is the steel sheet used in module case fabrication. Some variations

TABLE H.4

DATA FROM COMPUTER PROGRAM "CONDUIT"

	— Tube Length, diam, wall thickness scaled together —						Tube Length constant; wall thickness, diam. scaled					
Case No. →	0 (Present)	1	2	3	4	5	6	7	8	9	10	11
DOB-cm.	2.50	2,00	3.00	3.50	4.00	5.00	2.00	2.80	3.00	3.50	4.00	5.00
LOB-cm.	37.5	30.00	45.0	52.5	60.0	75.0	37.5	37.50	37.50	37.50	37.50	37.50
TB-cm.	,150	.120	.180	.210	.240	.300	.120	.168	.180	.210	.240	.300
No. of Tubes	326,061	454,872	248,128	197,008	161,472	116,241	365,625	307,576	296,862	274,429	256,694	230,571
WNA-g	284	178	424	605	832	1445	222	325	354	433	521	722
WS-g	414	297	544	685	836	1161	369	439	455	492	526	585
WCN-g	2108	1413	2975	4029	5292	8517	1743	2342	2503	2929	3388	4412
WB-g	135	69	234	371	554	1082	87	170	195	265	346	541
WALPH-g	67	54	82	97	115	154	54	76	81	97	114	153
DOCN-{cm.	4.63	4.16	5.11	5.58	6.06	7.03	4.16	4.91	5.10	5.57	6.05	7.00
DOCN-{(in.)	(1.82)	(1.64)	(2.01)	(2.20)	(2.39)	(2.77)	(1.64)	(1.93)	(2.01)	(2.19)	(2.38)	(2.76)
TCN-{cm.	.178	.159	.196	.214	.232	.269	.159	.188	.196	.214	.232	.268
TCN-{(in.)	(.070)	(.063)	(.077)	(.084)	(.091)	(.106)	(.063)	(.074)	(.077)	(.084)	(.091)	(.106)
DIAS-{cm.	4.28	3.84	4.72	5.16	5.60	6.49	3.84	4.54	4.71	5.15	5.59	6.47
DIAS-{(in.)	(1.685)	(1.51)	(1.86)	(2.03	(2.20)	(2.56)	(1.51)	(1.79)	(1.85)	(2.03)	(2.20)	(2.55)
LOCN-{cm.	53.20	44.20	61.81	70.10	78.15	93.71	54.62	52.41	51.90	50.74	49.71	47.97
LOCN-{(in.)	(20.94)	(17.40)	(24.33)	(27.60)	(30.77)	(36.89)	(21.50)	(20.63)	(20.43)	(19.98)	(19.57)	(18.89)
WCB-g	41	30	54	68	84	116	37	44	45	49	53	59

Legend: DOB = O.D. of beta-tube; LOB = Active beta-tube length; TB = beta-tube wall thickness; WNA = Wt. of sodium; WS = Wt. of sulfur;
WCN = Wt. of steel containers per cell; WB = Wt. of beta-alumina; WALPH = Wt. of alpha-alumina separator; DOCN = O.D. of steel containers;
TCN = Wall thickness of steel containers; DIAS = I.D. of steel containers; LOCN = Outside length of steel containers;
WCB = Wt. of carbon

TABLE II.5

CELL FABRICATION - MATERIAL COSTS PER BATTERY

Case No. ⟶	0(Present)	1	2	3	4	5	6	7	8	9	10	11
Sodium	$ 30,000	26,230	34,080	38,610	43,500	54,480	26,310	32,370	34,020	38,520	43,320	53,910
Sulfur	15,000	15,000	15,000	15,000	15,000	15,000	15,000	15,000	15,000	15,000	15,000	15,000
Steel Containers	400,000	374,000	429,600	461,600	496,800	576,800	370,800	419,200	432,000	468,000	506,000	592,000
β-alumina	112,000	79,856	147,728	185,920	227,472	320,432	80,864	132,944	147,168	185,136	225,904	317,296
α-alumina	79,000	88,796	73,549	69,125	67,071	64,859	71,416	84,451	86,900	96,301	105,781	127,585
Carbon	35,000	35,735	35,070	35,070	35,490	35,350	35,385	35,420	34,965	35,210	35,630	35,595
Summation	671,000	619,637	735,027	805,325	885,333	1,066,921	599,775	719,385	750,053	838,167	931,635	1,141,386

in module size occur as cell dimensions and numbers of cells change. Table H.6 indicates how such changes are reflected in material cost for steel sheet. The combined incremental costs for cell and module case materials are shown in Table H.7.

H.2.2. Labor Costs

Eighty percent of the total labor man-hours (26,000 per battery) is devoted to 12 operations, and these were evaluated for effect of beta-alumina tube size. All other operations require individually less than 500 man-hours per battery. Those considered were:

1. Electrolyte tube fabrication
2. Sulfur container-form flange and cut to length
3. Sodium container-form flange and cut to the length
4. Glass sealing electrolyte tube to separator
5. Cell assembly by thermo-compression bonding
6. Cathode current collector assembly
7. Fill and seal sodium and sulfur containers
8. Attach current collectors to cells
9. Bundle assembly
10. Module case fabrication
11. Module assembly
12. Paint exterior panels

For the above 12 operations, the total incremental labor in terms of man-hours and cost (overheaded at 150%) is given in Table H.8.

TABLE H.6

COST OF STEEL SHEET FOR MODULE CASES IN 100 MWH BATTERY AS A FUNCTION OF β-TUBE SIZE

Steel Sheet Cost - (cost per case 0)x(Module No. Ratio, $\frac{N_i}{N_o}$)x(Area Ratio $\frac{A_i}{A_o}$)

Cost for Case 0 = $294,000

Case	No. Modules	$\frac{N_i}{N_o}$	$\frac{A_i}{A_o}$	Steel Sheet Cost
0	960	1.000	1.000	$294,000
1	957	.997	.966	291,946
2	940	.979	1.018	293,007
3	933	.972	1.057	302,057
4	951	.991	1.188	346,129
5	963	1.003	1.277	376,364
6	923	.961	1.116	315,308
7	927	.966	1.117	317,232
8	899	.936	1.135	312,334
9	909	.947	1.153	321,016
10	907	.945	1.257	349,232
11	926	.965	1.385	392,938

TABLE H.7

INCREMENTAL COST COMPARED TO PRESENT DESIGN FOR CELL MATERIALS PLUS STEEL SHEET FOR MODULE CASES

Case No.	ΔCell Materials	ΔModule Case Steel	ΔSum/Battery
0	0	0	0
1	- 51,363	- 2,054	- 53,417
2	+ 64,027	- 993	+ 63,034
3	+134,325	+ 8,057	+142,382
4	+214,333	+52,129	+226,462
5	+395,921	+82,364	+478,285
6	- 71,225	+21,308	- 49,917
7	+ 48,385	+23,232	+ 71,617
8	+ 79,052	+18,334	+ 97,387
9	+167,167	+27,016	+194,183
10	+260,635	+55,232	+315,867
11	+470,386	+98,938	+569,324

Note: Original (Case 0) total material cost, without overhead is $2,477,000. Percentage changes, therefore, range from -2.16% to +23.0% on original cost.

TABLE H.8

SUMMARY - INCREMENTAL LABOR COSTS/BATTERY
AS A FUNCTION OF β-ALUMINA TUBE SIZE

Case	β-Tube Diameter cms.	Δ Man-Hrs. Required $(H_i - H_o)$	Δ Labor Cost @ $18.75/hr. w/150% O.H.
0	2.50	0	0
1	2.00	+3,979	+ 74,606
2	3.00	-3,152	- 59,100
3	3.50	-4,730	- 88,688
4	4.00	-5,535	-103,781
5	5.00	-7,415	-139,031
6	2.00	+2,216	+ 41,550
7	2.80	+ 203	+ 3,806
8	3.00	- 973	- 18,244
9	3.50	-1,396	- 26,175
10	4.00	-2,251	- 44,206
11	5.00	-2,379	- 44,606

H.2.3. Total Incremental Labor and Materials Costs

Overheaded labor cost increments from Table H.8 and materials cost increments from Table H.6 (with 10% overhead on materials added) are plotted graphically against the outside diameter of the beta-alumina tubes (DOB) in Figure H.1. Included also are curves for the sum of the materials and labor increments for each case. Cases 0-5 have simultaneous variations in beta-tube diameter, length and wall thickness. Cases 6-11 have essentially constant tube length and variations in tube diameter are accompanied principally by changes in wall thickness.

H.2.4. Conclusions

With the labor and overhead rates ($7.50/hour and 150%) established for this study, changes in factory cost per 100 MWH battery brought about by variations in beta-tube dimensions are dominated by materials costs increments.

Minimum cost appears to lie in the smaller tube size range, between 2 and 3 centimeters O.D.

If, as seems likely, the actual labor overhead should be higher than the 150% assumed, the tube size for minimum manufacturing cost would shift to a slightly larger diameter.

References

1. Proposed Criteria for Estimating the Capital Costs of Advanced Battery Systems for Utility Energy Storage, EPRI Project 787-1 Interim Report, Arthur D. Little, Inc., Cambridge, MA, November 1976.

2. An Assessment of Energy Storage Systems for Use By Electric Utilities, EPRI Project 225, Final Report (EPRI Report No. EM-264), Public Service Electric and Gas Company, Newark, NJ, July 1976.

3. Sodium-Sulfur Battery System, ERDA Report No. EY-76-C-02-2565* 000-4, Annual Report For The Period May 19, 1975 - May 19, 1976, Dow Chemical Company, Walnut Creek, CA, November 1976.

4. Improvements of Electrolyte and Seal Technology For Sodium-Sulfur and Sodium-Antimony Trichloride Load-Leveling Batteries, EPRI Project 726-1 Final Report, Compagnie Generale de Electricite, Marcoussis, France, May 1977.

List of Figure Captions

Figure H.1 Incremental Labor and Material Costs Per Battery as a Function of Beta-Alumina Tube Size

List of Tables

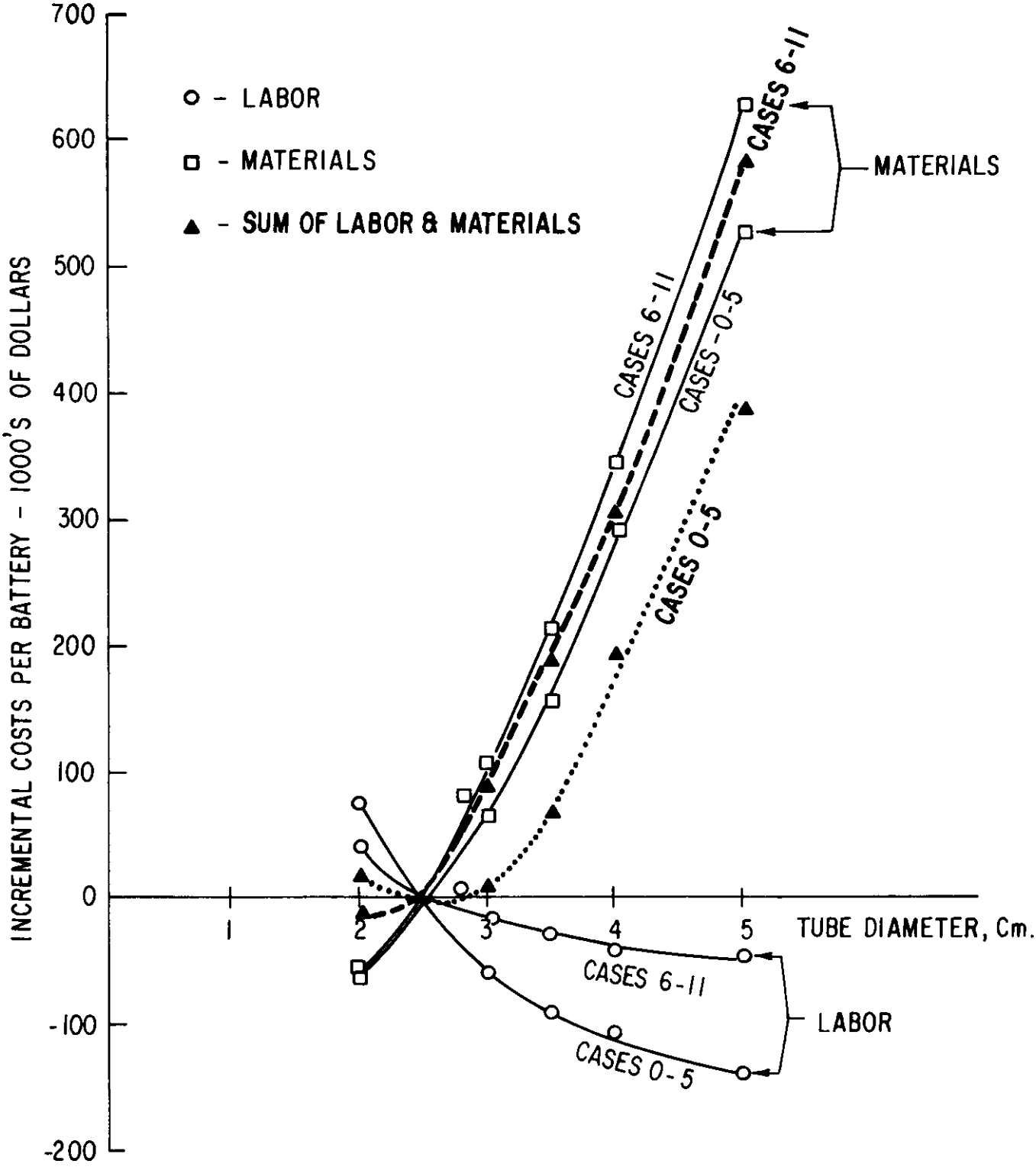

Figure H.1. Incremental Labor and Material Costs Per Battery As a Function of Beta-alumina Tube Size

Section I

DESCRIPTION OF COMPONENTS PROVIDED FOR THERMAL CONTROL OF MODULES

The system of components provided with each module for thermal purposes, is illustrated in Fig. I.1. It comprises the components described below. The dimensions and performance features are considered later.

(1) The nine "bundles" of cells. Each bundle consists of a matrix of 5 x 8 cells, with the cell axes vertical and the gas flow vertically in the interstitial spaces between adjacent cells.

(2) Busbar Straps. Each strap feeds electrical current to or from a set of 5 cells. One set of straps is connected to the upper portion of the cells (sodium reservoir). Two other sets of straps are connected to the sulfide container tube--one set near the top of the tubes, the other set near the bottom. A small horizontal distance is provided between successive bundles of a module for electrical connections to the bottom.

(3) Inlet and outlet manifolds for distributing and collecting the gas which flows through the bundles. Each

manifold serves the entire module of 360 cells. The gas flow direction between the cells is vertically upward. The gas supply to the lower (inlet) manifold is at the same end as the gas removal from the upper (outlet) manifold, so that the manifold flow arrangement is of the so-called "counterflow" type.

(4) A radial-flow fan or blower. The impeller axis direction is horizontal. A conventional scroll is provided. It discharges the gas vertically downward in a duct which connects the scroll to the inlet of the heat exchanger. The fan sucks the gas downward from the upper manifold through a rectangular duct.

(5) An electric motor which drives the fan impeller. The impeller is mounted directly on the extended shaft of this motor. This shaft is supported only by the bearings of the motor, in order to avoid location of a bearing in the high-temperature (over 300 deg C) region where the impeller operates. The shaft extension from the motor is to be relatively long (several inches), in order to provide space for substantial thermal insulation surrounding the shaft, and to increase the thermal resistance, axially, of the shaft metal. Cooling of the shaft immediately adjacent to the motor can be provided by a rotating disk provided with radial fins.

(6) A liquid, circulated by a pump, for cooling the gas which circulates through the module. The choice of liquid here proposed is known under the trade name "Therminol" in this country and is called "Santotherm" in Europe. It is sold by Monsanto. It is useable in the temperature range 150 to 425 deg C.

(7) Two finned-tube heat exchangers. One is designed to have a face area the same as the cross-section of the gas manifold which feeds gas to the cell matrix and is located just upstream of the inlet end of that manifold, drawing gas from the fan scroll through a duct thermally insulated from the cell-matrix region. The other heat exchanger is provided to cool the liquid by ambient air or any other convenient heatsink. It can be located wherever is most convenient for access to the cooling air.

(8) A control system, not shown in Fig. I.1, for maintaining the temperature of the gas within a specified range, and for also maintaining the temperature of the liquid within the same or a somewhat lower specified range. The gas temperature is to be controlled by controlling, by a thermostat, the flow of liquid to the gas-liquid exchanger. The liquid temperature is to be controlled by controlling, by a thermostat with sensor in the liquid, the flow of cooling air to the liquid-to-air heat exchanger.

(9) A source of heat, with thermostatic control, to be used only when the electrical losses in the cells are so low that the heat loss through the thermal insulation of the container walls tends to reduce the gas temperature below the desired range. This heat source can be an electrical resistor, for example, a "Calrod" element, located either in the liquid system or in the gas-flow system.

(10) Thermal insulation for the walls containing a set of many modules. The set of modules is to comprise four layers of modules, one above the other, with each layer containing several modules side-by-side. The insulation material must have an upper temperature limit of well above 350 deg C. The materials known commercially as "Refrasil" or "Fiberfrax" satisfy this requirement and have relatively low thermal conductivity.

Some thermal insulation may also be desirable for the vertical wall immediately adjacent to the row of cells nearest to the fan region. The gas around the fan is hotter (when the battery is generating appreciable heat) than the gas entering the cell region, so without insulation of this vertical wall, the gas flowing between the wall and the cells would rise more rapidly in temperature than it would from only the heat given off by the cells. The amount of insulation needed can be established by tests of a mock-up; such tests will be needed for other reasons also, namely, to measure the nonuniformities of temperature from cell to

cell and to modify, if necessary, the profile of one or both manifolds, and the spacings between the last rows of tubes and the adjacent walls, to reduce the non-uniformities.

I.1 The Dimensions and Performance Features of the System Components and the Reasons Underlying the Design Choices

I.1.1 Dimensions For The Cells And Their Spacing

The presently considered cell arrangement has an equilateral triangle configuration (in order to save space), with the following dimensions:

Outside diameter of cell tube	4.93 cm
Centerline pitch of cell tubes	5.59 cm
Thickness of busbar straps (uniform)	0.51 cm
Minimum clearance between cells where straps not present	0.66 cm
Minimum clearance betweeen cells where straps are present	0.15 cm

The above centerline spacing of the cells is chosen in order to make the minimum clearance between cells very small, as small as seems reasonable in consideration of the possibility of some variation from manufacturing tolerances in dimensions. The smaller the spacing, the smaller will be the temperature rise of the tube surface above the adjacent gas, except perhaps at very small clearances (which tend to reduce seriously the local velocity of the gas).

At one end of every alternate row of tubes a "dummy" half tube, generating no heat, is to be provided, and likewise at

the other end of the other rows. The same is true for the rows of tubes in the direction 90 degrees to the rows first considered here. The reason for these dummy half tubes is to prevent serious non-uniformity of the gas velocity which would tend to occur if the dummy half tubes were replaced by empty space.

I.1.2 Busbar Strap Dimensions

The busbar strap cross-section should be uniform, over the set of five tubes fed by the strap, in order to prevent non-uniform resistance to the gas flow.

A tentative choice of cross-section of 1.29 cm^2, with cross-section dimensions of 2.54 cm vertically and 0.51 cm horizontally, is used as the basis for gas pressure drop calculations.

I.1.3 Vertical Dimensions of the Inlet and Outlet Manifolds

The sum of the vertical dimensions of the two manifolds (inlet and outlet) of a module is here chosen as 61 cm (2.0 ft) in order to utilize all the space said to be available for this use. But this space is not divided equally. By making the vertical heights of outlet and inlet manifolds in the ratio 1.57 ($=\pi/2$), the pressure drop across the cell matrix is caused to become uniform (Ref. 1, Section 404.3, p. 3). Accordingly, the vertical dimensions of the inlet and outlet manifolds are to be, respectively, 23.8 cm (=0.78 ft) and 37.2 cm (=1.22 ft).

The cross-section of each manifold is to be uniform in the streamwise direction as a first trial design. Flow tests may show, however, that some small taper, not necessarily uniform, may yield even smaller non-uniformity of flow distribution through the tube matrix.

I.1.4 Dimensions and Performance of the Fan and Scroll

The following set of dimensions and rotational speed represent merely a trial example (selected from Sections 409.2 and 409.9 of Ref. 1), which is calculated to provide an acceptable combination of gas flow and pressure difference for the chosen flow circuit. The gas flow chosen is that which would yield a gas temperature rise of 15 deg C for the maximum heat generation per cell considered, namely 12.5 watts per cell (estimated for a temperature of 350 deg C). The chosen gas flow thereby calculated is 6.14 lb/hr per cell. The number of cell spaces (including the dummy half-tubes) is 421 (whereas the number of active cells is 360). The resulting value of gas flow is 2585 lb/hr (=1172 kg/hr).

For a gas temperature of 325 deg C, the density of nitrogen is .0356 lb/ft^3. This yields, for the above mass flow, a volume flow rate of 1210 ft^3/min (=34.3 m^3/min).

Axial width of impeller:	0.25 ft (=7.63 cm)
Outer diameter of impeller:	0.75 ft (=22.9 cm)
Radius of scroll at scroll outlet:	0.75 ft (=22.9 cm)
Width of scroll axially:	0.54 ft (=16.5 cm)
Breadth of scroll outlet (90° to axis)	1.3 ft (=39.7 cm)

Pressure developed by the fan for above flow:
(=393 nt/m^2)

Power input to the fan, for the module: 560 watts

Power allocation per cell, for 360 active cells:
1.58 watts/cell

Considerations of commercial availability, for impellers made of material suitable for the high temperatures involved, may make selection of some other impeller configuration preferable.

I.1.5 Thermal Considerations for the Fan Motor and Shaft

The design of the fan shaft has been discussed above. The limitation to axial length of the fan extension will be the mechanical strength and vibration susceptibility. The stiffness and strength can be increased by use of a hollow instead of a solid shaft. The particular dimensions will require analysis and then test confirmation.

The motor will presumably operate, in spite of design to reduce heat flow to it, at such high temperatures that the electrical insulation will have to be capable of standing relatively high temperature. Determination of the temperature to be encountered will require analysis, test, or both, after a tentative detailed design of impeller and shaft is selected.

I.1.6 Choice of Fluid For Removing the Heat From The Gas

A liquid, rather than air, is chosen as the fluid for removing the heat from the gas. The reason is that the space inside the module, for the ducts required for supplying and removing the air, and for the air-filled portion of the heat exchanger, would be far greater than for a liquid.

The liquid can be piped to a location near, but outside, the module proper, where it can be cooled by ambient air in an automotive-type "radiator". The details of this liquid-cooling system remain to be worked out, but seem likely to introduce no serious difficulties.

I.1.7. Dimensions and Performance of the Gas-to-Liquid Heat Exchanger

The following set of dimensions represent a tentative choice which is found by calculation to yield acceptable heat-transfer and pressure-drop performance. The details of the heat-exchanger surface elements, and generalized performance curves are those presented in Fig. 10-83 of Ref. 3.

Core dimensions in direction of gas flow:
0.577 ft (=17.6 cm)

Horizontal width of core (for 8 1/2 cell rows):
1.35 ft (=41.2 cm)

Vertical dimension of core (same as manifold):
0.78 ft (=23.8 cm)

Number of rows of .0335 ft dia. tubes:
8 rows horizontally
9 rows vertically

Liquid flow path:
two paths in parallel, so a set of 8 rows can be in series, to approximate counter flow of gas and liquid

The performance data are as follows:

Mass flow rate of gas:
2585 lb/hr

Mass flow rate of liquid:
1200 lb/hr (=2.7 gal/min)

Temp. change of liquid = temp change of gas = 15 deg C

Velocity of liquid:
5 ft/sec (=1.52 m/sec)

Mean temperature difference between gas and liquid:
8.1 deg C

Gas pressure drop in heat exchanger:
0.83 inch water (=207 newt/m^2)

Liquid pressure drop (incl. U-bends):
9.3 lb/in2 (=64,000 newt/m^2)

Pump power output for liquid, for module of 360 active cells:
11 watts

Pump power per active cell:
.031 watt/cell

I.1.8 System For Controlling The Temperature of the Gas and of the Liquid

The following information supplements the brief description of the control system presented above.

The location of the temperature sensor used for controlling the gas temperature is at the gas inlet to the heat exchanger. This is the location of the highest gas temperature in the gas-flow circuit.

The output of the gas-temperature sensor will be used to control the liquid flow rate. At maximum flow rate of the liquid, the liquid temperature rise in the heat exchanger will equal (as already mentioned) the gas temperature drop in that heat exchanger. For low heat generation, the temperature change of the gas, for the same gas flow rate as before, will be small, but the temperature change of the liquid will be much larger, and the log mean temperature difference between

the gas and liquid will be relatively small.

The location of the temperature sensor used for controlling the liquid temperature is to be at the liquid inlet to the gas-liquid heat exchanger. The output of this sensor is to be used to control (as previously mentioned) the rate of flow of coolant air to the liquid-to-air heat exchanger.

The tentative choice of temperature range for the gas, at the gas inlet of the gas-liquid heat exchanger, is 323 to 325 deg C. At the maximum heat load here assumed (12.5 watts per cell for 360 active cells), the corresponding gas temperature at the heat exchanger gas outlet is lower by 15 deg C, namely, 208 to 310 C.

The tentative choice of temperature range for the liquid, at the liquid inlet to the gas-liquid heat exchanger, is 300 to 302 deg C. This allows the calculated 8 deg C gas-to-liquid temperature difference in the heat exchanger.

Some gas flow is to be maintained at all times to avoid danger of "pockets" of gas at temperatures outside the desired temperature range. To save fan power at times of low electrical heat generation, there may be provided speed control of some type which then would provide a fan speed well below the normal full speed.

I.1.9. Location of the Heat Source For Times of Low Electrical Heat Input

Two alternative locations for this heat source have been

mentioned above, namely in the liquid flow circuit or in the gas flow circuit. Location in the liquid flow circuit seems preferable from considerations of uniformity of temperature in the gas stream. A heat source located in the gas stream might not distribute its heat uniformly over the cross-section of the gas stream without a considerable cost penalty.

I.1.10. Heat Loss Through The Thermal Insulation For Tentatively Chosen Thicknesses

The following thickness choices are here proposed, and have been used as the basis for the calculation of the heat losses of the modules in various different locations in the insulated enclosure which contains many modules.

Thickness for the side walls and rear end wall:
2.0 ft (=61 cm)

Thickness for the top and bottom of the enclosure:
1.0 ft (=30.5 cm)

Thickness of the front wall:
the average effective thickness for the heat loss through that insulation and through the fan shaft to the motor: 0.2 ft (=6 cm)

The calculated heat losses for these thicknesses are as follow:

For an assumed temperature difference of 325 - 20 = 305 deg C

For a module in the top or bottom layer and adjacent to a side wall:
345 w for 360 cells = 0.96 w per cell

For a module in the top or bottom layer but not adjacent to a side wall:
213 w for 360 cells = 0.59 w per cell

For a module not in the top or bottom layer, but adjacent to a side wall:

269 w for 360 cells = 0.75 w per cell

For a module not in the top or bottom layer, and not adjacent to a side wall:

144 w for 360 cells = 0.40 w per cell

I.2 Results of Approximate Calculations of Temperature-Rise Increments

In order to avoid too high or too low temperature at any location in the matrix of cells, throughout the operating cycle, the maximum temperature rise, at the hottest spot (at the time of maximum heat generation), above the controlled coolant temperature, must be suitably limited. The design objective of the cooling system here proposed is to limit the hot-spot temperature rise above coolant liquid supply temperature to 48 deg C, with a maximum controlled liquid supply temperature of 302 deg C and a minimum liquid supply temperature of 300 deg C.

Achievement of this objective is indicated by the following calculated results for the various increments of the total rise of temperature. The calculations are based on reasonably conservative assumptions, but tests will be needed to confirm or refine those assumptions.

Temp. rise of gas above liquid in heat exchanger, with counter flow, and equal steamwise temperature change of liquid and gas:	8 deg C
Temp. rise of cell surface above inlet gas if axial conduction is accounted for:	36 deg C

Radial temp. increment inside the cell, to hot spot:	8.4 deg C
Benefit of temp. lag behind steady state, due to rapidly rising heat generation at time of maximum heat generation.	-7.4 deg C
Total rise about liquid supply temperature	45 deg C

I.3 Results of Approximate Calculations of Pressure-Drop Increments in the Gas-Flow System

The presently proposed configurations for the fan and for the gas-to-liquid heat exchanger are trial designs, chosen to establish feasibility of the proposed cooling system. The calculated results here summarized do indeed indicate that the fan can provide a pressure amply adequate to produce the presently proposed gas flow with the chosen manifolds and cell spacing.

The pressure-drop increments, as calculated for the dimensions listed in I.1., I.1.2, and I.1.3 above, are as follows:

Gas friction for vertical flow between cells where no straps:	.0061 in. water
Gas friction for vertical flow past straps:	.0058 in. water
Pressure losses at contractions of cross-section vertical flow:	.029 in. water
Subtotal for vertical flow between cells:	.041 in. water
Acceleration in outlet manifold: (=velocity head in inlet of inlet manifold)	.038 in. water
Pressure drop of gas in heat exchanger (item 2.7 above)	.83 in. water
Total of above values: (the minimum fan requirement)	0.91 in. water

Available for additional restrictions for vertical flow between the cells, as discussed below:	0.67 in. water
Total system pressure drop provided by presently proposed (item 2.4 above) fan:	1.58 in. water

Provision of additional flow restriction, for the flow vertically between the cells, is recommended for two reasons, namely: (1) because it can reduce the amount of non-uniformity of gas flow through the matrix of 360 cells, and (2) because it can be used to reduce the increment of temperature rise of surface temperature of the cell above the local gas temperature.

Non-uniformity of flow distribution is likely for two reasons, as follows. There is a small, but appreciable, additional pressure drop increment required to cause the 90-degree change of flow direction (from the manifold to the vertical flow), which is greatest where the manifold velocity is highest, and negligible where the manifold velocity is low. The maximum value of this increment is about .003 inch water. Secondly, there is likely to be appreciable non-uniformity of velocity of gas leaving the outlet face of the heat exchanger (due to non-uniformity of velocity leaving the fan scroll and to the 90-degree turn of gas direction from scroll to heat exchanger). The <u>average</u> velocity of gas at the manifold inlet is .038 inch of water, as noted above, so non-uniformities can be more than negligible compared to the pressure drop (.041) through the cell matrix.

The alternative forms of flow restrictions deserving future consideration include the following:

(a) Vertical rods, of triangular or cusp-shaped cross-section, in the interstitial spaces between adjacent cell tubes.

(b) Co-axial tubes, of circular cross-section and thin walls surrounding each cell tube, with spacing "knobs" or "pins" or tiny vertical rods to prevent eccentricity of position and to provide support. The additional tubes could be omitted in the regions where attachment of the busbar straps would otherwise interfere.

(c) A "header" plate at the bottom end of the cells, with suitably-sized round orifice holes lined up with the spaces for vertical flow between the cells. These would not appreciably help the convection heat transfer, but the ease of providing uniformity of the flow restrictions is attractive.

References

1. Fluid Flow Data Book, General Electric Co., Corporate Research & Development, Schenectady, NY (1977).

2. Heat Transfer Data Book, General Electric Co., Corporate Research & Development, Schenectady, NY (1977).

3. W.M. Kays and A.L. London, Compact Heat Exchangers, McGraw-Hill Book Co., New York, NY (1964).

List of Figure Captions

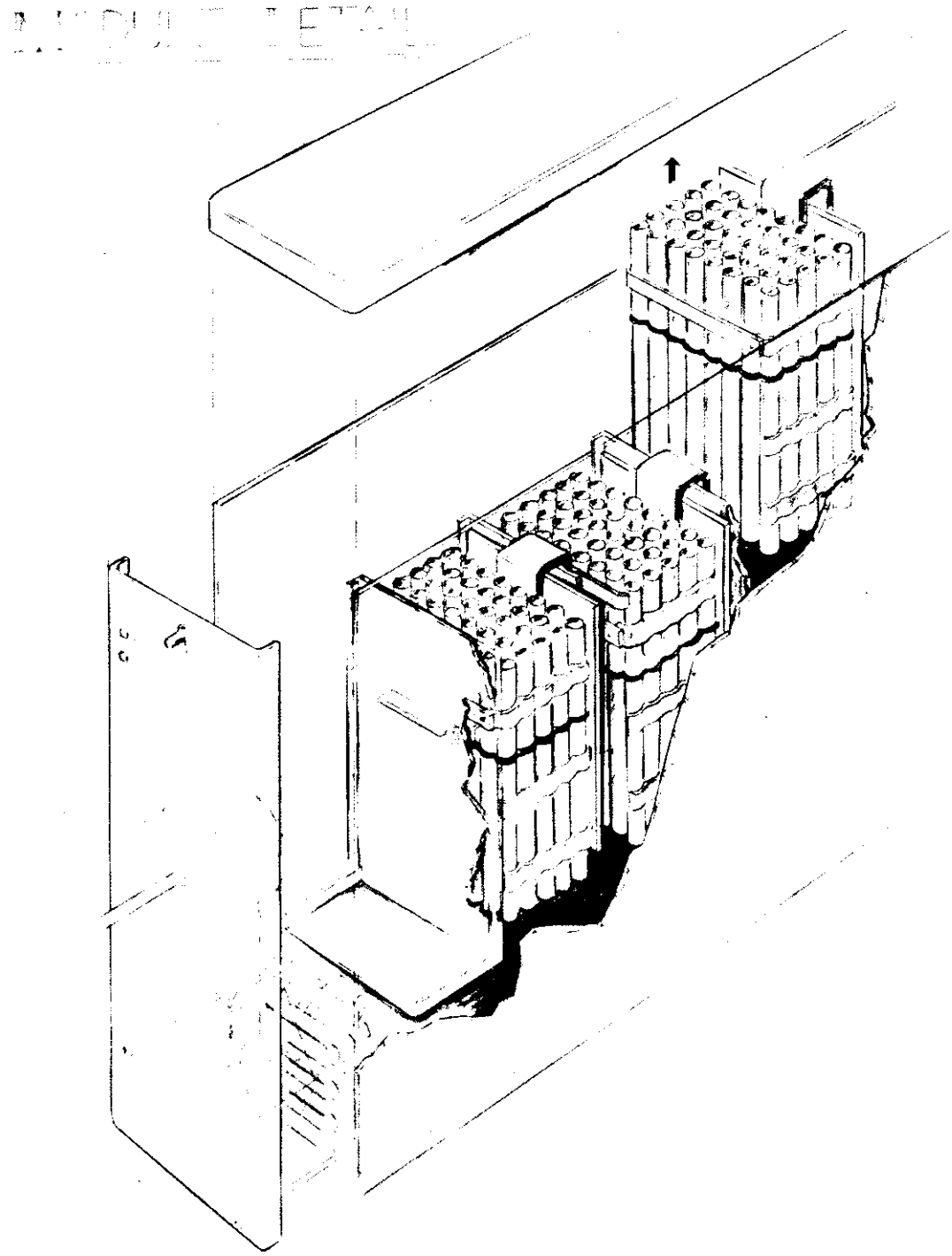

Figure I.1. Module Components Provided for Thermal Purposes

Section J

SUPPORTING RESEARCH

During the report period research was conducted in the following areas to support the development-oriented tasks:

1. Sulfur Electrode Studies
2. Real Time X-Radiography of Na/S Cells
3. Analytical Methods for Determination of Na in Beta-Alumina
4. Sulfur Purification
5. Mechanisms of Seal and Container Degradation
6. Mechanism of Ion Transport in Beta-Alumina: NMR Studies

This section provides summaries of research done in the areas of sulfur electrode and cell x-radiography.

J.1 Sulfur Electrode Studies

The sulfur electrode studies that relate to the sodium-sulfur battery are primarily concerned with establishing the electrode kinetics at the carbon/sodium polysulfide interface. Although an appreciable understanding of the electrochemistry now exists, there is often some ambiguity when these results are applied to actual cell performance. The intent of this report is to consider the influence of the interface on certain cell properties. Sulfur electrode contributions to cell resistance and the distribution of electrochemical reactions occurring within it are presented.

J.1.1 Carbon Mat Resistance

An accurate determination of the carbon mat resistance is absolutely required if the two topics mentioned above are to be properly assessed. The resistance of the mat is extremely sensitive to its bulk density. Therefore measurements must be made under simulated operating conditions to minimize the potential for error.

A cell was constructed (Fig. J.1) which resembled the sulfur electrode in sodium-sulfur cells. The high sulfur resistivity ensured that conduction would be electronic (via carbon fibers). Thus, a graphite rod replaced the usual beta-alumina tube and served as the counter electrode. Mat 32/sulfur plugs were fabricated in the usual manner and the unsaturated mat layers were

wrapped normally. The resistance (at 1 KHz) was measured as a function of temperature.

Three configurations were employed; a) mat 32/sulfur plug with high resistance mat covering the counter electrode, b) mat 32/sulfur plug with mat 32 covering the counter electrode and c) mat 32/sulfur plug. Condition (a) corresponds to the sulfur electrode normally used and (c) allows the mat 32 resistance to be evaluated directly. From (b) one may determine whether a contact resistance exists between an unsaturated layer of mat and a sulfur impregnated mat. The results are shown in Fig. J.2. When the sulfur melts it improves the electrical contact within the system and lowers the resistance commensurately. The temperature dependence of the transition depends upon the heating rate and perhaps the wetting behavior of the originally unsaturated layer. Item (c) is not graphed because it is identical to (b) i.e., there is no evidence of a contact resistance.

Clearly the high resistance of case (a) resulted from the presence of the resistive mat. Additional d.c. measurements were performed and only ohmic behavior was observed. Agreement with the 1 KHz values was excellent. The resistance for case (a) was approximately 10 ohms while that of (b) was 0.18 ohms. Some variation occurred because the measuring cell was not leaktight and sulfur was vaporized. Mat resistivities were calculated from the formula

$$R = \frac{\rho}{2\pi L} \ln \frac{r_1}{r_2} \qquad (1)$$

where R is the measured resistance, ρ the resistivity, L the length of the mat, r_1 the outer radius and r_2 the inner one. For mat 32 and the high resistance mat the resistivities are 9.97 ohm-cm and 2725 ohm-cm, respectively. These values are essential for the calculations performed in the following sections. It is also significant to note that this procedure may be used in the future to evaluate and predict the behavior of other carbon mat products in sodium-sulfur cells.

J.1.2 Calculation of Cell Resistance

The simplest representation for the cell resistance of a sodium-sulfur cell is a series resistance approach

$$R_c = R_{Na} + R_\beta + R_{m/ps} + R_{mc} \qquad (2)$$

where R_c is the cell resistance and Na, β, m/ps and mc refer to the contributions made by the sodium, beta-alumina electrolyte, mat/polysulfide matrix and metal container respectively. The large conductivities of the two metals allows R_c to become

$$R_c \simeq R_\beta + R_{m/ps} \qquad (3)$$

The mat/polysulfide matrix consists of a highly porous

carbon mat (>95% porosity) saturated with molten polysulfide. Electrochemical reactions occur between the two phases (see below). Thus a parallel resistance path exists and,

$$R_c \simeq R_\beta + \frac{R_m R_{ps}}{R_m + R_{ps}} \qquad (4)$$

Resistivities for beta-alumina are routinely measured in our laboratory, resistivities of various polysulfide compositions are available in the literature[1] and R_m was discussed above. Since the resistivities for sodium polysulfides are so much less than that of the carbon mat one would expect that the second term in Eq. (4) reduces to R_{ps}. This is shown in Table J.1. Thus, the cell resistance is merely the sum of the beta-alumina and sodium polysulfide resistances.

$$R_c \simeq R_\beta + R_{ps} \qquad (5)$$

Table J.2 indicates how the cell resistance depends upon polysulfide composition and beta-alumina resistivity. For the appropriate conditions (e.g., $Na_2S_{4.2}$ and $\rho_\beta = 10\ \Omega$-cm) the values from the table agree extremely well with the lowest observed cell resistances. Thus, the model appears to offer a viable means of predicting minimum cell resistance.

Table J.1

Determination of $R_{m/ps}$

Composition	$Na_2S_{3.2}$	$Na_2S_{4.2}$	$Na_2S_{5.1}$
Resistivity (ohm-cm)	2.67	4.05	5.60
Resistance (ohms)	0.0493	0.0748	0.1034
$R_{m/ps}$* with R_m = 10Ω	0.0491	0.0742	0.1023
$R_{m/ps}$* with R_m = 5Ω	0.0488	0.0737	0.1013

$$*R_{m/ps} = \frac{R_m \, R_{ps}}{R_m + R_{ps}}$$

Table J.2

Calculation of Cell Resistance

Beta-Alumina Resistivity (ohm-cm)	Sodium Polysulfide Composition		
	$Na_2S_{5.1}$	$Na_2S_{4.2}$	$Na_2S_{3.2}$
15	0.1840	0.1554	0.1299
10	0.1572	0.1286	0.1031
7	0.1109	0.0900	0.0722

J.1.3 Electrochemical Reaction Rate Distribution in the Sulfur Electrode

Description of the Model

The analysis of current distribution in porous electrodes has been treated by several investigators[2,3] and subsequently applied to the sodium/sulfur system[4,5]. Gibson[4] considered a uniform concentration of polysulfide with linear polarization (i.e., polarization represented by an ohmic resistance) while Kao and Wayner[5] treated the nonuniform case. In this report, a modified version of the uniform concentration model is applied to the 16 Ah prototype Na/S cell.

The system analyzed is shown in Fig J.3. It consists of a unit crossectional area slice of carbon mat saturated with molten Na_2S_4. The beta-alumina electrolyte is a distance L from the metal container. Radial symmetry exists in the battery and this enables a one-dimensional model to be developed (i.e., perpendicular to the electrodes). A brief derivation is outlined below. The procedure followed for one type of carbon mat is analogous to that previously presented[4]. The derivation for the two carbon mat configurations is somewhat more involved.

Single Carbon Mat: In these calculations the reaction rate distribution is obtained for prototype cells that use only one type of carbon mat in the sulfur electrode. Different values were chosen for the mat resistance. Other parameters were as follows;

I_o = current density = 100 ma/cm^2

R_m = melt resistivity/cm = 4 ohm/cm (i.e., Na_2S_4)

L = carbon thickness = 0.66 cm

Figures J.4-J.6 illustrate how the spatial distribution of the reaction products are dependent upon resistivities of the melt and carbon components. When the melt resistivity is much greater than that of the carbon mat (i.e., high conductivity mat) most of the reaction occurs at the beta-alumina interface. This situation predicts that upon charging the cell, sulfur deposition is liable to passivate the electrode and impede cycling into the two phase region. If the polysulfide melt is more conductive than the carbon mat (Fig. J.5) reaction is concentrated at the metal electrode. This condition may promote the formation of insoluble polysulfide films (e.g., Na_2S_2) which limit current flow[6] or possibly enhance container corrosion. In the case where the resistivities are equal (Fig. J-6) the reaction rates are greatest at both electrodes. Once again poor cycling performance is expected because of passivating films. Figure J.6 represents a good approximation of the potential distribution if mat 32 is the only type of carbon in the sulfur electrode.

A homogeneous distribution of reaction rate would presumably provide the best cycling performance. None of the arrangements calculated for a single type of carbon mat offered this condition. The placement of a high

resistance mat adjacent to the beta-alumina tube improves this situation.

Two Carbon Mats: In this calculation a second region is created to account for the high resistivity mat. The characteristics of the two regions are;

Region I (corresponding to mat 32 plug):

$I = 0.9I_o = 90$ ma/cm^2, $R_c = 10\Omega$/cm

$L = 0.58$ cm, $R_m = 4\ \Omega$/cm

Region II (corresponding to high resistance mat):

$I = 0.1$, $I_o = 10$ ma/cm^2, $r_c = 2500\ \Omega$/cm

$L = 0.08$ cm, $R_m = 4\ \Omega$/cm

It is assumed that only a fraction of the total current (10%) is associated with region II and that the high mat resistivity causes most of the current to be carried in the melt. Therefore, at the boundary between regions I and II, virtually no current is carried by mat 32 and $d\phi c/dx \simeq 0$. A discontinuity arises in the potential distribution (Fig. J.7) and the reaction rate is considerably larger at the boundary than at the beta-alumina interface. This prevents sulfur from depositing on the electrode during charge and enables successful cell operation to occur in the two phase region. The 10% allotted to region II is arbitrary. A more generalized approach is presently being developed.

Outline of Mathematical Treatment

Single Carbon Mat: The potential distribution in the sulfur electrode is obtained by essentially solving Poisson's Equation.

$$-\frac{1}{r_c}\frac{d^2\phi c}{d_x^2} = \frac{\delta I_c}{\delta x} \text{ and } \frac{-1}{R_m}\frac{d^2\phi m}{d_x^2} = \frac{\delta I_m}{\delta_x} \qquad (6)$$

where the subscripts c and m represent the carbon and melt values of R, the resistance per unit length, ϕ, the electrostatic potential and I, the current flux. δI_c is the change in electronic current over the increment δx within the carbon. Thus at any point

$$\delta I_c = -\delta I_m \text{ with } I_c + I_m = I_o \qquad (7)$$

From equations (6) and (7)

$$-\frac{1}{r_c}\frac{d^2\phi_c}{d_x^2} = \frac{1}{R_m}\frac{d^2\phi_m}{d_x^2} \qquad (8)$$

This equation is then solved by using the appropriate boundary conditions. At the metal container (x = 0) the current is totally electronic and from Ohm's law

$$\frac{d\phi_c}{d_x} = -R_c I_o \text{ , } \frac{d\phi_m}{d_x} = 0 \qquad (9)$$

At the beta-alumina electrode (x = L) all the current is ionic

$$\frac{d\phi_c}{d_x} = 0, \ \phi_m = 0 \text{ (arbitrary reference point}^{(2)}\text{)} \qquad (10)$$

Within the mat/polysulfide phase, current is transferred from the carbon to the melt by electrochemical reactions. The local reaction rate is given by

$$-\frac{\delta I_c}{\delta x} = \frac{\phi_c - \phi_m}{\gamma} \tag{11}$$

Although γ has been considered a constant[4], it actually reflects the local resistance of the carbon/melt interface and is quite dependent on r_c.

Equation (8) is solved by applying the boundary conditions (9) and (10) and substituting (11)[4]. The value of ϕ_c at X = L is obtained once general expressions for $\phi_c(x)$ and $\phi_m(x)$ are available. Then (11) may be used in the form

$$\frac{1}{\gamma}\int_0^L (\phi_c-\phi_m)\, d_x = -\int_0^L dI = I_o \tag{12}$$

to determine the unknown.

Two Carbon Mats: The procedure followed in this case is analogous to the one presented above. Each region,however, is solved separately. For region I (mat 32, between x = 0 and x = a)

$$-\frac{1}{r_{c1}}\frac{d^2\phi_{c1}}{d_x^2} = \frac{1}{R_m}\frac{d^2\phi_{m1}}{d_x^2} \tag{13}$$

is the starting point while for region II (high resistance mat)

$$-\frac{1}{R_{c2}}\frac{d^2\phi_{c2}}{d_x^2} = \frac{1}{R_m}\frac{d^2\phi_{m2}}{d_x^2} \tag{14}$$

is used.

At x = a, additional boundary conditions are necessary. The high mat resistance suggests that nearly all the current is ionic and therefore at the end of region I

$$\frac{d\phi_c}{d_x} \simeq 0, \quad \frac{d\phi_m}{d_x} \simeq -R_m I_o \tag{15}$$

Region II is solved similarly to that of the single mat case. To find the unknown values of ϕ_c at x = a and x = L, equation (12) is used. A certain fraction of the total current, I_o, must be proportional to the different regions. Equation (12) is modified in region I to be

$$\frac{1}{\gamma} \int_0^a (\phi_c - \phi_m) d_x = -0.9 \int_0^a dI = 0.9 I_o \tag{16}$$

(90% was based on the ratio of mat thicknesses). In region II the coefficient for I_o is 0.1. The solution to the differential equations is somewhat more involved, but straightforward nonetheless.

J.2 X-Radiography of Sodium-Sulfur Cells

In a previous report the usefulness of x-radiography for evaluating Na-S cells was established with room temperature photographs, taken before and after cycling[7]. The electrochemical performance was found to depend on the distribution of sulfur and carbon in the cathode, wetting of the beta alumina surface by sodium polysulfide and sulfur, deterioration of the carbon current collector and corrosion of the metal container walls. The results, which were

obtained at room temperature, suggested it would be possible to use x-radiography as a supplement to electrochemical methods for investigating operating Na-S cells. This section describes the application of x-radiography at high temperature to observe physical and structural changes in Na-S cells as they are charged and discharged.

The conversion of chemical free energy to electricity proceeds by sequences of reactions which are accompanied by mass transport of reactants and products toward and away from the electrodes. The chemical and physical changes during cycling are understood in a general way from the Na-S phase diagram[8] and measurements of the voltage-current characteristics[9] in cells at different states of charge. The overall reaction requires the transfer of electrons, ions and molecules through interfaces joining phases of disparate properties. The existence of equilibrium conditions throughout the cell, particularly at high current density, is doubtful since the cathode is a high viscosity mixture of polymeric sulfur, ionic sodium polysulfide and carbon fibers.

Knowledge of the concentration and physical movement of active materials during discharge and charge are needed to design electrode and cell configurations for optimum performance. Some information has been obtained by analyzing the contents of quenched cells[10]. The cells contain sodium and sodium polysulfides, all highly reactive and unstable

in the atmosphere, and the determinations are difficult and inexact. In addition, Na-S cells operate above 325°C with molten reactants and the real distribution of active materials during cycling is obscured by structure and volume changes which take place when the multi-component mixture solidifies.

The primary objective of this study was to ascertain if x-radiography could be applied to obtain useful information about Na-S cells as they operated under realistic test conditions. It was recognized that resolving details in 2-dimensional radiographs of a complex 3-dimensional structure would be severely limited without taking simultaneous photographs from different directions. Accordingly, visual examination was extended by quantitative densitometry and masking techniques to reveal changes in x-ray opacity as the cell was charged and discharged.

Experimental

The equipment for heating, cycling and photographing Na-S cells was assembled in a radiation-shielded cabinet x-ray system (Hewlett-Packard, Faxitron Model 43805N). The apparatus was rotated on its side to obtain a horizontal beam to radiograph cells with liquid contents in a vertical orientation. The unit was modified for horizontal operation by attaching an auxiliary reservoir to the oil-filled enclosure that housed the high voltage transformers.

Figure J.8 is a schematic drawing of an oven that was built for heating and radiographing the cells. The test

cell was heated by two 375 W infrared quartz lamps with radiation focused by gold-plated brass elliptical reflectors. The temperature was maintained at 330 $\pm$ 10°C by controlling the output of the quartz lamp with a thermocouple attached to the cell wall. The furnace was aluminum alloy lined with 1/4" insulation. Windows 1 1/2" x 5 1/2" high covered with aluminum foil radiation shields were incorporated for the x-ray beam. Water circulated through the front and rear panels prevented the x-ray cabinet from overheating and enabled film to be brought close to the cell.

Preliminary and line-up photographs were made on Polaroid Type 57 film. Radiographs for densitometering and differential radiography were made on Kodak Industrex M2 and Single Coated R film. The film to source distance was 100 cm and exposure times ranged from 3 to 20 minutes at 80 kVp and 3 ma.

Figure J.9 is a drawing of a Na-S test cell. The cell is composed of a sodium reservoir, closed-end tubular beta alumina solid electrolyte separator, sulfur-carbon felt cathode, and seals for insulating the cathode from the anode. The sodium and sulfur containers were aluminum and steel, respectively. Current and voltage probes were welded to the sodium and sulfur containers and passed through an opening near the top of the oven. Cells were cycled at 2A (108 ma/cm^2) and 4A (216 ma/cm^2) while monitoring cell voltage, resistance and open circuit potential.

X-ray densities were measured with a Joyce-Loebel densitometer. Films were scanned with a beam 0.1 mm wide, 1 mm high along a path in the center of the sulfur electrode and perpendicular to the cell axis. Densities in a sequence of radiographs were normalized with respect to a constant reference density in each film to compensate for variations in x-ray voltage, exposure time and film processing.

Difference radiographs were made by combining radiographs of partially discharged cells with masks into a sandwich and printing the combination on photographic paper. Masks were prepared by contact printing x-radiographs of the fully charged and fully discharged cell on Kodak Ektapan film. A satisfactory mask when combined with its precursor resulted in a nearly structureless neutral grey image.

J.2.1 Results and Discussion

According to the phase diagram (Fig. J.10) discharge of a Na-S cell at 340°C proceeds in two stages:

(1) $2Na + 5S \rightleftharpoons Na_2S_5$

(2) $nNa + Na_2S_5 \rightleftharpoons [1 + 1/2n]\ Na_2S_{(\frac{10}{2+n})}$ $\quad 0<n<4/3$

The product of the first stage is a 2-phase liquid of S and Na_2S_5. Sulfur is consumed until the Na/S ratio exceeds that of Na_2S_5. A single phase sodium polysulfide melt with variable composition is formed in the second stage. Discharge is terminated at Na_2S_3 to avoid precipitation of solid Na_2S_2. Many of the usual features that are encountered cycling Na-S cells are due to the different properties of the

sulfur electrode in the 1-phase and 2-phase region.

First Cycle Behavior

The electrochemical performance of Na-S cells during the first few cycles is erratic, usually characterized by high initial resistance and occasionally by difficulties cycling through the 2-phase/1-phase boundary. Radiographs were taken of a freshly assembled cell as it was heated from room to operating temperature, then discharged and recharged at 340°C. Of particular interest was whether improvements in performance could be related to observable changes in the electrodes.

Radiographs taken as the cell was heated are shown in Fig. J.11a, b, c. At room temperature the electrodes are extremely non-uniform (Fig. J.11a). The sodium reservoir contains a large central cavity and several bubbles, a consequence of the volume decrease when sodium crystallized. The sulfur electrode has myriad voids, purposely incorporated to accomodate the sodium polysulfide that is formed when the cell is discharged. The distribution of sulfur through the reservoir is completely determined by the carbon felt current collector. There virtually is no sulfur in a thin layer of high resistance carbon mat that is incorporated at the beta alumina surface to prevent formation of a resistive sulfur layer when the cell is charged.

Figure J.11b shows the state of the cell at 154°C when both sodium and sulfur are liquid. The sodium cavity is filled, leaving a few residual bubbles that probably

are gas pockets stabilized by an oxide film. The sulfur electrode is unchanged, even though at this temperature sulfur is a fluid liquid composed of S_8 molecules.

Figure J.11c was taken at 340°C. The gas bubbles in the sodium reservoir have disappeared, probably released to the open space above the liquid when the film of sodium oxide dissolved. Negligible intercalation into the voids of the sulfur electrode has taken place and the dispersion of sulfur through the electrode appears to have been completely determined by the properties of the carbon felt when the cell was loaded.

The test cell was discharged and recharged at 2A, equivalent to 108 ma/cm^2. Cycling was interrupted for the x-ray exposures, which required 15 minutes, and measurements were made of cell voltage, open circuit potential (OCV) and cell resistance (R_c). No difficulty was encountered cycling the cell at near theoretical capacity or discharging through the 2-phase boundary. The OCV, R_c and average composition of the cell during discharge and charge are summarized in Table J.3. R_c initially was high but decreased to normal by complete discharge. R_c remained small while the cell was recharged until the composition of the sulfur electrode exceeded 95% sulfur. The changes in open circuit potential during the first cycle are slightly anomalous but readily accounted for by inhomogeneous non-equiblirium distributions of sodium polysulfide and sulfur. Figure J.12 displays R_c and OCV as a function of charge during the first cycle.

Table J.3

First Cycle of Na-S Cell at 108 ma/cm^2

Ampere Hours	OCV (Volts)	R_c (Ohms)	Sulfur Electrode Composition (Percent)
Discharge			
0	2.08		100 S
.25	2.08	1.30	99 S, 1 Na_2S_5
2.25	2.08	.65	94 S, 7 Na_2S_5
4.25		.47	86 S, 14 Na_2S_5
6.25	2.04	.42	71 S, 29 Na_2S_5
8.25	2.01	.37	36 S, 64 Na_2S_5
10.26	1.96	.34	$Na_2S_{4.44}$
12.25	1.89	.21	$Na_2S_{3.77}$
15.25	1.88	.19	$Na_2S_{3.00}$
Charge			
2.00	2.05	.16	$Na_2S_{3.45}$
4.00	2.08	.16	$Na_2S_{4.08}$
6.13	2.08	.17	$Na_2S_{5.00}$
8.00	2.08	.17	75 S, 25 Na_2S_5
10.50	2.08	.18	82 S, 18 Na_2S_5
12.00	2.08	.18	90 S, 10 Na_2S_5
13.20	2.08	.21	91 S, 9 Na_2S_5
13.60	2.08	.30	93 S, 7 Na_2S_5
13.80	2.08	.54	97 S, 3 Na_2S_5

Figure J.13 is a representative set of radiographs taken as the cell discharged. The transfer of sodium from the sodium reservoir to the sulfur electrode is shown by the sodium level in the upper container. The voids in the sulfur electrodes are gradually filled with sodium polysulfide as the cell discharges (Fig. J.13a-g). The filling of the interstices is irregular and many voids, both large and small, remained unfilled at complete discharge.

Radiographs of the charge part of the cycle are shown in Figure J.14. The interstices in the carbon current collector are slowly depleted of sodium polysulfide as sodium is pumped back into the sodium reservoir. To a first approximation the original void structure is regenerated. The distribution of sulfur and sodium polysulfide apparently depends only on the state of charge and the original properties of the carbon felt.

Midway through discharge the radiographs undergo a subtle change in appearance. The change occurs about when R_c and OCV attain normal values. The transition will be discussed more fully in the section on composition gradients and phase change. At this point attention is directed toward the possibility that the transition from high to low resistance during the first discharge is due to an increase in dimensions of Na_2S_5 regions until they overlap and form a quasi-continuous interconnected conducting film which extends throughout the extended sulfur electrode.

Differential Radiography and Local Electrochemical Efficiency

Figure J.13 and Figure J.14 show the sulfur distribution is not uniform but they do not give a clear indication of where and how sodium polysulfide forms. Factors which make it difficult to distinguish the locations of sulfur and sodium polysulfide are the non-uniform structure of the carbon current collector, the small difference in x-ray absorption coefficients and overlapping of details in the 2-dimensional projected image. Two alternate approaches for abstracting information from radiographs of the active materials are described in this and the following section.

During the second cycle the cell was discharged and charged at 4A (216 ma/cm^2) instead of 2A to increase the composition gradients. High resolution of fine details was deemed not important for this aspect of the study and x-ray exposures were made without interrupting cycling. The radiographs therefore describe the average situation over a period of time and chemical composition.

The performance of the cell at 4A was quite good, considering the high current density. The electrical parameters and composition during the cycle are summarized in Table J.4 and R_c and OCV are plotted as a function of charge in Fig. J.15. R_c was small through most of the cycle, rising sharply at the beginning and end of recharge. The rapid increase in R_c for a short time at the beginning of charge took place after the cell had floated at OCV

Table J.4

Second Cycle of Na-S Cell at 216 ma/cm^2

Ampere Hours	OCV (Volts)	R_C (Ohms)	Sulfur Electrode Composition (Percent)
Discharge			
0	2.08	>.250	100 S
1.45	2.08	.215	96 S, 4 Na_2S_5
2.93	2.08	.157	92 S, 8 Na_2S_5
5.89	2.06	.140	74 S, 26 Na_2S_5
7.40	2.05	.135	54 S, 46 Na_2S_5
8.91	2.03	.130	12 S, 88 Na_2S_5
9.67	2.02	.128	$Na_2S_{4.73}$
11.17	1.97	.125	$Na_2S_{4.10}$
12.66	1.91	.123	$Na_2S_{3.62}$
13.69	1.88	.153	$Na_2S_{3.34}$
14.47	1.85	.213	$Na_2S_{3.16}$
Charge			
.29	1.89	.335	$Na_2S_{3.23}$
.97	1.94	.485	$Na_2S_{3.39}$
1.72	1.99	.138	$Na_2S_{3.59}$
2.17	2.03	.145	$Na_2S_{3.72}$
3.21	2.06	.150	$Na_2S_{4.06}$
3.97	2.07	.170	$Na_2S_{4.36}$
4.71	2.08	.190	$Na_2S_{4.68}$
5.47	2.08	.198	8 S, 92 Na_2S_5
6.40	2.08	.198	40 S, 60 Na_2S_5
7.32	2.08	.198	56 S, 44 Na_2S_5
8.10	2.08	.198	69 S, 31 Na_2S_5
9.55	2.08	.200	81 S, 18 Na_2S_5
11.05	2.08	.203	90 S, 10 Na_2S_5
11.82	2.08	.203	92 S, 8 Na_2S_5
12.62	2.08	.210	95 S, 5 Na_2S_5
13.33	2.08	.520	97 S, 3 Na_2S_5

overnight. The cell performance was nearly normal, compared to the first cycle, and constant potential for sulfur saturated with Na_2S_5 was observed over a large segment of the cycle.

A differential radiographic technique was developed to observe the changes in the distribution of sulfur and polysulfide which took place when the cell was cycled. In order to see the difference between a fully charged and partially discharged cell the radiograph of the discharged cell was combined with a mask. The mask was a contact print on photographic film of the radiograph of the fully charged cell. The positive radiograph and negative mask were combined in a sandwich and printed on photographic paper to make a difference print that will be referred to as a Δ-radiograph. The Δ-radiograph shows density in locations where absorption of x-rays in the discharged cell is greater than in the charged cell.

Figure J.16a is a Δ-radiograph after 0.25 Ah discharge, included primarily for judging the quality of masking. It shows structure cancellation is adequate in the sulfur electrode but the mask does not compensate completely for sharp density gradients. Figure J.16a was made near the beginning of discharge when the average composition was 0.06 Na_2S_5 + 0.945S. There are high concentrations of Na_2S_5 in specific locations, for example, near the α-Al_2O_3 seal, in the high resistance carbon mat, at the bottom of the beta alumina tube. The non-uniformity

of discharge is more apparent in Figure J.16b (0.88 Na_2S_5 + 0.12S) and in Fig. J.16c (single phase, $Na_2S_{3.3}$).

Figure J.16d, e, f is a similar sequence made when the cell charged. To study charge the mask is a negative of the radiograph obtained from the completely discharged cell. Light areas in the Δ-radiograph are regions that are depleted of sodium polysulfide as a result of charging. Figure J.16d is at the beginning of charge and still in the 1-phase field ($Na_2S_{3.4}$). Figure J.16e ($Na_2S_{4.0}$) and Figure J.16f (0.44 Na_2S_5 + 0.56S) establish that the locations which accumulated sodium polysulfide first during discharge are the first to be depleted on charge. Accordingly, the flow of active material when Na-S cells cycle is reversible and locally balanced throughout the sulfur electrode.

Composition Gradients and Phase Changes

The large differences in electrochemical efficiency that were found at various locations in the sulfur electrode probably influence the rate and current density at which cells can be cycled to a greater extent than the quantity of charge that can be stored or released. Attaining high capacity is related to the availability of sodium polysulfide and sulfur at critical stages of the cycle. A possible experimental method for determining the concentration and location of the various sulfur species is from measurements of x-ray absorption, as shown by the mass absorption coefficients at 40 keV; μ_m for S, Na_2S_5, Na_2S_3 = 0.903, 0.790, 0.739 cm^2/g,

respectively. Unfortunately, interpretation of x-ray absorption in test cells is severely handicapped by the irregular void distribution and the cylindrical geometry. An x-ray beam perpendicular to the cell axis is attenuated by passing through regions of changing composition, variable density and different path length.

Some quantitative data have been abstracted from the radiographs by densitometering the films and studying the effect of cycling on the transmitted x-ray intensity at particular locations in the sulfur electrode. The measurements reported at this time are qualitative and depend on comparisons between many films that were exposed, developed and densitometered independently.

Figure J.17 is a densitometer trace of a radiograph of a partially discharged cell. The principle features are absorption peaks due to the central electrode at (a), walls of the beta alumina tube at (b) and walls of the steel container at (c). In addition, there are regions of high transmission through voids. The absorption peak due to one of the walls of the beta alumina (on the left side) is obscured because at that location there is a broad transmission band due to voids.

Optical densities at five locations in the sulfur electrode were interpolated from densitometer scans of the radiographs taken during the second cycle of the test cell. The locations were (1) in the high resistance mat

on the beta alumina surface, (2) outside the mat but close to the beta alumina, (3) midway between the beta alumina and cell wall, (4) near the cell wall, (5) at the cell wall. The effect of discharging and charging the cell on the x-ray intensity at these locations is shown in Fig. J.18. During the first 30-50 percent of discharge the intensity is sensibly constant, then decreases rapidly to a plateau which remains approximately constant until it increases when the cell is discharged completely. When the cell was recharged the reverse changes in x-ray density take place except the initial plateau is extended. An interesting feature of the data is that as the cell discharges the boundary moves closer to the cell wall.

The system is too complex to arrive at a complete model of the electrode from the limited data that is available but the transition between high and low transmitted intensity probably is at the boundary between 2-liquids and 1-liquid in the Na-S phase diagram. This is consistent with requiring more discharged sodium to effect transition farther from the sodium electrode. The plots in Figure J.18 indicate transformation occurs more uniformly through the extended sulfur electrode during recharging. The reason for decreased absorption in the nearly completely discharged cell may be related to the formation of Na_2S_2 deposits as a consequence of the high current density.

Caution is to be used interpreting the magnitudes of x-ray absorption, especially comparing measurements at different locations. The beam through the electrode near

the outside wall is attenuated by a moderately homogeneous Na-S composition, whereas the beam close to the beta alumina surface is attenuated by material over the entire composition range.

Resolution. High temperature x-radiography will also be useful to investigate deterioration and corrosion of components in Na-S cells under active electrochemical cycling conditions. The resolution of detail that easily is attainable with the present film technique is illustrated in Fig. J.19. The radiograph was made through a cell wall 0.005" thick with 30 keV x-rays and Kodak R single emulsion film. The beta alumina tube and container walls are clearly resolved and it is estimated that features with moderate difference in density could be seen and measured to $< 0.005\mu m$.

J.2.2 Summary

X-radiography has been used to observe the flow of electrochemically active materials in a Na-S cell as it discharged and charged at high temperature. Differential and densitometric techniques were applied to detect differences in electrochemical activity at various locations in test cells and to observe composition changes in the extended sulfur electrode.

At its present state of development, radiography could be applied to determine the effect of design and material changes on the distribution of active materials during cycling and thus reduce the time required to optimize parameters for the Na-S battery. The method easily can be

improved by radiographing cells from several directions and using x-ray detectors to measure x-ray absorption. Computerized tomography could be used to resolve details in the cell interior.

Fundamental studies of model systems carried out in consort with potential and cyclic voltammetry measurements could clarify the thermodynamics and kinetics of the sulfur/sulfide electrode reactions. For investigations of this nature it probably would be desirable to build thin rectangular cells with homogeneous current collectors.

References

1. B. Cleaver, A. J. Davies and M. D. Hames, Electrochim. Acta 18, 719 (1973).
2. J. S. Newman and C. W. Tobias, J. Electrochem. Soc. 109, 1183 (1962).
3. J. Euler and W. Nonnenmacher, Electrochim. Acta 2, 268 (1960).
4. J. G. Gibson, J. Appl. Electrochem. 4, 125 (1974).
5. Y. K. Kao and P. C. Wayner, J. Electrochem. Soc. 123, 632 (1976).
6. R. D. Armstrong, T. Dickinson and M. Reid, Electrochim. Acta 20, 709 (1975).
7. W.L. Roth, General Electric Corporate Research and Development Report No. 75CRD135, June (1975).
8. G.T. Pearson and P.L. Robinson, J. Chem. Soc., 1473 (1930).
9. M.W. Breiter, J.B. Bush, Jr., S.P. Mitoff, O. Muller and W.L. Roth, Energy Storage, The Electrochem. Soc. (1976).
10. O. Muller, Private Communication.

Figure Captions

Fig. J.1 Experimental arrangement for determining mat resistance.

Fig. J.2 Mat resistance vs. temperature for two configurations.

Fig. J.3 Schematic of sulfur electrode system modelled.

Fig. J.4 Reaction rate distribution for $R_m > R_c$.

Fig. J.5 Reaction rate distribution for $R_m < R_c$.

Fig. J.6 Reaction rate distribution for $R_m = R_c$.

Fig. J.7 Reaction rate distribution for two mat system.

Fig. J.8 Oven for high temperature radiography. Left - Interior with test cell. Right - Front and back plate. a - Na-S test cell. b - Quartz heater. c - Reflector. d - Insulation. e - Port for current and voltage probes. f - Heater terminal. g - Oven wall. h - Clamping bolt. i - Water channel. j - X-ray window.

Fig. J.9 Na-S test cell. a - Glass seal. b - Mechanical seal. c - Glass spacer. d - Loading tube. e - Sodium. f - Insulator. g - Alpha alumina ring. h - Beta alumina tube. i - Sulfur and carbon felt. j - Metallic container.

Fig. J.10 Na-S phase diagram.

Fig. J.11 Radiographs of cell heated to operating temperature the first time. a - Room temperature. b - 154°C. c - 340°C. The square metal tab, sphere and bands are electrical connections for filling and cycling.

Fig. J.12 Open circuit voltage and cell resistance of Na-S cell during first cycle. Current density 108 ma/cm^2.

Fig. J.13 Radiographs of Na-S cell taken during first discharge. a - Fully charged. b - 0.25 Ahr. c - 2.25 Ahr. d - 4.25 Ahr. e - 6.25 Ahr. f - 8.25 Ahr. g - 15.25 Ahr.

Fig. J.14 Radiographs of Na-S cell taken during first recharge. a - Fully discharged. b - 2.00 Ahr. c - 4.00 Ahr. d - 6.13 Ahr. e - 8.00 Ahr. f - 10.50 Ahr. g - 13.80 Ahr.

Fig. J.15 Open circuit voltage and cell resistance of Na-S during second cycle. Current density 216 ma/cm^2.

Fig. J.16 Δ-radiographs of Na-S cell cycled at 216 ma/cm^2. Dark areas are regions in which sodium polysulfide formed during discharge. Light areas are regions from which sodium polysulfide was depleted during charge.

Fig. J.17 Densitometer trace of radiograph taken on Na-S cell after 12.25 Ahr discharge. a - Electrode in center of beta alumina tube. b - Beta alumina wall. c - Metal cell wall. The broad maximum to the left of the beta-alumina tube is due to x-ray transmission through voids in the carbon/sulfur electrode. The distance between the cell walls is 1".

Fig. J.18 X-ray transmission at various locations in Na-S cell. The curves give the variation of X-ray transmission Δ mm from the surface of the beta-alumina tube.

Fig. J.19 Enlarged section of partially discharged Na-S cell radiographed at 340°C on Kodak R film. The metal container is 1" diameter and the wall thickness was reduced to 0.005". The structure at lower left is a density wedge for densitometering and making Δ-radiographs.

List of Tables

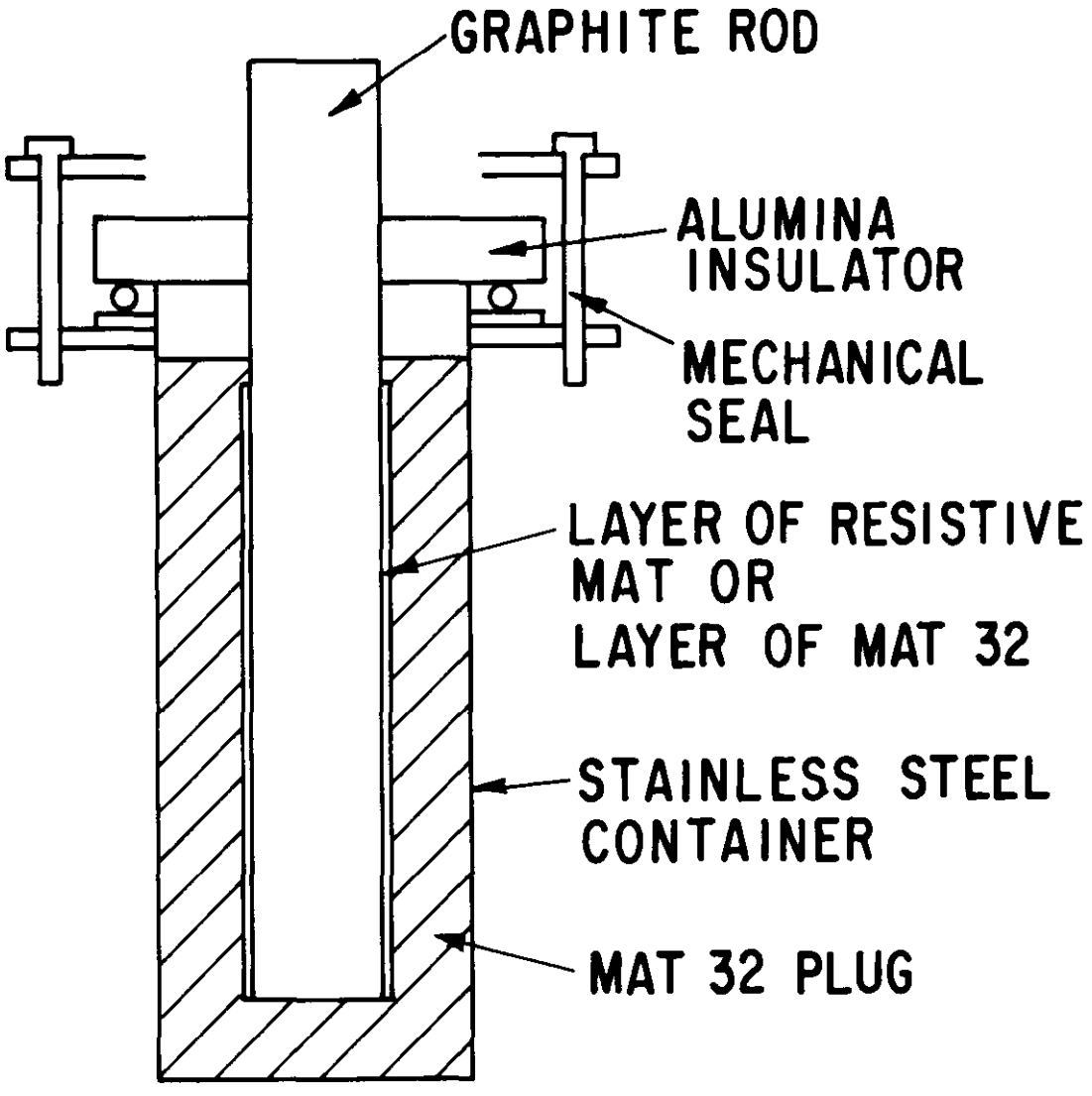

Figure J.1. Experimental Arrangement for Determining Mat Resistance

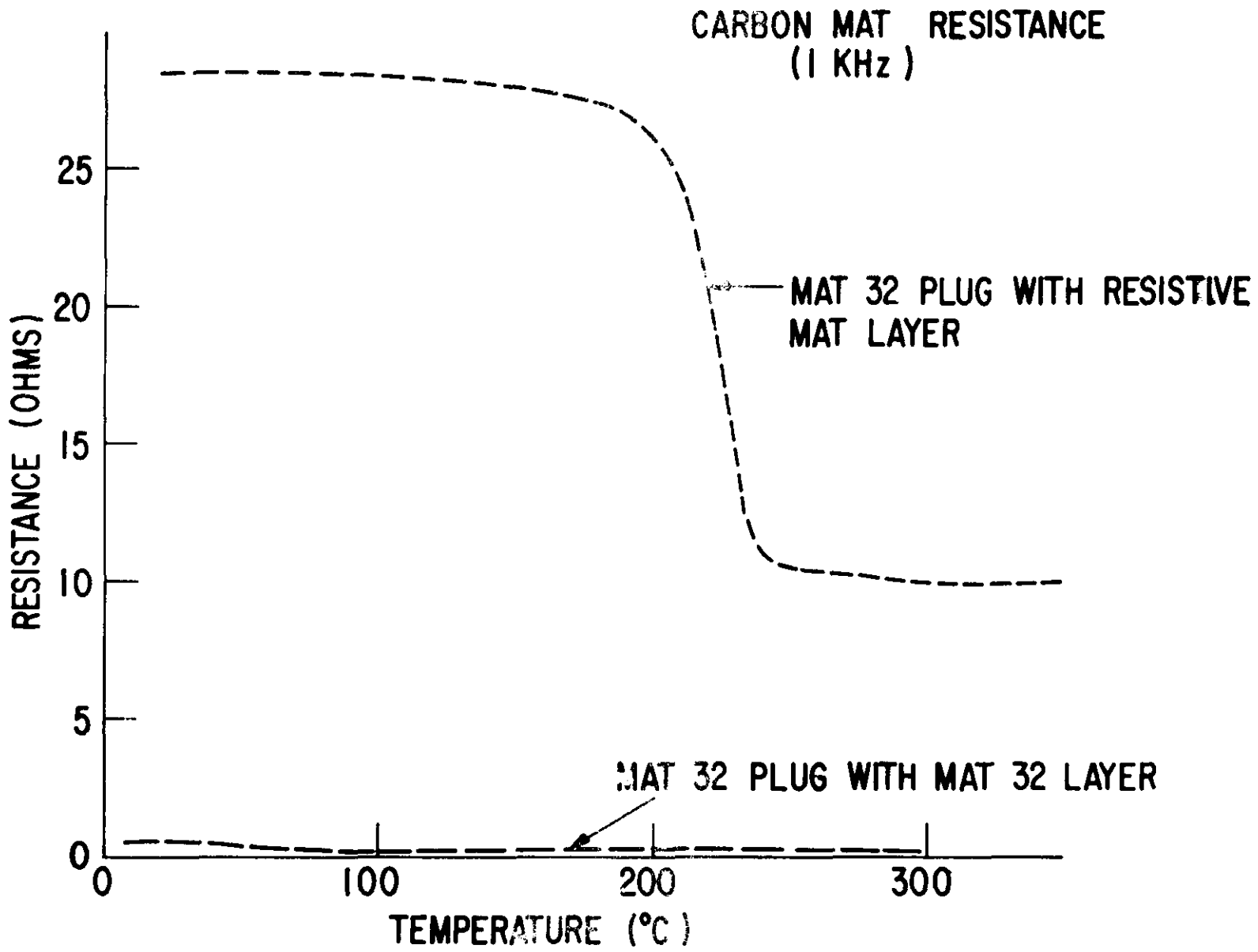

Figure J.2. Mat Resistance vs. Temperature for Two Configurations

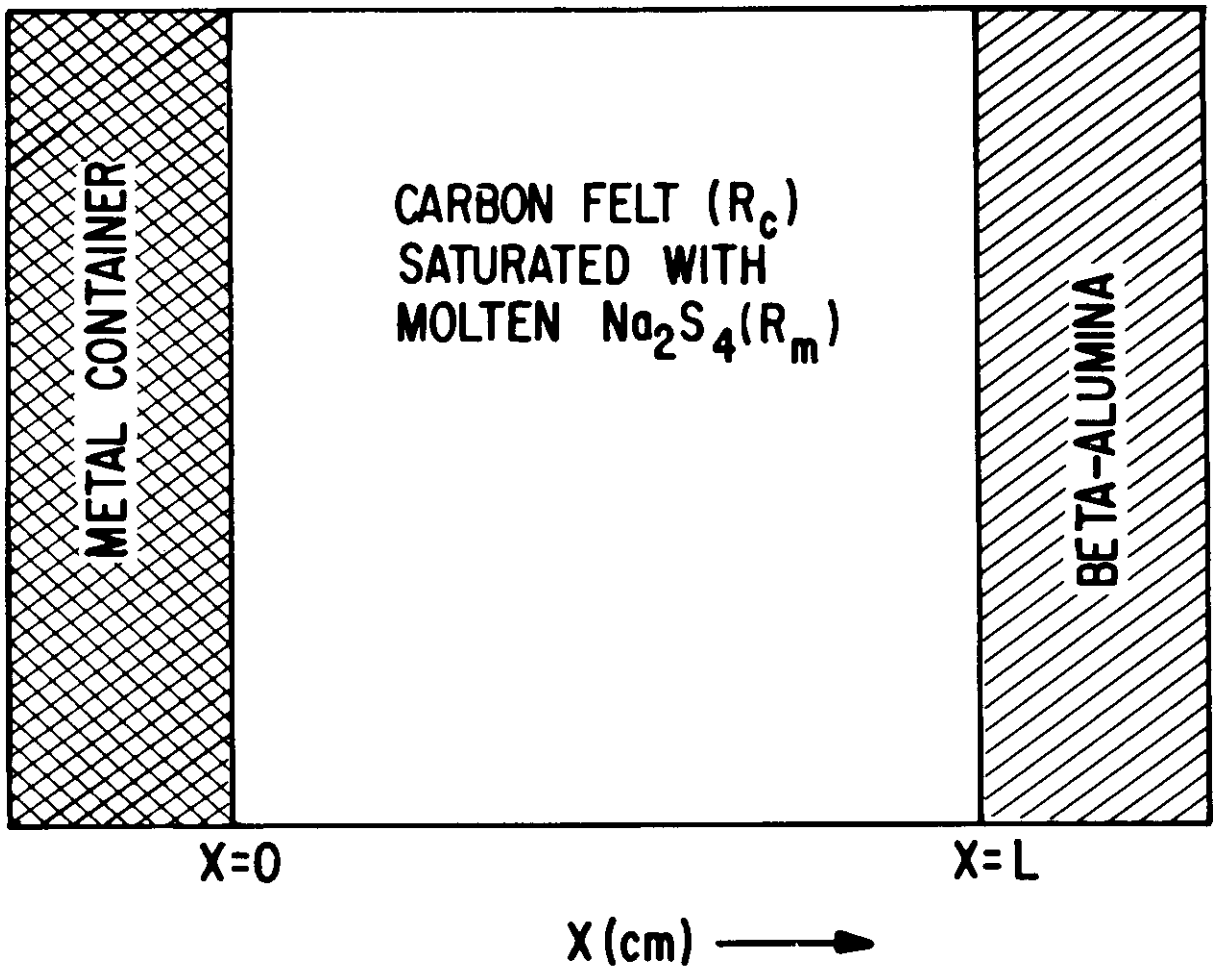

Figure J.3. Schematic of Sulfur Electrode System Modelled

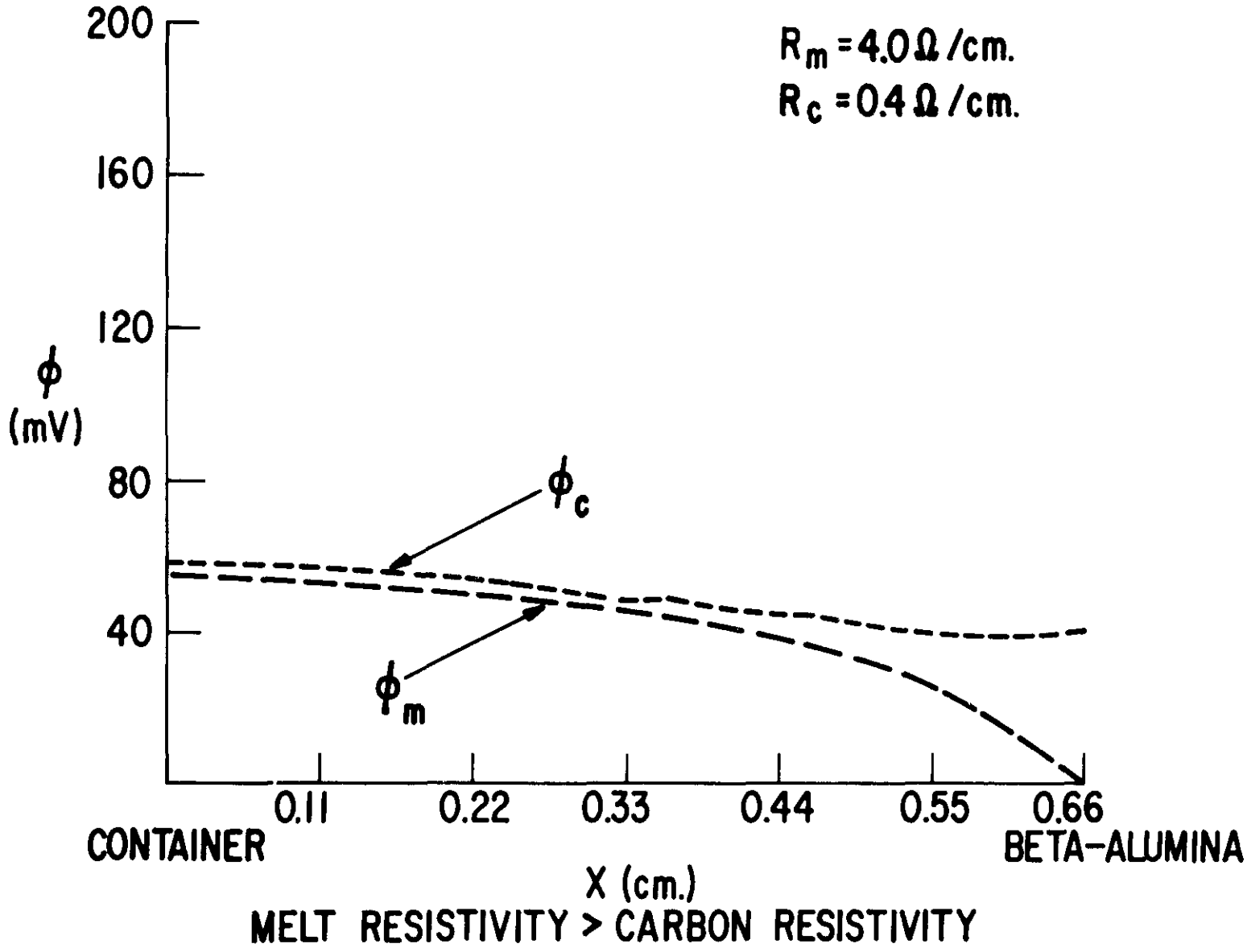

Figure J.4. Reaction Rate Distribution for $R_m > R_c$

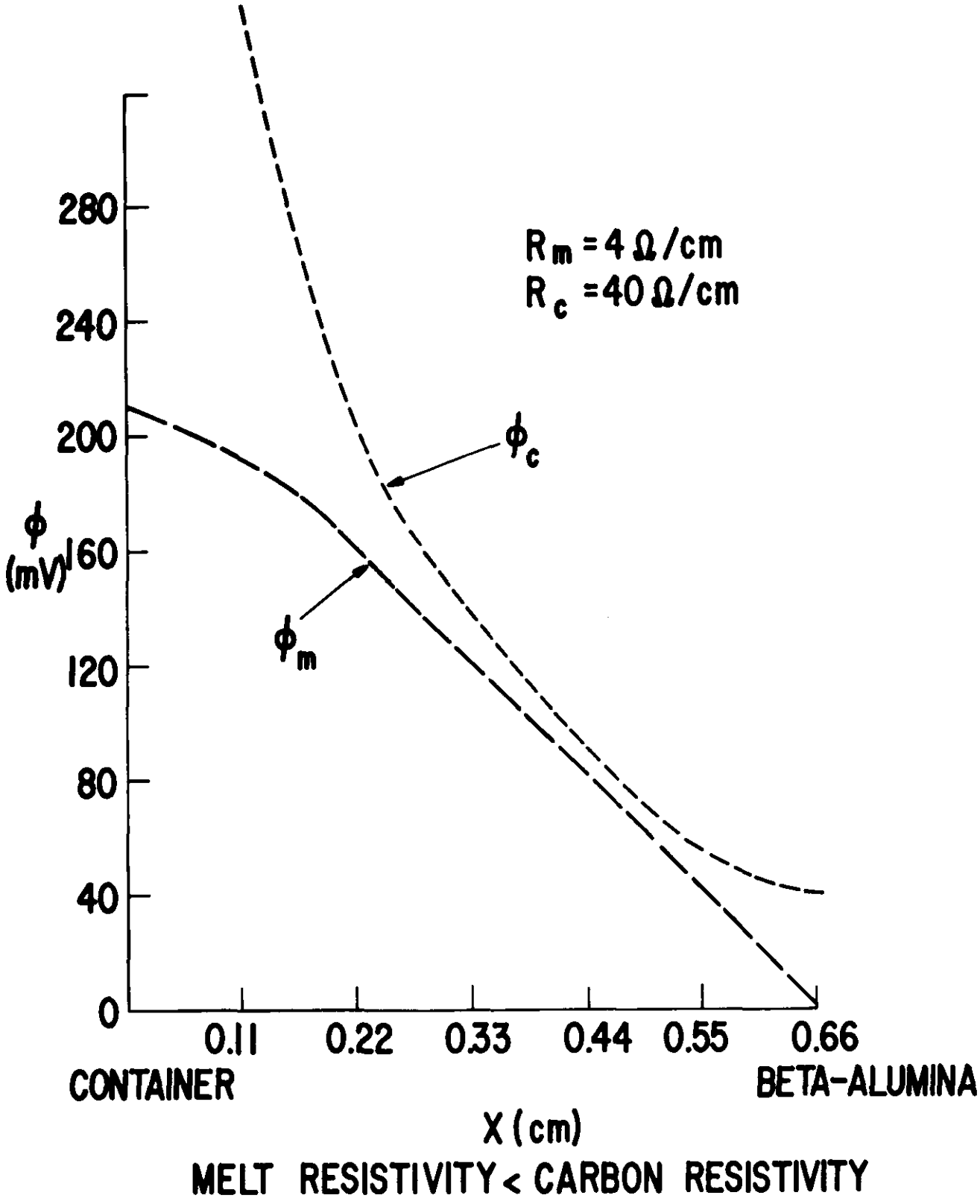

Figure J.5. Reaction Rate Distribution for $R_m < R_c$

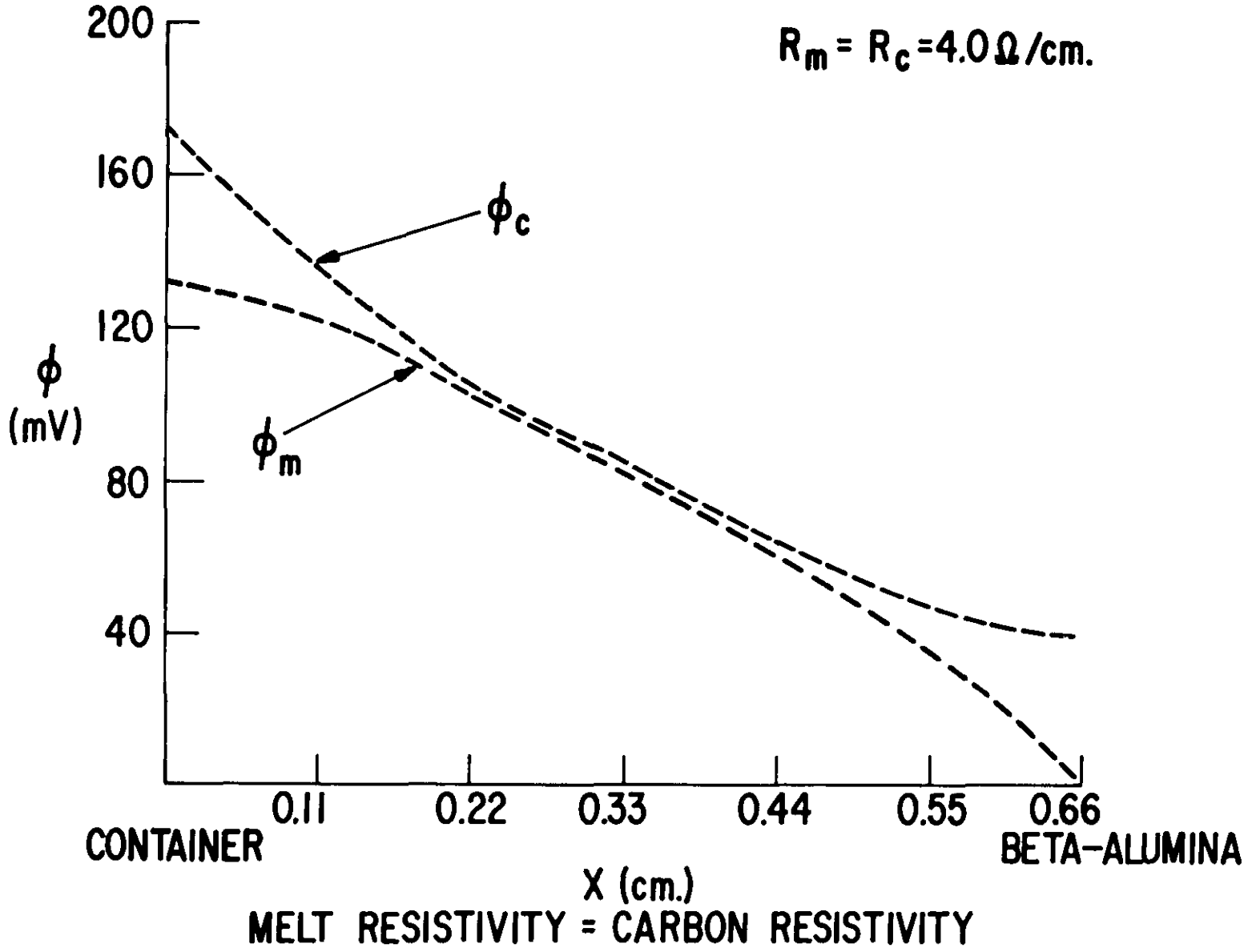

Figure J.6. Reaction Rate Distribution for $R_m = R_c$

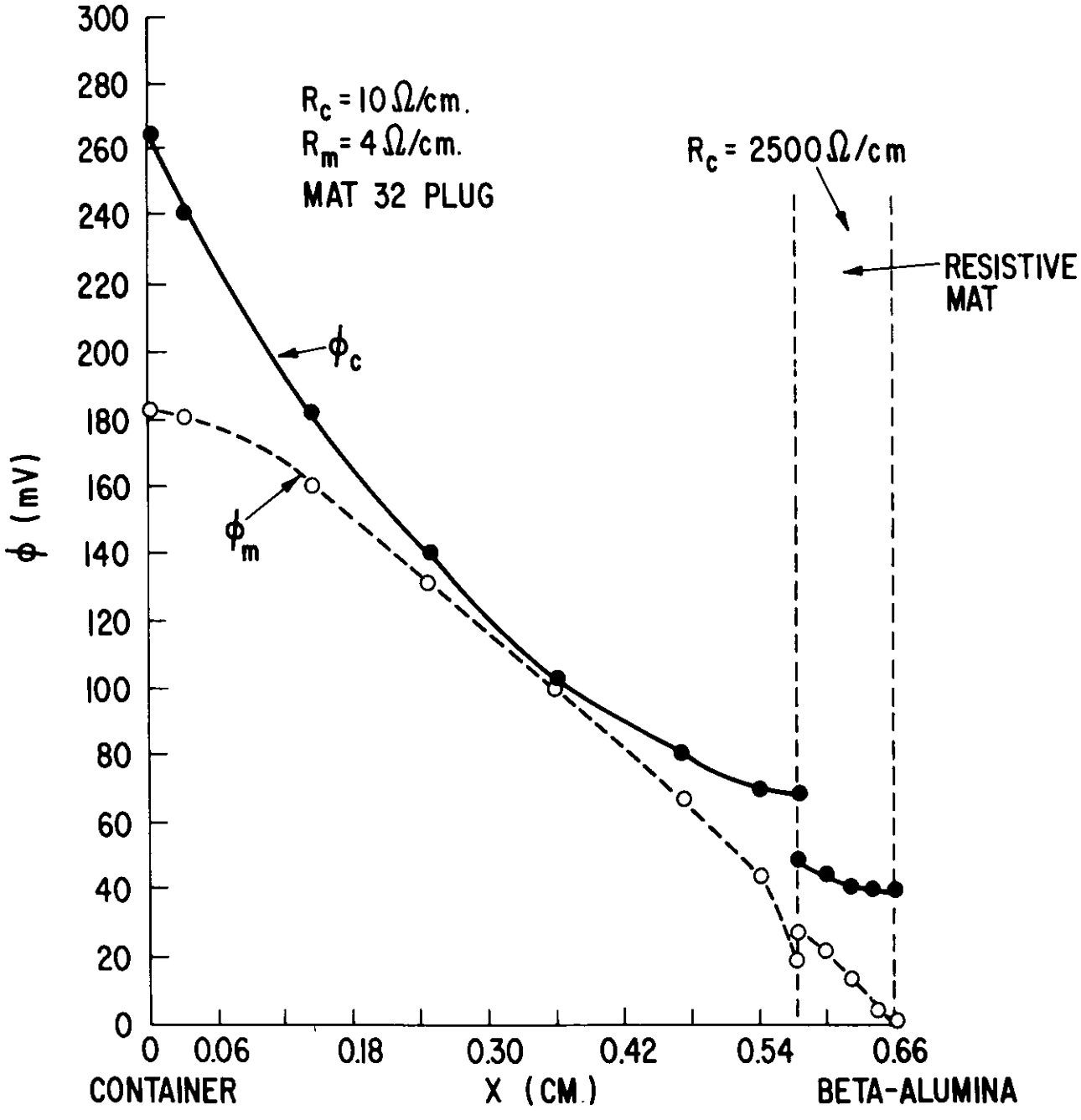

Figure J.7. Reaction Rate Distribution for Two Mat System

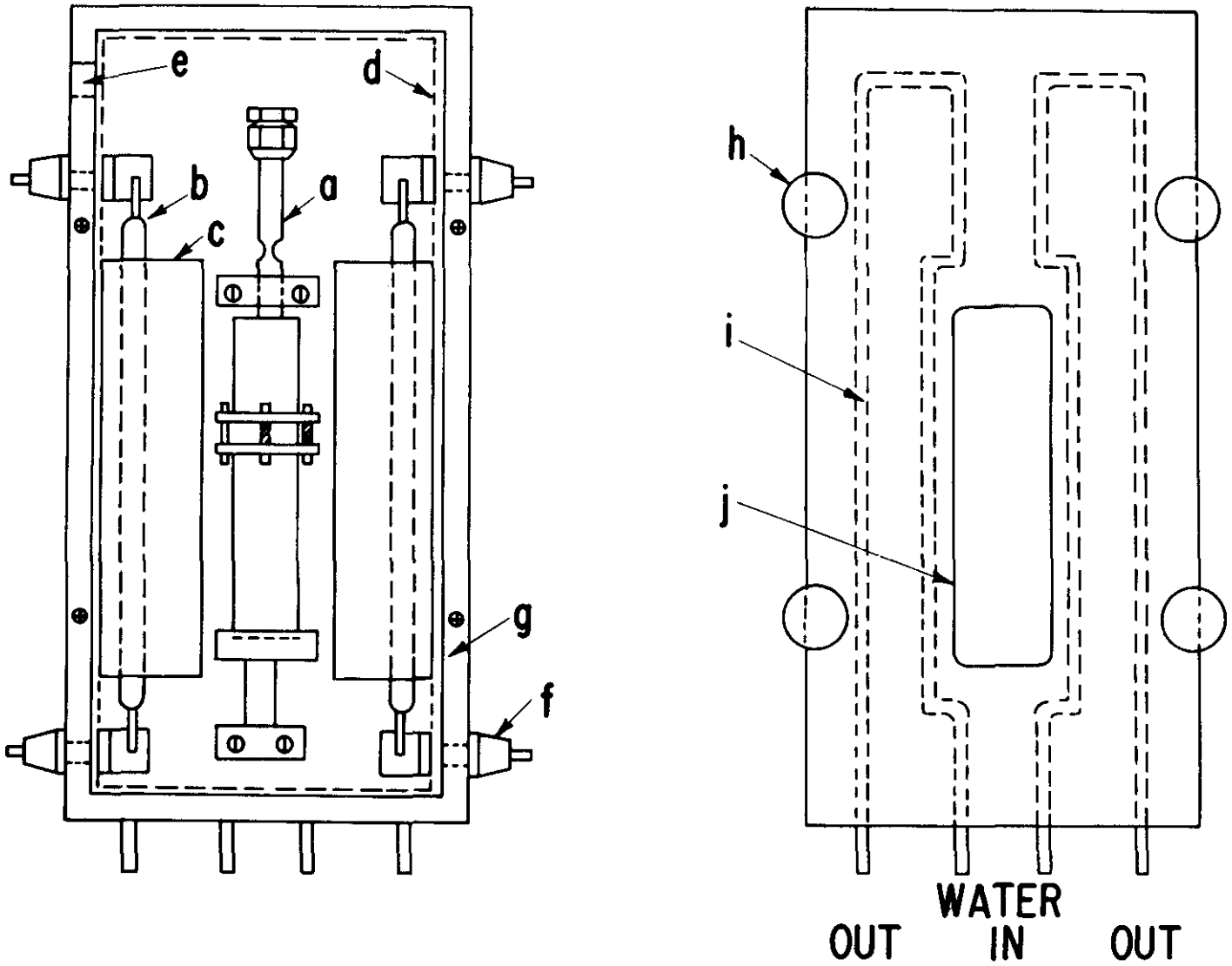

Figure J.8. Oven for High Temperature Radiography. Left - Interior with test cell. Right - front and back plate. a - Na-S Test Cell. b - Quartz heater. c - Reflector. d - Insulation. e - Port for current and voltage probes. f - Heater terminal. g - Oven wall. h - Clamping bolt. i - Water channel. j - X-ray window.

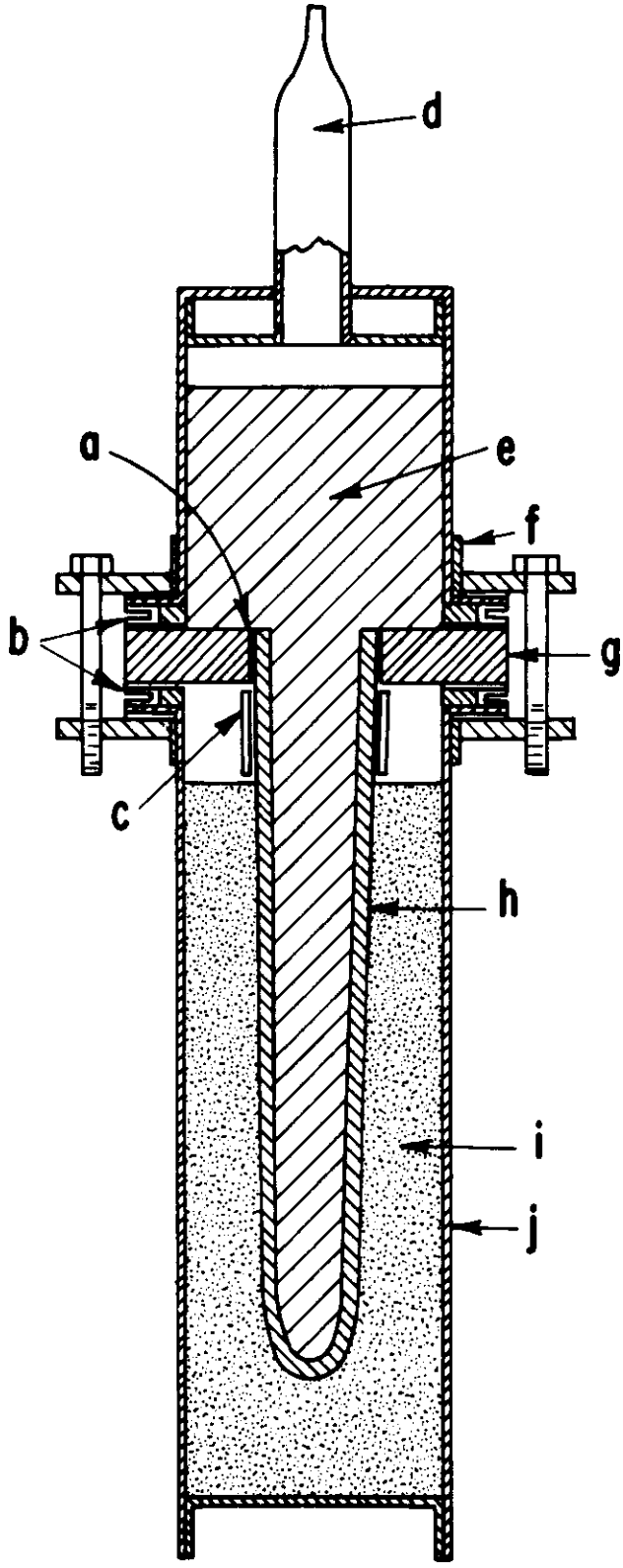

Figure J.9. Na-S Test Cell. a - Glass Seal. b - Mechanical Seal. c - Glass Spacer. d - Loading Tube. e - Sodium. f - Insulator. g - Alpha alumina ring. h - Beta alumina tube. i - Sulfur and carbon felt. j - Metallic container.

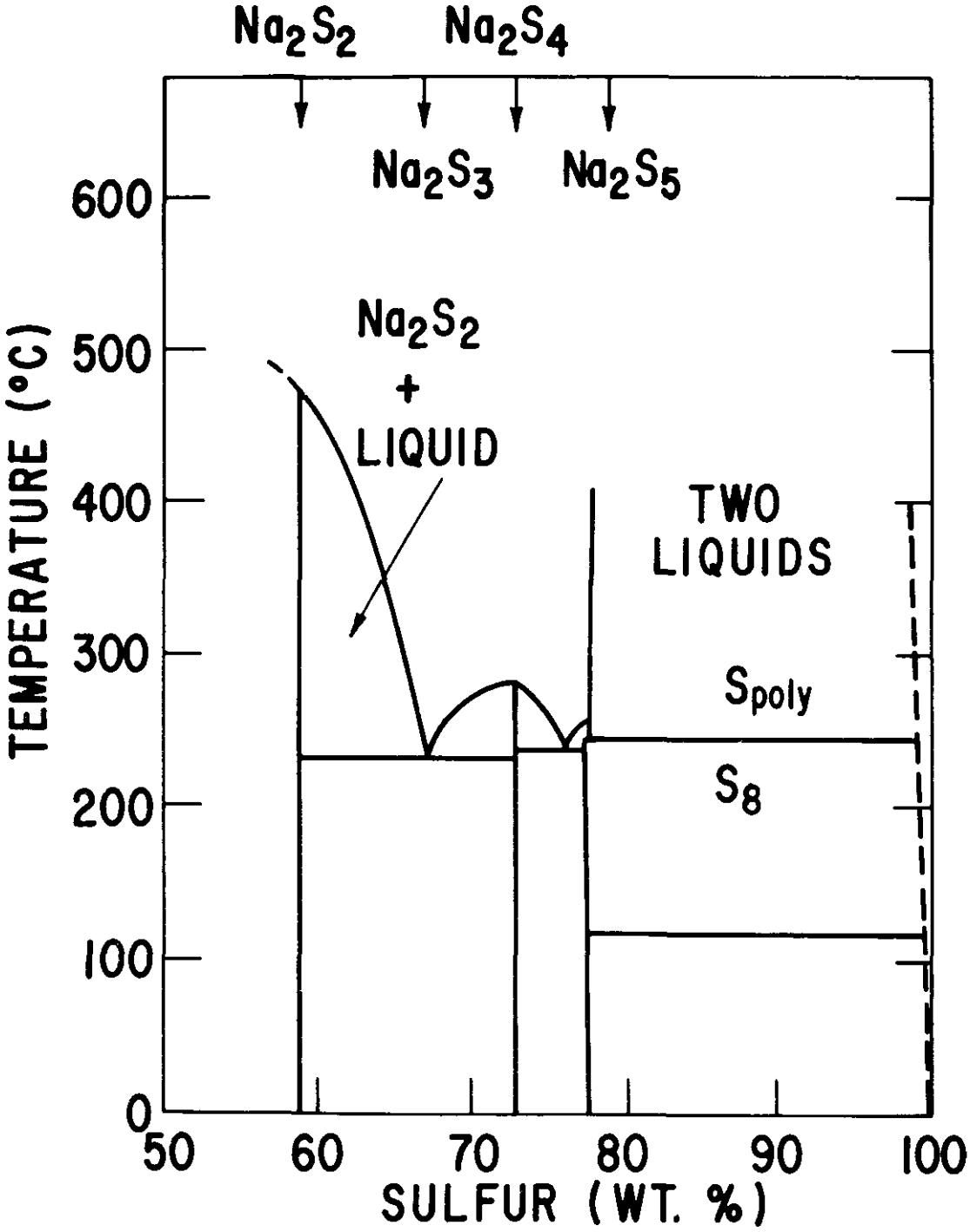

Figure J.10. Na-S Phase Diagram

Figure J.11. Radiographs of Cell Heated to Operating Temperature the First Time. a - Room temperature. b - 154°C. c - 340°. The square metal tab, sphere and bands are electrical connections for filling and cycling.

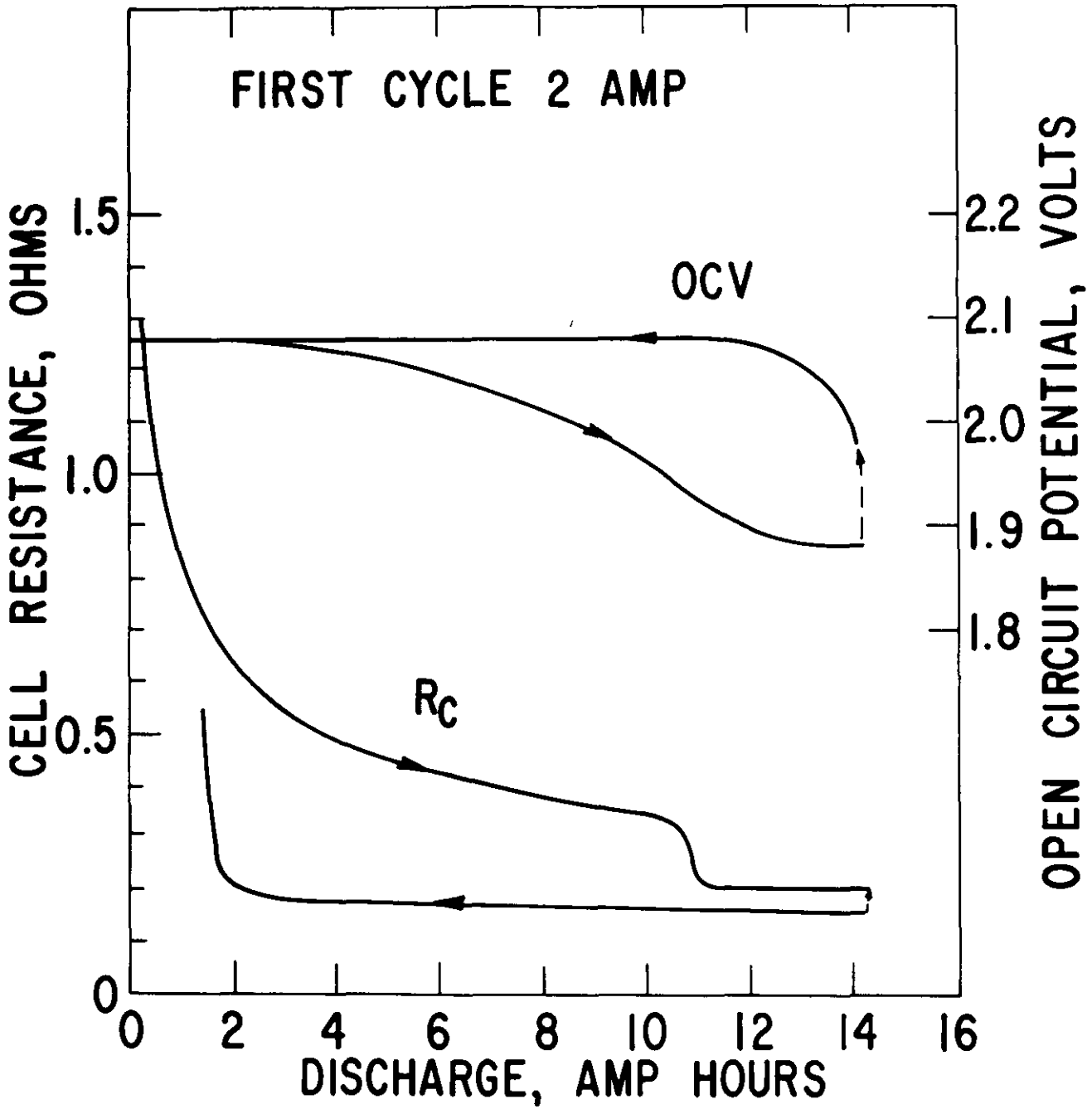

Figure J.12. Open Circuit Voltage and Cell Resistance of Na-S Cell During First Cycle. Current density 108 ma/cm^2.

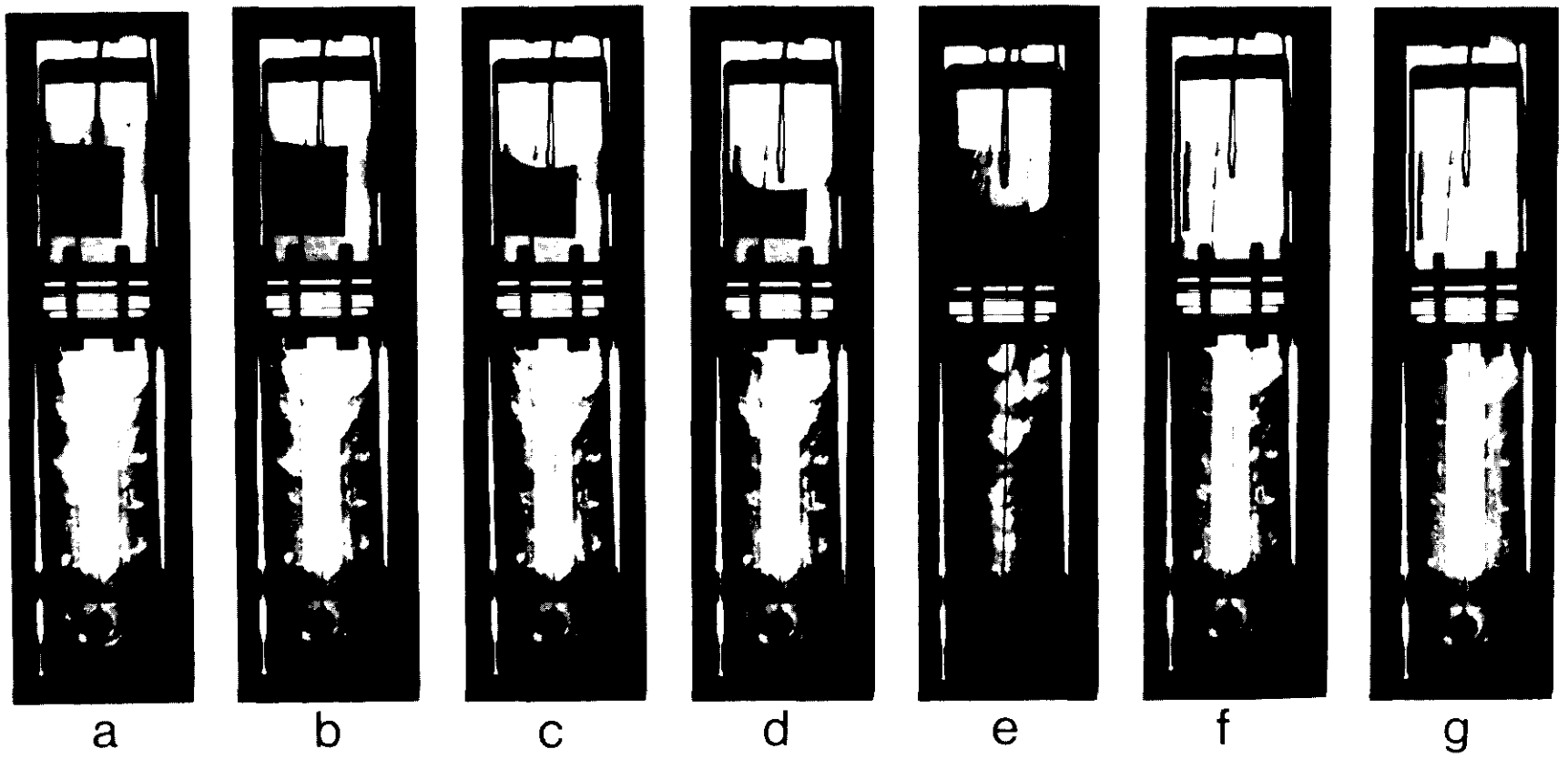

Figure J.13. Radiographs of Na-S Cell Taken During First Discharge. a - Fully charged. b - 0.25 Ahr. c - 2.25 Ahr. d - 4.25 Ahr. e - 6.25 Ahr. f - 8.25 Ahr. g - 15.25 Ahr.

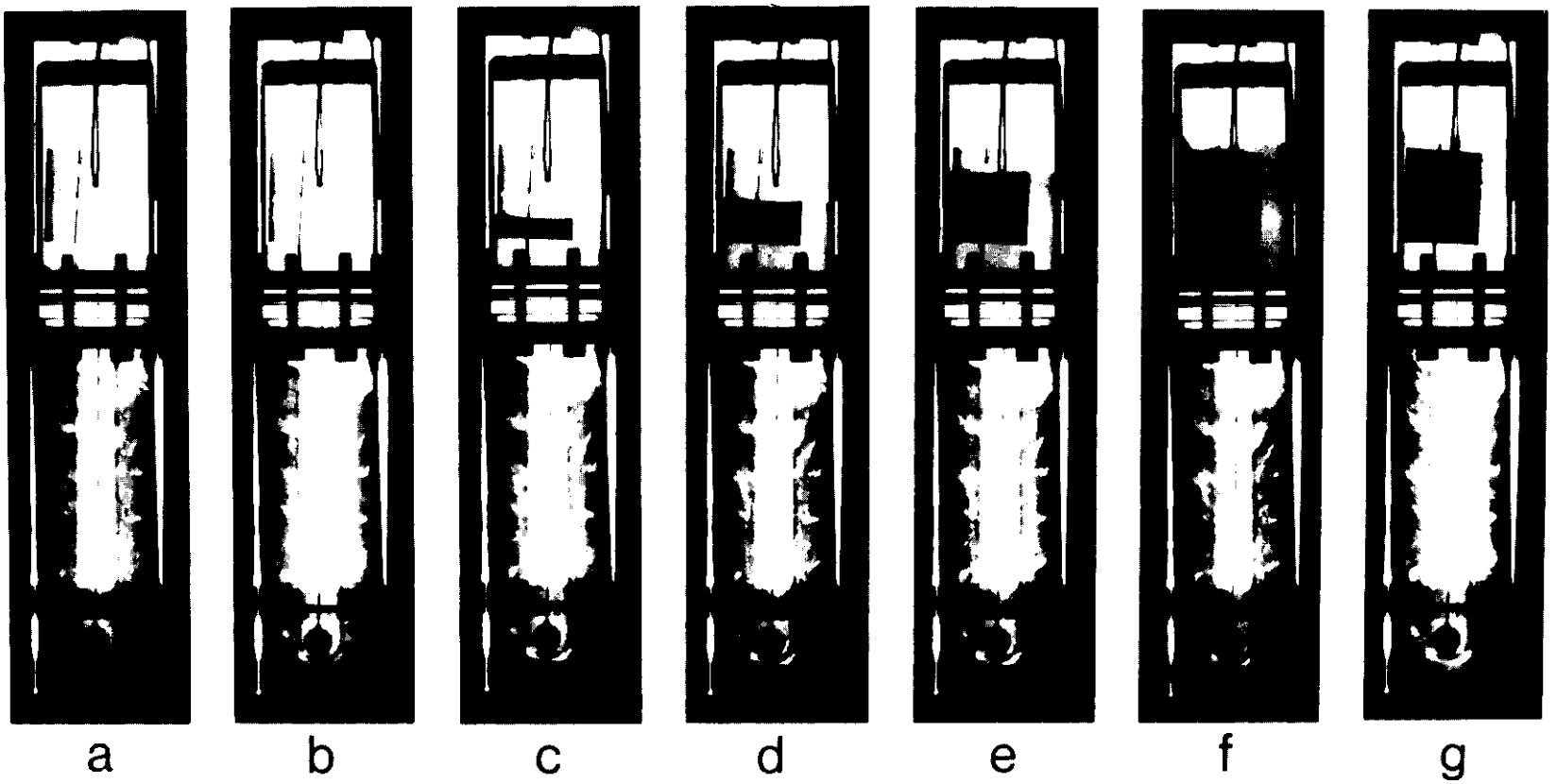

Figure J.14. Radiographs of Na-S Cell Taken During First Recharge. a - Fully discharged. b - 2.00 Ahr. c - 4.00 Ahr. d - 6.13 Ahr. e - 8.00 Ahr. f - 10.50 Ahr. g - 13.80 Ahr.

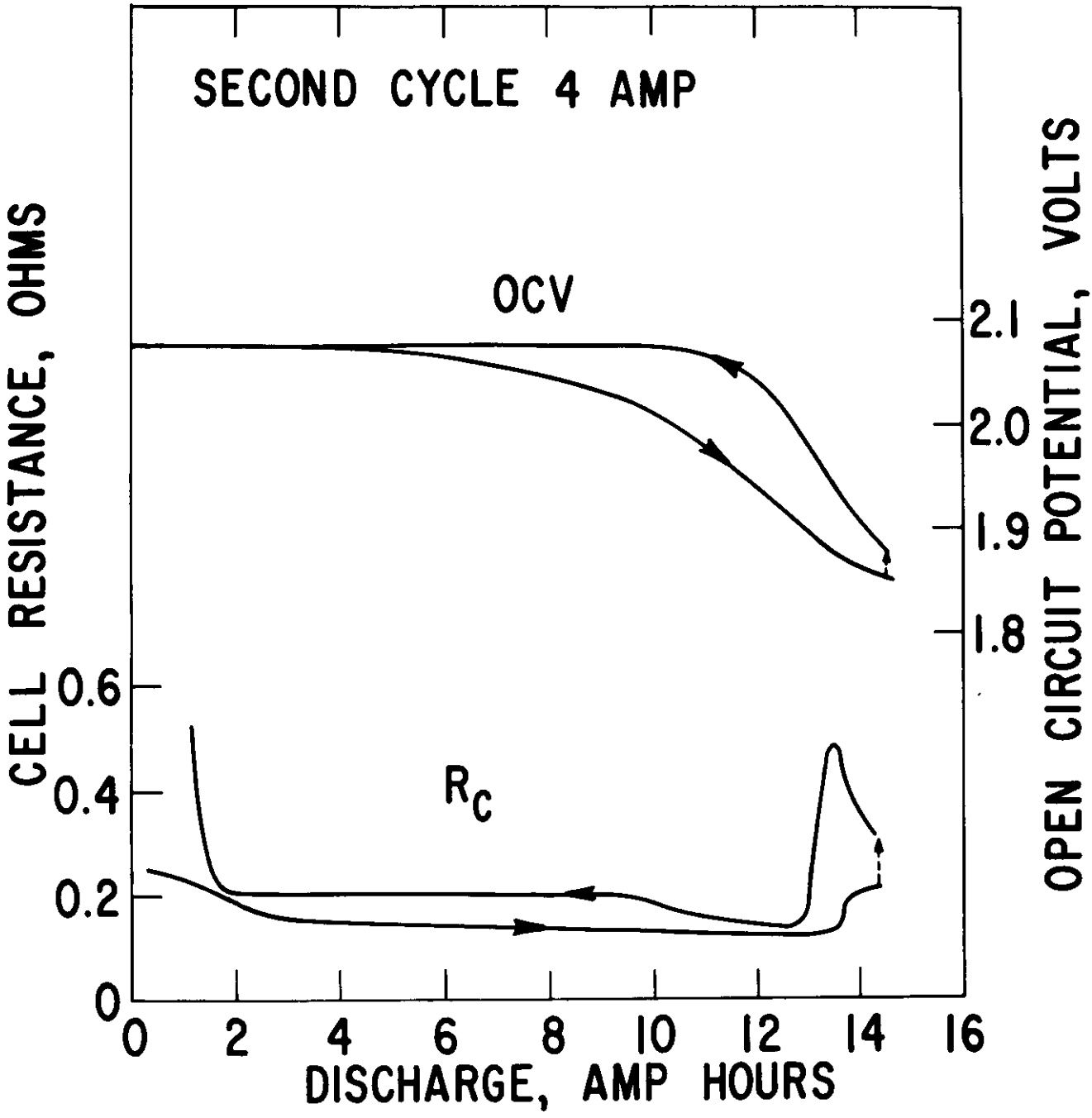

Figure J.15. Open Circuit Voltage and Cell Resistance of Na-S During Second Cycle. Current density 216 ma/cm^2.

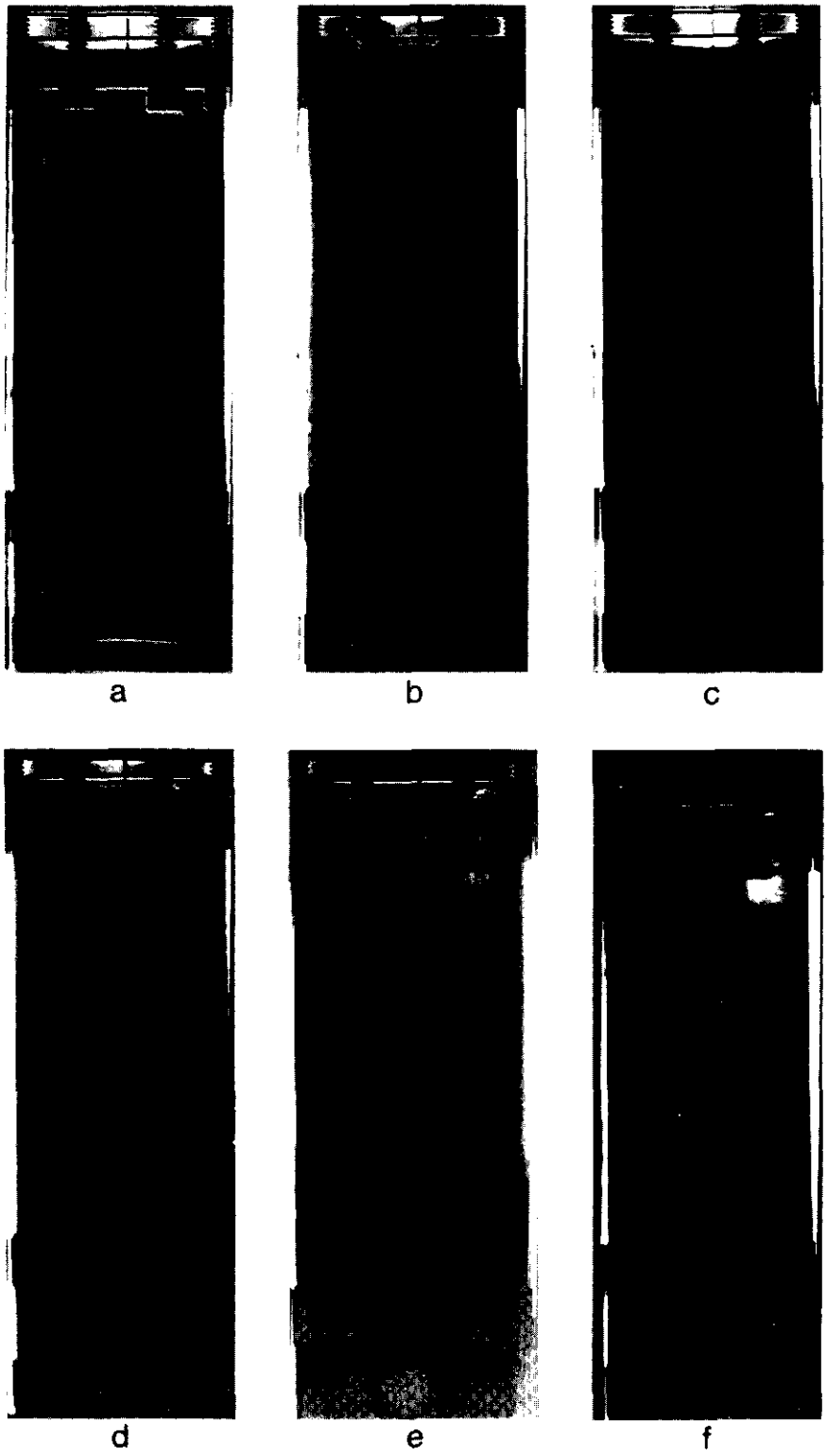

Figure J.16. Δ-Radiographs of Na-S cell Cycled at 216ma/cm^2. Dark areas are regions in which sodium polysulfide formed during discharge. Light areas are regions from which sodium polysulfide was depleted during charge.

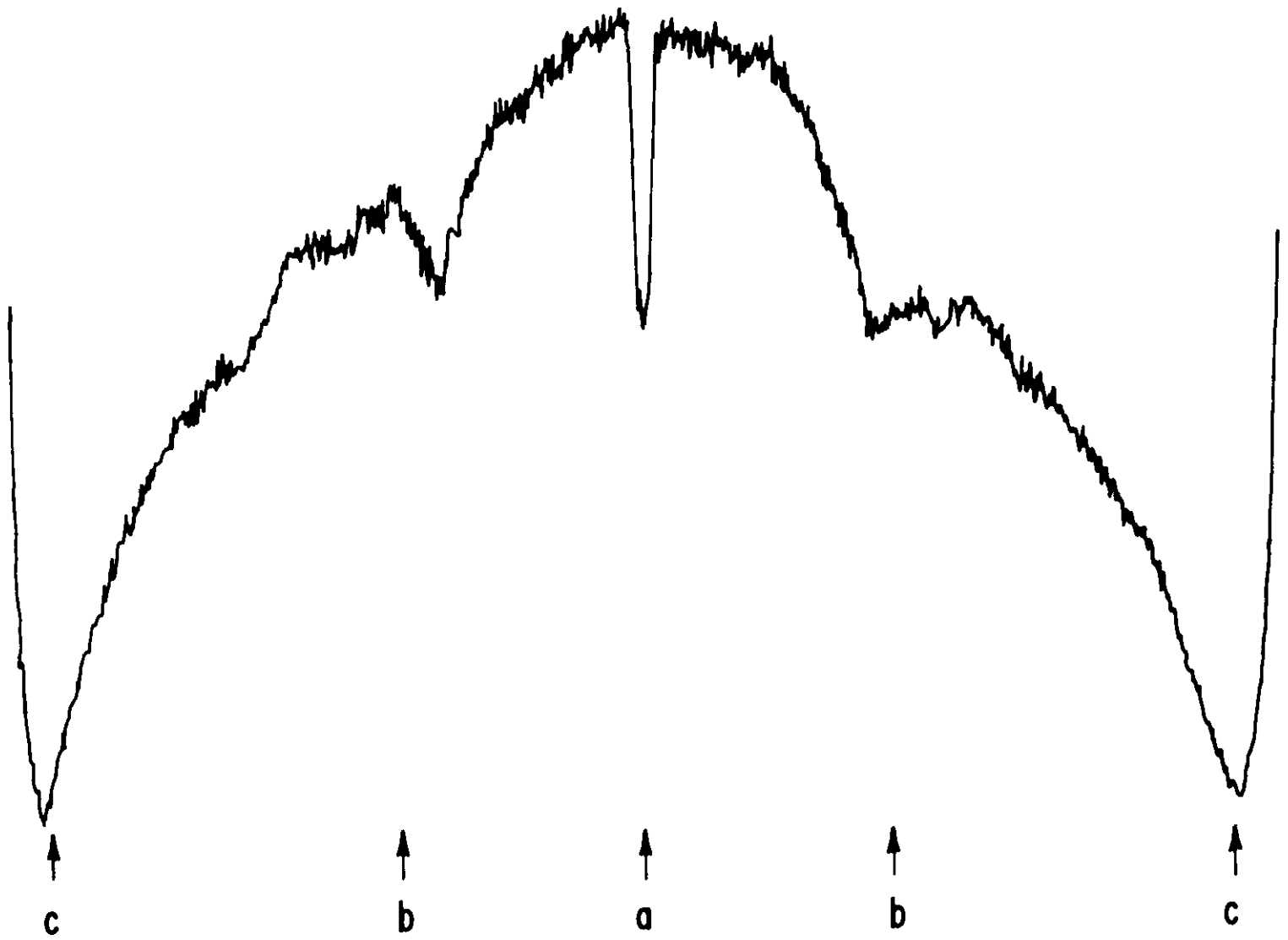

Figure J.17. Densitometer trace of radiograph taken on Na-S cell after 12.25 Ahr discharge. a - Electrode in center of beta alumina tube. b - Beta alumina wall. c - Metal cell wall. The broad maximum to the left of the beta-alumina tube is due to x-ray transmission through voids in the carbon/sulfur electrode. The distance between the cell walls is 1".

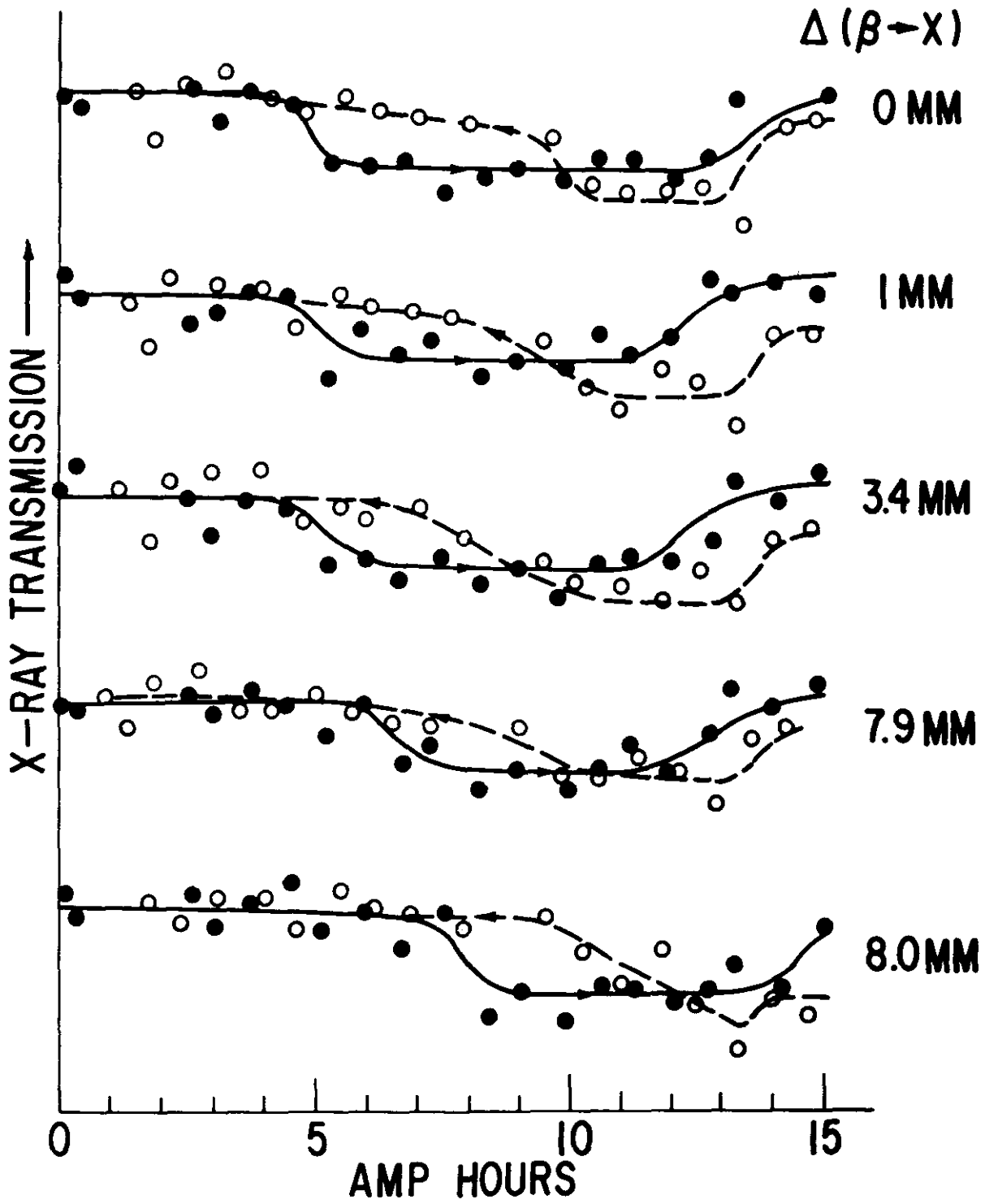

Figure J.18. X-ray Transmission at Various Locations in Na-S Cell. The curves give the variation of x-ray transmission Δ mm from the surface of the beta-alumina tube.

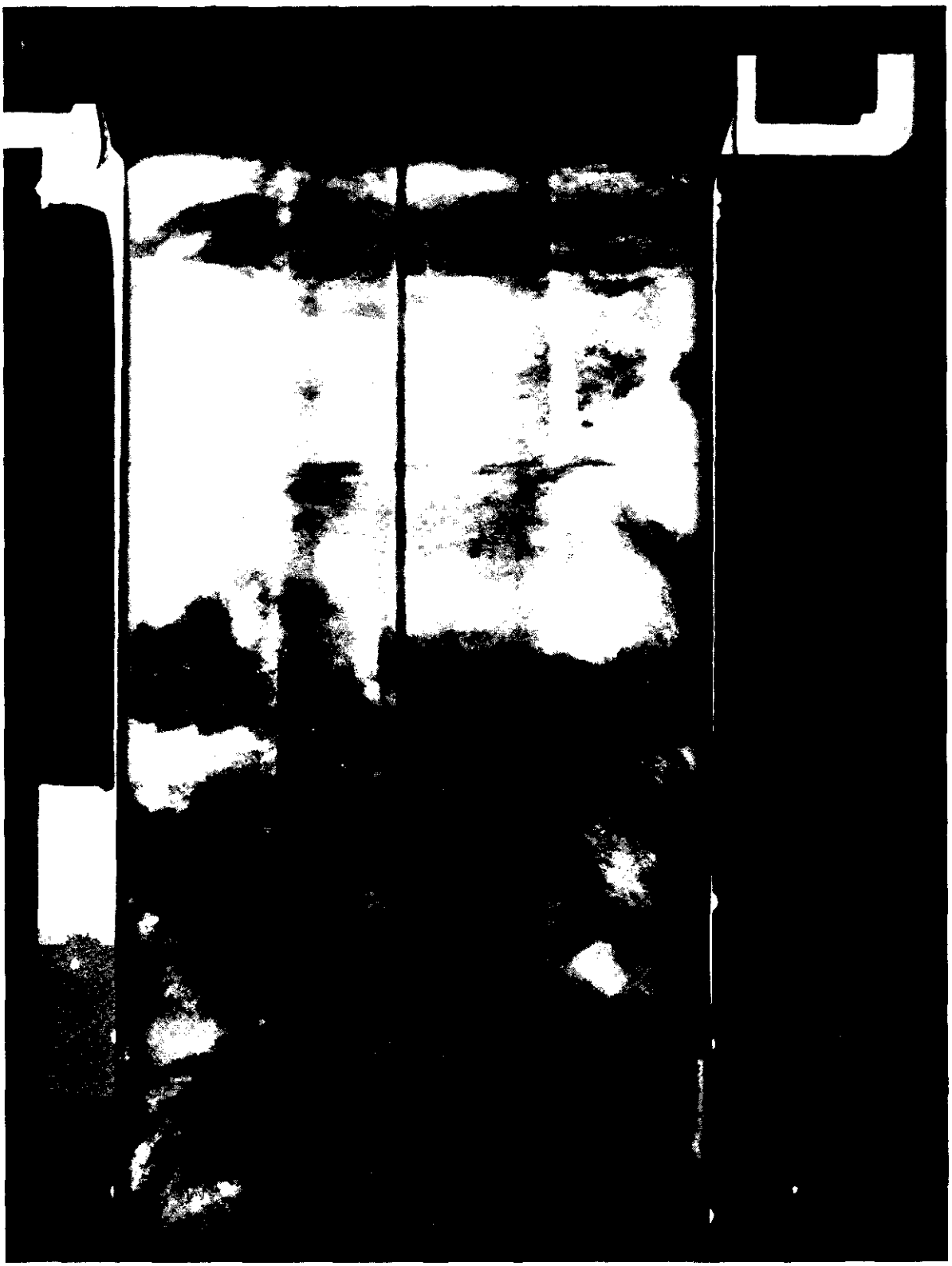

Figure J.19. Enlarged Section of Partially Discharged Na-S Cell Radiographed at 340°C on Kodak R Film. The metal container is 1" diameter and the wall thickness was reduced to 0.005". The structure at lower left is a density wedge for densitometering and making Δ-radiographs.

Section K

SCALE-UP ACTIVITIES

The sodium-sulfur battery development program at General Electric now stands at a crossroads. The program emphasis is shifting from feasibility demonstration with laboratory test cells to detailed design, development and demonstration of battery systems of much larger scale. The program therefore faces the usual but difficult challenges associated with scale-up of laboratory processes and devices.

This Section describes briefly the actions taken during 1977 in the areas of cell size and component production scale-up as well as safety, manufacturing process development, battery controls, and failure modes analysis. In many cases, work has just started (under an Add-On Contract); in other areas, substantial progress has been made. Listed and described below are fourteen areas directly related to program scale-up.

K.1 Design of Full Size Cell

The basic principles of cell design were described in Section G. When the design calculations and iterations have

been completed a preferred design is established; the program is currently in that stage.

The full size cell construction will be approached in two simultaneous programs, the first cells to be constructed will use a mechanical exterior seal similar to those used in the 16 Ah cells and the superseding program will use cells constructed using thermocompression-bonded seals with inward turned flanges (see Fig. G.1). A separate study has been undertaken for design of equipment to satisfactorily form steel containers with inward flanges.

The exact dimensions, projected performance, and number of cells required per MWh are consistent with the economic analysis given in Section H.

K.2 Ceramic Fabrication

Scale-up on this task falls into two categories: that involved with fabrication of larger sized tubes and that concerned with larger production rates.

Ceramic tubes have been formed both by isostatic pressing and electrophoresis. The tubes formed with an Olin isostatic

press are of a size to be built into cells for the BEST battery. However, a scale-up by a factor of about 20 times in mass was required of tubes formed by electrophoretic deposition. Surprisingly only two new problems were encountered in forming large tubes. There was a tendency for the wall thickness to be larger near the bottom or closed end after deposition. In the worst case the ratio of wall thicknesses amounted to 1.7. The other problem was occasional cracking of the green tube during removal of the amyl alcohol vehicle. Both problems were readily overcome: the former by circulation of the suspension during deposition and the latter by more uniform drying of the deposit along the length of the tube.

Work related to scale-up in production rate presently involves three kinds of activities:

1. Selection and qualification of more cost effective reagents for carrying out processing.
2. Selection and qualification of equipment for performing operations on a larger scale, and
3. Close examination of individual processing steps for purposes of simplification and even of elimination in some instances since there is considerable "over-processing" in present laboratory scale operations.

K.3 Interior Seals

The selection of the sealing glass to be used to seal the alpha-alumina insulator to the beta-alumina tube has been the subject of intensive study. After several months of cell and accelerated (higher temperature) testing, a satisfactory borate type glass has been formulated, which is (1) resistant to sodium attack, (2) resistant to reactions with alpha or beta-alumina, and (3) satisfactory from the sealing operation viewpoint.

Several seals have been made to beta-alumina tubes of the full 28 mm O.D. and disks of alpha-alumina of the mechanical seal design size without failure by cracking and they were helium leak-tight.

A study has also been in progress to examine stress levels in various alpha-to-beta seal designs. The existence of mechanical stress in the area of this seal is probably a significant contribution to some of the failures observed in the small prototype cells.

Scale-up of the seal size will increase the risk of failure. The work of this task will be used as a guide in the design of the larger seals. It will include determination of stress levels, risk analysis (analysis of various factors contributing to the risk of rupture), and life prediction as limited by critical size crack growth.

K.4 Exterior Seals

The size scale-up for seals between the alpha alumina insulator disk and the sulfur and sodium containers has been successfully accomplished using mechanical seals. Several full size seals have been made using alpha-alumina disks, and one with a beta-alumina tube segment which were all helium leak-tight. These techniques will be used to seal the first full size test cells.

Two programs are in progress to scale up the thermo-compression bonding seal which was developed at CGE Laboratories de Marcoussis and successfully duplicated at GE using small metal sulfur and sodium containers. In the first program critical parameters are being examined to see if any new scale-up problems result from the increase in cell dimensions.

A separate program has been undertaken with a more engineering-oriented goal. Here an experimental study has started where semiproduction apparatus is being developed to make the seals and establish the most practical time schedules and type of machinery required to produce required tolerances for BEST Facility cells.

K.5 Continuous Coating Process

Experiences at GE and at CGE have shown that low carbon steel with a particular type of chromium-rich coating makes a long lasting, low resistance, economical sulfur container material which is also well suited to the thermocompression

bonding process. This container has been chosen for full size cells. The coating is presently applied in a batch process. A much more suitable process, from the standpoint of efficiency, yield, and quality control, would be a continuous process; work is underway to develop such a continuous process.

K.6 Sulfur Purification

In anticipation of the future need to purify large amounts of sulfur on a routine basis, an activity has been initiated to determine and develop a high volume, high rate purification process. The following alternatives have been investigated:

1. Direct scale-up of the presently used Bacon-Fanelli process.[1]
2. Commercial sulfur filtration processes.
3. Alternative mechanical (nonfiltration) processes.
4. Alternative, commercial sources of sulfur (and thus avoid purification).

It was concluded that 1 and 3 were viable alternatives for our goal of developing an in-house capacity to purify 700 lbs of sulfur per year in the 1978-79 time frame. It was also found that "by-product" sulfur which is available only in tank-car lots is very low in hydrocarbons which are thought to be the cause of poorer cell performance. This material is very inexpensive and could be the long term solution.

K.7 Cell Filling

Filling sequence, methods, and apparatus have been planned for large cells. The sodium will be loaded into full-size cells in the molten state with a special loading device, which will meter the sodium amount by ultrasonic detection. The apparatus is being constructed.

The sulfur graphite plugs will be made in molds. Three castings will be required for each cell. Molds have been fabricated and successful castings have been made.

K.8 Cycling Apparatus

Cycling of full size cells requires several different types of apparatus. The status of those required for the cycling of large cells is outlined below.

- Furnace for maintaining cells at a constant temperature (300-350°C). A new oven has been procured which is of a size sufficient to hold 30 cells on test at a time. It has forced air circulation so that temperature is uniform to within 2 or 3 degrees centigrade. The furnace is currently being modified to provide for insertion and removal of cells with current, voltage, and individual thermocouple leads.
- Power supplies and switching circuitry have been designed and constructed to supply power and to provide current reversal and open circuit periods for up to twenty cells at adjustable constant current up to fifty amps per cell.

- Computer terminal interfacing. The system for large cell cycling has been made compatible with the system previously developed for the cycling of small cells so that the same device and tape recorder system may be used to switch individual cells from charge to discharge and the reverse depending on operating voltages or time of cycle as used with small cells. The magnetic tape recordings of cell voltages will be used with modifications to the computer programs to obtain the same type of computer cell cycling information as with small cells.

K.9 Safety

Over a year ago some experimental studies on safety were undertaken. The tests were performed on 16 Ah cells. No serious problems were observed on cells this small, so further safety tests were deferred until full size cells were to be made. Now that cell size scale-up is in progress a very detailed safety review and analysis is underway. The study includes aspects of:

- Design
- Component Manufacture
- Assembly
- Shipping/Storage
- Erection
- Operation

The program is considering the following aspects of the safety question.

- Identification of potentially hazardous conditions or processes which are not sufficiently controllable so as to represent a potential short or long term failure.
- Recommendations of design, manufacturing, storage, or operational procedures which would be expected to reduce the likelihood of hazardous failure occurring.
- Recommendations aimed at minimizing the effects of one or more levels of hazardous failure, after the battery is in service.
- Identification of mechanical, electrical or other tests which might be required to determine that certain of the design, manufacturing or other aspects of the battery system might have for failure.

K.10 Failure Modes and Effects Analysis, and Reliability Analysis

These two analyses were initiated in September 1977. The former study will be emphasized (perhaps exclusively during 1977) as it is more appropriate for the Na/S project at its current stage of development. The FMEA will examine all the failure modes of each individual component of the battery system, and analyze the effects of the failure mode on the rest of the battery system as well as on the sensing and control systems and on the "outside world". It is therefore a system level study. The results are presented in a formal tabular scheme. A maintainability study examines the expected rate of component failure and the level and frequency of replacements which will be required to maintain a required reliability. It is thus very important from the standpoint of system economics.

K.11 Electrical Bundling of Cells

The major program objective for 1978 is to assemble one or two full size "bundles" of cells (see Fig. G.2). To prepare for that goal, two parallel activities have been started. At CGE-Marcoussis small test cells are being connected in parallel to observe cycling behavior of such a bundle. Although such a bundle has no direct relationship with the full size bundle designed by GE, an experimental assessment of the technical problems and their severity will result. At GE, performance of a bundle consisting of 40 cells with different capacity/ resistance vs. cycle life characteristics is being modeled and computer-analyzed.

K.12 Battery Control Strategy Study

This study is directed toward comparing the possible benefits of operating the sodium-sulfur battery system in different modes using various control strategies and examining the effects on battery life and efficiency in utility application. The sub-station and distribution control functions which may be required to operate this battery system using the above control strategies will also be studied.

K.13 Module Design Mock-ups

Module design has progressed to the point that detailed thermal and coolant flow must be verified experimentally before commitment to a final design, in the form of full-size fluid flow and heat transfer mock-ups. In turn this has required that the mock-ups represent a realistic near-final design because adequate coolant flow and heat transfer modeling cannot be accomplished without complete physical details of the module construction. Therefore all the engineering phases of the program are currently being put together to construct module mock-ups.

K.14 Manufacturing Process Development

The manufacturing cost of sodium-sulfur batteries will ultimately depend on materials and manufacturing processes, the latter being responsible for capital equipment and labor cost levels. The overall economic prospects for the battery, therefore, will be difficult to assess until the critical manufacturing steps have been validated to an acceptable extent. At GE, the following activities have been initiated for these reasons:

- Metal Joining Processes Development
  This task experimentally addresses three metal joining steps which are critical to the scaled-up cells. 1) Connection of the current collector straps to the outside of the sodium and sulfur containers. 2) Welding of the end caps to the bottom of the sulfur containers (which in the preferred assembly method will be filled with sodium at this point). 3) Closure of the filling tube at the top of the sodium container after filling with sodium.

- Cell Connectors Forming Process Development
  Cell Connectors are straps of metal formed around each cell in a bundle. The precision required in their shape is so high that even the straps for the first experimental bundles cannot be handmade. An automatic forming method must be developed which is an objective of this task. Study of problems associated with current collector forming may lead to a different design concept.

- Thermocompression Bonding Equipment Development
  An equipment with multiple stations is being fabricated to study the potential economic benefits of automation and reduction in processing time.

- Fabrication of Containers With Inward Flanges
  The Mark IIIA cell design (see Fig. G.1) calls for Na- and S-containers with sealed flanges turned inward to increase packing density and improve thermal control. Manufacturing studies are in progress to assess the problems, if any, in this approach.

In addition, the viability of continuous coating (for S-container) concepts are being assessed in the laboratory as discussed above.

References

1. R. Bacon and R. Fanelli, Ind. & Engr. Chem., Vol. 34, p. 9 (1942).

PART THREE

COMPAGNIE GENERALE d' Electricite

PROGRESS REPORT

Section L

SEAL AND CONTAINER EVALUATION

Beginning January 1, 1977, CGE-Marcoussis undertook investigations in the following areas:

1. Ceramic-to-Metal Seals
2. Ceramic-to-Ceramic Seals
3. Containers for the Sulfur Compartment

The investigations emphasized in-cell evaluation of CGE-generated concepts. Concept optimization and supporting research were carried out under a CGE-sponsored parallel program. This Section provides a brief summary of the concept evaluation activities at CGE.

L.1 Ceramic-to-Metal Seals

The seals described in this section are the ones normally used at Marcoussis in studies of the sodium-sulfur system. Seals were fabricated between an alpha-alumina disc (25 mm diameter) and a metallic reservoir of 50 mm length. Two types of seals were investigated; (a) direct thermocompression and (b) brazed seals. They were characterized in terms of leaktightness, resistance to thermal cycling, corrosion and electrochemical cycling behavior and mechanical properties.

L.1.1 Direct Thermocompression Seals

Different reservior materials were tested; aluminum for the Na compartment, stainless steels and chromium-clad materials (iron, mild steel) for the S compartment.

The apparatus used for bonding was identical to that described in EPRI Report 726-1. One conclusion of this report was that high purity Al washers were required for the Al-ceramic interface. Thus, the seals tested in this study were constructed with a pure aluminum ring or disc between the ceramic and the reservoir.

Test Results

In order to characterize the degree of seal leak-tightness, a coefficient was established which described

the level of hermiticity. These coefficients range from 0 to 9 (Figure L.1), 9 representing complete tightness (leak level < 2.10^{-10} std cc sec^{-1} of He). 89 seals with aluminum reservoirs were tested and only 2 showed a slight leak (coefficient 8). The reject percentage is therefore on the order of 2% (Figure L.2).

Not all the other materials were capable of producing leaktight seals. Chromium-clad armco iron and 304 stainless steel were unable to form coherent interfaces at the reservoir/washer interface. Photomicrographs indicated the presence of fissures in this region. On the other hand chromium-clad mild steel and 430 stainless steel were consistently successful in obtaining hermetic seals. In subsequent bonding studies only chromium-clad mild steel was considered in detail because of its importance to industrial production.

Figure L.3 shows the appearance of such a seal. The even flow and distribution of the aluminum ring indicates the uniformity with which pressure was applied. Excellent leaktightness was once again obtained. 47 seals with chromium-clad mild steel reservoirs were evaluated and 44 were hermetic (94% - Figure L.4).

Thermal cycling was evaluated by subjecting a number of seals through 10 thermal treatments. The temperature was raised to 400°C and then rapidly cooled to ambient. No leaks were observed.

Test cells for sodium corrosion (static) were constructed (Figure L.5) and filled with sodium by electrolysis from molten sodium nitrate. They were placed in an oven operating in air at a temperature fixed at 400°C. Observations were conducted each week on the cells, and lifetimes in excess of 5,000 hours have been obtained for aluminum reservoirs. With chromium-clad mild steel samples, no apparent leakage has been observed over periods of 1500 hours.

In addition to the static tests, Na/Na cells containing two aluminum (type 1050) reservoirs were prepared and cycled. Two configurations of aluminum gaskets were assessed; O-ring (i.e., circular cross-section) and disc (rectangular cross-section). Three test temperatures were employed (330, 365, and 400°C), with a d.c. current density of 100 mA/cm^2 across the beta-alumina and current inversion every 40 minutes.

At 330°C the cells with O-ring seals exhibited an essentially constant resistance (Figure L.6) without any functioning problems up to 2600 hours. In the disc geometry a slight variation occurred after 500 hours of cycling (Figure L.7), however, at 365°C constant behavior was observed (Figure L.8). The O-ring sample at this temperature was terminated after 1800 hours because of fracture of the beta-alumina (Figure L.9).Subsequent analysis verified that the seals were structurally sound. At 400°C the disc specimen achieved 500 hours of cycling without any apparent change in behavior (Figure L.10). The O-ring seal at 400°C was terminated after 2000 hours of cycling following a rapid

rise in cell resistance and then an electrical short (Figure L.11). The larger than expected cell resistance (∿200 mΩ) during operation probably resulted from poor wetting of the cell components by sodium. Analysis of the failed cell indicated that the seal of the compartment containing the solid electrolyte had fractured. Sodium flow through this break interrupted electrical contact and produced a rapid resistance increase. Subsequent sodium flow along an exterior quartz tube resulted in an external short circuit.

Sodium-sulfur cells with aluminum compartments for sodium and chromium clad mild-steel containers for sulfur were constructed and cycled at 330°C. Cells continue to function satisfactorily after 5500 hours of cycling. One cell was voluntarily terminated at 500 hours in order to determine whether degradation was occurring. The seals were essentially unaffected. Only a thin passivating layer of aluminum sulfide on the aluminum washer was observed. The diffusion layer between the chromium-clad steel and aluminum exhibited no change in dimensions from its initial value. It is unlikely that this region is susceptible to long-term diffusion effects.

L.1.2 Brazed Metal Seals

Ceramic-metal seals can also be fabricated by a brazing technique. The inability of the braze to adequately wet the ceramic requires that the alpha-alumina be adequately metallized. The materials and procedures used in fabrication

are discussed below.

The brazes used to obtain satisfactory ceramic-metal seals in Na-S cells should satisfy the following conditions:

1) resist corrosion by the reagents (sodium, sodium polysulfides),

2) conveniently wet the parts to be assembled.

Various types of brazes were examined, and their weight variations determined after one month exposure at 400°C in sodium or sodium polysulfides. Brazes containing noble metals (e.g., Ag-Cu, Ag-Pd, Au-Ni) were rapidly attacked by sodium. Brazes composed of Fe, Ni, or Cr were stable in contact with liquid sodium, without any evidence of surface reaction. However, the braze surface became covered with crystals of nickel sulfide when in contact with sodium polysulfide. Diffusion of the reagent was limited by an underlying chromium sulfide layer. The behavior of these brazes is therefore analogous to that of stainless steels.

The molten braze does not wet the ceramic used as an insulating support (dense alpha-alumina manufactured by CERAVER containing a low level of vitreous phase). A preliminary metallization of the ceramic is therefore required in order to obtain a seal. Two techniques were examined:

1) use of active metals

2) hard metallization.

In the active metal process the alumina surface is covered by titanium or zirconium hydride. During the braze

operation, the material decomposes and provides a transient layer which the braze film wets. An adherent film is formed upon cooling.

Studies conducted as part of the C.G.E. in-house program identified tungsten as the most effective hard metallization and titanium hydride as the active metal. Seals were made using these two techniques but those with tungsten were not leaktight. An investigation revealed that the metallized layer had completely dissolved in the braze metal. Titanium hydride, however, was able to produce leaktight seals.

Test Results

All seals tested were fabricated by using a titanium hydride metallization in conjunction with a Fe-Cr-Ni braze. 347 stainless steel was the reservoir material. The ability to form leaktight seals was dependent upon processing conditions. A study concerning the influence of the various operating parameters is presently being conducted as part of the C.G.E. in-house program.

Seals must possess the necessary mechanical strength in order to meet the requirements of sodium-sulfur cell fabrication and operation. Five tensile tests on leaktight seals were performed. The test geometry was slightly different from that of the usual cell, however the stresses involved do indeed correspond to realistic conditions and constraints that component parts often experience. Table L.1 lists the measured failure loads. In all cases the parts

Table L.1

TENSILE FAILURE LOADS OF BRAZED SEALS

Seal No.	Load at Failure (N)
9	7.550
12	6.180
16	8.240
24	7.650
25	9.520

All parts failed due to fracture of alpha-alumina

failed due to fracture of the alumina and it is clear that the brazed seals possess the necessary mechanical integrity.

The braze geometry used in these tests was such that the alumina insulator was placed in a state of compression upon cooling. The maximum admissible stress value for the steel part is that of its elastic limit. On reheating the mechanism is reversed. There is an initial decrease of the compressive stress, followed at higher temperatures by a tensile stress at the brazed seal. This may affect seal leaktightness. Five leaktight parts were tested after heating respectively to 200, 300, 350, 400 and 450°C in air. Those subjected to temperatures higher than 350°C showed evidence of leakage. This limiting temperature depends on the expansion coefficients of the materials used, and is independent of the brazing procedure employed.

Future Program

In the thermocompression bonding work, seals with 1050 aluminum and chromium-clad mild steel will be emphasized. Lifetesting will be continued as will the corrosion and electrochemical cycling studies. The brazed seal approach will also be evaluated. In particular, thermal cycling effects and corrosion resistance will be examined.

L.2 Ceramic-to-Ceramic Seals

In this section the fabrication and properties of the glass seal existing between alpha and beta-alumina is discussed. A second variety, the direct high-temperature seal, was developed

as part of the C.G.E. in-house program. This seal is presently at the initial stage of evaluation.

L.2.1 Glass Seal Fabrication

The technique involves depositing a glass suspension on the open end of the beta-alumina tube and then heating to the vitrification point of the glass. The tube is put in contact with the alpha-alumina disc and heating this combination to the glass softening temperature allows the tube to slip into the appropriate region machined in the alpha-alumina. Slow cooling completes the seal preparation. The glass used for this type of seal must satisfy certain conditions:

1) Corrosion resistance to cell reagents (in particular to Na)

2) Sealing temperature less than 1200°C to avoid risk of Na_2O loss from the beta-alumina.

3) Capable of wetting the ceramic surface while avoiding chemical interaction.

L.2.2 Test Results

A sodium corrosion test (400°C for one month) indicated that certain commerical potassium-free glasses could be used. Two borosilicate glasses, S 750-06 and S 750-02 were particularly attractive because of their expansion coefficient and high softening temperature ($\sim$900°C).

Seals constructed with these two glasses were subjected to the following thermal cycle:

1) Heating from the room temperature to 400°C in 30 minutes

2) Cooling from 400°C in 30 minutes.

Seals with S 750-06 glass were able to resist at least 5 of these thermal cycles without the appearance of cracking in the seal area. In contrast, S 750-02 glass seals were rarely capable of enduring 5 cycles, and fracture occurred in the beta-alumina adjacent to the glass.

The different thermal behaviors may be traced to the nature of the reactions between glass and beta-alumina. The exposure of beta-alumina to a drop of S 750-02 glass at 1000°C for one hour led to the formation of reaction products in the solid electrolyte (Figure L.12). These dendrites appear at temperatures as low as 800°C and their growth depends on temperature and time of exposure. For example, 20 hours at 1200°C produces a transformation of essentially the entire thickness ($\sim$1 mm) of the beta-alumina tube. Analysis with an electron probe microanalyzer indicates the absence of sodium and silicon in the dendrites (Figure L.13), and it is therefore reasonable to assume that they consist of alpha-alumina. The presence of this second phase explains the formation of cracks during thermal cycling of the seals.

Sodium-sodium cells that utilize the S 750-06 sealing glass were constructed and cycled at 330°C, 365°C and 400°C. This test assesses the durability of the glass in molten sodium and an electric field. None of the cells were terminated due to glass seal failure. Some brown discoloration of the surface was observed. Several cells continue on test after

4000 hours of cycling. Another group of sodium-sodium cells were constructed with an improved glass sealing technique developed in the C.G.E. in-house program. These function well after 500 hours of cycling at 330°C.

The work on the chemical resistance of the glass to sodium will be continued. Emphasis will be placed on the influence of the discoloration on long-term seal quality. Directly-formed high temperature seals will also be evaluated.

L.3 Containers for the Sulfur Compartment

Static corrosion testing and electrochemical cycling procedures were used to evaluate various candidate materials for the sulfur container. The former serves as an effective screening test. Two stainless steels, 304 and 430, were subjected to molten sodium polysulfide. The Na_2S_5 composition was prepared using $Na_2S \cdot 9H_2O$ as starting material. Two thermal treatments were used in obtaining the pure sulfide;

(1) Vacuum evaporation at 75°C during a period of 130 hours.

(2) Heating at 150°C for 18 hours under reducing atmosphere (argon plus hydrogen).

The dry residue was mixed with sulfur in a glove-box and melted to obtain Na_2S_5. This convenient method of preparation does not give a perfectly anhydrous product, and may lead to a premature attack of stainless steels with formation of iron sulfide (Figure L.14). To obtain data under more significant conditions, specimens were introduced into the cathode compartments of Na-S cells containing Na_2S_5 prepared

by partial discharge in-situ. Under these conditions, a considerable reduction in corrosion rate was observed. It appears, therefore, that corrosion of stainless steel is sensitive to the presence of moisture and perhaps oxygen in the melt. Materials having Cr-rich coatings (mild steel and Armco iron) were tested under identical conditions. One month exposure at 330°C led to no detectable weight changes. This type of test was terminated and replaced by electrochemical cycling methods.

In this part of the program sodium-sulfur cells with sulfur containers consisting of a Cr-rich coating on mild steel were constructed and cycled at 330°C. An initial test was terminated at the end of one month. No variations in cell capacity or resistance were observed during this period. Cycling of another cell was terminated after 6 months at 330°C, and the chromium content of the polysulfide melt was analyzed by atomic absorption spectroscopy. The quantity determined (8 ppm) was of the same order as that in the previous study (5 ppm).

These results indicate the ability of the chromium layer to protect the mild steel container without forming a passivating product. This enables the material to serve as an effective current collector.

Future work in this area will emphasize the behavior

of mild steel with Cr-rich coating in contact with the graphite-felt sodium polysulfide mixture. Changes in the morphology of the chromium sulfide will be studied as a function of cycling lifetime.

L.4 Summary

Two types of ceramic-metal seals were evaluated. Direct thermocompression seals yielded extremely positive results. Chemical stability in sodium and sodium polysulfide was demonstrated and Na-S cells constructed with these seals have been on test for over 5500 hours. Thermal cycling did not affect seal leaktightness. Over 90% of the seals fabricated were hermetic. Brazed metal seals were also studied. Although excellent mechanical strengths were noted, thermal cycling stability was limited. Testing programs are continuing in both areas.

Sealing glasses were evaluated and encouraging results were obtained. Despite some evidence of sodium attack, cells continue on test after 4000 hours of cycling.

Stainless steel and containers with Cr-rich coatings were subjected to various corrosion tests. Materials with Cr-rich coatings were extremely effective in suppressing corrosion. After 6 months of cell cycling, only a few microns of a chromium sulfide layer was evident and the quantity of chromium in the melt was barely noticeable.

List of Figure Captions

List of Tables

LEAKTIGHTNESS
DEFINITION OF CLASSES

No.	LEAK IN STD. CC. SEC.$^{-1}$ He
9	$< 2 \cdot 10^{-10}$ (LEAKTIGHT)
8	$2 \cdot 10^{-10} - 10^{-8}$
7	$10^{-8} - 3 \cdot 10^{-8}$
6	$3 \cdot 10^{-8} - 10^{-7}$
5	$10^{-7} - 3 \cdot 10^{-7}$
4	$3 \cdot 10^{-7} - 10^{-6}$
3	$10^{-6} - 3 \cdot 10^{-6}$
2	$3 \cdot 10^{-6} - 10^{-5}$
1	VACUUM $< 10^{-5}$ mm Hg
0	VACUUM $> 10^{-4}$ mm Hg

Figure L.1. Leaktightness Coefficients

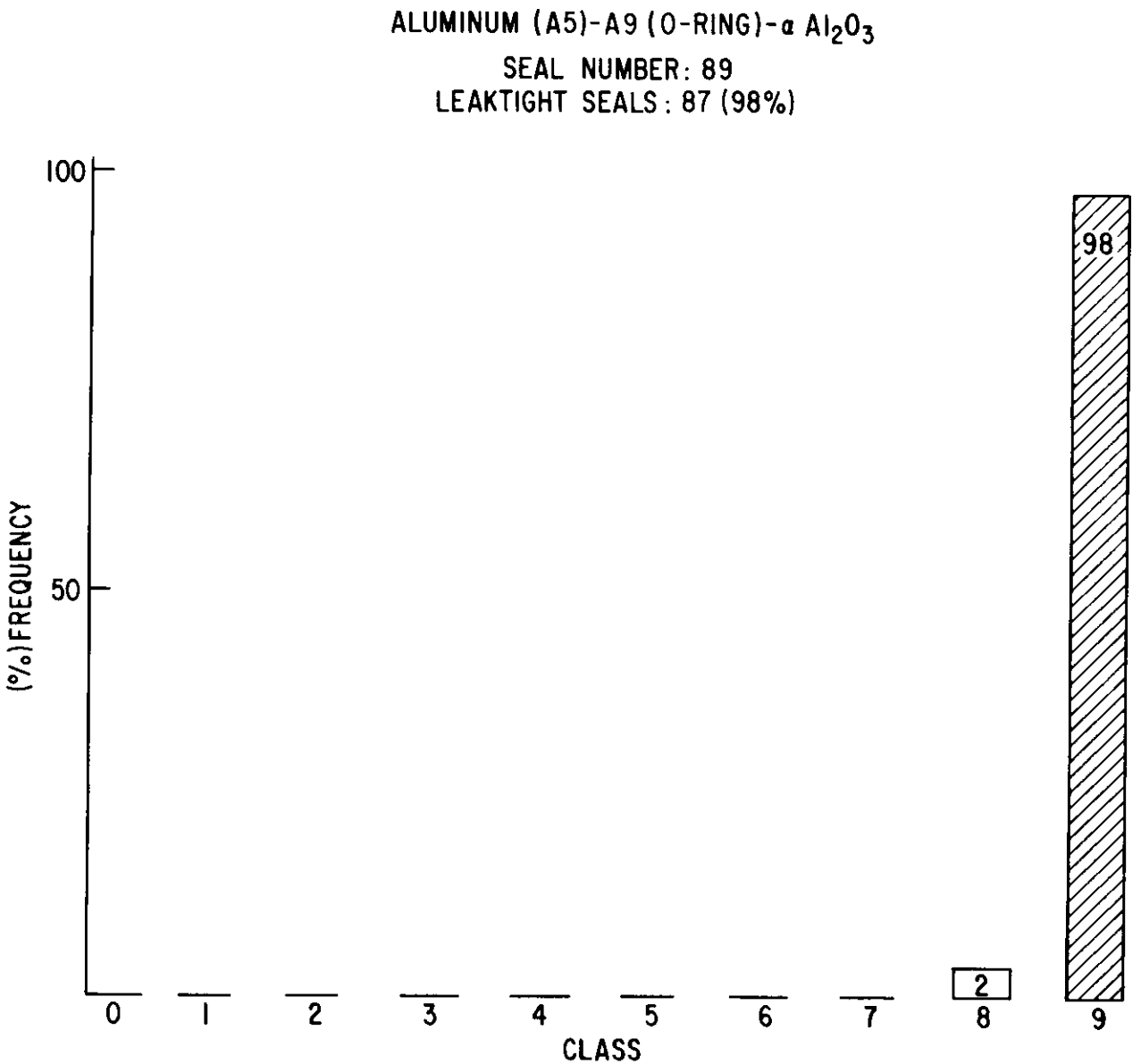

Figure L.2. Leaktightness Frequency for the System Aluminum (A5)-A9(O-Ring)-Alpha-Al_2O_3

Figure L.3. Cross-section of Chromized Steel-aluminum-alumina Seal

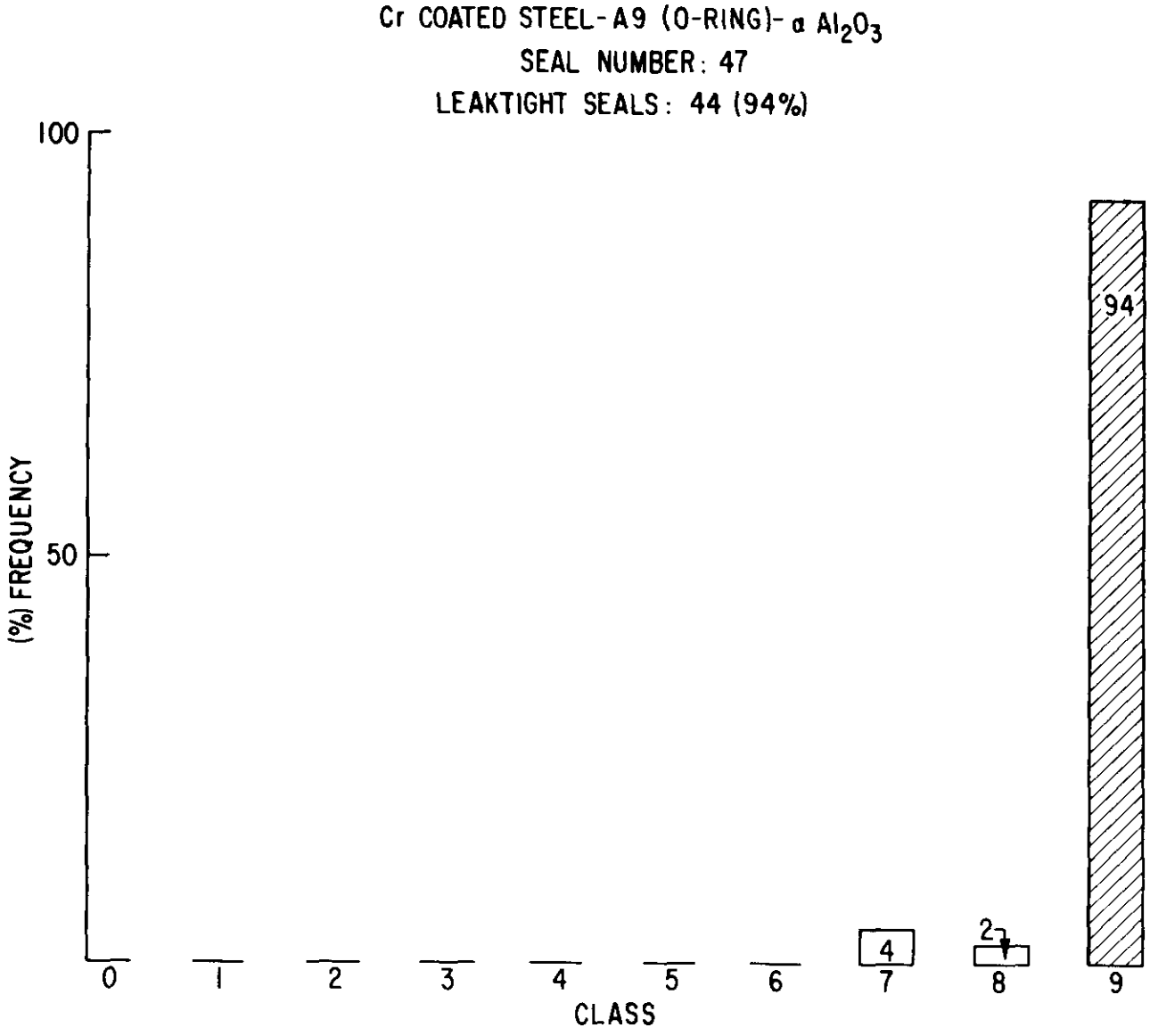

Figure L.4. Leaktightness Frequency for the System Cr-coated Steel-A9(O-Ring)-Alpha-Al_2O_3

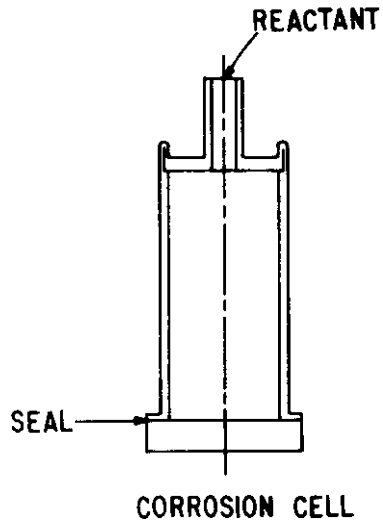

Figure L.5. Corrosion Cell for Sodium Durability

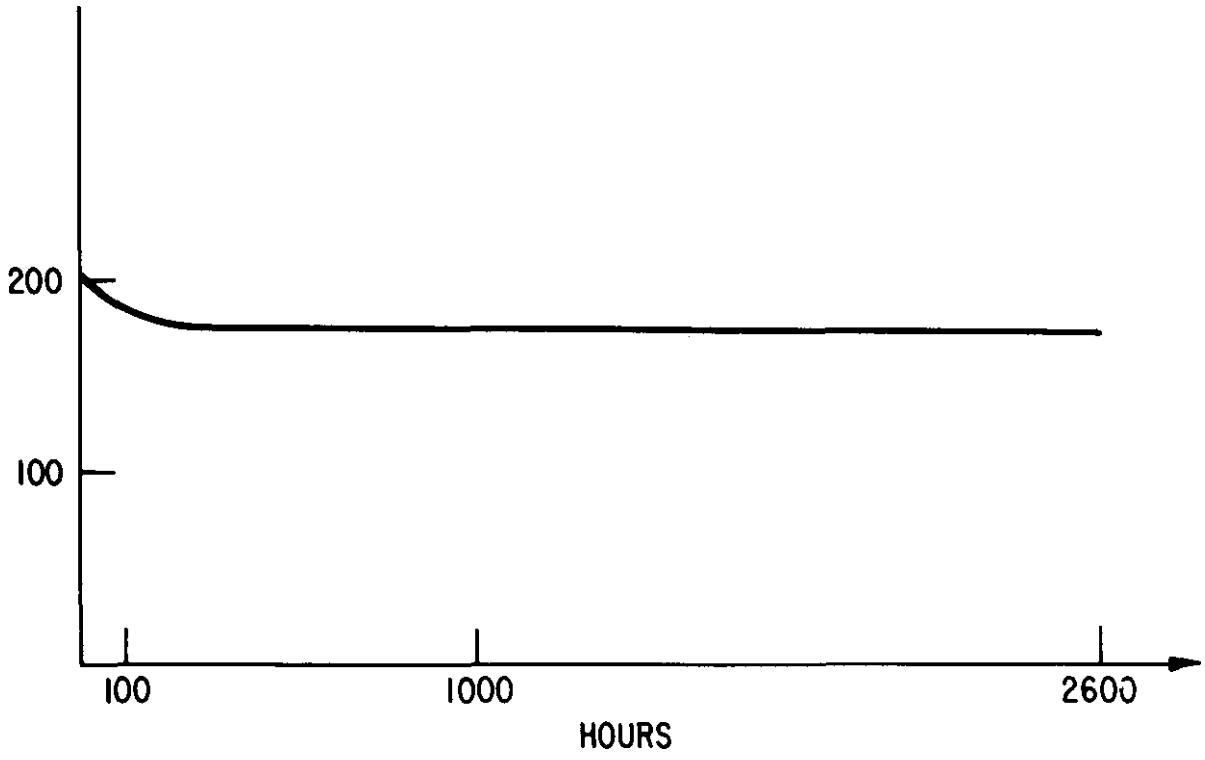

Figure L.6. Resistance of Na/Na Cell at 330°C - O-Ring Washer

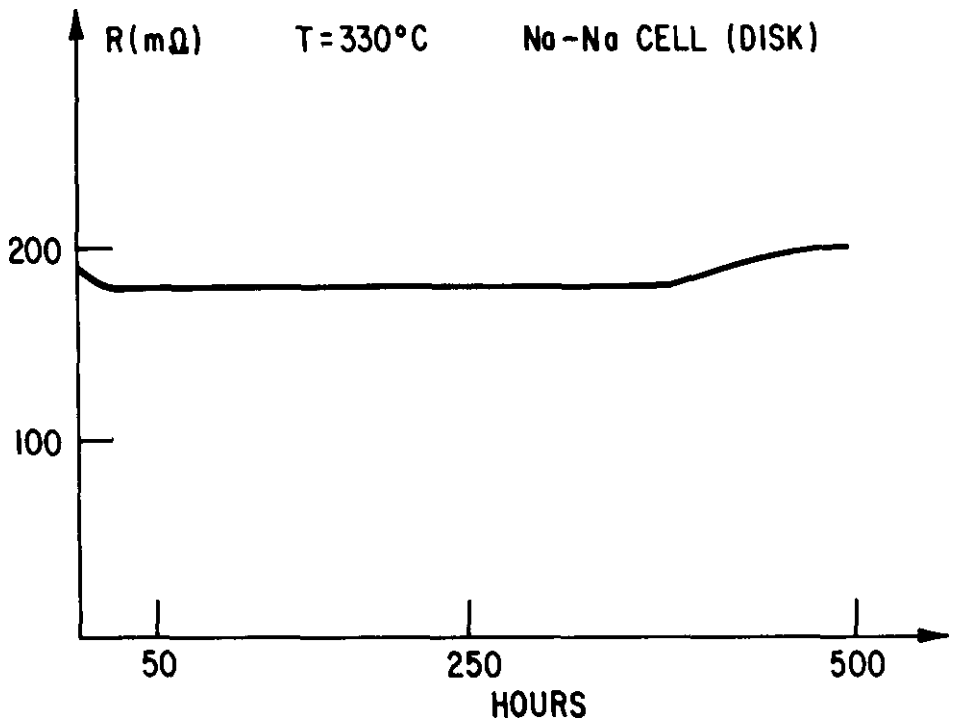

Figure L.7. Resistance of Na/Na Cell at 330°C - Disc Washer

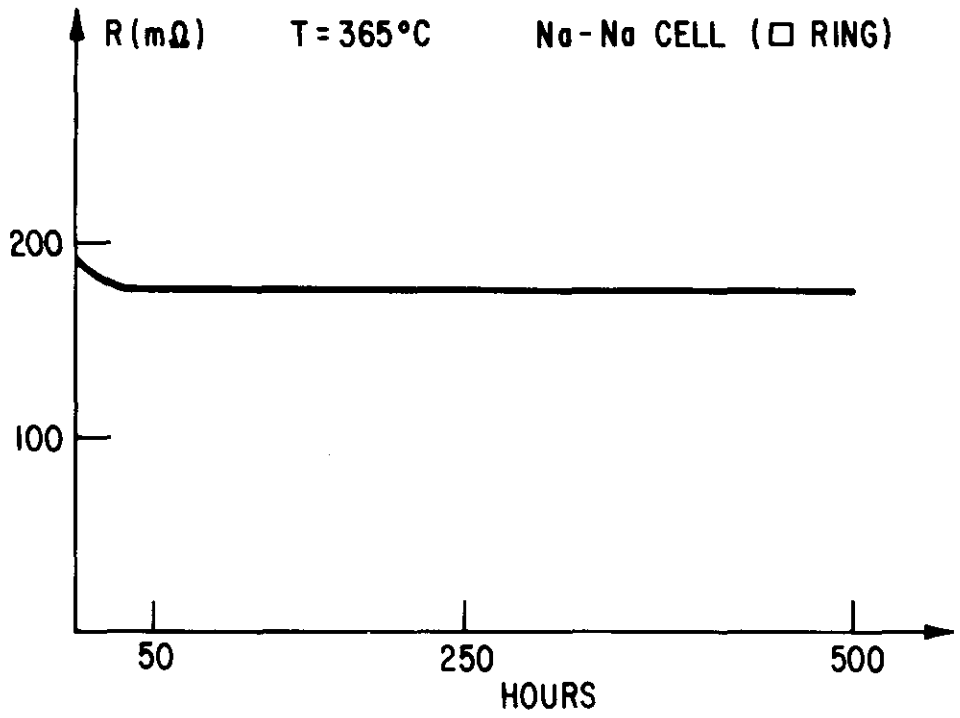

Figure L.8. Resistance of Na/Na Cell at 365°C - Disc Washer

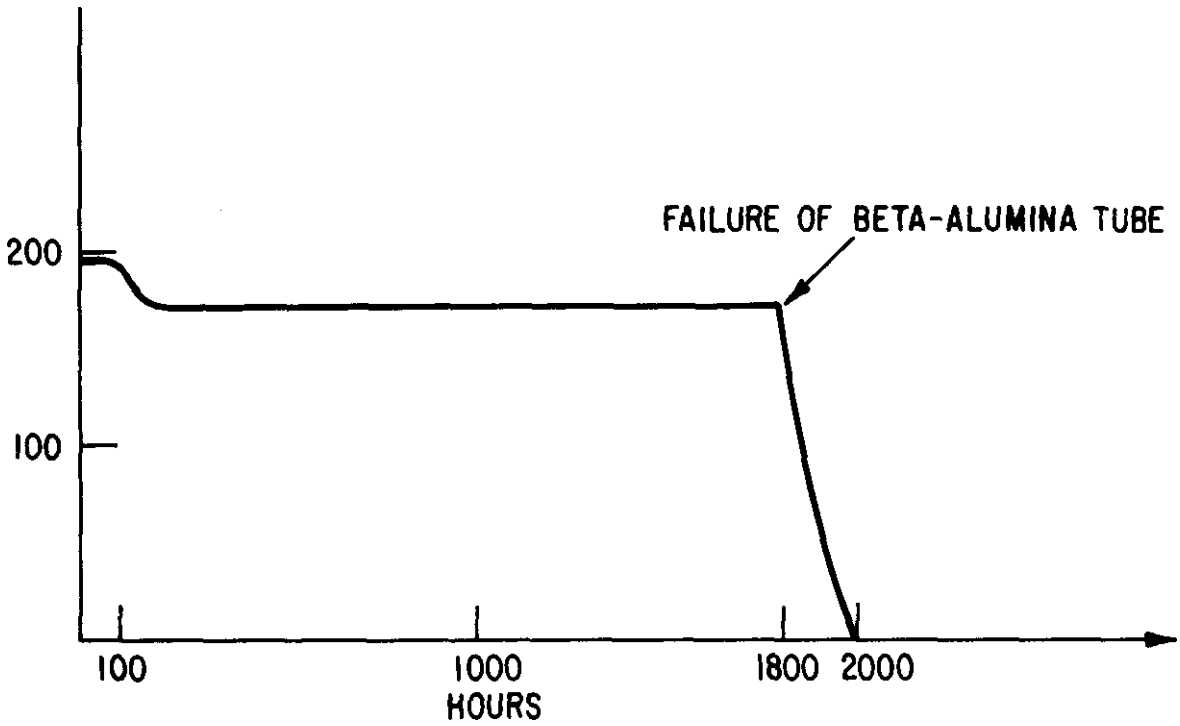

Figure L.9. Resistance of Na/Na Cell at 365°C - O-Ring Washer

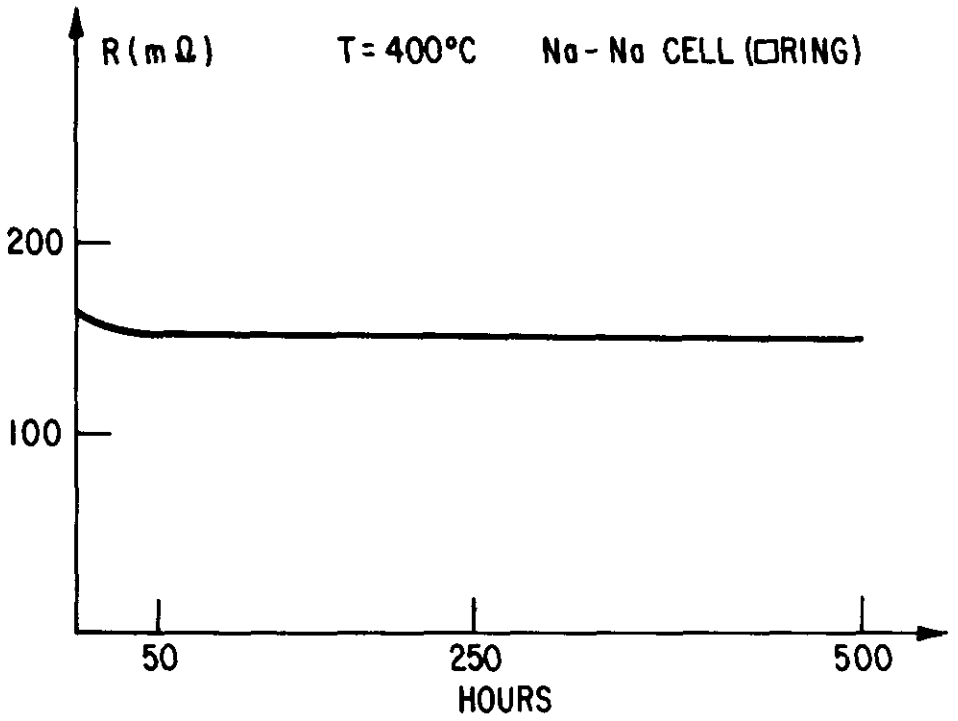

Figure L.10. Resistance of Na/Na Cell at 400°C - Disc Washer

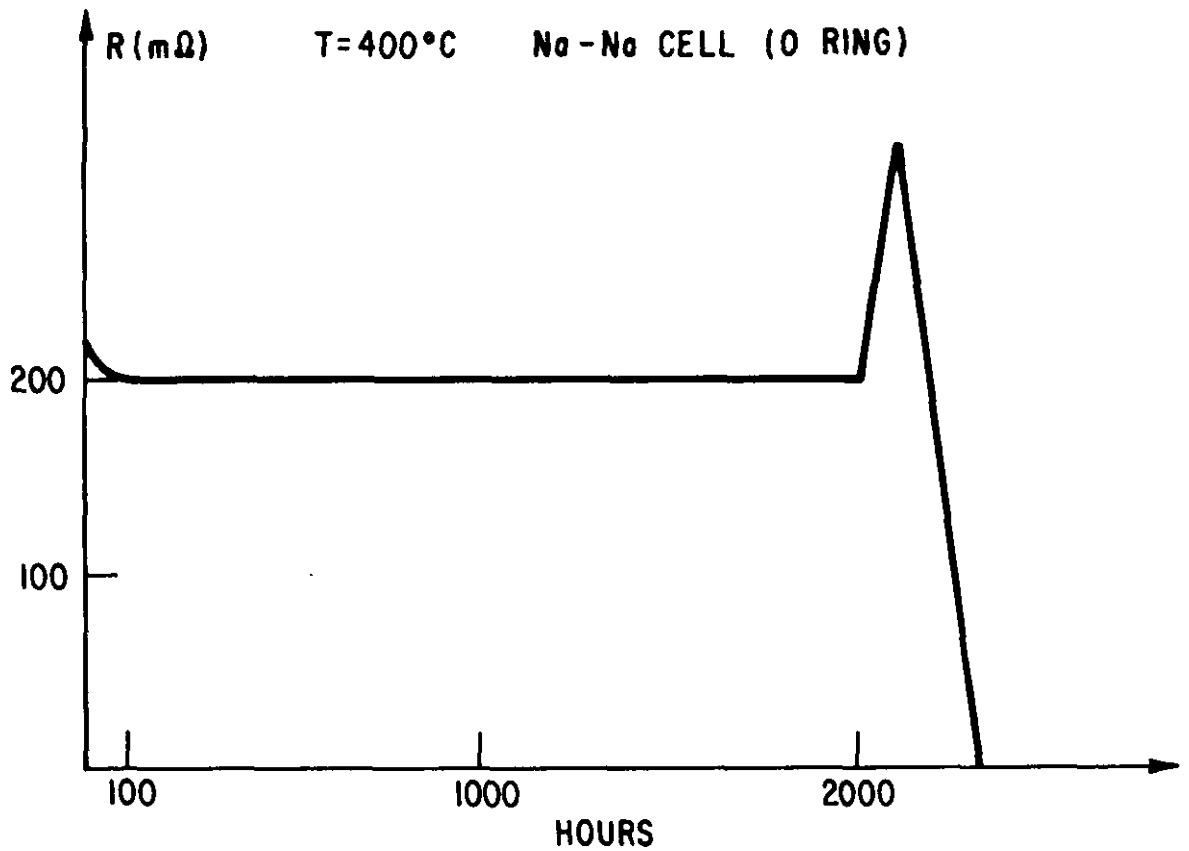

Figure L.11. Resistance of Na/Na Cell at 400°C - O-Ring Washer

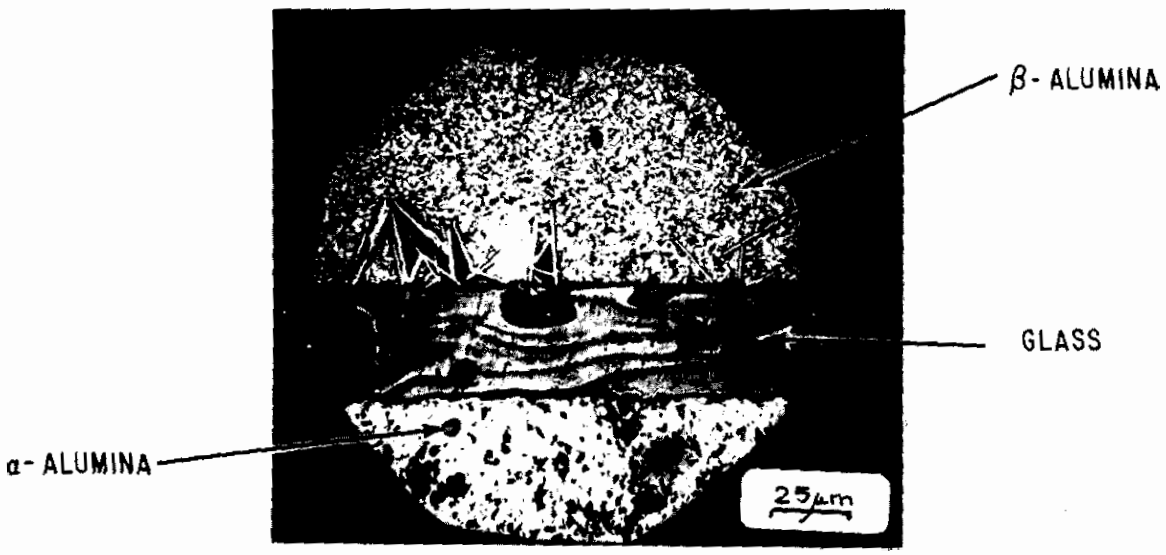

Figure L.12. Cross-section of Beta-alumina/Glass/Alpha-alumina Seal

SODIUM X-RAY IMAGE

Figure L.13. Microprobe Analysis of Dendrite

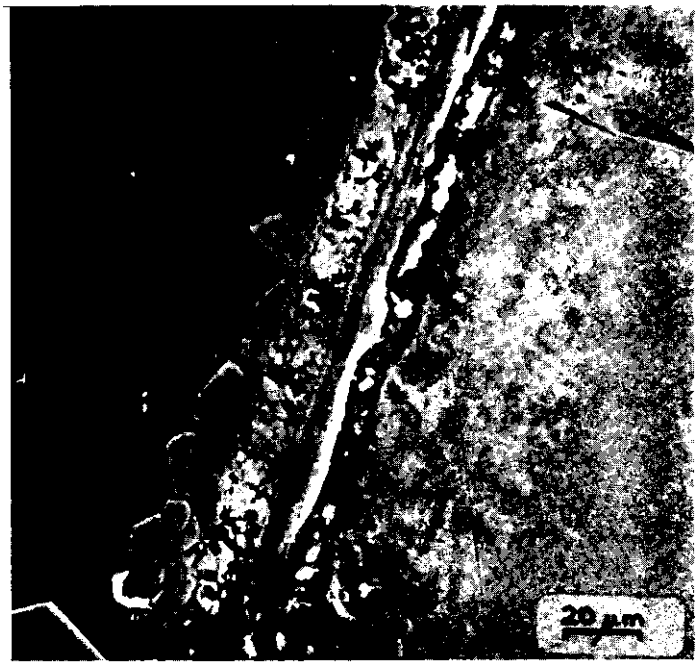

SCANNING ELECTRON MICROGRAPH

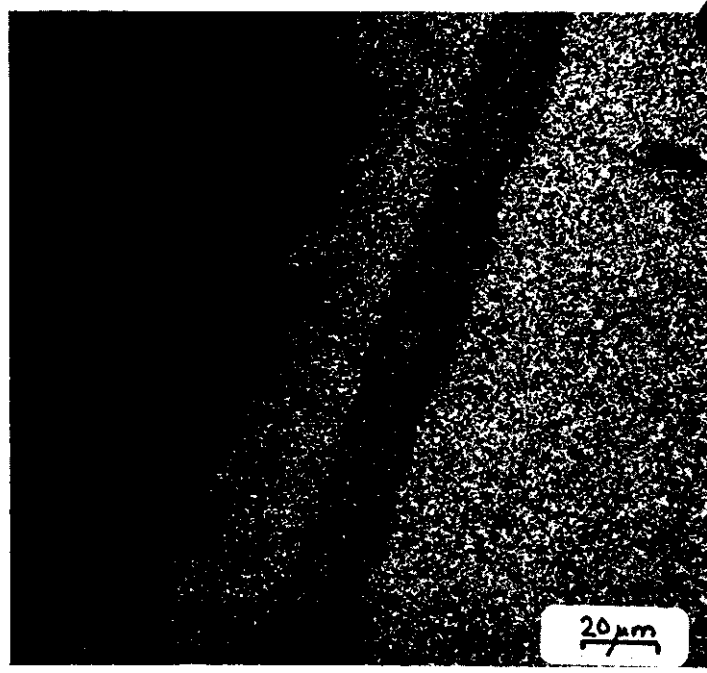

IRON X-RAY IMAGE

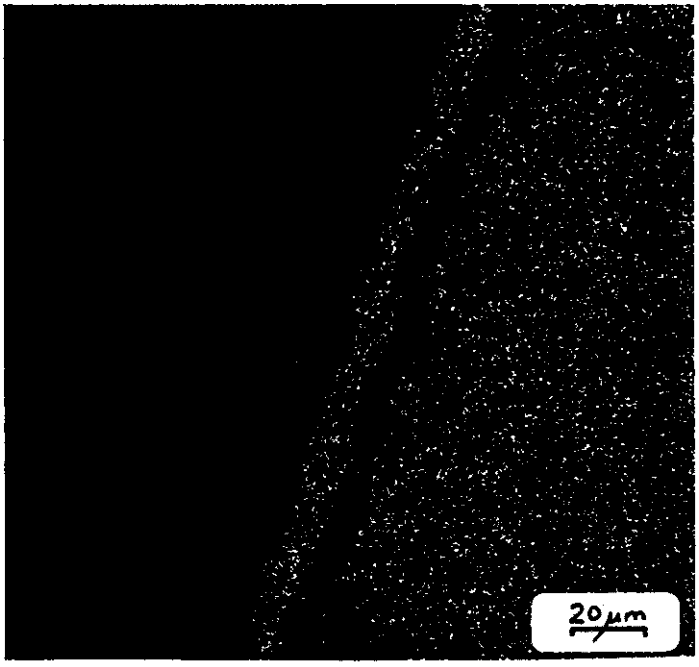

CHROMIUM X-RAY IMAGE

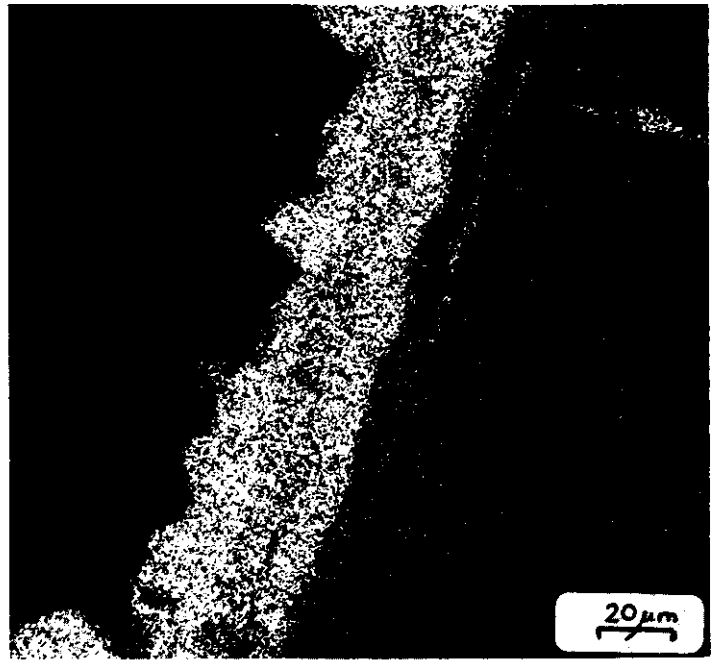

SULFUR X-RAY IMAGE

Figure L.14. Corrosion of Stainless Steel in Na_2S_5

PART FOUR

CONCLUDING REMARKS

Section M
CHALLENGES AND PLANS

As expected of most major R&D programs, the mix of technological challenges faced and addressed by Project RP128 continues to change with progress. In 1974, the majority of our test cells failed due to electrolyte degradation. Much to our satisfaction, that problem has been solved. On the other hand, the seals did not present any problem in 1974, for the electrolyte failed much before the seals. Now the seals limit the life of our test cells. Work is in progress to improve the chemical stability of the glass seal between the beta-alumina tube and the alpha-alumina insulator. Work is also in progress to replace the mechanical seals. These mechanical seals have served a very useful function so far; they allowed us to work with a basic cell design (that is amenable to modification) and to advance the state-of-the-art in cell performance. However, the mechanical seals impose non-uniform stresses on the alpha-alumina header, and very long seal life appears to be inattainable. These seals also present some cost challenges. A number of highly promising exterior seal concepts are now under evaluation at General Electric and at Compagnie Generale de Electricite.

The major challenges in the area of beta-alumina electrolyte now relate to lowering of resistivity (both bulk and surface) without sacrificing the outstanding physicochemical properties already achieved. Prognosis for success in this area is excellent.

Corrosion of the sulfur container presents another problem. Here the challenge lies in developing an alloy, a ceramic or a coated composite that is (1) resistant to sulfur/polysulfide attack, (2) electrically conductive, (3) safe from thermal/mechanical standpoints, and (4) cost-effective. Investigations during 1974-75 at GE demonstrated that sintered, high-density SiC performed extremely well in cell tests and accelerated tests. Unfortunately, this material appeared to present cost problems. At present, a number of approaches to protect low carbon-steels through metallic coatings/claddings are under evaluation. Certain proprietary chromium-based coatings have performed in an outstanding manner during tests conducted in 1977. It is our belief that the container problem is finally nearing a cost-effective solution.

The sodium-sulfur battery program at General Electric now stands at a crossroads. The program emphasis is steadily shifting from demonstration of basic technological feasibility in the laboratory to detailed engineering and demonstration of large battery systems. The program is therefore facing

and addressing the usual but difficult challenges associated with scale-up of laboratory processes and devices.

As this report has shown, significant progress has been made in the areas of battery system design and manufacturing engineering and economics. The challenges of more space and equipment, larger size of cell components, higher rates of production, and more manpower are being addressed. Furthermore, studies on safety, battery control alternatives, and failure modes and effects have been initiated. Analytical and experimental work has begun on "bundling" of cells. Finally, preliminary process development work has started in areas where manufacturing feasibility and/or cost are key issues. Development of continuous coating processes is one such area; another area is fabrication of cell-interconnectors.

In summary, many difficult technological barriers have been overcome, promising approaches are being pursued to solve existing problems, scale-up activities have been initiated, and a sound groundwork has been laid for the next phase of the program.

Section M
CHALLENGES AND PLANS

As expected of most major R&D programs, the mix of technological challenges faced and addressed by Project RP128 continues to change with progress. In 1974, the majority of our test cells failed due to electrolyte degradation. Much to our satisfaction, that problem has been solved. On the other hand, the seals did not present any problem in 1974, for the electrolyte failed much before the seals. Now the seals limit the life of our test cells. Work is in progress to improve the chemical stability of the glass seal between the beta-alumina tube and the alpha-alumina insulator. Work is also in progress to replace the mechanical seals. These mechanical seals have served a very useful function so far; they allowed us to work with a basic cell design (that is amenable to modification) and to advance the state-of-the-art in cell performance. However, the mechanical seals impose non-uniform stresses on the alpha-alumina header, and very long seal life appears to be inattainable. These seals also present some cost challenges. A number of highly promising exterior seal concepts are now under evaluation at General Electric and at Compagnie Generale de Electricite.

The major challenges in the area of beta-alumina electrolyte now relate to lowering of resistivity (both bulk and surface) without sacrificing the outstanding physicochemical properties already achieved. Prognosis for success in this area is excellent.

Corrosion of the sulfur container presents another problem. Here the challenge lies in developing an alloy, a ceramic or a coated composite that is (1) resistant to sulfur/polysulfide attack, (2) electrically conductive, (3) safe from thermal/mechanical standpoints, and (4) cost-effective. Investigations during 1974-75 at GE demonstrated that sintered, high-density SiC performed extremely well in cell tests and accelerated tests. Unfortunately, this material appeared to present cost problems. At present, a number of approaches to protect low carbon-steels through metallic coatings/claddings are under evaluation. Certain proprietary chromium-based coatings have performed in an outstanding manner during tests conducted in 1977. It is our belief that the container problem is finally nearing a cost-effective solution.

The sodium-sulfur battery program at General Electric now stands at a crossroads. The program emphasis is steadily shifting from demonstration of basic technological feasibility in the laboratory to detailed engineering and demonstration of large battery systems. The program is therefore facing

and addressing the usual but difficult challenges associated with scale-up of laboratory processes and devices.

As this report has shown, significant progress has been made in the areas of battery system design and manufacturing engineering and economics. The challenges of more space and equipment, larger size of cell components, higher rates of production, and more manpower are being addressed. Furthermore, studies on safety, battery control alternatives, and failure modes and effects have been initiated. Analytical and experimental work has begun on "bundling" of cells. Finally, preliminary process development work has started in areas where manufacturing feasibility and/or cost are key issues. Development of continuous coating processes is one such area; another area is fabrication of cell-interconnectors.

In summary, many difficult technological barriers have been overcome, promising approaches are being pursued to solve existing problems, scale-up activities have been initiated, and a sound groundwork has been laid for the next phase of the program.